Characterisation of Novel Lipids Generated by Activated Human Platelets via COX-1

Maceler Aldrovandi

A thesis submitted to Cardiff University for the degree of

Doctor of Philosophy

2013

DECLARATION

This work has not previously been accepted in substance for any degree and is not concurrently submitted in candidature for any degree.

Signed: *Macder Aldrovandi*   Date: 01/05/2014

STATEMENT 1

This thesis is being submitted in partial fulfilment of the requirements for the degree of PhD.

Signed: *Macder Aldrovandi*   Date: 01/05/2014

STATEMENT 2

This thesis is the result of my own independent work/investigation, except where otherwise stated. Other sources are acknowledged by explicit references.

Signed :   *Macder Aldrovandi*   Date: 01/05/2014

STATEMENT 3

I hereby give consent for my thesis, if accepted, to be available for photocopying and for interlibrary loan, and for the title and summary to be made available to outside organisations.

Signed: *Macder Aldrovandi*   Date: 01/05/2014

Acknowledgements

It would not have been possible to accomplish this thesis without the help and support of the kind people around me, to only some of whom it is possible to give particular mention here. They have all been generous with their advice and with their time and I would like to thank and acknowledge them here.

First and foremost I would like to express my sincere gratitude to my supervisor Professor Valerie O'Donnell for her infectious enthusiasm for science, her expert guidance on lipidomics and above all her support, patience and good humour while supervising this thesis. I would also like to thank Dr Peter Collins for the good advice, support and expertise on haemostasis.

I would like to express my deepest gratitude to all past and present members of the O'Donnell research group for their scientific advice, become good friends and provide welcome distractions from work. I would like to thank, in particularly, Dr Sarah Lauder and Dr Christopher Thomas for their significant contributions to the revision of this thesis and for their never failing patience and good humour. I am also grateful to Dr David Slatter for his great help with PGE_2/D_2-PE quantification.

I would like to offer my thanks to Dr Robert Murphy, Professor of pharmacology, University of Colorado, who has been invaluable for his expertise in lipidomics and for being generous with his time and advice. In addition, for the insights he has shared and for kindly providing purified COX enzymes, I would like to express my gratitude to Dr Lawrence Marnett, Professor of chemistry, Vanderbilt University.

I would also like to thank my parents and my sister. They were always supporting me and encouraging me with their best wishes.

Last but certainly not least I would like to thank my dearest husband Tiago without whom this process would have seemed impossible. An inspiration in so many ways, I certainly would not come this far without you. Thanks for always be there cheering me up and supporting me throughout this adventure. You have my thanks and my love always.

Publications

Full papers

Thomas CP, Clark SR, Hammond VJ, <u>Aldrovandi M</u>, Collins PW, O'Donnell VB. Identification and quantification of aminophospholipid molecular species on the surface of apoptotic and activated cells. Nat Protoc. 2014 Jan; 9(1):51-63.

<u>Aldrovandi M</u>, Hammond VJ, Podmore H, Hornshaw M, Clark SR, Marnett LJ, Slatter DA, Murphy RC, Collins PW, O'Donnell VB. Human platelets generate phospholipid-esterified prostaglandins via cyclooxygenase-1 that are inhibited by low dose aspirin supplementation. J Lipid Res. 2013 Nov; 54(11):3085-97.

Clark SR, Thomas CP, Hammond VJ, <u>Aldrovandi M</u>, Wilkinson GW, Hart KW, Murphy RC, Collins PW, O'Donnell VB. Characterization of platelet aminophospholipid externalization reveals fatty acids as molecular determinants that regulate coagulation. Proc Natl Acad Sci U S A. 2013 Apr 9; 110(15):5875-80.

<u>Aldrovandi M</u> & O'Donnell VB. Oxidized PLs and vascular inflammation. Curr Atheroscler Rep. 2013 May; 15(5):323.

Presentations

Aldrovandi M, Hammond VJ, Clark SR, Murphy RC, Collins P, O'Donnell VB. Thrombin-stimulated platelets acutely generate phospholipid-esterified prostaglandins (2011). Postgraduate Research Day, Cardiff University, UK. (Poster)

Aldrovandi M, Hammond VJ, Clark SR, Murphy RC, Collins P, O'Donnell VB. Thrombin-stimulated platelets acutely generate phospholipid-esterified prostaglandins (2012). Gordon Research Conference on Oxygen Radicals. Ventura, CA, USA. (Poster)

Aldrovandi M, Hammond VJ, Clark SR, Murphy RC, Collins P, O'Donnell VB. Thrombin-stimulated platelets acutely generate phospholipid-esterified prostaglandins (2012). 4th European Workshop on Lipid Mediators. Paris, France. (Poster)

Aldrovandi M, Slatter D, Murphy RC, Marnett LJ, Collins P, O'Donnell VB. Thrombin-stimulated platelets acutely generate PGE_2-PE and PGD_2-PE that are inhibited by aspirin *in vivo* (2013). Young Life Scientists' joint symposium 2013, Cardiovascular Medicine: Bridging Basic and Clinical Researchers. London, UK. (Poster)

Aldrovandi M, Slatter D, Murphy RC, Marnett LJ, Collins P, O'Donnell VB. Thrombin-stimulated platelets acutely generate PGE_2-PE and PGD_2-PE that are inhibited by aspirin *in vivo* (2013). 14th Annual UK Platelet Group Meeting. Birmingham, UK. (Poster)

Aldrovandi M, Slatter D, Murphy RC, Marnett LJ, Collins P, O'Donnell VB. Thrombin-stimulated platelets acutely generate PGE_2-PE and PGD_2-PE that are inhibited by aspirin *in vivo* (2013). 13th International Conference. Bioactive Lipids in Cancer, Inflammation and Related Diseases. San Juan, Puerto Rico. (Poster)

Summary

Initially, prostaglandins (PGs) were considered to only exist as free acid mediators. Although, formation of PG glycerol esters and PG ethanolamides by cellular cyclooxygenase (COX)-2 has been reported, generation of complex oxidised lipids via COX-1 has not been considered. In this study, formation of sixteen unique PG-containing phospholipids generated by agonist-activated human platelets is demonstrated using lipidomic approaches. Precursor scanning-tandem mass spectrometry identified a group of specific lipids comprising PGE_2, PGD_2 and two previously undescribed PG-like molecules (named PGb and PGc), attached to four phosphatidylethanolamine (PE) phospholipids (16:0p/, 18:1p/, 18:0p/ and 18:0a/). PGb and PGc were also detected as free eicosanoids and their structures remain to be characterised. These novel lipids formed within 2-5 minutes of platelet activation by thrombin, collagen or ionophore and required activation of several intracellular signalling intermediates, including cytosolic phospholipase A_2 (cPLA$_2$), p38 mitogen-activated protein kinase (MAPK), *src* tyrosine kinases, phospholipase C (PLC) and cytosolic calcium. Unlike free PGs that are secreted, PG-PEs remain cell associated, suggesting an autocrine mode of action. Aspirin supplementation *in vivo* (75 mg/day) or *in vitro* (1 mM) blocked their generation, indicating that COX-1 is required. Pharmacological studies using inhibitors of fatty acyl re-esterification significantly reduced formation of PG-PEs. Furthermore, purified COX-1 was unable to directly oxidise PE *in vitro*. Collectively, these indicate that PG-PEs are initially formed as free PGs via COX-1, and then rapidly esterified into PEs. In summary, this is the first demonstration of acute generation of PG-PEs in agonist-activated human platelets from endogenous substrate via COX-1. These unique lipids may represent additional bioactive molecules from this key platelet enzyme.

Abbreviations

A23187	Calcium ionophore
AA	Arachidonic acid
ACD	Acid-citrate-dextrose acid
AEA	Arachidonyl-ethanolamide
AG	Arachidonyl-glycerol
AMP	Adenosine monophosphate
amu	atomic mass units
ATP	Adenosine-5'-triphosphate
BAPTA/AM	1,2-bis-(o-Aminophenoxy)-ethane-N,N,N',N'-tetra-acetic
BEL	Broenol lactone
Ca^{+2}	Calcium
CAT	Calibrated automated thrombography
CID	Colision-induced-dissociation
CoA	Coenzyme A
COX	Cyclooxygenase
$cPLA_{2\alpha}$	Cytosolic phospholipase $A_{2\alpha}$
cps	counts per second
DMPE	Dimyristoyl phosphatidylethanolamine
DMSO	Dimethyl sulfoxide
DSPC	1,2-distearoyl-sn-glycero-3-phosphocholine
DTPA	Diethylenetriaminepentaacetic acid
EGTA	Ethylene glycol tetraacetic acid
Fe^{2+}	Ferrous ion
Fe^{3+}	Ferric ion
FTMS	Fourier transform mass spectrometry
HCD	Higher collision dissociation
HDOHE	Hydroxydocosahexaenoic acid
HETE	Hydroxyeicosatetraenoic acid
HPLC	High pressure liquid chromatography
IP_3	Inositol 1,4,5-triphosphate
$iPLA_2$	Calcium-independent PLA_2
ITMS	Ion trap mass mode
KETE	keto-eicosatetraenoic acid
LC	Liquid chromatography
LC-FACS	Long chain fatty acyl-CoA synthetase
LOX	Lipoxygenase
LPCATs	Lysophosphatidylcholine acyltransferase
LPS	Lipopolysaccharide

m/z	Mass to charge ratio
MAPK	Mitogen-activated protein kinase
MRM	Multiple reaction monitoring
MS	Mass spectrometry
MS/MS	Tandem mass spectrometry
NET	Neutrophil extracellular trap
ng	Nanograms
NSAID	Nonsteroidal anti-inflammatory drug
OOEPC	Oleyloxyethyl phosphocholine
OxPAPC	1-palmitoyl-2-arachidonyl-sn-3-glycero-phosphoryl-choline
OxPL	Oxidised phospholipid
PAR	Protease-activated receptor
PC	Phosphatidylcholine
PE	Phosphatidylethanolamine
pg	Picograms
PG	Prostaglandin
PGD_2	Prostaglandin D_2
PGDS	Prostaglandin D synthase
PGE_2	Prostaglandin E_2
PGES	Prostaglandin E synthase
PI	Phosphatidylinositol
PI3Ks	Phosphatidylinositide 3-kinases
PIP_2	Phosphatidylinositol 4,5-bisphosphate
PKC	Protein kinase C
PL	Phospholipid
PLA_2	Phospholipase A_2
PLC	Phospholipase C
ppm	part-per-million
PS	Phosphatidylserine
SAPE	1-stearoyl-2-arachidonoyl-sn-glycero-3-phosphoethanolamine
SAPS	1-stearoyl-2-arachidonoyl-sn-glycero-3-phospho-L- serine
SEM	Standard error of the mean
$sPLA_2$	secretory PLA_2
TF	Tissue factor
TP	Thromboxane receptor
TxA_2	Thromboxane A_2
TxB_2	Thromboxane B_2
vWf	von Willebrand factor

Contents

Chapter 1 – General Introduction

Chapter 2 – Materials and Methods

Chapter 3 – Identification of novel Phospholipid-esterified Prostaglandin Generated by Activated Human Platelets

Chapter 6 – Studies on the Mechanism of Free and Esterified Prostaglandin Formation by Activated Human Platelets

Chapter 7 – Investigating the requirement for COX-1 in the Generation of Esterified Prostaglandins by activated human platelets

Chapter 8 – Studies on the Mechanism of COX-1 Oxidation of Free or Esterified Arachidonic Acid in Human Platelets

Chapter 9 – Characterisation of Receptor and Signalling mediators Regulating Esterified and Free Prostaglandin Formation by Activated Human Platelets

Chapter 10 – Studying PGE2 Esterification into Lysophospholipids using Rat Liver Microsomes and Characterising the Ability of Esterified Prostaglandins to Regulate Coagulation

List of Figures

List of Schemes

List of Tables

Chapter 1

Introduction

1.1 Platelets

Human platelets are small enucleate cell fragments that play important roles in the physiological and pathological processes of haemostasis, inflammation, tumour metastasis, wound healing and host defence. After erythrocytes, platelets are the most abundant corpuscle in the blood, normally circulating at a range between $150 - 400 \times 10^9$ per litre (Thon & Italiano, 2012). An average healthy adult produces approximately 100 billion platelets each day, with a single megakaryocyte capable of generating more than 5,000 thousand (Thon & Italiano, 2012). Platelets are the smallest corpuscular component of circulating blood and have a diameter of 2 - 3 μm. The average physiological lifetime of a platelet is normally just 8 – 10 days with a daily renewal of about 20 % of the total platelet count (Nayak *et al.*, 2013). Approximately two thirds of the platelets circulate in the bloodstream before they are cleared by macrophages in the spleen and by Kupffer cells in the liver. The remaining third are stored in the spleen and are released when needed (Schmidt *et al.*, 1991).

Platelets derive from cytoplasmic fragmentation of megakaryocytes in the bone marrow and are released into the circulation. The transition from immature cells to platelets initiates with the development of megakaryocyte thick pseudopods, leading to pro-platelet formation. Towards the final stage of megakaryocyte maturation, the entire megakaryocyte cytoplasm is converted into a mass of pro-platelets from which the nucleus is eventually extruded. Individual platelets are then released from pro-platelet into the sinusoidal blood vessels of the bone marrow (Italiano *et al.*, 2007; Bluteau *et al.*, 2009; Thon & Italiano, 2010).

The unstimulated platelet surface is generally smooth and packed with functional receptors to enable platelet activation and interactions with other blood cells and platelets (Semple *et al.*, 2011). The membrane is metabolically active with a surface canalicular connection system that permeates the cytoplasm and provides a large surface area. Platelets contain mitochondria, microtubules and several granules, which upon

activation, can fuse with the platelet membrane and release their content into the extracellular space (Figure 1.1). In addition, platelets contain a dense tubular system (DTS), a derivative of the smooth endoplasmic reticulum of the megakaryocyte, which regulates platelet activation by sequestering or releasing calcium (Ebbeling *et al.*, 1992). A schematic representation of a platelet and its organelles is shown in Figure 1.1.

1.1.1 Platelets and coagulation

During their lifetime, most platelets flow in the circulatory system in a quiescent state and never undergo firm adhesion. Only when the endothelial cell layer of vessel walls is damaged by traumatic injury or pathological alteration, as found in atherosclerosis, do they undergo fast activation, granule secretion and aggregation, leading to a haemostatic plug. To ensure a rapid and effective response, platelets are very sensitive towards external stimuli. Upon activation, they experience a dramatic shape change from a discoid to a more stellate form with long pseudopodia.

Following disruption of vascular integrity, coagulation is initiated by the exposure of cells expressing tissue factor (TF), such as adventitial fibroblasts and epithelial cells surrounding organs (Figure 1.2) (Drake *et al.*, 1989). Then, Factor (F) VII present binds to TF, together forming a very high affinity complex (TF:FVIIa) in the presence of calcium on the phospholipid surfaces expressed by platelets (Higashi et al., 1996; Eigenbrot *et al.*, 2001; Adams & Bird, 2009). The generation of TF:FVIIa complex results in a proteolytic cleavage of Factor X (FX) to form the activated protease FXa. Also, conversion of the zymogen FVII to the serine protease FVIIa results in the activation of FIX by the TF:FVIIa complex. The activated FX, in the absence of its activated cofactor FVa, generates only small amounts of thrombin. Trace amounts of thrombin formed in this initiation stage of coagulation is not sufficient to commence significant fibrin polymerization. However, it is enough to back-activate FV and to convert FVIII and FXI to the proteases FVIIIa and FXIa, respectively.
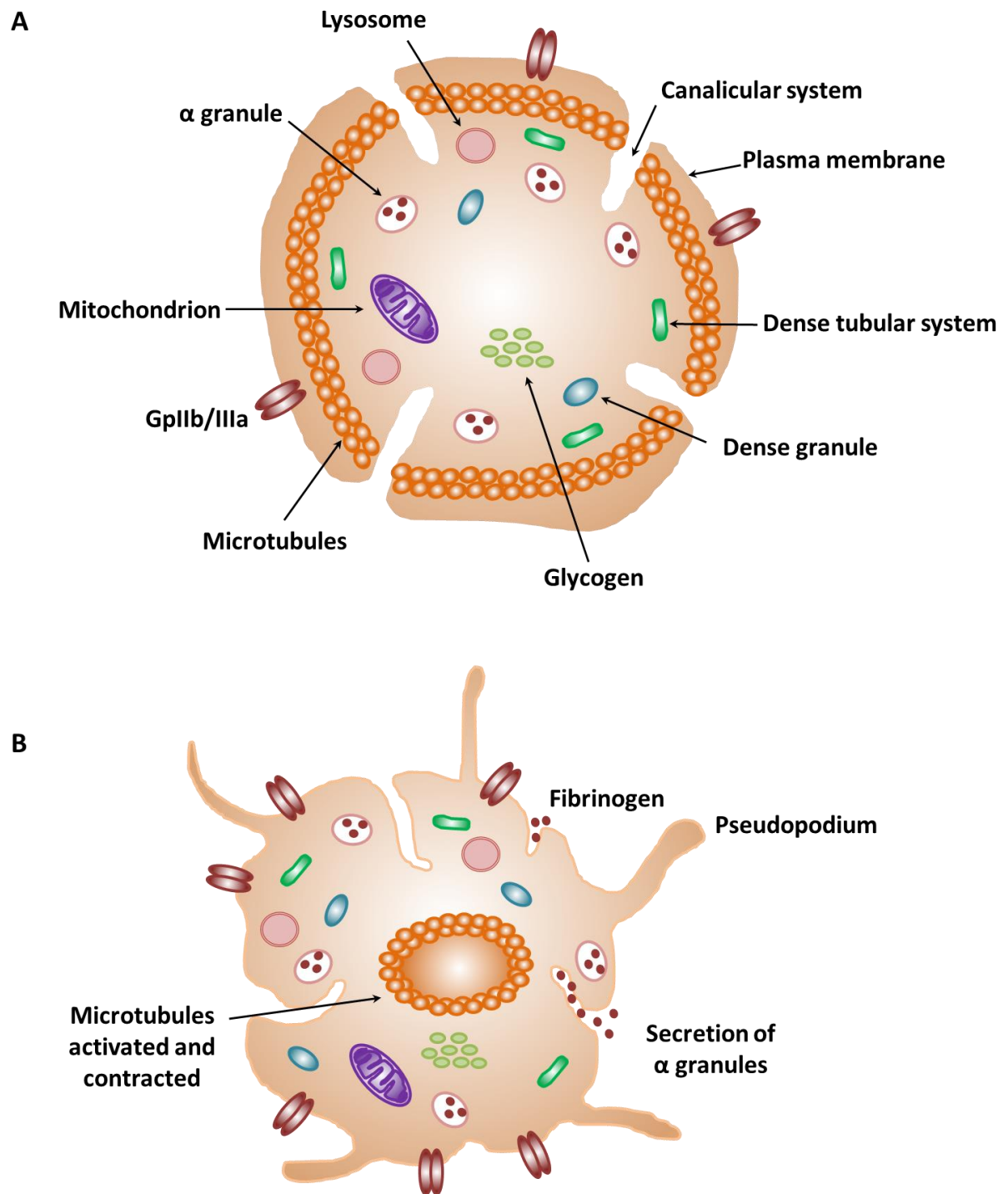
Figure 1.1: Schematic representation of a platelet and its organelles. *Panel A.* The unstimulated platelet. *Panel B.* The activated platelet. Upon agonist activation, activated platelets release their α-granules content (fibrinogen, fibronectin, platelet-derived growth factors, platelet factor 4, transforming growth factor β, von Willebrand and coagulation factors) and change shape, from a lentiform shape to a spiny sphere.
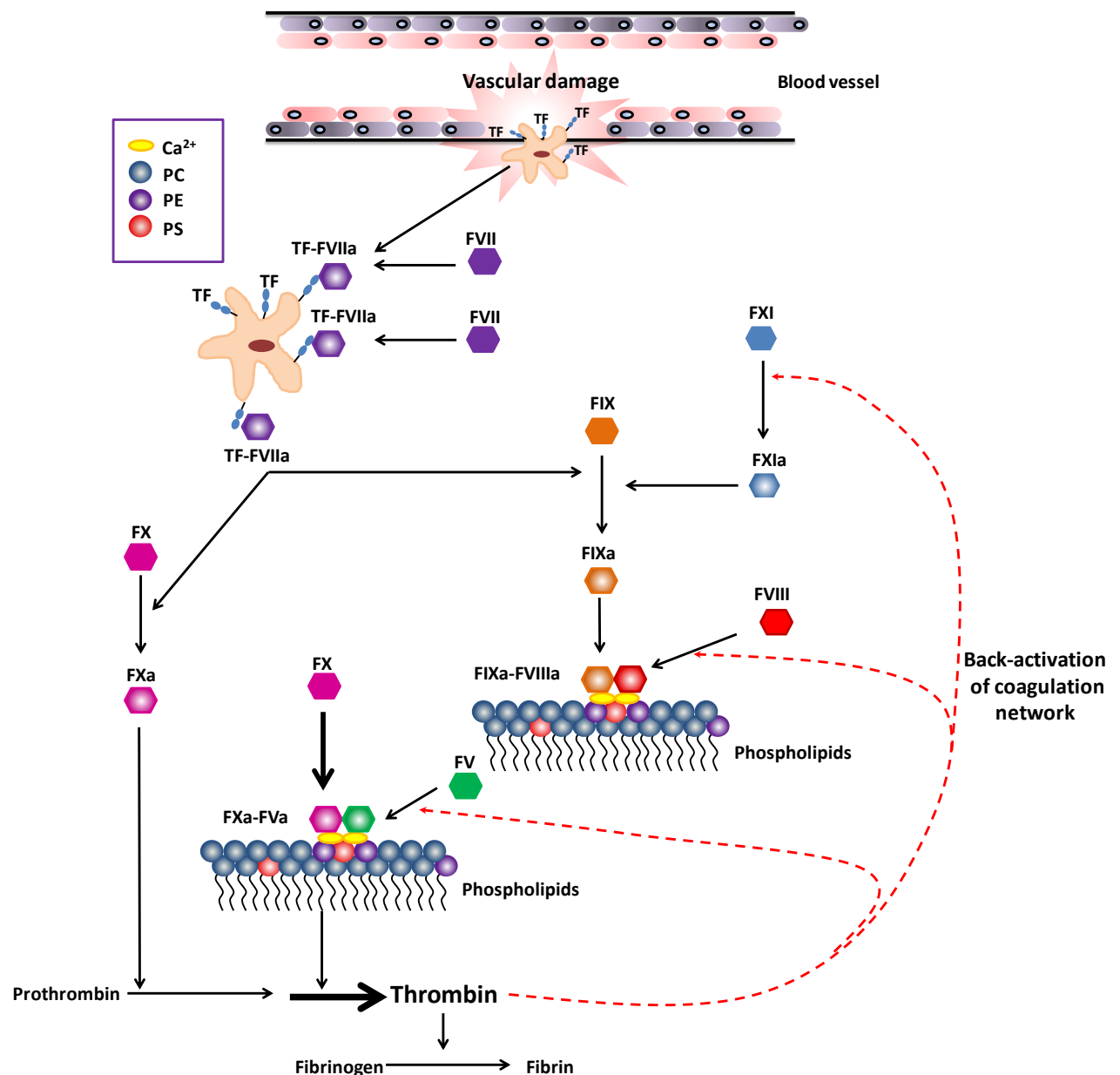
Figure 1.2: The haemostasis network. Physiologically, blood coagulation is initiated upon exposure of subendothelial TF to the circulating FVII, together forming a very high affinity complex (TF:FVIIa). Conversion of the FVII to FVIIa results in the activation of FIX and FX by the TF:FVIIa complex. Initially, only small amounts of thrombin is formed, enough to activate FV and to convert FVIII and FXI to FVIIIa and FXIa, respectively. In the amplification phase, FXIa activates FIXa that forms a complex with FVIIIa. The tenase complex (FVIIIa:FIXa) activates sufficient FXa that, together with FVa, form the prothrombinase (FVa:FXa) complex. Together, the tenase and the prothrombinase complexes lead to the explosive generation of thrombin.

In the amplification phase of coagulation, FXIa activates FIXa, which forms a complex with FVIIIa (Figure 1.2). The tenase complex (FVIIIa:FIXa) activates sufficient FXa that, in the presence of calcium ions, forms a one-to-one complex with Factor Va (FVa:FXa, prothrombinase complex) on the surface of anionic phospholipids expressed by activated platelets (Ahmad *et al.*, 2003; Mackman, 2009; Fay, 2004).

Collectively, the tenase and the prothrombinase complexes lead to the explosive generation of thrombin, which is responsible for the conversion of soluble plasma protein fibrinogen to fibrin. Consequently, the insoluble fibrin polymer gives rise to a haemostatic plug, whose main function is to rapidly prevent the loss of body fluids without compromising blood flow.

1.2 Phospholipids

Phospholipids, also referred to as glycerophospholipids, are the major components of cell membranes. They play a crucial role in the biochemistry of all living cells. Due to their amphipathic nature, phospholipids form a bilayer that is crucial to cell survival, providing a semi-permeable barrier to the surrounding environment and functional roles in cellular processes, such as cell signalling, secretion and internalisation (Vance & Vance, 2002; Fahy *et al.*, 2005; Fahy *et al.*, 2011).

Phospholipids consist of a glycerol backbone connected to two nonpolar fatty acids at sn1 and sn2 and a phosphate-containing polar headgroup at the sn3 position (Figure 1.3). In eukaryotes, phospholipids may be subdivided into distinct classes, based on the nature of the polar headgroup, including phosphatidylethanolamine (PE), phosphatidylcholine (PC), phosphatidylserine (PS), phosphatidylinositol (PI) and phosphatidylglycerol, which can influence membrane function.

In phospholipids, the sn2 fatty acid is attached to the glycerol backbone via an acyl group, while, the sn1 can be linked either through an acyl, plasmalogen or ether bond. The acyl group is a carbonyl group (>C=O) attached to either an alkyl or aryl group. It has the formula RCO-, where R represents an alkyl group attached to the CO group with a single

bond and the carbon and oxygen atoms linked by a double bond (Stoke, 2013). Whereas, plasmalogens are a subclass of phospholipids characterised by the presence of a saturated group at the sn1 position on the glycerol chain bonded by a vinyl ether linkage, while the sn2 position is most commonly occupied by polyunsaturated fatty acids, particularly arachidonic acid (AA), linked by an ester bond (Nagan & Zoeller, 2001). The fatty acid at the sn1 can also be linked to the glycerol chain via an ether linkage (C–O–C), which is stable to both alkaline and acidic conditions while vinyl ether bonds open under acidic conditions to form aldehydes (Albert *et al.*, 2001).

The fatty acyl chains are highly variable at both the sn-1 and sn-2 positions, varying in terms of carbon chain length and degree of unsaturation (Marcus *et al.*, 1969). Arachidonic acid, an important precursor of many lipid mediators, is one of the fatty acids commonly found at sn-2 position and is cleaved by enzymes, such as phospholipase A_2 (PLA_2), generating fatty acid substrate for oxidation by cyclooxygenases (COX) and lipoxygenases (LOX) (Levy, 2006; Triggiani *et al.*, 2005).

1.2.1   *Phospholipids of the platelet plasma membrane*

Cellular membranes are composed of bilayers with each leaflet presenting a different phospholipid composition. In platelet phospholipids, PC constitutes approximately 38 % of the membrane and PE 27 %, with PS and PI together contributing only about 15 % (Shick & Panetti, 2006). The phospholipids in the resting platelet plasma membrane are asymmetrically organized; PC and sphingomyelin (SphM) are enriched in the outer monolayer, while PE and PS are more dominant in the inner layer (Shick & Panetti, 2006). The adenosine triphosphate (ATP)-dependent aminophospholipid-specific translocase is responsible for quickly transporting PS and PE from the cell's outer-to-inner leaflet, keeping the plasma membrane asymmetry (Zwaal & Schroit, 1997).
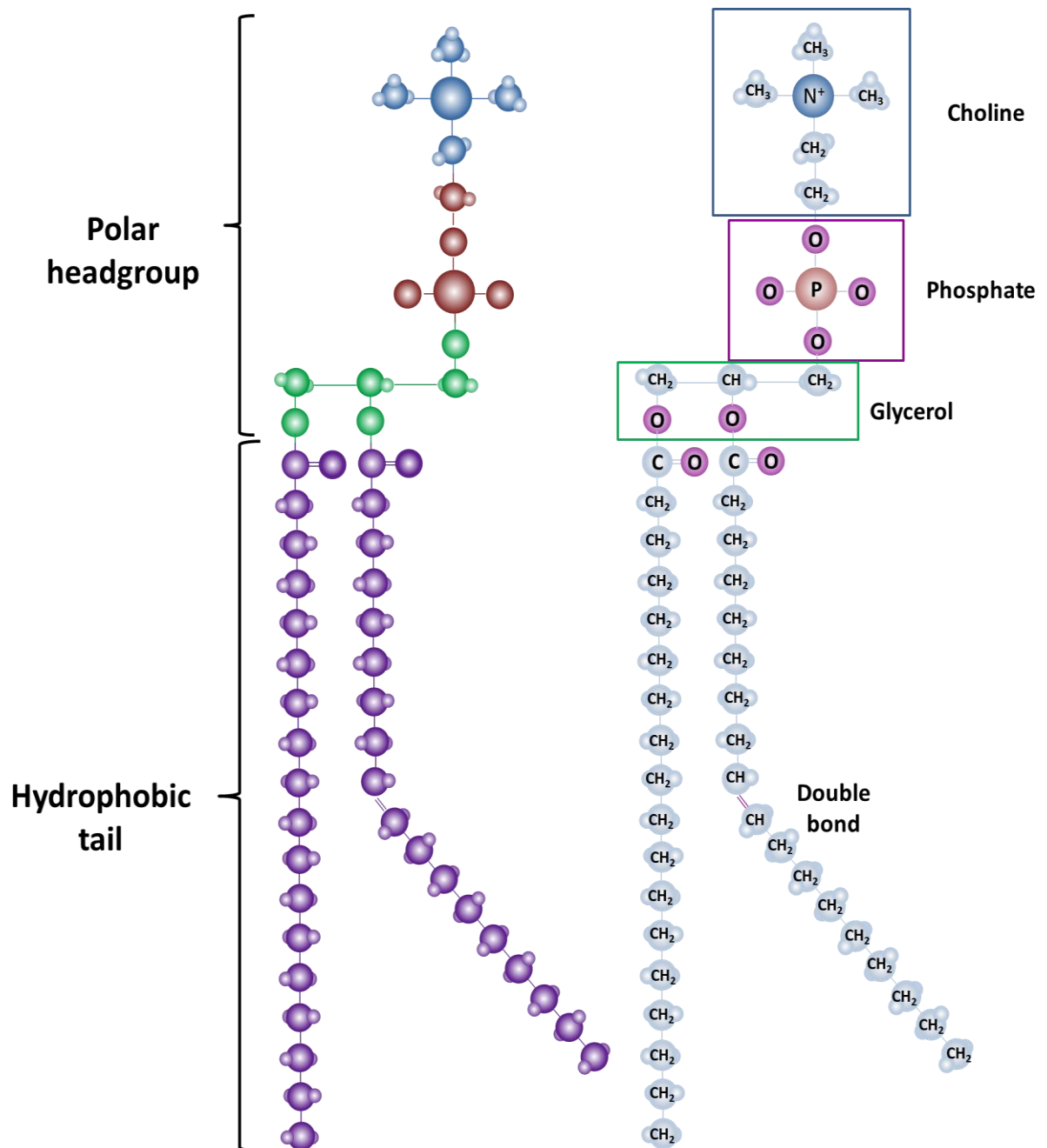
Figure 1.3: Structure and composition of a phospholipid molecule. Phospholipids consist of a glycerol backbone, a phosphate group and an organic head group. The presence of a double bond classifies the fatty acid attached as unsaturated. Modified from http://www.nature.com/scitable/topicpage/cell-membranes-14052567.

However, upon platelet activation, this asymmetry is rapidly lost due to the exposure of aminophospholipids, such as PS and PE, on the outer surface of the platelet by a flip-flop mechanism (Bevers et al., 1983; Zwaal & Schroit, 1997). This process is attributed to scramblase, a protein facilitating bidirectional movement of phospholipids between the two leaflets (Wolfs *et al*., 2005). Thus, on the outer-leaflet of an activated platelet membrane, PS (with its negative net charge) and PE will be exposed (Falls *et al*., 2000). The exposure of PS and PE together with Ca^{2+} provides a binding site for the coagulation factor complexes and, thereby, enabling thrombin generation and clot formation (Zwaal *et al*., 1998; Sims *et al*., 1989).

Following platelet activation, fatty acids, such as AA, are hydrolysed from membrane phospholipids by cellular phospholipases (Levy, 2006). These free fatty acids then can act as substrate for LOX and COX-dependent enzymatic oxidation, generating a diverse range of bioactive lipid metabolites (Mustard *et al*., 1980; Thomas *et al*., 2010; Morgan *et al*., 2010). In platelets, 12-hydroxyeicosatetraenoic acid (12-HETE) results from the enzymatic oxidation of AA by 12-LOX, while prostaglandin H_2 (PGH$_2$) is formed via COX-dependent oxygenation of the arachidonate (Coffey *et al*., 2004b; Smith *et al*., 2000; Rouzer & Marnett, 2009). PGH$_2$ undergoes further enzymatic metabolism to form more stable compounds, leading ultimately to prostanoids, such as prostaglandin E_2 (PGE$_2$), prostaglandin D_2 (PGD$_2$) and thromboxane A_2 (TxA$_2$) that, in platelets, have only been reported as free forms (Rouzer & Marnett, 2003). In contrast, 12-HETE can either be released by activated platelets or be esterified, generating oxidised phospholipids (OxPLs) (Thomas *et al*., 2010).

1.3 Enzymatic and non-enzymatic formation of OxPLs

Oxidation of esterified polyunsaturated fatty acids can be initiated either by enzymatic or non-enzymatic mechanisms (Bochkov *et al*., 2010). The non-enzymatic generation of OxPLs is mediated by free radicals, such as nitric oxide, superoxide, hydrogen peroxide and hydroxyl radical (•OH), often generated by activated phagocytes during chronic inflammation (Bochkov *et al*., 2010). Esterified polyunsaturated fatty acids are highly

susceptible to reactive oxygen species, which can initiate hydrogen abstraction, resulting in addition of oxygen and subsequently the formation of hydroperoxides (Bochkov *et al.*, 2010). An array of mechanisms can then yield secondary peroxidation products in an enzyme-independent manner.

Elevated levels of non-enzymatically formed OxPLs have been measured in both rabbit models and human atherosclerotic lesions (Watson *et al.*, 1997; Waddington *et al.*, 2001; Podrez *et al.*, 2002). Accumulation of OxPLs in the atherosclerotic lesion is known to both initiate and drive disease progression. Oxidised 1-palmitoyl-2-arachidonyl-sn-3-glycero-phosphoryl-choline (OxPAPC) has been identified as a key regulator of atherosclerosis mediating chemokine synthesis and monocyte adhesion to endothelial cells, leading to inflammatory reactions and pro-atherogenic events (Gargalovic *et al.*, 2006; Bochkov *et al.*, 2010).

Separate to non-enzymatic lipid oxidation described above, we have found that upon cellular activation, human neutrophils, monocytes and platelets can generate both free eicosanoids and esterified OxPLs enzymatically via the LOX pathway (Clark *et al.*, 2011; Hammond *et al.*, 2012; Thomas *et al.*, 2010; Kozak *et al.*, 2000; Kozak.*et al.*, 2002). In the past 6 - 7 years a number of different esterified-HETE species generated via LOX have been identified and characterised (Maskrey *et al.*, 2007; Morgan *et al.*, 2009; Morgan *et al.*, 2010; Thomas *et al.*, 2010; Clark *et al.*, 2011; Hammond *et al.*, 2012). Esterified-HETEs were shown to present distinct biological and physical properties (Thomas *et al.*, 2010; Clark *et al.*, 2011; Hammond *et al.*, 2012).

Up to now, prostaglandins (PGs) were considered to exist only as free acid mediators. However, Marnett and colleagues demonstrated in 2000 that PGE_2 and PGD_2 were generated in macrophage cell lines by COX-2 oxidation of endogenous arachidonyl-glycerol (2-AG) and arachidonyl-ethanolamide (AEA) (Kozak *et al.*, 2000; Kozak.*et al.*, 2002). The oxidation products, PGE_2-G/PGD_2-G or PGE_2-EA/PGD_2-EA elicit different effects to free PGE_2 and PGD_2, for example, PGE_2-G triggers rapid calcium mobilisation, inositol trisphosphate (IP_3) synthesis, and activation of protein kinase C (PKC) in a PGE_2-independent manner (Nirodi *et al.*, 2004). Whilst COX-2 can oxidise complex substrates

including AEA and 2-AG, the constitutive isoform COX-1 is only able to utilise AA as substrate, and it is not yet known to be a source of esterified eicosanoids.

In the following sections, the major findings of what is currently known about enzymatic formation of OxPLs by acutely activated immune cells and platelets are summarised. Also, a brief description of their known biological actions under homeostatic and pathological conditions is presented.

1.3.1   OxPLs generated by human monocytes and murine macrophages

Peripheral human monocytes express high levels of 15-LOX that, upon stimulation with Th2 cytokines (interleukin (IL)-4 and IL-13), generate 15-HETE (Roy & Cathcart, 1998; Kuhn & Thiele, 1999; Morgan *et al.*, 2009). Similarly, naïve murine peritoneal macrophages express the functional equivalent homolog 12/15-LOX (Morgan *et al.*, 2009). This enzyme is constitutively active under basal conditions (Dioszeghy *et al.*, 2008). Nevertheless, ionophore can further enhance 12/15-LOX activity in both peripheral human monocytes and murine peritoneal macrophages (Dioszeghy *et al.*, 2008).

In 2007, Maskrey and colleagues identified a family of four esterified 15-HETEs, comprising one diacyl (18:0a/15-HETE-PE) and three plasmalogen PE species (18:0p, 18:1p, 16:0p/15-HETE-PE) formed by murine resident macrophages and human peripheral monocytes (Figure 1.4) (Maskrey *et al.*, 2007). This new family of OxPLs were detected both basally (0.5 - 3 ng/10^6 monocytes) and on activation (~7 ng/10^6 monocytes) with calcium ionophore, corresponding to nearly 30 % of the total 15-HETE produced (Maskrey *et al.*, 2007; Morgan *et al.*, 2009). In contrast to free 15-HETE that is released, esterified HETEs remain cell associated, implying an autocrine mode of action. The enzymatic generation of HETE-PEs was confirmed by MS/MS and chiral chromatography, which showed the predominance of the 15(*S*)-HETE enantiomer. Moreover, stable isotope labelling demonstrated that HETE-PEs were generated by direct PE oxidation via 15-LOX (Maskrey *et al.*, 2007; Morgan *et al.*, 2009). This result is consistent with the already known ability of the 15-LOX isoform to directly oxidise phospholipids.

IL-4 and IL-13 are Th2 cytokines known to induce ciliated epithelial cell differentiation into mucus producing goblet cells, contributing to asthma severity and lung allergy. Studies have shown that the expression of 15-LOX in human asthmatic epithelial cells is considerably increased by IL-4 and IL-13 (Kondo *et al*., 2002; Kondo *et al*., 2006; Morcillo & Cortijo, 2006; Brown *et al*., 2001). Human bronchial epithelial cells were reported to generate two 15-HETE-PEs (16:0p/15-HETE-PE and 18:1p/15-HETE-PE) via 15-LOX in response to IL-13 in culture (Zhao *et al*., 2009). These were shown to enhance expression of MUC5AC, resulting in hypersecretion of mucus in asthma (Zhao *et al*., 2009). Furthermore, IL-13 induced 15-LOX causing 15-HETE-PE products to bind to PE-binding protein-1 (PEBP1), resulting in its dissociation from Raf-1 and activation of extracellular-signal-regulated kinase (ERK), in human bronchial epithelial cells (Zhao *et al*., 2011).

In 2012, Uderhardt and colleagues published their findings showing that OxPLs present on the surface of resident peritoneal macrophages function as binding sites for soluble receptors recognised by apoptotic cells. They also showed that 12/15-LOX expressing resident peritoneal macrophages were responsible for non-inflammatory clearance of apoptotic cells (Uderhardt *et al*., 2012). In addition, during inflammation, apoptotic cell uptake was initiated by freshly recruited inflammatory monocytes (Uderhardt *et al*., 2012). Oxidised PE was found to inhibit the uptake of apoptotic cells by infiltrating cells through binding to milk fat globule-EGF factor 8 (MFG-E8) (Uderhardt *et al*., 2012). This suggests that 12/15-LOX enzyme is the main element coordinating the regulation of apoptotic cell clearance and maintenance of immunological tolerance.

More recently, Hammond and co-workers identified two additional families of LOX-derived lipids in human IL-4 monocytes and murine peritoneal macrophages, consisting of hydroperoxyeicosatetraenoic acid (HpETE) and ketoeicosatetraenoic acids (KETE) attached to the PE (Hammond *et al*., 2012). LC/MS/MS analysis identified KETE-PEs as 18:0a, 18:0p, 18:1p and 16:0p, comprising of three plasmalogen bound and one acyl linked at sn1 (Figure 1.4). As for HETE-PEs, they are formed on ionophore activation but at lower levels. KETE-PEs are absent in macrophages from 12/15-LOX deficient mice, confirming the involvement of LOX in their generation. Miller and co-workers have previously shown that 12/15-LOX$^{-/-}$ macrophages are incapable of mounting a normal

phagocytic response *in vitro* (Miller *et al*., 2001). Consistent with these findings, Hammond and O'Donnell recently observed that 12/15-LOX$^-$/$^-$ macrophages contain larger amounts of cytoplasmic vesicles and anomalous mitochondria, suggesting a defective autophagy or exosomal processing (unpublished data, 2012).

It is proposed that HpETE-PEs are initially formed via LOX and then reduced to HETE-PEs by cellular glutathione peroxidases. These reduced lipids are subsequently oxidised by 15-hydroxyprostaglandin dehydrogenase (15-PGDH), resulting in the formation of cell-associated 15-KETE-PEs (Figure 1.5). Recent studies utilising 15-PGDH inhibitor demonstrated that 15-KETE-PEs are generated by direct oxidation of pre-formed HETE-PEs by LOX and PGDH (Hammond *et al*., 2012).

In macrophages, both 15-HETE-PE and 15-KETE-PE are shown to activate peroxisome proliferator-activated receptor-γ (PPARγ) transcriptional activity in a dose dependent manner. Hence, it appears that these lipids can act indirectly either being released as free PPARγ ligands via PLA$_2$ hydrolysis, or via upstream regulation of the expression of PPARγ (Hammond *et al*., 2012). 15-HETE-PE may decrease inflammatory signalling by binding to toll-like receptor 4 (TLR4) accessory proteins, including CD14 and lipopolysaccharide (LPS)-binding protein (LPB) (Morgan *et al*., 2009). Thus, impairing activation of TLR4 may result in elevated PPARγ signalling and anti-inflammatory effects (Necela *et al*., 2008; Huang *et al* 1999).

New families of lipid mediators generated by 12/15-LOX in immune cells, such as those described above, are expected to mediate anti-inflammatory function *in vivo* and may be of potential therapeutic benefit for chronic inflammatory diseases.
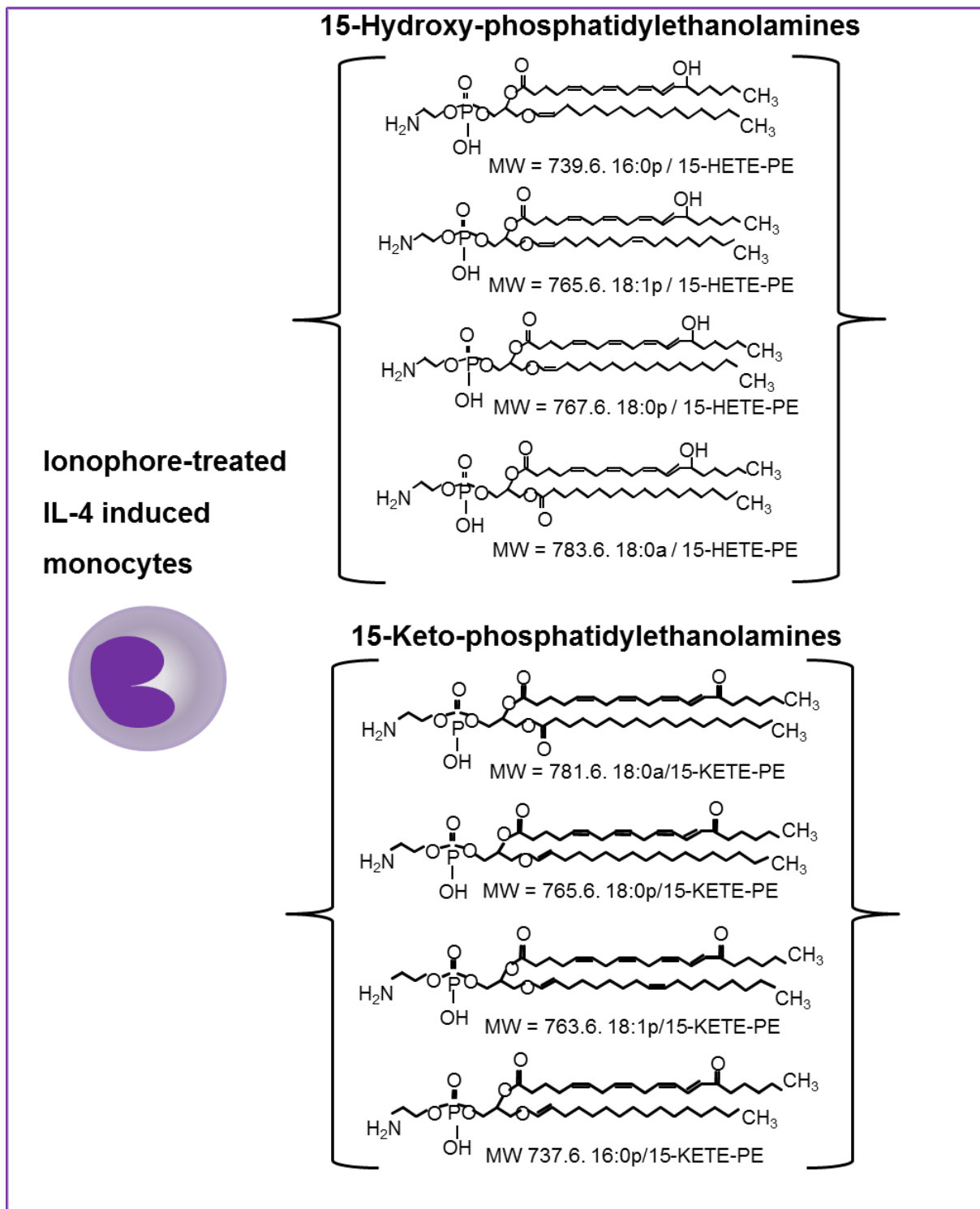
Figure 1.4: Chemical structures of 15-HETE-PEs and 15-KETE-PEs generated by activated human monocytes.
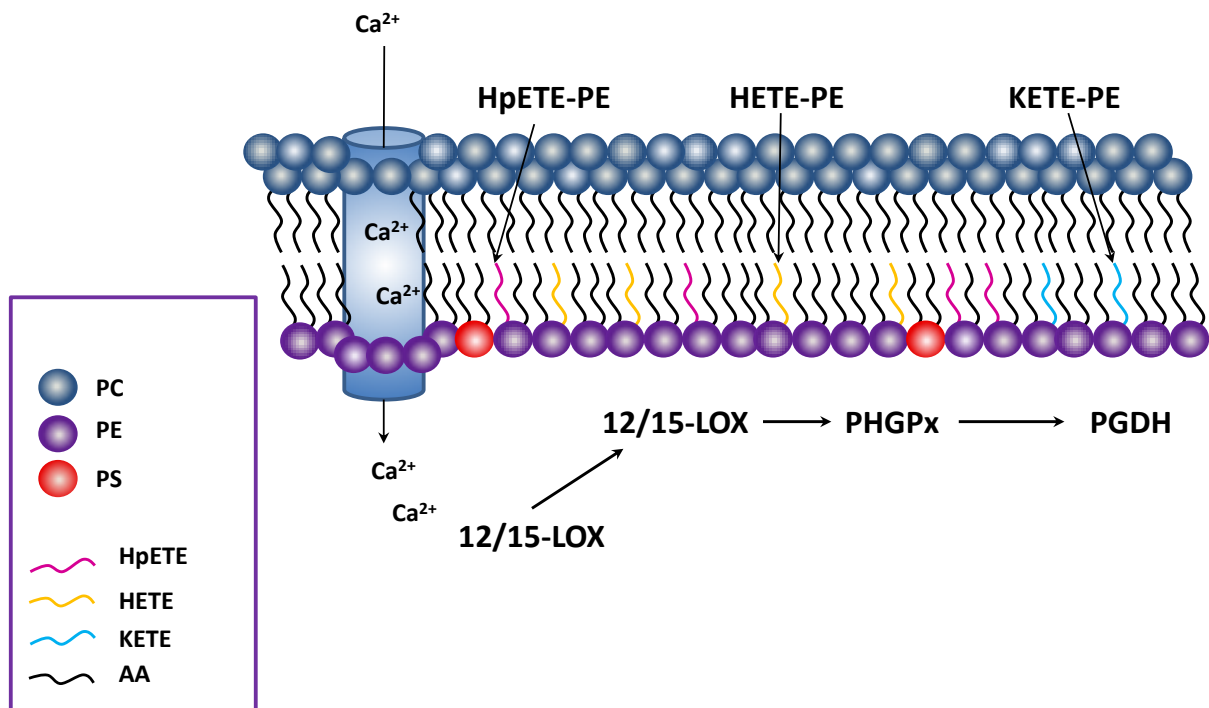
Figure 1.5: Schematic representation of mechanism of formation of 12- and 15-HETE-PEs generated by human monocytes and murine peritoneal macrophages. IL-4–cultured monocytes and peritoneal macrophages already express HETE-PEs and KETE-PEs in the cell membranes, but upon ionophore activation their levels are increased approximately 2-fold. Generation involves direct oxidation of membrane phospholipids. PHGPx, phospholipid hydroperoxide glutathione peroxidase; PGDH, prostaglandin dehydrogenase.

1.3.2 OxPLs generated by human platelets

In human platelets, COX-1 and a platelet-specific 12-LOX isoform are known to mediate oxidation of free fatty acids. Agonist-mediated platelet stimulation acutely activates both enzymes in a calcium-dependent manner. Upon activation, 12-HETE is synthesised and released by platelets (Thomas *et al*., 2010). However, its function remains controversial as 12-HETE has been reported to be without direct effect on platelet activity as well as pro- and anti-thrombotic (Yeung & Holinstat, 2011). On the contrary, TxA$_2$, a platelet COX-1 product, is well known to induce platelet aggregation through thromboxane receptors (Dogné *et al*., 2000).

Recently, six molecular species of esterified 12-HETE have been shown to be generated in agonist-activated human platelets, consisting of four PEs (16:0p, 18:1p, 18:0p and 18:0a/12-HETE-PE) and two PCs (16:0a, 18:0a/12-HETE-PC) via 12-LOX, Figure 1.6 (Thomas *et al*., 2010). Following activation with thrombin, collagen or ionophore, esterified 12-HETEs are formed within 5 min with levels approximately 6 ng/4 x 10^7 platelets (PE) and 18 ng/4 x 10^7 platelets (PC) generated in response to thrombin. Furthermore, formation of 12-HETE-PE/PCs is not detectable in 12-LOX deficient mouse platelets (Aldrovandi *et al.,* unpublished data, 2012).

Experiments using agonist peptides confirmed 12-HETE-PE and 12-HETE-PC generation through activation of protease activated receptor (PAR)-1 and 4. Also, formation of esterified 12-HETEs was shown to require several intracellular signalling mediators, including calcium, *src* tyrosine kinase, protein PKC and secretory PLA$_2$ (sPLA$_2$) (Figures 1.7). Stable isotope labelling revealed that free 12-HETEs are initially formed and subsequently esterified into PEs (Thomas *et al*., 2010). Esterified 12-HETEs account for approximately one-third of the total 12-HETE synthesised remaining primarily cell-associated, while free 12-HETE is secreted. Consistent with previous observations reporting pro-coagulant activities by non-enzymatically OxPLs, 12-HETE-PCs are also capable of enhancing tissue factor-dependent thrombin generation *in vitro*, Figures 1.8 (Weinstein *et al*., 2000; Pickering *et al*., 2008; Thomas *et al*., 2010; Slatter *et al.,* unpublished data, 2012).
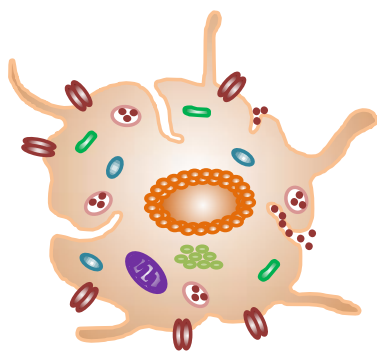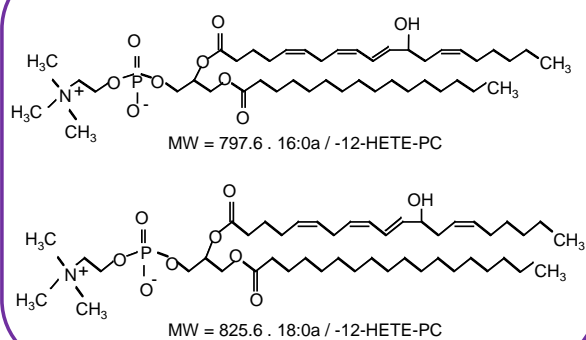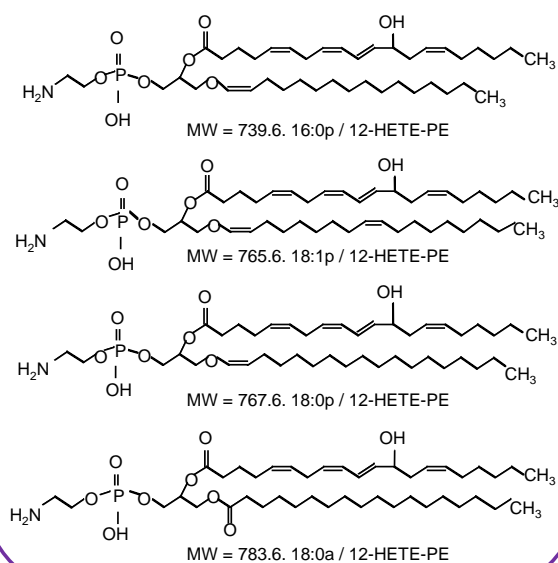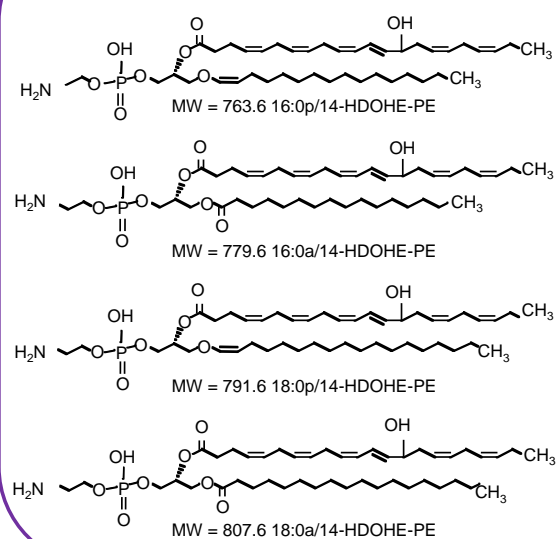
Figure 1.6: Chemical structures of 12-HETE-PEs and 14-HDOHE-PEs generated by activated human platelets.
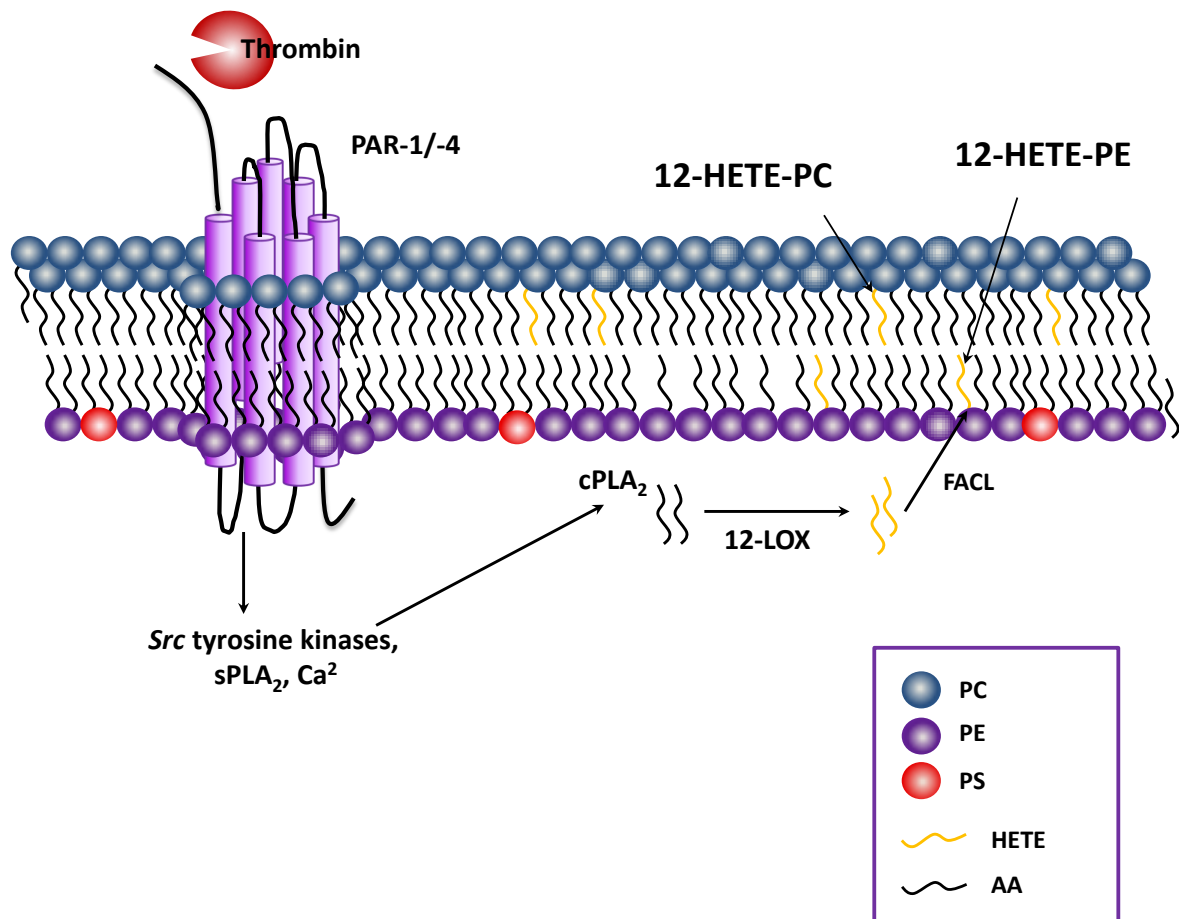
Figure 1.7: Schematic representation of mechanism of formation of 12-HETE-PE/PCs in human platelets. 12-HETE-PE/PCs are generated in response to thrombin activation of PAR-1 and PAR-4, via several signalling intermediates. Hydrolysis of arachidonate by cPLA$_2$ and calcium is required. cPLA$_2$, cytosolic phospholipase A$_2$; sPLA$_2$, secretory phospholipase A$_2$; PIP$_2$, phosphatidylinositol 4,5-bisphosphate; IP$_3$, Inositol trisphosphate; LOX, lipoxygenase; FACL, fatty acyl CoA ligase; PLC, phospholipase C.
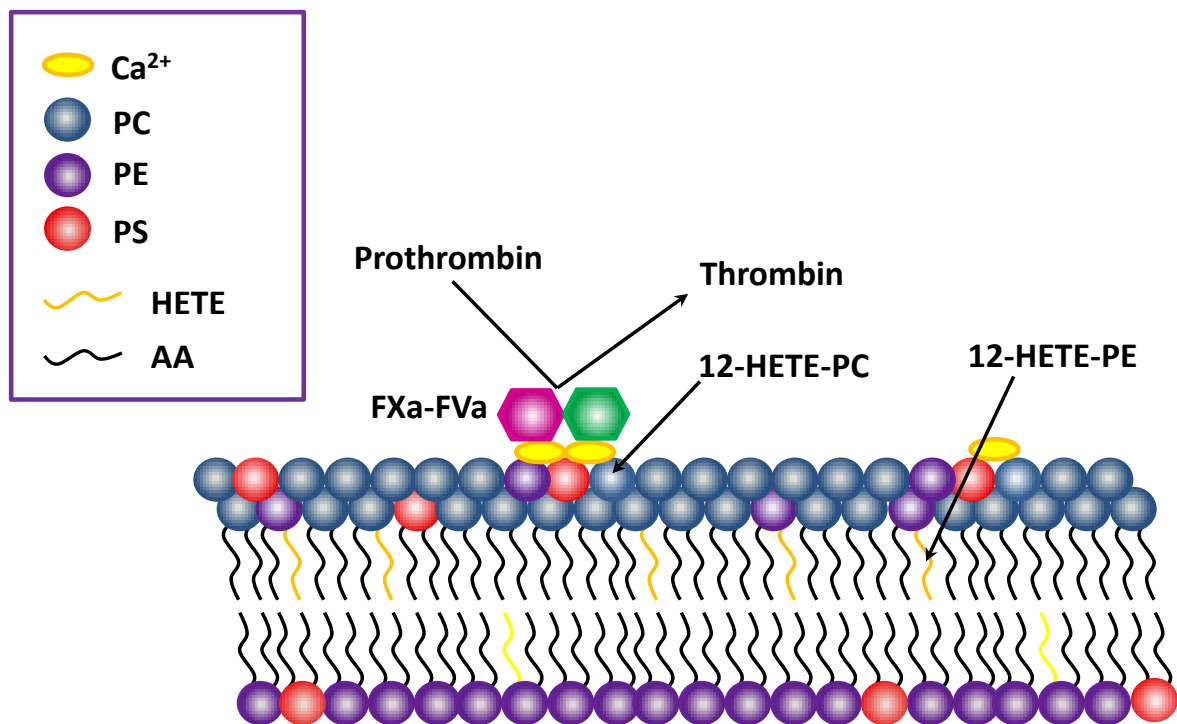
Figure 1.8: Potential mechanism of action of 12-HETE-phospholipids in human platelets. Following their generation, small amounts of 12-HETE-PEs translocate to the outside of the plasma membrane and 12-HETE-PCs can enhance tissue factor-dependent thrombin generation *in vitro*.

Several additional phospholipid-esterified hydroxy-fatty acids are also synthesised via 12-lipoxygenase in activated human platelets. These comprise two plasmalogen (16:0p, 18:0p) and two diacyl (16:0a, 18:0a) PE species, where the 12-HETE is substituted by 12-LOX-oxidised docosahexaenoic acid (DHA). These lipids contain predominantly the 14-hydroxydocosahexanoic acid (HDOHE) positional isomer, Figure 1.6 (Morgan *et al*., 2010). Following thrombin activation, esterified HDOHEs are acutely formed within 2 min. They are generated in a calcium dependent manner, at lower levels ($4 - 2$ ng/4×10^7 platelets) that esterified 12-HETEs.

HDOHE-PEs are also formed though the same pathway as esterified 12-HETEs, by 12-LOX oxidation of free DHA followed by re-esterification of 14-HDOHE into phospholipids (Morgan *et al*., 2010). Although formation of several esterified LOX-products by thrombin-activated platelets have been reported, generation of phospholipid-esterified eicosanoids formed via COX-1 has not been described.

1.3.3   OxPLs generated by human neutrophils

Neutrophils are an essential part of the innate immune system and also the most abundant white cells in the circulation of mammals. Upon agonist activation of neutrophils, 5-LOX generates 5-HpETE, which undergoes further processing to the more stable 5-HETE and leukotriene B$_4$. Clark and co-workers have recently reported acute generation of 5-LOX derived lipids in primary human neutrophils that comprise four esterified 5-HETEs: one diacyl PC (16:0a/5-HETE-PC) and three plasmalogen PE species (18:0p/, 18:1p/, 16:0p/5-HETE-PE), Figure 1.9 (Clark *et al*., 2011). They form immediately after activation with bacterial peptides, chemokines and chemical stimuli, such as phorbol and calcium ionophore, within 2 min, with levels of total esterified 5-HETEs reaching approximately 0.4 ng/10^6 neutrophils. Similar to 12-HETE-PE/PC in platelets, arachidonic acid is initially oxidised by 5-LOX, generating free 5-HETE, which is then rapidly esterified into lysophospholipids.
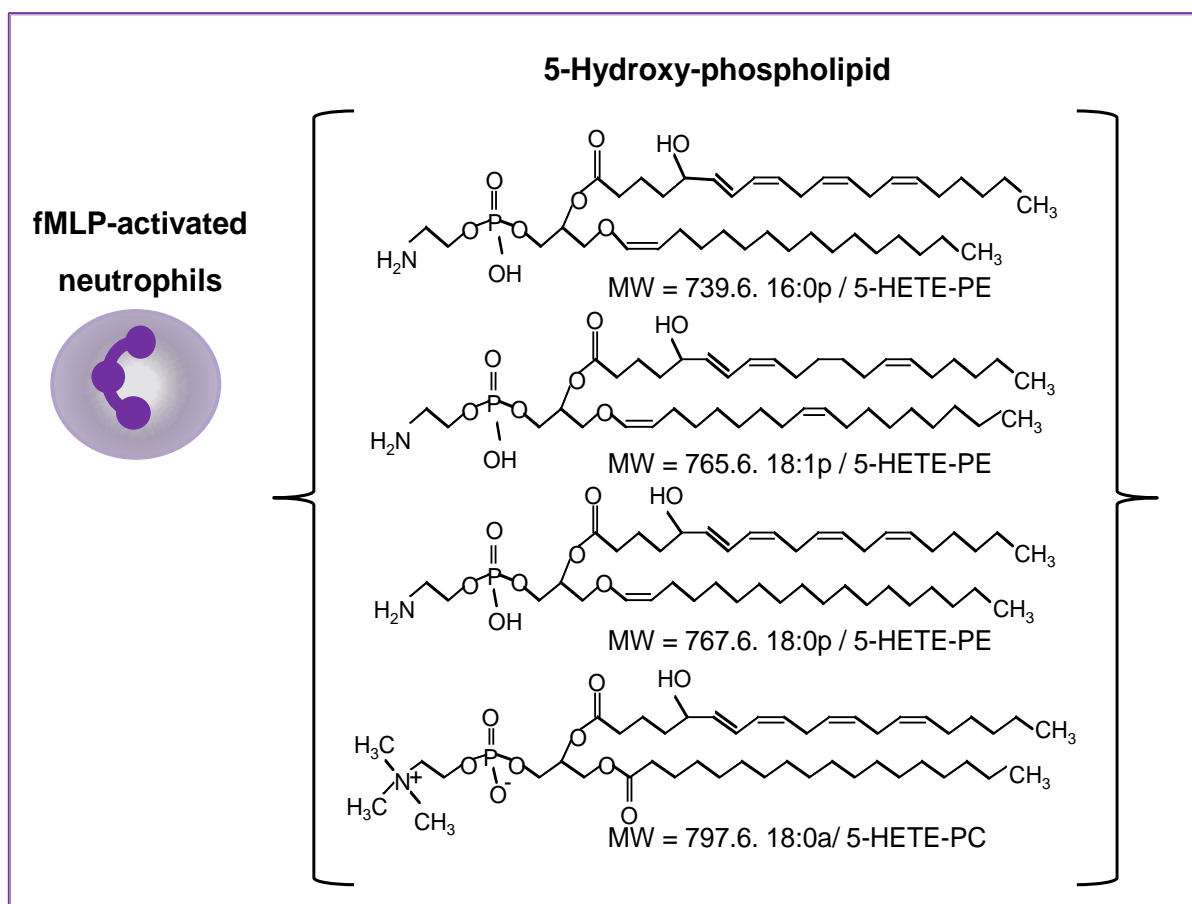
Figure 1.9: Chemical structures of 5-hydroxy-phospholipids generated by activated human neutrophils.

Unlike free 5-HETE, esterified 5-HETEs remain cell associated, mainly confined to nuclear and extranuclear membrane. Studies using inhibitors demonstrate that esterified 5-HETEs are generated via a highly coordinated mechanism, involving calcium, phospholipase C (PLC), cytosolic PLA_2 ($cPLA_2$), $sPLA_2$, mitogen-activated protein kinase/extracellular signal-regulated kinase kinase 1 and 5-LOX activating protein (FLAP), Figures 1.10. *In vitro* studies revealed that 5-HETE-PEs regulate several neutrophil activities, including superoxide generation and neutrophil extracellular trap (NET) release (Clark *et al*., 2011).

1.4 Cyclooxygenase enzymes

In addition to LOX, COX enzymes are also capable of generating potent lipid mediators via AA oxygenation in platelets and immune cells. COX also known as prostaglandin H synthase (PGHS) or prostaglandin endoperoxide H synthase (E.C.1.14.99.1), is a bifunctional membrane bound hemoprotein that catalyses the first committed steps in prostanoid biosynthesis, converting AA to PGH_2. This enzyme is responsible for the generation of important biological mediators termed prostanoids, including prostaglandins, prostacyclin and thromboxane (Smith *et al*., 1996; Marnett *et al*., 1999; Smith *et al*., 2000). Mammals express two distinct isoforms of COX; COX-1 and COX-2, which are separate gene products. COX-1 and COX-2 are of similar molecular weight, approximately 70 and 72 kDa, respectively. These proteins are 65 % homologous in amino acid sequence with near identical catalytic sites (Simmons *et al*., 1991).

In terms of their molecular biology, the most significant difference between COX-1 and COX-2 is the substitution of isoleucine at position 523 in COX-1 with valine in COX-2 (Vane *et al*., 1998). This allows the isoforms to be inhibited differentially. The smaller Val523 residue in COX-2 allows the inhibitor access to a hydrophobic side-pocket while this is denied by the longer side chain of Ile in COX-1 (Vane *et al*., 1998). They also differ in their expression regulation and tissue distribution. COX-1 is constitutively expressed in most cell types and tissues and is considered a "housekeeping gene".
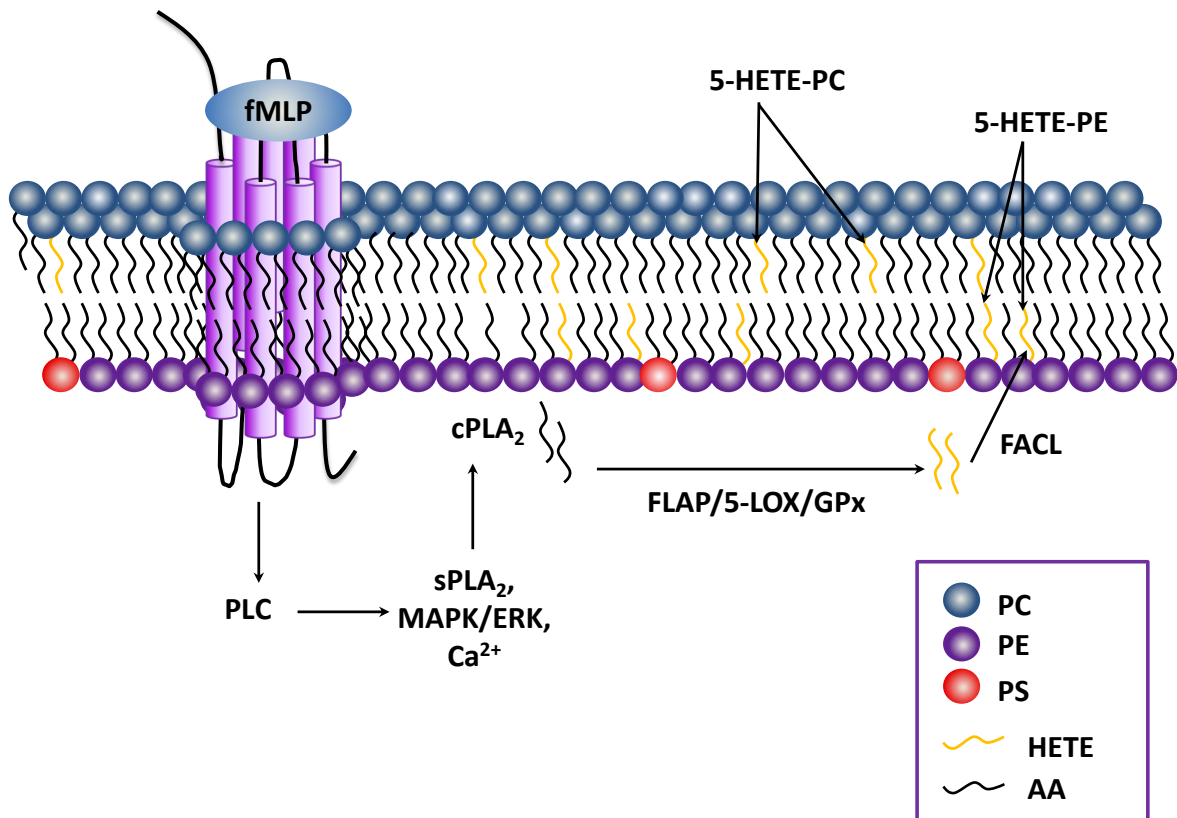
Figure 1.10: Schematic representation of mechanism of formation of 5-HETE-PE and 5-HETE-PC by human neutrophils. Formation of the lipids is promoted via receptor dependent stimuli, including bacterial peptides, and intracellular signalling mediators. AA is cleaved from phospholipids by cPLA$_2$ and then is oxidised by 5-LOX, reduced by GPX, and re-esterified into the phospholipid membrane. fMLP indicates N-formyl-methionine-leucine-phenylalanine; PLC, phospholipase C; cPLA$_2$, cytosolic phospholipase A$_2$; FACL, fatty acyl Coenzyme A ligase; and GPx, glutathione peroxidase.

This isoform is of particular importance for gastrointestinal function and participates in physiological activities such as platelet aggregation, gastric mucosa protection and renal electrolyte homeostasis. In contrast, COX-2 is absent from most tissues in normal conditions but highly induced in response to inflammatory stimuli such as IL-1β and tumour necrosis factor-α (TNF-α), growth factors and LPS (Vane *et al.*, 1998; Kang *et al.*, 2007; Smith *et al.*, 1996; Chell *et al.*, 2006; Parazzoli *et al.*, 2012; Greene *et al.*, 2011). Thus the major function of COX-1 is homeostatic, while COX-2 is mostly involved in inflammation. Also, it has been suggested that COX-1 is responsible for the initial prostanoid response to inflammatory stimuli, while generation of these lipid mediators during the progression of inflammation occurs mainly via COX-2 (Gilroy *et al.*, 1998; Langenbach *et al.*, 1995; Noguchi *et al.*, 1996; Tilley *et al.*, 2001).

The discovery that COXs are the major target for nonsteroidal anti-inflammatory drugs (NSAIDs) has led to increased interest in cyclooxygenase function. Inhibition of COX enzymes by NSAIDs acutely reduces pain, fever and inflammation. In the last few decades, long-term use of aspirin has been associated with reduction of the incidence of fatal thrombotic events (Hall & Lorenc, 2010). The central role of platelets in cardiovascular atherothrombosis has led to low dose aspirin becoming a well-established antiplatelet therapy.

This thesis focuses on the discovery of novel free and esterified prostaglandin generated by thrombin-activated platelets through COX-1 and, thus, the rest of this introduction will focus on COX-1, unless otherwise stated.

1.4.1   History and evolution of cyclooxygenase

Goldblatt and von Euler were the pioneers of prostanoid studies in the early 1930s. Prostaglandins were first extracted from semen, prostate, and seminal vesicles and were shown to lower blood pressure and cause smooth muscle contraction, the effects of which could not be ascribed to the tissue hormones known at the time (Goldblatt, 1933; von Euler, 1935; Greene *et al.*, 2011). These new, unknown substances were named "prostaglandins" by von Euler because he believed they were generated in the prostate

gland. In 1958, Bergstrom and Sjiovall purified and determined the structure of the first two prostaglandin isomers, corresponding to PGE_1 and $PGF_{1\alpha}$ (Bergstrom & Sjiovall, 1960a, Bergstrom & Sjiovall, 1960b). Two research groups led by David van Dorp in Holland and by Sune Bergstrom and colleagues in Sweden, in 1964, independently showed AA as the precursor of prostaglandins (van Dorp *et al.*, 1964; Bergstrom *et al.*, 1964). Later, Samuelsson and co-workers characterised the cyclooxygenase reaction, through which AA is enzymatically converted to endoperoxide-containing prostaglandin G_2 (PGG_2) (Hamberg & Samuelsson, 1973; Hamberg *et al.*, 1974; Smith & Lands, 1972). The discovery and characterisation of prostaglandins was the basis of Nobel Prize, in 1982, that was awarded to Bergstrom, Samuelsson, and Vane.

COX-1 was first purified from sheep and bovine seminal vesicles (rich enzyme sources) in the 70s, followed by the cloning of the PGHS-1 gene in 1988 (Hemler *et al.*, 1976; van der Ouderaa *et al.*, 1977; Miyamoto *et al.*, 1976; Ogino *et al.*, 1978; Yokoyama & Tanabe, 1989; Merlie *et al.*, 1988; DeWitt & Smith, 1988). Also in the 70s, it was discovered that COX-1 displays two catalytic activities, a peroxidase and a cyclooxygenase activity, which were later found to be at separate sites (Miyamoto *et al.*, 1974; O'Brien & Rahimtula, 1976; Marshall & Kulmacz, 1988). It was in 1971, 74 years after aspirin was first marketed, that Sir John Vane first demonstrated that the popular commercial available aspirin and other NSAIDS act by blocking the COX-1 and, therefore, uncovering the mechanism of action of this class of drugs (Vane, 1971). Soon, speculations on whether there was more than one COX began to appear. Observations from studies on COX-1 auto-inactivation rates, inhibition by NSAIDs and time course profiles of PGE_2 and $PGF_{2\alpha}$ generation led to the discovery of COX-2 (Lysz & Needleman, 1982; Lysz *et al.*, 1988). In 1985, Habenicht reported that human platelet-derived growth factor could stimulate an early (10 min) as well as a late (2 - 4 h) prostaglandin peak of generation in Swiss 3T3 cells, suggesting a constitutive and an inducible COX enzyme, subsequently named COX-1 and COX-2, respectively (Habenicht *et al.*, 1985). Later, in the early 90s, the existence of the inducible COX-2 enzyme was confirmed by the identification of a separate gene, of which overexpression induces PGH_2 generation and this activity was inhibited by NSAIDs (Simmons *et al.*, 2004).

COX-1 is a member of the myeloperoxidase superfamily and appears to have evolved from peroxidase ancestors. Based on observations from reconstruction studies of the evolutionary relationships of the peroxidase–cyclooxygenase superfamily, it appears that before organisms developed an acquired immunity, their antimicrobial defence depended on enzymes that were recruited upon pathogen invasion and could produce antimicrobial reaction products (Zamocky *et al*., 2008). Therefore, it is postulated that COX isoforms differentiated very early in the evolutionary history as part of the foundation of the innate immune system. Up to now, all vertebrates investigated including mammals, birds, bony and cartilaginous fishes express both COX-1 and COX-2 (Chandrasekharan & Simmons, 2004).

Since their discovery in the early twentieth century, COX-1 and COX-2 have become the most thoroughly studied and best understood mammalian oxygenases and are still the basis of numerous on-going studies worldwide.

1.4.2   The structure of mammalian COX-1

A landmark study elucidating the three dimensional structure of sheep COX-1 was first published by Picot and co-workers in 1994 (Picot *et al*., 1994). Later in 1996, human and mouse COX-2 were crystallised (Kurumbail *et al*., 1996; Luong *et al*., 1996). Comparison of COX-1 and COX-2 from the same species showed 60 – 65 % sequence identity (Smith *et al*., 2000). COX-1 is as homodimer with a molecular mass of 70 kDa and is a protein with 600 amino acids in size, which is then processed into a mature form by removal of the signal peptide (Smith *et al*., 2011). Each COX monomer is composed of three distinct structural domains, an epidermal growth factor (EGF) domain at the short N-terminal, a neighbouring α-helical membrane-binding domain (MBD), and a large globular catalytic domain at the C-terminus containing the cyclooxygenase and the peroxidase active sites (Picot *et al*., 1994).

1.5 Regulation of COX-1 expression

The human COX-1 gene (*Ptgs1*), located on chromosome 9 (locus 9q32–q33.3), is approximately 22 kilo-base pairs in length and is transcribed as a 2.8 kb mRNA (Yokoyama & Tanabe, 1989; Kraemer *et al*., 1992; Tanabe & Tohnai, 2002). COX-1 displays the characteristics of a "housekeeping" gene (Kraemer *et al*., 1992; Wang *et al*., 1993; Xu *et al*., 1997). Under normal physiological conditions, COX-1 is constitutively expressed in many mammalian tissues and cells, including seminal vesicles, platelets, monocytes, renal collecting tubes and vascular endothelial cells (Otto & Smith, 1995).

The molecular mechanism underlying the regulation of COX-1 gene has not been fully characterised. Also, it is an oversimplification to consider that COX-1 is only constitutive expressed, as COX-1 levels have been shown to change during development, to be downregulated in epithelial cells and upregulated in several cell types under the influence of specific factors.

1.6 Cellular localisation of COX-1

COX-1 is an integral membrane protein equally distributed on the lumenal surfaces of the endoplasmic reticulum (ER) and nuclear envelope (Otto & Smith, 1994; Regier et al., 1995; Morita et al., 1995). Within the nuclear envelope, COX-1 is present on both inner and outer nuclear membranes, in similar proportions (Spencer et al., 1998). It appears that COX-1 functions predominantly in the ER (Morita et al., 1995). In platelets, COX-1 is predominantly, if not almost exclusively, located in the intracellular membranes, more specifically in the dense tubular system (Gerrard et al., 1976; Carey et al., 1982).

1.7 Mechanisms of enzyme catalysis

COX-1 catalyses two distinct reactions, a cyclooxygenase reaction in which two O_2 molecules are inserted into the carbon backbone of AA to yield PGG_2 and a peroxidase reaction in which PGG_2 undergoes a two-electron reduction to PGH_2 (Figure 1.11). PGH_2 is rapidly converted into several bioactive products such as PGD_2, PGE_2, PGI_2 and TxA_2 through PGD, PGE, PGI and thromboxane synthase, respectively. Both reactions occur at physically distinct locations but at functionally interacting sites. The peroxidase reaction occurs at a heme-containing active site situated near the protein surface, while the cyclooxygenase reaction occurs in a hydrophobic channel in the core of the enzyme.

1.7.1   Cyclooxygenase reaction

The branch-chain reaction mechanism model was first proposed by Ruf and co-workers in 1988, describing the interplay of the cyclooxygenase and peroxidase activities (Figure 1.12) (Dietz *et al.*, 1988). The newly synthesised COX enzyme has an absolute requirement for peroxides to activate and sustain the cyclooxygenase activity of COX enzyme (Smith & Lands, 1972).

In this model, a substrate peroxide (ROOH) reacts with the heme group [(PPIX)Fe^{3+}] at the peroxidase active site of COX, initiating a two-electron oxidation that yields Compound I, which contains Fe^{4+} and a porphyrin radical cation [(PPIX$^\bullet$)$^+Fe^{4+}$O], with concomitant formation of the corresponding alcohol (ROH) (Figure 1.13). The oxidised heme group in turn oxidises a neighbouring tyrosine residue, most likely tyrosine 385, to yield peroxidase Intermediate I, which has a tyrosyl radical and an oxyferryl heme (Fe^{4+}=O), and the subsequent conversion of intermediate I to compound II. Alternatively, the porphyrin radical cation undergoes one-electron reduction generating compound II [(PPIX)Fe^{4+}O] and a second one-electron reduction restores the resting enzyme (Rouzer & Marnett, 2003).
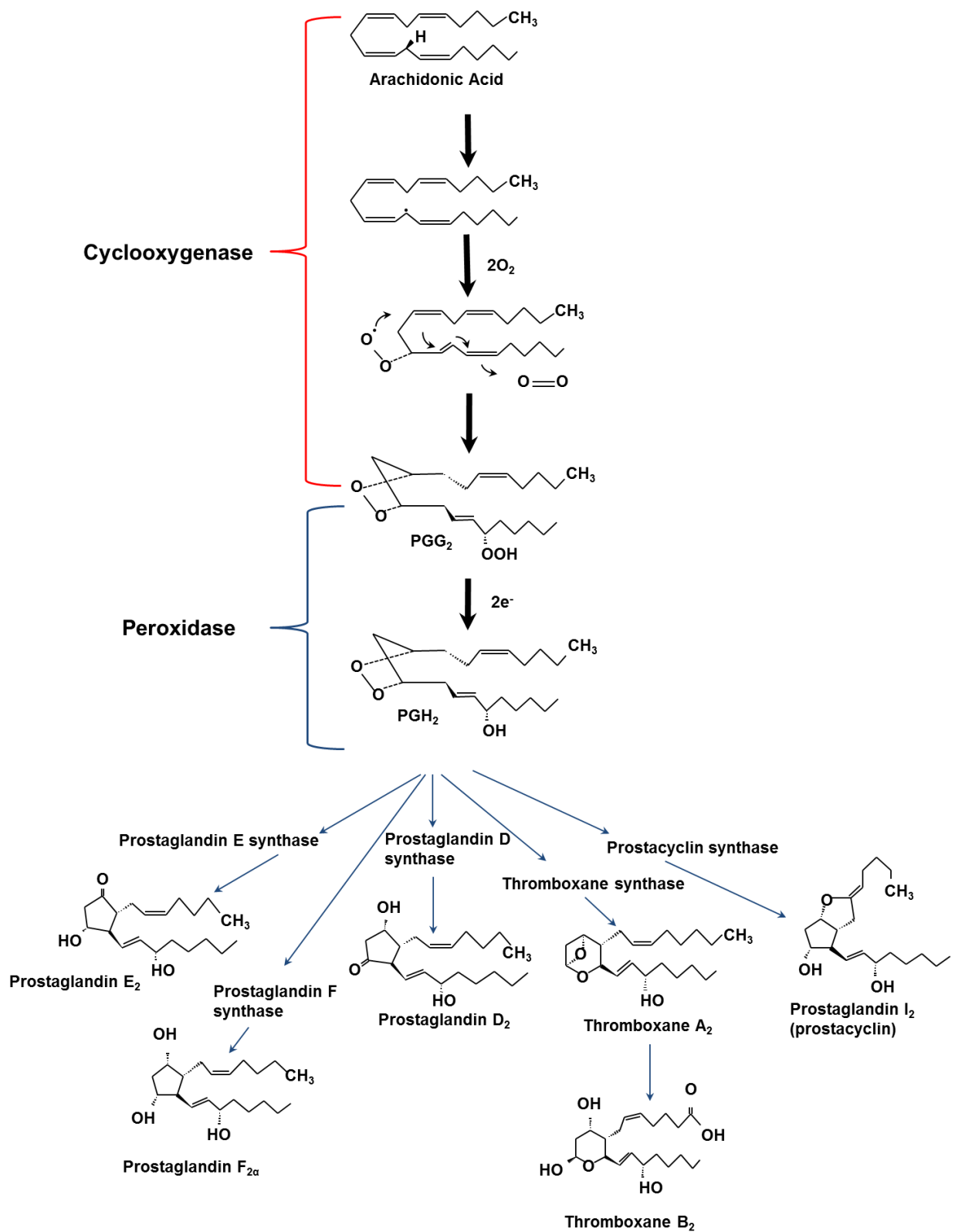
Figure 1.11: Cyclooxygenase and peroxidase reactions catalysed by COX-1.
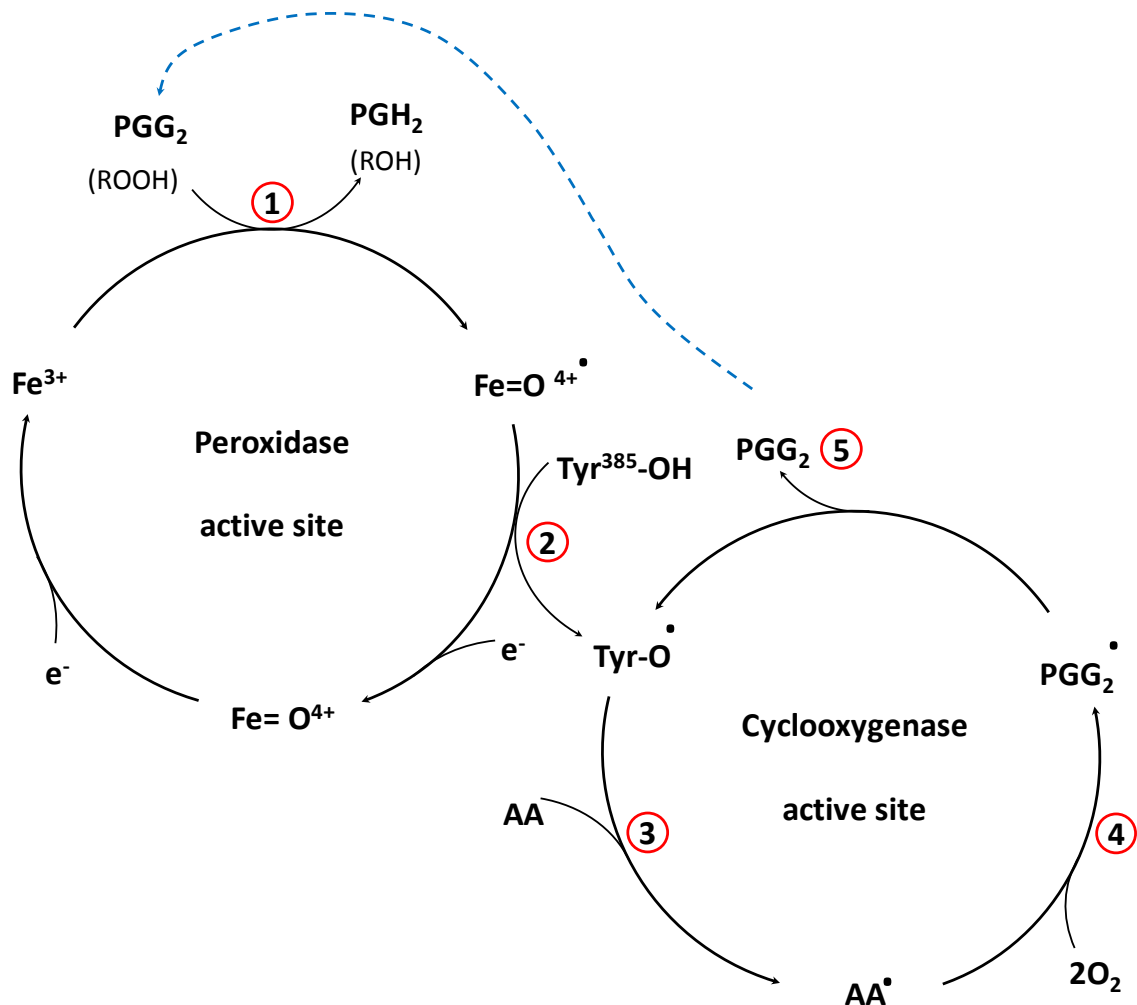
Figure 1.12: Peroxidase and cyclooxygenase catalysis. (1) First, an oxoferryl protoporphyrin radical ($Fe^{4+}=O^{\bullet}$) in the heme in the peroxidase active site is produced when endogenous oxidant(s) oxidises ferric heme (Fe^{3+}) through a two-electron oxidation. (2) The Tyr 385 residue in the cyclooxygenase active site is activated, through a single electron oxidation reaction with the Fe^{4+} protoporphyrin radical, to produce a tyrosyl radical. In the first step of the oxygenation process (3), the 13-*proS* hydrogen of AA in the cyclooxygenase active site is abstracted by the tyrosyl radical to produce the arachidonyl radical. (4) This is followed by the reaction of the arachidonyl radical with two molecules of oxygen, to yield PGG_2. (5) Then PGG_2 diffuses (dotted line) to the peroxidase active site and is reduced to PGH_2 by the peroxidase activity (1). AA, arachidonic acid; Fe^{3+}, ferric heme; $Fe=O^{4+\bullet}$, oxo-ferryl $Fe^{4+\bullet}$ porphyrin radical; Tyr-OH, active site tyrosine; Tyr-O$^{\bullet}$, tyrosyl radical. Modified from Chandrasekharan & Simmons, 2004.
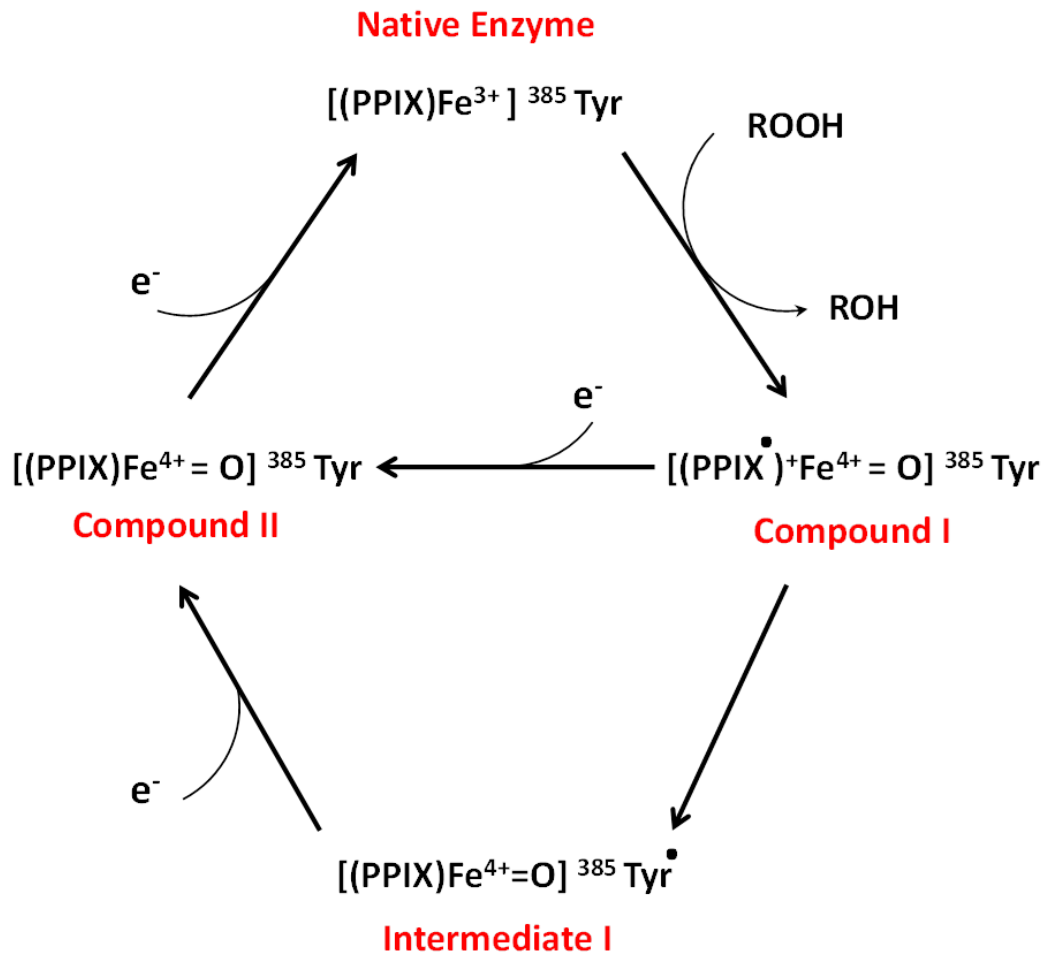
Figure 1.13: Mechanism for the COX peroxidase reaction. Native enzyme ([(PPIX)Fe^{3+}]) reacts with substrate peroxide (ROOH), reducing it to the corresponding alcohol (ROH) and converting the enzyme to compound I ([(PPIX$^{\bullet}$)$^+$Fe^{4+}O]). Two sequential one-electron reductions using peroxidase reductant as the electron source convert compound I to compound II ([(PPIX)Fe^{4+}O]) and then back to native enzyme. Also, compound I can quickly be converted to intermediate I ([(PPIX)Fe^{4+}O]tyr$^{\bullet}$) and the subsequent reduction of intermediate I to compound II. Modified from Rouzer & Marnett, 2003.

The cyclooxygenase activity is dependent on heme oxidation, on the peroxidase active site, but continuous peroxidase activity is not necessary for cyclooxygenase activity, as the tyrosyl radical is regenerated in each catalytic cycle. *In vitro*, hydroperoxides contaminating commercial fatty acid preparations, including AA, are responsible for the initial oxidation of the heme groups of a small fraction of COX enzymes, and the remaining COX molecules are then activated auto-catalytically by newly generated PGG_2.

Finally, when an appropriate fatty acid such as AA enters the COX channel, the enzyme correctly positions the 13-*proS* hydrogen of the AA for removal (Picot *et al.*, 1994). When AA is appropriately positioned, the cyclooxygenase reaction begins with the abstraction of the 13-*proS* hydrogen from AA to form an arachidonyl radical. The tyrosyl radical centred on the phenolic oxygen of tyrosine (Tyr) 385 is responsible for the abstraction of the hydrogen atom from AA (Figure 1.14). The resulting radical migrates to carbon 11. This is followed by sequential addition of O_2 at carbon 11 to generate an 11*R*-hydroperoxyl radical which in turns forms a carbon 11 to carbon 9 endoperoxide moiety that cyclises. A second cyclisation occurs, in which a bond is formed between carbon 8 and carbon 12 to form the prostanoid five-membered ring and another radical is generated, which is delocalised over carbon 13 to carbon 15. This is followed by addition of O_2 at carbon 15 to form a 15-hydroperoxy radical. In the final stage, the hydroperoxy radical abstracts a hydrogen atom from Tyr 385, yielding hydroperoxy endoperoxide PGG_2 and completing the catalytic cycle. Activated COX would continue to turnover, in the presence of substrate, until radical induced inactivation occurs (Smith *et al.*, 2000).

COX-1 is primarily found in cells in its inactive form waiting to react with a hydroperoxide activator (e.g., lipid peroxide), so that it can oxidise a fatty acid. It is suggested that an endogenous oxidant binds to the peroxidase active site forming a ferryl-oxo-porphyrin radical that abstracts an electron from Tyr 385, thus, generally a tyrosyl radical required for cyclooxygenase activity (Simmons *et al.*, 2004). However, it is not known which endogenous compound(s) initiates the heme oxidation in the peroxidase active site *in vivo*.
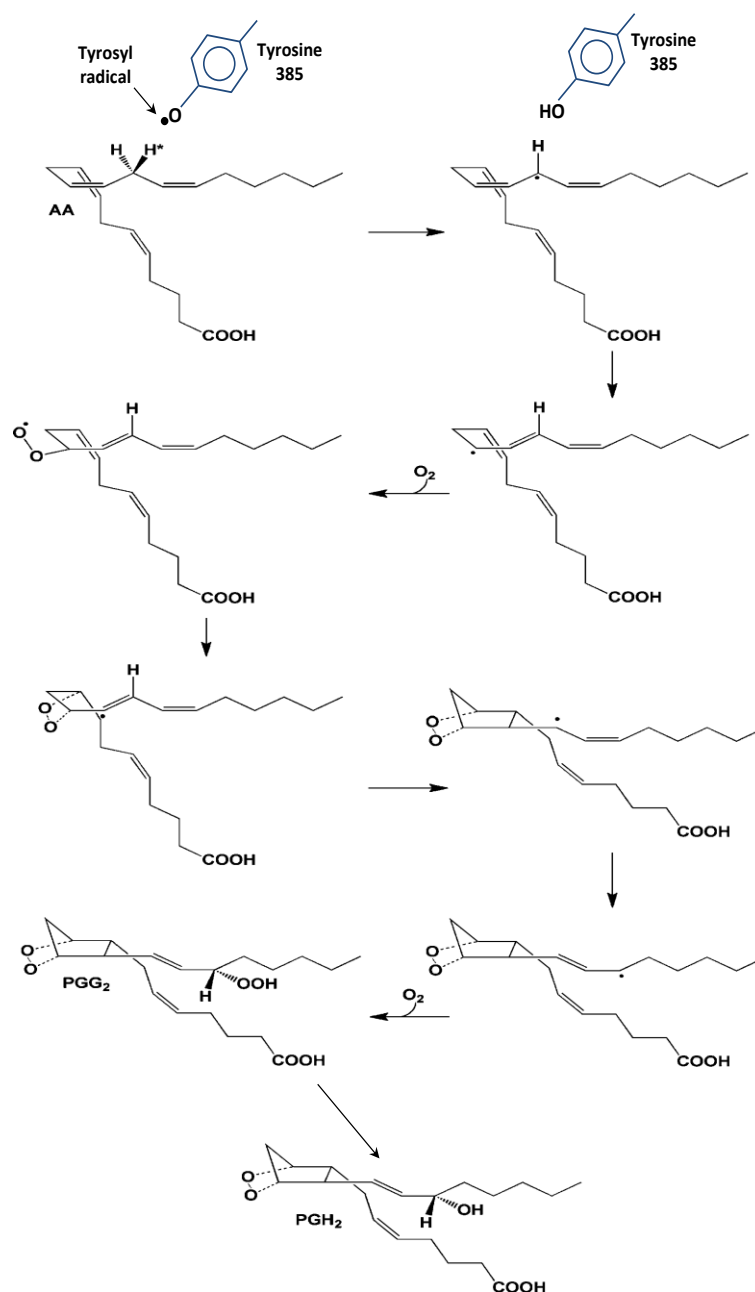
Figure 1.14: Proposed mechanism for the cyclooxygenase reaction. Arachidonic acid 13-pro-(S) hydrogen atom removal. Formation of an arachidonyl radical. Migration of the resulting radical to C11. Addition of O_2 to C11 to generate an 11-hydroperoxyl radical. Endoperoxide formation. Cyclization to form the prostanoid five-membered ring. Radical migration from C13 to C15. Addition of the second O_2 followed by a reduction of the peroxyl radical, yielding hydroperoxy endoperoxide PGG_2. Reduction of the hydroperoxide group of PGG_2 to form PGH_2. Modified from Rouzer & Manett, 2011.

It is possible that many compounds serve as a physiological heme oxidant for the peroxidase active site, for instance hydroperoxides and alkyl peroxides (Smith *et al.*, 2011). The inorganic oxidant peroxynitrite, which is derived from the condensation of nitric oxide and superoxide, has been reported as a possible physiological heme oxidant in macrophages (Marnett *et al.*, 1999).

1.8 Suicide Inactivation of COX-1

The COX-1 feedback activation mechanism allows large amounts of potent prostaglandins and other biomolecules to be synthesised. Thus, rigorous regulatory mechanisms are required to prevent deleterious effects. Suicide inactivation is the irreversible self-inactivation of both cyclooxygenase and peroxidase activities which represent the ultimate regulation of prostanoid production, limiting cells' ability to synthesise PGs and thromboxane (Marshall *et al.*, 1987). COX-1 has a short half-life of less than 2 min, even in the presence of sufficient substrate (Simmons *et al.*, 2004). Indeed, Smith and Lands were one of the first to observe that COX-1 undergoes self-inactivation in the presence of fatty acid substrates (Smith & Lands, 1972).

Inactivation of COX-1 peroxidase activity is independent of peroxide species and concentrations (Wu *et al.*, 1999; Wu *et al.*, 2001). This strongly suggests that the self-inactivation process originates after formation of Compound I and, probably, with Intermediate II occurring at slower rate than cyclooxygenase inactivation (Wu *et al.*, 1999; Wu *et al.*, 2001). POX activity remains, even after cyclooxygenase activity is completely lost (Wu *et al.*, 2001). On the other hand, cyclooxygenase inactivation appears to be dependent on the structure of the peroxide, the peroxidase reducing substrate and the fatty acid substrate (Smith *et al.*, 2011).

It has been proposed that distinct damage can occur at the peroxidase and cyclooxygenase sites during side reactions of Intermediate II, which forms during reaction of COX-1 with peroxide and contains two strong oxidants, a ferryl heme in the peroxidase site and a tyrosyl free radical in the cyclooxygenase site. This implies that peroxidase inactivation involves the oxyferryl heme group whereas cyclooxygenase inactivation

involves the tyrosyl radical (Wu *et al.*, 2003; Wu *et al.*, 2007; Tsai & Kulmacz, 2010). Nevertheless, little is known about the chemical changes that occur in the enzyme related to peroxidase or cyclooxygenase auto-inactivation events (Tsai & Kulmacz, 2010).

1.9 Inhibition of COX by aspirin

The annual consumption of aspirin worldwide is estimated to be 100 billion tablets, showing how popular this nonsteroid anti-inflammatory drug has become since first marketed in 1897. The success of the most widely used drug in the world is due to its broad pharmacological actions, including anti-inflammatory, anti-pyretic and analgesic effects with relatively minor side effects.

Acetyl salicylic acid or aspirin (Figure 1.15) has the ability to suppress the production of prostaglandins and thromboxane by causing irreversible inactivation of COX-1/-2 and, consequently, inhibiting the formation of prostaglandins (Roth *et al.*, 1975).
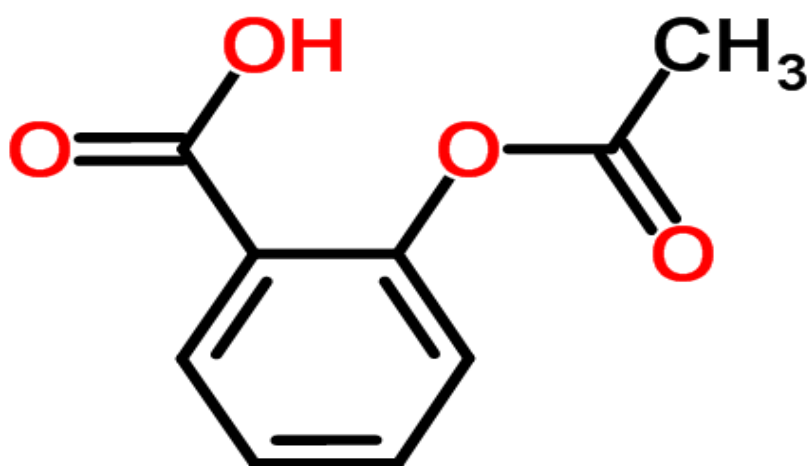
Figure 1.15: Aspirin structural formula.

The cyclooxygenase active site is created by a long, hydrophobic channel that is the site of binding of aspirin-like drugs (Picot *et al.*, 1994). Like other NSAIDs, aspirin diffuses into the COX active site through the mouth of the channel and travels to the constriction point formed by arginine (Arg) 120, Tyr 355, and glutamine (Glu) 524 (Simmons *et al.*, 2004). At this point in the channel, the carboxyl of aspirin forms a weak ionic bond with the side chain of Arg 120, which is situated near the opening of the catalytic channel (Loll *et al.*, 1995). It has been proposed that the binding of aspirin to Arg 120 through the carboxylate moiety puts the molecule in the correct orientation to subsequently acetylate serine (Ser) 530 (Loll *et al.*, 1995). Ser 530 lies along the wall of the hydrophobic channel near Tyrosine (Tyr) 385 and is the site of aspirin acetylation (Figure 1.16).

Aspirin acts as an acetylating agent where an acetyl group is covalently attached to the Ser 530, in the active site of the COX enzyme (Loll *et al.*, 1995). The acetyl group protrudes into the cyclooxygenase active site preventing AA access to Tyr 385 (Figure 1.16) (Loll *et al.*, 1995). Thus, aspirin irreversibly inhibits prostanoid synthesis by directly blocking AA from binding to the enzyme. This makes aspirin different from other NSAIDs (such as diclofenac and ibuprofen), which are reversible inhibitors.

Aspirin acetylates platelet COX-1 in the pre-systemic circulation before its metabolism by the liver. This way, inhibition of platelet function occurs at very low doses of aspirin, such as 75 mg. At this concentration, aspirin has no effect on PGI_2 generation by endothelial cells or other systemic effects. Thus, low-dose (75 mg) aspirin blocks only platelet COX-1, consequently inhibiting thromboxane production. As platelets are unable to replace inactivated COX-1 because they are enucleate, these cells lose their ability to aggregate until new platelets are formed, which, in humans, is within 7 to 10 days (Vesterqvist & Gréen, 1984). Therefore, daily 75 mg dose is the usual prescription administrated to patients at high risk of heart attacks and strokes.
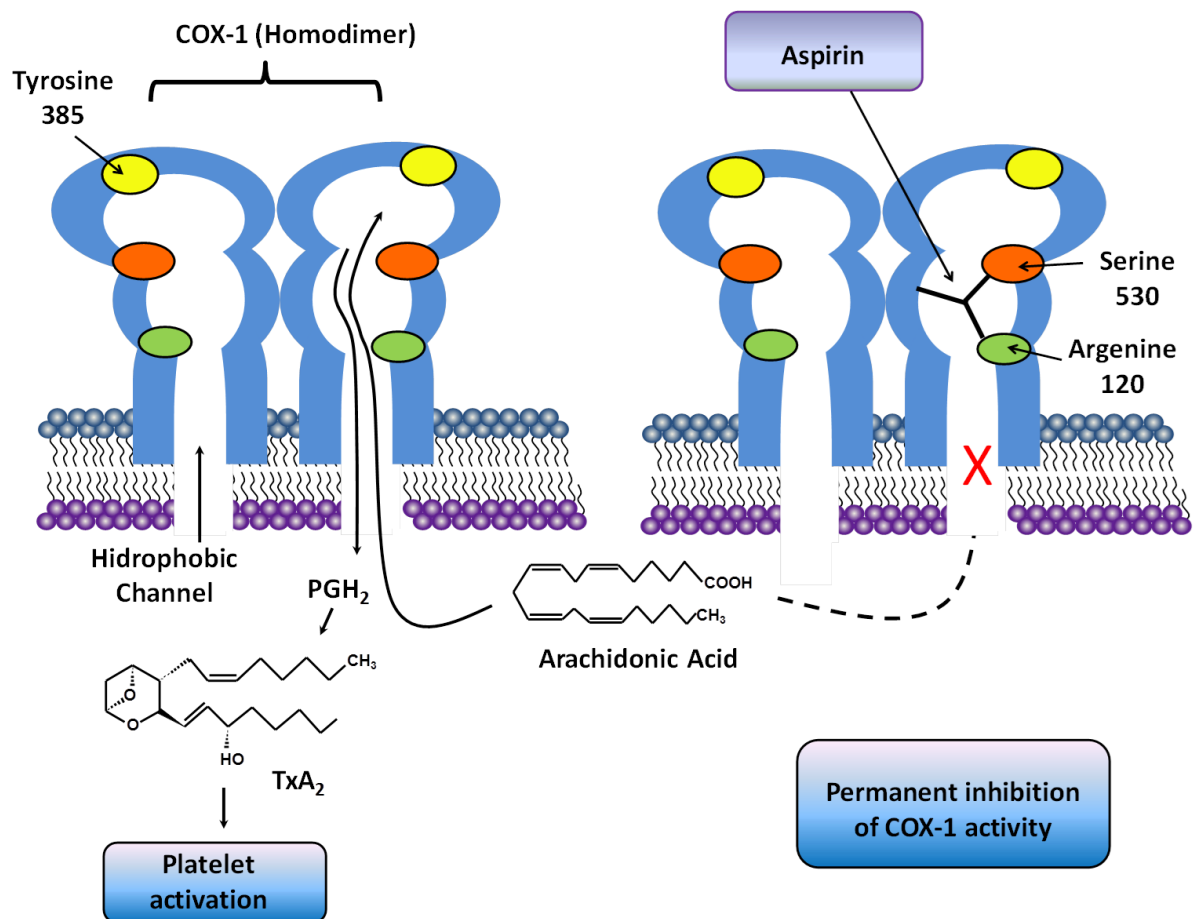
Figure 1.16: Aspirin irreversibly inhibits platelet COX-1 enzyme. Its substrate, arachidonic acid, is converted to PGH_2, which is consequently converted to TxA_2 by thromboxane synthase. The carboxylic acid groups of aspirin bind weakly to arginine 120 at the mouth of the channel. Aspirin acetylates serine 530 in a narrow region of COX-1's hydrophobic pocket and thereby sterically inhibits the passage of arachidonic acid to the so-called active site of the enzyme. Modified from Sweeny *et al.*, 2009.

1.10   The importance of discovering novel COX-1 derived lipids

COX-1 is a major regulator of platelet function, including aggregation, shape change, degranulation and P-selectin expression (Kaplan & Jackson, 2011). This is assumed to be via generation of pro-aggregatory TxA_2, which signals through activation of thromboxane receptor (TP). However, clinical trials with thromboxane synthase inhibitors have been unsatisfactory, mainly due to an increase in PGH_2, which can itself induce platelet aggregation (Fiddler & Lumley, 1990; Watts *et al.*, 1991).

The use of aspirin as an antithrombotic drug is based on the hypothesis that inhibition of platelet COX-1 prevents pathological thrombosis by reducing TxA_2 formation. However, it is likely that the antithrombotic effect of aspirin is not only due to the inhibition of TxA_2 formation but also because of the blockade of all COX-1 products that function as pro-thrombotic and pro-inflammatory agents, including previously undescribed products.

In recent years, it has become clear that OxPLs play an important role not only during chronic inflammation but also in maintaining homeostasis. Although the formation of glyceryl prostaglandins (PGE_2-G and PGD_2-G) via COX-2 has been reported in macrophage cell lines, generation of esterified prostaglandins via COX-1 has not been described. Platelets express both COX and LOX isoforms. In 2010, Thomas and colleagues reported the formation of OxPLs by activated platelets. Since these are formed by esterification of HETEs, it is also possible that platelets also esterify COX-derived prostaglandins. Esterified prostaglandins could be involved in a diverse array of processes within the host including haemostasis, membrane lipid remodelling, wound healing and modulation of immune responses during infection and inflammation. The identification of new bioactive platelet lipids may provide a possible target for therapeutic intervention for a variety of platelet-driven pathologies, including atherosclerosis and thrombosis.

1.11   Overall thesis aims

Studies performed in this thesis will utilise a lipidomic approach to investigate the formation of novel families of esterified prostaglandins generated by agonist-activated human platelets. Upon identification of previously unreported lipid species the aims of this thesis are to: (1) perform a complete structural characterisation and quantification of the lipids; (2) determine whether they originate via COX-1 and whether they are formed by direct phospholipid oxidation or esterification of newly formed prostaglandins; (3) investigate the signalling pathways involved in the formation of the lipids through the use of pharmacological inhibitors; (4) and finally, *in vitro* studies using liposomes will investigate a potential role of esterified prostaglandins in coagulation.

CHAPTER 2

2   Materials and Methods

2.1 Materials

During the course of this project, experiments were conducted utilising various materials and methods. The first section of this chapter lists all the materials used during this project whether prepared in the laboratory or commercially available kits, and identifies the source of the materials. The second section describes the methods employed, including, in the case of commercial kits, methods in accordance with the manufacturers' instructions.

2.1.1   Chemicals

5Z,8Z,11Z,14Z-Eicosatetraenoic acid (arachidonic acid) fatty acyl standard, PGE_2, PGD_2, 11β-PGE_2 and 8-iso-PGE_2 lipid standards and triacsin C were purchased from Enzo Life Sciences Ltd (Exter, UK). 1,2-dimyristoyl-sn-glycero-3-phosphoethanolamine (DMPE), 1-stearoyl-2-arachidonoyl-sn-glycero-3-phosphoethanolamine (SAPE), 1-stearoyl-2-arachi-donoyl-sn-glycero-3-phospho-L-serine (SAPS), 1,2-distearoyl-sn-glycero-3-phosphocholine (DSPC), 1-octadecanoyl-sn-glycero-3-phosphocholine (18:0 lyso PC), 1-octadecanoyl-sn-glycero-3-phosphoethanolamine (18:0 lyso PE) was purchased from Avanti Polar Lipids inc. (Alabaster, Alabama, USA). PGE_2-d_4, PGD_2-d_4, AA-d_8, TxB_2-d_4, 12-HETE-d_8, arachidonic acid and selective COX-1 inhibitor (Sc-560) were from Cayman Chemical Company (Ann Arbor, Michigan, USA). Collagen was from Pathway Diagnostics Ltd (Surrey, UK). PAR-1 and -4 agonists were from Tocris Biosciences (Bristol, UK). Inhibitors of intracellular signalling pathways, PP2, p38i (mitogen-activated protein kinase (MAPK) inhibitor), oleyloxyethylphosphocholine (OOEPC), cytosolic phospholipase $A_{2\alpha}$ inhibitor (c$PA_{2\alpha}$i) (N-((2S,4R)-4-(Biphenyl-2-ylmethyl-isobutyl-amino)-1-[2-(2,4-difluoro-benzoyl)-benzoyl]-pyr-rolidin-2-ylmethyl}-3-[4-(2,4-dioxothia-zolidin-5-ylidene-methyl)phenyl] acryl amide, HCl), bromoenol lactone (BEL), Gö 6850, U73112 and wortmannin were from Calbiochem (Beeston, Nottingham, UK). Ovine PGHS-1 and wild-type murine PGHS-2 were kindly

provided by Dr Lawrence J Marnett (Vanderbilt Institute of Chemical Biology, Vanderbilt University, Nashville, TN, USA). Corn Trypsin Inhibitor (CTI) and recombinant tissue factor were purchased from Cambridge Biosciences (Cambridge, UK). Thrombin Calibrator was purchased from Diagnostica Stago UK Ltd (Reading, UK). Aspirin 75 mg enteric coated tablets were from Boots UK Ltd. All high-performance liquid chromatography grade solvents were from Thermo Fisher Scientific (Hemel Hempstead, Hertfordshire, UK). All other reagents were from Sigma-Aldrich Company Ltd (Poole, Dorset, UK) unless otherwise stated.

2.1.2   General buffers and solutions.

Acid-citrate-dextrose (ACD) buffer.

85 mM trisodium citrate, 65 mM citric acid, 100 mM glucose, pH 5.0.

Tyrode's buffer.

134 mM NaCl, 12 mM NaHCO$_3$, 2.9 mM KCl, 0.34 mM Na$_2$HPO$_4$, 1 mM MgCl$_2$, 10 mM Hepes, 5 mM glucose, pH 7.4.

Extraction mix solvent.

1 M acetic acid, 2-propanol, hexane (2:20:30, v/v/v).

Hydrolysis buffer.

150 mM NaCl, 5 mM CaCl2, 10 mM Tris (trizma base), pH 8.9.

Phosphate buffer.

100 mM potassium phosphate, pH 7.4.

Liposome buffer.

20 mM HEPES, 140 mM NaCl, pH 7.35.

Hepes buffer.

20 mM HEPES, 140 mM NaCl, pH 7.35, 5 mg/ml BSA.

Fluo-buffer.

20 mM HEPES, 140 mM NaCl, pH 7.35, 60 mg/ml BSA, 0.02 % sodium azide.

Sodium citrate buffer.

136 mM trisodium citrate in PBS.

Sucrose buffer.

0.1 mM potassium phosphate, 0.25 M sucrose, 1 mM EDTA, pH 7.5.

2.2 Methods

2.2.1 Blood collection and platelet isolation.

All blood donations were approved by the Cardiff University School of Medicine Ethics Committee and were with informed consent (SMREC 12/37, SMREC 12/10), and were according to the Declaration of Helsinki. Whole blood was collected from healthy volunteers free from non-steroidal anti-inflammatory drugs for at least 14 days. Approximately 40 ml of blood was taken via forearm venepuncture into ACD (ratio of blood:ACD, 8.1: 1.9, v/v). Blood containing ACD (50 ml total) was separated into two 50 ml falcon tubes, followed by centrifugation at 250 X g in a centrifuge (Heraeus Labofuge 400e, DJB Labcare Ltd, Buckinghamshire, UK), with brake mechanism off, for 10 min at room temperature. The resulting platelet-rich-plasma (PRP) was aspirated into a clean 50 ml falcon tube and centrifuged at 900 X g, with brake mechanism off, for 10 min at room temperature. Platelet-poor-plasma (PPP) was then discarded and the remaining platelet pellet was resuspended in 10 ml Ca^{2+} free Tyrode's buffer containing ACD (9:1 v/v). Resuspended platelets were then centrifuged at 800 X g, with brake mechanism off, for 10 min at room temperature (Thomas *et al*., 2010). After the last centrifugation step, supernatant was discarded and platelet pellet was resuspended in 3 ml Tyrode's buffer.

2.2.1.1 Platelet isolation from buffy coat.

All buffy coats were obtained from the Welsh Blood service. Buffy coat containing approximately 50 ml of anticoagulated blood, composed predominantly of white blood cells and platelets, was separated into five 50 ml falcon tubes. Then, 20 ml of Tyrode's buffer containing ACD (9:1 v/v) was added to each tube. The diluted blood was centrifuged for 10 min at 250 X g with brake mechanism off. Next, plasma was transferred to a clean falcon tube and centrifuged at 900 X g for 10 min (brake off). Plasma was carefully discarded and the platelet pellet was resuspended in 10 ml of Tyrode's buffer containing ACD (9:1 v/v). Platelets were then centrifuged for 10 min at 800 X g (brake off), the supernatant was discarded and the platelet pellet was carefully resuspended with 10 ml Tyrode's buffer.

2.2.1.2 Platelet density analysis.

The platelet number was evaluated after diluting 1:100 in a Tyrode's buffer/Trypan Blue solution (445 µl Tyrode's buffer, 50 µl of electrostatically charged exclusion dye (Trypan Blue). Platelets were counted over a grid of 25 squares using a haemocytometer and their concentration was calculated using the followed equation:

$$
\begin{aligned}
&Concentration\ of\ platelets\ in\ original\ mixture\\
&= \left[\left(\frac{number\ of\ platelets\ counted}{number\ of\ squares\ counted}\right) \times 25\right] \times (dilution\ factor)\\
&\times (10^4)\ \times total\ original\ volume\ mixture
\end{aligned}
$$

Platelets were then diluted at a concentration of 2 x 10^8 per ml in calcium free Tyrode's buffer.

2.2.1.3 Platelet activation.

Washed human platelets, at a concentration of 2 x 10^8 per ml in Ca^{2+} free Tyrode's buffer, were aliquoted into 1.5 ml eppendorf tubes followed by addition of 1 mM $CaCl_2$ with gentle agitation and incubated at 37^oC for 5 min. Platelet samples were then activated with several agonists including thrombin (0.2 U/ml), collagen (10 µg/ml) and calcium ionophore (10 µM) for 30 min at 37^oC prior to lipid extraction.

2.2.1.4 Time course experiments.

Platelet samples were analysed at several time points (0, 5, 10, 30, 60, 120 and 180 min). Washed human platelets were collected and isolated, as described in section *2.2.1*, and activated with several agonists as described in section *2.2.1.4*. After the specific time points had been reached, the activated platelet samples were transferred into 10 ml glass extraction vial containing extraction solvent and 5 ng of each internal standard followed by lipid extraction as described below (section *2.2.2*).

2.2.2   Lipid extraction.

Prior to extraction, 5 ng each of di-14:0-phosphatidylethanolamine (DMPE), PGE_2-d_4 and PGD_2-d_4 was added to samples as internal standards. Where quantified, 5 ng each of TxB_2-d_4 and 12-HETE-d_8 were also added. Lipids were extracted by adding a solvent mixture (1 M acetic acid, isopropyl alcohol, hexane (2:20:30, v/v/v)) to the sample at a ratio of 2.5 ml of solvent mixture to 1 ml of sample, vortexing, and then adding 2.5 ml of hexane (Zhang *et al*., 2002). After vortexing and centrifugation for 5 min at 4 °C, lipids were recovered in the upper hexane layer. The samples were then re-extracted by addition of an equal volume of hexane. The combined hexane volumes were evaporated to dryness using a Rapidvap N2/48 evaporation system (Labconco Corporation) and resuspended in methanol and analysed for free and esterified prostaglandins by liquid chromatography/tandem mass spectrometry (LC/MS/MS).

2.2.3 Mass Spectrometry Analysis.

The identification of phospholipid-esterified eicosanoids described in this thesis utilised mostly mass spectrometry methods. Mass spectrometry (MS) is a powerful tool in the field of lipidomics, allowing for identification, characterisation and quantitation of various lipid classes. A MS in simple terms functions to detect the mass-to-charge ratio (*m/z*) and abundance of the various analytes generated during ionisation of a sample extract.

2.2.3.1 Precursor scanning.

Precursor scanning of platelet lipid extracts was carried out in order to identify ions that generate daughter ions with a *m/z* of 351.2 on collision-induced dissociation. Lipid extracts were separated by reverse-phase HPLC using a Luna 3 μm C18 (2) 150 mm × 2 mm column (Phenomenex, Torrance, CA) with a gradient of 50 – 100 % B over 10 min followed by 30 min at 100 % B [A, methanol/acetonitrile/water (1 mM ammonium acetate) at a ratio 60:20:20; B, methanol, 1 mM ammonium acetate] with a flow rate of 200 μl.min $^{-1}$. MS was carried out using a 4000 Q-Trap (Applied Biosystems, Foster City, California, USA). The declustering potential (DP) was set at -140 V and the collision energy (CE) at -45 V. Spectra were acquired scanning Q1 from 650 - 950 atomic mass units (amu) over 5 s with Q1 in negative mode set to the daughter ion of interest, *m/z* 351.2 [M-H]$^{-}$.

2.2.3.2 Phospholipid reverse-phase LC/MS/MS.

LC-MS/MS analysis of lipids relies exclusively on soft ionisation techniques that create intact gas-phase ions from biomolecules, enabling accurate measurement of molecular weight. Briefly, the technique consists of introducing lipid samples in solution, within the mass spectrometer electrospray chamber, where the sample is introduced through a hypodermic needle at a high voltage charging the surface of the emerging liquid and dispersing it into a fine spray of charged droplets, electrospray (Mann *et al.*, 2001; Fenn *et al.*, 1989). Molecules within the electrospray evaporate and are then ionised in atmosphere (Mann *et al.*, 2001). After ionisation, charged molecules travel through three

quadrupoles (Q1, Q2 and Q3) to a detector. The first (Q1) and the third (Q3) quadrupoles act as mass filters, and only let stable masses through the detector (Mann *et al.*, 2001). Charged molecules can then be contained in the middle (Q2) quadrupole and undergo collision-induced-decomposition (CID) using inert gas such as argon, helium or nitrogen (Maskrey & O'Donnell, 2008). This causes fragmentation of precursor ions (intact molecule) into product ions, also known as parent and daughter ions, respectively. The fragments then pass through Q3 to the detector.

Phospholipids were separated by reverse-phase HPLC using a Luna 3 μm C18 (2) 150 X 2 mm column (Phenomenex, Torrance, CA) based on the hydrophobicity of the sn1 fatty acid, and gradient as described in detail in Section *2.2.3.1*. Products were monitored by LC/MS/MS in negative ion mode, on a 4000 Q-Trap, using the specific parent to daughter transitions; collision energies and declustering potential for each analyte are specified in Table 2.1.

2.2.3.3 Eicosanoid reverse-phase LC/MS/MS.

Free fatty acids were separated on a C18 Spherisorb ODS2, 5 μm particle size, 150 x 4.6 mm (Waters Ltd., Elstree, Hertfordshire, UK) with gradient elution of. 50 − 90 % B over 20 min at 1 ml.min^{-1} (A, water:acetonitrile:acetic acid at 75:25:0.1; B, methanol:aceto-nitrile:acetic acid at 60:40:0.1). Products were monitored by LC/MS/MS in negative ion mode, on a 4000 Q-Trap, using the specific parent to daughter transitions, collision energy and declustering potential for each analyte as described in Table 2.2. PGE_2, PGD_2, TxB_2 and 12-HETE were quantified using PGE_2-d_4, PGD_2-d_4, TxB_2-d_4 and 12-HETE-d_8 as internal standards run in parallel under the same conditions.

Table 2.1: Parent and daughter m/z and MS conditions for analytes.

PE Phospholipid Structure	Analysed Transition [M-H]$^-$	Declustering Potential (V)	Collision Energy (V)
PE(14:0/14:0)	634.5/227.2	-140	-45
16:0p/PGE$_2$/D$_2$-PE	770/271	-140	-60
18:1p/PGE$_2$/D$_2$-PE	796/271	-140	-60
18:0p/PGE$_2$/D$_2$-PE	798/271	-140	-60
18:0a/PGE$_2$/D$_2$-PE	814/271	-140	-60
16:0p/PGb-PE 16:0p/PGc-PE	770/351	-140	-45
18:1p/PGb-PE 18:1p/PGc-PE	796/351	-140	-45
18:0p/PGb-PE 18:0p/PGc-PE	798/351	-140	-45
18:0a/PGb-PE 18:0a/PGc-PE	814/351	-140	-45
16:0p/12-HETE-PE	738/179	-140	-45
18:1p/12-HETE-PE	764/179	-140	-45
18:0p/12-HETE-PE	766/179	-140	-45
18:0a/12-HETE-PE	782/179	-140	-45

Table 2.2: Fatty acid transitions *m/z* and MS conditions for analytes.

Analyte	Q1 Mass (amu)	Q3 Mass (amu)	Declustering Potential (V)	Collision Energy (V)
PGE$_2$ PGD$_2$	351	271	-55	-26
PGb	351	207	-55	-26
PGc	351	165	-55	-26
TxB$_2$	369	169	-50	-22
12-HETE	319	179	-85	-20
PGE$_2$-d$_4$ PGD$_2$-d$_4$	355	275	-55	-26
TxB$_2$-d$_4$	373	173	-50	-22
12-HETE-d$_8$	327	184	-85	-20

2.2.3.4 Enhanced product ion (EPI) analysis.

In enhanced product ion analysis, Q1 acts as a filter by selecting a specific precursor ion by its *m/z* value. These ions are transferred to a collision chamber (Q2) where they are bombarded with a collision gas, and fragment. The daughter ions produced are then detected in Q3. EPI analysis uses ion trapping, where ions can accumulate in Q3 for a specified time and can be scanned simultaneously. The ion trap settings were as follow with the LIT fill time set at 200 ms and the Q3 entry barrier set at 8.00 V, declustering potential -50 V and the collision energy set at -30V.

All MS data acquired using 4000 Q-Trap (Applied Biosystems, Foster City, California, USA) were analysed by Analyst^{TM} software.

2.2.3.5 Targeted MS/MS using an LTQ Orbitrap Velos.

The LTQ Orbitrap Velos used in this study combines the tandem mass spectrometry competence of the linear ion trap (LTQ) with the high resolution fast scanning and mass accuracy of the Orbitrap for precursor and product ions measurements, providing rapid and high quality accurate data for elucidation of unknown compounds.

In the LTQ Velos, ions are generated by heated electrospray, a soft ionization process which transforms ions predominantly pre-formed in solution into ion in the gas phase. Then, ions are driven towards the ion transfer tube, passing through the S-lens which consists of a set of stainless apertures that act focusing ions into a tight beam as they travel through the device (Michalski *et al.*, 2012). At the S-lens exit, ions are transferred into the square quadrupole and from there into the octopole, which main purpose is to transmit only selectively charged ions from the S-lens to the ion trap, allowing neutral or ions of opposite polarity to be lost to vacuum before to be transferred into the ion trap (Michalski *et al.*, 2012). In the high pressure cell (HPC), all ions are first trapped, regardless of mass, in the ion trap through the voltage applied to the electrodes and stabilised by helium gas. Once ions are trapped, several modes of operation can be trigged, such as full scan in which all of the ions are collected in the HPC and transferred directly into the low pressure cell (LPC), from where they are ejected travelling towards to the Orbitrap analyser. In MS/MS, ions are trapped (step 1) and a single ion is isolated (step 2) and fragmented (step 3) in the HPC, generating product ions which are detected on the LPC. In the case of any higher level of analysis, for instance MS^3 or MS^n, steps 2 and 3 can be repeated several times in order to generate the desired end product.

Ions ejected from the LPC are transferred into a multipole, where ions are packed and guided to the next piece of device. The multipole is followed by an ion storage device based on trapping ions, termed C-trap, which can accumulate a significant ion population by employing an electrostatic field (Perry *et al.*, 2008). The C-trap allows the stored ions to be either injected directly into the Orbitrap analyser or undergo fragmentation in the HCD collision cell first, HCD stands for higher collision dissociation (HCD), and then injected into the Orbitrap analyser (Makarov & Sciegelova, 2010). Thus, the C-trap works

as a "T-piece" allowing interface with additional devices. In order to acquire mass accuracy of product ions, the precursor ions are isolated in the LTQ Velos, transferred to the C-trap into the HCD collision cell, from where they are transferred back into the C-trap and then into the Orbitrap.

The Orbitrap mass analyser consists of two electrodes, a central electrode termed spindle, around which ions are forced to move in a spiral, and an outer electrode (Perry *et al.*, 2008). When ions are injected into the Orbitrap a strong electrical field inside the trap pushes them towards the equator of the Orbitrap analyser (a central spindle electrode) where they are electrostatic trapped, initiating axial oscillation along the axis and rotation around the central electrode, resulting in an intricate spiral (Perry *et al.*, 2008; Makarov & Sciegelova, 2010; Makarov, 2000). The combination of orbital motion and harmonic axil oscillations allows a larger trapping capacity, consequently, leading to an increased space-charge capacity (Perry *et al.*, 2008). The harmonic ion oscillations along the central electrode produces an image current, which is then acquired as a time-domain signal by the two split halves of the outer electrode (Perry *et al.*, 2008). The time-domain signal contains all the characteristic frequency observed over a period of time that ions are measured. The fast Fourier transform (FT) operation converts the recorded time-domain into a frequency spectrum, which is then converted into a *m/z* spectra through mathematical calculations (Scigelova *et al.*, 2011). Therefore, as masses are represented by frequencies and the last can be measured very accurately because is completely independent of the energy and the position of the ions, high mass accuracy and high mass resolution can be achieved.

Purified lipid extracts were separated by negative reverse-phase HPLC on a C18 Hypersil Gold, 1.9 μm, 100 x 2.1 mm column on an LTQ Orbitrap Velos mass spectrometer (Thermo Fisher Scientific, Hemel Hempstead, Hertfordshire, UK) using a linear mobile phase gradient (A, methanol/acetonitrile/water containing 1 mM ammonium acetate, at a ratio 60:20:20; B, methanol, 1 mM ammonium acetate) with a flow rate of 200 μl.min^{-1}. The starting conditions consisted of 50 % B and were maintained for 10 min. The gradient then increased to 100 % B over 15 min and then finally returned to the initial conditions for 5 min to allow equilibration. The analyses on the LTQ Orbitrap instrument

were performed using heated electrospray ionization (h-ESI) in negative ion mode at sheath, auxiliary, and sweep gas flows of 30, 10, and 0, respectively. The capillary and source heater temperatures were set to 275 and 250 °C, respectively. Resolving power of 30,000 in full scan mode was used. LC/MS of parent ions were monitored using accurate mass in FTMS mode. Negative MS/MS spectra were acquired using higher energy collision-induced-dissociation (HCD). Data dependent MS^3 of *m/z* 351 was carried out in ITMS on the LTQ Ion Trap.

All MS data acquired using LTQ Orbitrap Velos mass spectrometer (Thermo Fisher Scientific, Hemel Hempstead, Hertfordshire, UK) were analysed by Xcalibur^{TM} software.

2.2.3.6 Normal-phase HPLC–UV.

Normal-phase HPLC–UV was used to determine phospholipid headgroup. Platelet lipid extracts resuspended in normal phase solvents [50:50 of solvents A:B (A, hexane:propan-2-ol, 3:2; B, solvent A:water, 94.5:5.5)] were separated on a Spherisorb S5W 4.6 x 150-mm column (Waters Ltd., Estree, Hertfordshire, UK) at a flow rate of 1.5 ml.min^{-1} (Dugan *et al.*, 1986). Absorbance was monitored at 205 nm and products identified by retention time comparison using a mixture of standard phospholipids (bovine brain PC and PE, 25 mg/ml). Fractions were collected at 30 sec intervals and analysed by direct flow injection, with no column attached, in reverse phase solvents [50:50 of solvents A:B (A, methanol:acetonitrile:water, 1 mM ammonium acetate, 60:20: 20; B, methanol, 1 mM ammonium acetate)] and a flow rate of 200 µl. min^{-1}, monitoring parent to daughter ion on a 4000 Q-trap. The time of elution of esterified prostaglandins were then compared with standard PE and PC for headgroup classification.

2.2.4 Purification of prostaglandin-PEs (PG-PEs).

Washed human platelets were activated with ionophore (10 μM for 30 min at 37°C) in the presence of 1mM $CaCl_2$ followed by lipid extraction as described above (section *2.2.2*). HPLC with UV detection was carried out using a Gilson HPLC system comprising 811D dynamic mixer, 306 pumps, 805 manometric module, and an Agilent 1100 series UV detector. Prostaglandin-PEs were purified from total platelet lipid extracts using a Discovery C18 column (25 cm x 4.6 mm, 5 μm particle size (Sulpeco)) at 1 ml.min^{-1}, and gradient of 50 % to 100 % mobile phase B (A: water, 1 mM ammonium acetate, B: methanol, 1 mM ammonium acetate) over 15 min, then held at 100 % B for 20 min. Fractions were collected with 60 sec intervals for subsequent analysis by LC/MS/MS. Prostaglandin-PEs were then analysed for the *m/z* of interest using phospholipid reverse-phase separation on an Applied Biosystems 4000 Q-Trap, as described in section *2.2.3.2*. Esterified prostaglandin-containing fractions were combined and evaporated to dryness using a Rapidvap N2/48 evaporation system (Labconco Corporation) and resuspended in methanol.

2.2.5 Phospholipase A_2 hydrolysis.

Purified prostaglandin-PE sample was subject to enzymatic-hydrolysis. Lipids were dried by evaporation under N_2 and resuspended in 1 ml hydrolysis buffer (described in section *2.1.2*). To this solution was added 200 μg/ml of snake venom phospholipase A_2 (PLA_2) and incubated for 60 minutes at 37°C. Following incubation, lipids were extracted as described in Section *2.2.2*. Following hydrolysis, prostaglandins released from the glycerol backbone were analysed using prostaglandin reverse-phase LC/MS/MS as described below in Section *2.2.6*.

2.2.6 Prostaglandin reverse-phase LC/MS/MS.

Prostaglandins were separated on a C18 Spherisorb ODS2, 5 μm particle size, 150 x 4.6 mm (Waters Ltd., Elstree, Hertfordshire, UK). MS/MS was carried out using an Applied

Biosystems 4000 Q-Trap. The solvent system was composed of 0.1 % formic acid in water (solvent A) and 0.1 % formic acid in acetonitrile (solvent B). The flow rate was 1 ml.min^{-1}. Solvent B was increased from 20 % to 42.5 % over 50 min, at 50 min was increased further to 90 % over 10.5 min to wash the column, and at 65.5 min, it was returned to 20 % over 1 min for column equilibration (Brose *et al*., 2011). Equilibration time between runs was 14 min.

2.2.7   *Synthesis of PGE$_2$/D$_2$-PE standards.*

Approximately 1×10^{11} platelets were isolated from two buffy coats as described in Section *2.2.1.2*, diluted in Tyrode's buffer to give a concentration of 2×10^8 platelets/ml, and activated using 10 µM of A23187, for 30 min at 37°C, in the presence of 1 mM CaCl$_2$. Following activation, platelet samples were spun at 900 X g for 5 min, the supernatant (containing free prostaglandins) removed and the platelet pellet resuspended in fresh Tyrode's buffer. Following extraction using hexane: isopropanol, as described in Section *2.2.2*, platelet lipid extracts were resuspended in 400 µl of methanol, from which 200 µl was taken and divided into two vials. A 100 µl aliquot was then dried and incubated with 200 µg/ml snake venom PLA$_2$ and the other 100 µl incubated with hydrolysis buffer only, as control. Both were incubated for 60 minutes at 37°C.

Following hydrolysis, 2 ng of PGE$_2$-d$_4$ and PGD$_2$-d$_4$ were added to each sample for quantification of PGE$_2$ and PGD$_2$, respectively. To account for differences in PGE$_2$/D$_2$-PE recovery during extraction, an internal standard (1,2-dimyristoyl-*sn*-glycero-3-phosphoethanolamine (DMPE)) was added to samples prior to lipid extraction. Following extraction, lipids were recovered as described in Section *2.2.2*, resuspended in methanol and analysed for PGE$_2$/D$_2$-PEs using reverse-phase LC/MS/MS, monitoring parent [M-H]$^-$ $\rightarrow$ 271, as described in Section *2.2.3.2*. PGE$_2$ and PGD$_2$ was also analysed using reverse-phase LC/MS/MS monitoring *m/z* 351.2 $\rightarrow$ 271, as described in Section *2.2.6*.

2.2.8 *Enzymology*

2.2.8.1 Protein quantification.

Ovine COX-1 and wild-type murine COX-2 were quantified using Bicinchoninic Acid (BCA) Protein Assay Kit (Thermo Scientific Pierce Protein Research Products), in accordance with the manufacturer's instructions. The assay was performed in triplicate on 1:20 dilutions of the ovine COX-1 and wild-type murine COX-2 protein in PBS buffer. 20 µl of each protein standard and sample was added to 200 µl of a 1:50 dilution of sulphate pentahydrate in bicinchoninic acid in 96 well plates and incubated at $37^{o}C$ for 30 minutes. The absorbance was recorded at 562 nm using a Multiscan plate reader (FLUOstar Omega, BMG Labtech). The protein sample concentration was determined by comparison to the standard curve.

2.2.8.2 Oxidation of free and phospholipid-esterified arachidonate by purified/ recombinant COX-1 and COX-2.

ApoCOX-1 or apoCOX-2 was reconstituted with 2 molar equivalents of hematin in phosphate buffer on ice for 20 min. The reconstituted enzyme (holoCOX-1 or holoCOX-1) was added to 1 ml phosphate buffer and 500 µM of phenol and incubated for 3 min at 37°C in the presence of 150 µM arachidonate (AA or AA-d_8). In some experiments, the same amount of AA was replaced with SAPE. The reaction was stopped by addition of ice-cold extraction mix solvent (described in Section *2.1.2*). Then, 5 ng each of DMPE, PGE$_2$-d_4 and PGD$_2$-d_4 was added as internal standards and lipids extracted. PGE$_2$ and PGD$_2$ were quantified by LC/MS/MS analysis, as described in Section *2.2.3.3*. In some experiments, 10 µM of the metal chelator diethylenetriaminepentaacetic acid (DTPA) was added to the reaction just before the addition of holoCOX-1. Formation of esterified and deuterated esterified prostaglandin was analysed by phospholipid reverse-phase LC/MS/MS, as described in Section *2.2.3.2*, in negative ion mode, on a 4000 Q-Trap. Formation of PGs and deuterated PGs was analysed by prostaglandin reverse-phase LC/MS/MS, as described in Section *2.2.6*, in negative ion mode, on a 4000 Q-Trap. Deuterated PGs were monitored using the specific transitions as described in Table 2.3. Deuterated esterified

prostaglandins were monitored using the specific parent to daughter transitions, as described in Table 2.4.

Table 2.3: Transitions *m/z* and MS conditions for deuterated prostaglandin analytes.

Analyte	Q1 Mass (amu)	Q3 Mass (amu)	Declustering Potential (V)	Collision Energy (V)
Deuterated PGE_2 and PGD_2	359	278	-55	-26
Deuterated PGb	359	213	-55	-26
Deuterated PGc	359	169	-55	-26

Table 2.4: Parent and daughter *m/z* and MS conditions for deuterated esterified prostaglandin analytes.

PE Phospholipid Structure	Analysed Transition [M-H]⁻	Declustering Potential (V)	Collision Energy (V)
Deuterated 16:0p/PGE_2/D_2-PE	778/278	-140	-60
Deuterated 18:1p/PGE_2/D_2-PE	804/278	-140	-60
Deuterated 18:0p/PGE_2/D_2-PE	806/278	-140	-60
Deuterated 18:0a/PGE_2/D_2-PE	822/278	-140	-60
Deuterated 16:0p/PGb-PE and 16:0p/PGc-PE	778/359	-140	-45
Deuterated 18:1p/PGb-PE and 18:1p/PGc-PE	804/359	-140	-45
Deuterated 18:0p/PGb-PE and 18:0p/PGc-PE	806/359	-140	-45
Deuterated 18:0a/PGb-PE and 18:0a/PGc-PE	822/359	-140	-45

2.2.9   Exogenous incorporation of added fatty acids by activated human platelets.

Human platelets were incubated with either 2 µg of AA-d_8, 5 ng of PGE$_2$-d_4 or 2.5 ng of PGD$_2$-d_4, in the presence of 0.2 U/ml of thrombin and 1 mM CaCl$_2$ (Smith *et al*., 1985). Cells were incubated for 30 min at 37°C and lipids extracted as described in section *2.2.2*. Formation of deuterated prostaglandins was analyzed using eicosanoid reverse-phase LC/MS/MS, monitoring specific transitions as described in Table 2.4. Generation of deuterated esterified prostaglandins was monitored using phospholipid reverse-phase LC/MS/MS, on a 4000 Q-trap, monitoring parent to daughter transitions as described in Table 2.5. In each table, the first analyte transition corresponds to deuterated-esterified prostaglandin formed upon incorporation of AA-d_8, while the second transition relates to the incorporation of either PGE$_2$-d_4 or PGD$_2$-d_4.

2.2.10 In vivo aspirin supplementation.

All human studies were approved by the Cardiff University School of Medicine Ethics Committee (Study No. 12/10) and were with informed consent. Healthy volunteers were recruited by advertisement. Exclusion criteria were a known sensitivity to aspirin. All subjects gave written informed consent, according to the Declaration of Helsinki. Following a 14-day NSAID-free washout period, blood samples were obtained for baseline determination of PGE$_2$/D$_2$-PE, PGb-PE and PGc-PE as well as PGE$_2$, PGD$_2$, PGb and PGc levels. Subjects were ask to take 75 mg/day aspirin for 7 days, then provided a second blood sample on the day after the last aspirin dose. Platelets were isolated and activated *ex vivo* using 0.2 U/ml of thrombin, in the presence of 1 mM CaCl$_2$, followed by lipid extraction.

Table 2.5: Parent and daughter *m/z* and MS conditions for analytes.

Phospholipid Structure	Analysed Transition [M-H]$^-$	Declustering Potential (V)	Collision Energy (V)
Deuterated 16:0p/PGE$_2$/D$_2$-PE	774/275 778/278	-140	-60
Deuterated 18:1p/PGE$_2$/D$_2$-PE	800/275 804/278	-140	-60
Deuterated 18:0p/PGE$_2$/D$_2$-PE	804/275 806/278	-140	-60
Deuterated 18:0a/PGE$_2$/D$_2$-PE	818/275 822/278	-140	-60
Deuterated 16:0p/PGb-PE and 16:0p/PGc-PE	774/355 778/359	-140	-45
Deuterated 18:1p/PGb-PE and 18:1p/PGc-PE	800/355 804/359	-140	-45
Deuterated 18:0p/PGb-PE and 18:0p/PGc-PE	804/355 806/359	-140	-45
Deuterated 18:0a/PGb-PE and 18:0a/PGc-PE	818/355 822/359	-140	-45

2.2.11 Generation of liposomes.

Lipids were dried in a glass vial by evaporation under N$_2$ and suspended in 500 µl liposome buffer (described in section *2.1.2*) with vortexing. Liposomes were then generated by ten freeze thaw cycles with liquid nitrogen, followed by passing through LiposofastTM mini-extruder with 100 nm pore membranes (Avestin) nineteen times. In

some experiments, 25 nM recombinant tissue factor was added to lipids in buffer before the freeze thaw cycles. Liposomes were prepared immediately before use, utilizing either lipid extracts from activated human platelets or commercial available lipid standards.

2.2.12 Synthesis of PGE$_2$-PE in vitro.

2.2.12.1 Generation of Rat liver microsomes.

Wistar strain male rats (6 weeks old) were decapitated and whole livers were immediately removed and kept on ice. Livers were washed with ice-cold PBS and perfused with 50 ml ice-cold trisodium citrate buffer to remove excess of blood. They were then minced and homogenized using a glass hand homogenizer in 200 ml of ice-cold sucrose buffer (pH 7.4), containing 1 mM ethylenediaminetetraacetic acid (EDTA). The homogenate was sequentially centrifuged at 5,000 X g for 10 min, 22,000 X g for 10 min and 43,500 X g for 10 min, at 4°C, with pellets discarded every time. Then, supernatant was centrifuged once again at 81,600 X g for 60 min, at 4°C, and pellet containing rat liver microsomes were resuspended in sucrose buffer. Microsomes were stored at - 80°C before use. The protein content of microsome pellets was measured by NanoDrop 1000 spectrophotometer.

2.2.12.2 Preparation of lysophospholipid/fatty acid solution.

Lysophospholipid/fatty acid solution was prepared by adding 80 μM of AA-d$_8$ and 80 μM of either 18:0 lyso PE or 18:0 lyso PC to a 0.3 ml reaction vial and solvent evaporated. In some experiment 80 μM of PGE$_2$ was replaced by 80 μM of PGE$_2$. Lipids were resuspended in 20 μl of ethanol and mixed vigorously by vortex. This was followed by 200 μl ultrapure water and samples again vortexed. When required, lysophospholipid/fatty acid solution was added to the reaction mix, the vial rinsed with 100 μl ultrapure water, vortexed and also added to the microsome reaction mix.

2.2.12.3 Esterification reaction procedure.

Microsome buffer mix was prepared by adding 3 ml of Tris-HCl (60 mM, pH 7.4), 1.6 mM of adenosine-5'-triphosphate (ATP), 1 mM of $MgCl_2.6H_2O$ and 80 µM of Coenzyme A to a 5 ml reaction vial. Then, microsomes were added at a concentration of 0.5mg/3ml. This was followed by addition of lysophospholipid/fatty acid solution, prepared as described in Section *2.2.12.1*. The resulting reaction mix solution was incubated for 1 h at 37°C, using Rapidvap N2/48 system (Labconco Corporation) with constant shaking and vacuum mechanism off. Following incubation lipids in solution were extracted by Bligh and Dyer method, as described below.

2.2.12.4 Lipid extraction by Bligh and Dyer

For each 1 ml of sample 3.75 ml of 1:2 (v/v) $CHCl_3$:MeOH was added and the sample vortexed. Then, 1.25 ml of $CHCl_3$ was added and again vortexed. Finally 1.25 ml of dH_2O was added, vortexed and centrifuged at 250g for 5 min at 4°C to give a two-phase system (aqueous top, organic bottom). The bottom phase was recovered by inserting a Pasteur pipette through the upper phase with gentle positive-pressure to avoid the upper phase to get into the pipette tip (Bligh & Dyer, 1959). The bottom layer was evaporated to dryness, using a Rapidvap N2/48 evaporation system (Labconco Corporation) and resuspended in methanol. Products were analyzed using phospholipid reverse-phase LC/MS/MS (as described in section *2.2.3.2*) in negative and positive mode on a 4000 Q-Trap, monitoring the specific parent to daughter transitions as described in Tables 2.6 – 2.8. The collision energies and declustering potential for each analyte are also specified in Tables 2.6 – 2.8.

Table 2.6: Parent and daughter ion transition and MS condition in negative mode for Lyso PC 18:0.

Phospholipid Structure	Analysed Transition [M-16]$^-$	Declustering Potential (V)	Collision Energy (V)
Lyso PC 18:0	508/283	-140	-45

Table 2.7: Parent and daughter ion transitions and MS conditions in negative mode for analytes.

Phospholipid Structure	Analysed Transition [M-H]$^-$	Declustering Potential (V)	Collision Energy (V)
Lyso PE 18:0	480/283	-140	-45
SA-AA-d$_8$-PC	802/311	-140	-45
SA-AA-d$_8$-PE	774/311	-140	-45
SA-PGE$_2$-PC	842/283	-140	-45
SA-PGE$_2$-PE	814/271	-140	-45
SA-PGE$_2$-d$_4$-PC	846/355	-140	-45
SA-PGE$_2$-d$_4$-PE	818/355	-140	-45

SA stands for stearic acid attached at the sn1 of the glycerol backbone.

Table 2.8: Parent and daughter ion transitions and MS conditions in positive mode for analytes.

Phospholipid Structure	Analysed Transition [M+H]$^+$	Declustering Potential (V)	Collision Energy (V)
Lyso PC 18:0	524/184	140	45
SA-AA-d$_8$-PC	818/184	140	45
SA-PGE$_2$-PC	858/184	140	45
SA-PGE$_2$-d$_4$-PC	862/184	140	45

2.2.13 Measurement of thrombin generation by Calibrated Automated Thrombography (CAT).

Plasma was obtained from whole human blood (gently drawn into 20 μg/ml corn trypsin inhibitor and 4 % sodium citrate) by two rounds of centrifugation (1500 and 2900 rpm for 10 min, respectively) and filtration to reduce endogenous microparticles (0.22 μm filter). Trigger solution was prepared by dilution of liposomes in HEPES buffer with 0.5 % BSA and addition of tissue factor. As a control, a trigger solution with recombinant tissue factor and no liposomes was prepared. To determine thrombin generation, plasma (80 μl) was added in triplicate to wells of a 96-well plate followed by 20 μl trigger solution. For each sample set, a separate calibrator well, containing thrombin calibrator (α2-macroglobulin-thrombin instead of liposomes) was used. The 96-well plate was warmed and placed into a Fluoroskan Ascent Reader (Thermo Electron) and automated addition of fluorogenic substrate (Z-Gly-Gly-Arg) in fluo-buffer (described in section *2.1.2*) for thrombin measurement was initiated. The final concentration of each component was 10 pM recombinant tissue factor, 5 mM fluorogenic substrate and 20 mM $CaCl_2$. The reaction was allowed to proceed for 60 min with thrombin measurements acquired every 15 seconds. The thrombin concentration reported represents the maximum amount of thrombin present during the assay period (Hemker *et al.*, 2003).

2.2.14 Statistical analysis.

Data are representative of at least three separate experiments, with samples run in triplicate for each experiment. Data are expressed as mean ± SEM. The statistical significance of the difference between 2 sets of data was assessed with the use of an unpaired, 2-tailed Student *t* test. When the difference between > 2 sets of data was analysed, 1-way analysis of variance was used, followed by Bonferroni multiple comparisons test, as indicated on legends. A p value less than 0.05 was considered statistically significant.

Chapter 3

3   Identification of Novel Phospholipid-esterified Prostaglandins Generated by Activated Human Platelets

3.1 Introduction

As described in Chapter 1, prostaglandins have long been known as free acid mediators but their generation as esterified lipids has not been studied in detail (Ricciotti & FitzGerald, 2011; Kozak *et al*., 2000; Kozak.*et al*., 2002). Herein, a targeted lipidomic approach will be employed to investigate the generation of esterified prostaglandins formed by thrombin-activated human platelets.

Previous studies by Thomas *et al* (2010) form the starting point of this thesis describing the characterisation of phospholipid-esterified 12*S*-hydroxy-eicosatetraenoic acid (12*S*-HETE) generated by agonist-activated human platelets (Thomas *et al*., 2010). These cells also express COX-1 that converts AA into lipid mediators, including prostaglandins and thromboxane, which are known to contribute to the development of atherosclerosis (Schober *et al*., 2011; McClelland *et al*., 2009). Since activated platelets generate OxPLs via LOX, it is hypothesised that these cells also have the potential to form phospholipid-esterified prostaglandins.

The method of analysis employed by Thomas *et al* (2010) to discovery phospholipid-esterified HETEs was precursor scanning electrospray ionisation tandem mass spectrometry (ESI-MS/MS), which will also be utilised for the work described herein. To identify prostaglandins attached to larger functional groups, lipid extracts from thrombin-activated human platelets will be scanned for precursors of *m/z* 351.2, the mass of the prostaglandin carboxylate anion. In this, the product ion (*m/z* 351.2) is selected in Q3 and the precursor masses scanned in Q1. Following this, lipid analysis will be carried out using multiple reaction monitoring (MRM), which enables detection of numerous compounds simultaneously by monitoring specific parent to daughter transitions (Masoodi *et al*., 2010).

3.1.1   Aims

The studies described in this chapter aim to:

- Use precursor scanning LC/MS/MS to identify esterified prostaglandins generated by thrombin-activated human platelets.

3.2 Results

3.2.1   Precursor scanning LC/MS/MS of lipid extracts from thrombin-activated platelets identifies novel phospholipids with a mass of 351 attached.

Lipid extracts from thrombin-activated platelets were subject to precursor-LC/MS/MS, which fragments using collision-induced dissociation (CID) and scans for a functional group of interest in Q3. Analysis using negative precursor-LC/MS/MS for *m/z* 351.2 (the carboxylate anion of several prostaglandin species) demonstrated several ions that were largely absent in control platelets and elevated on thrombin activation (Figure 3.1 A, marked by*). Spectra acquired in this retention time window demonstrated four prominent ions at *m/z* 770.6, 796.6, 798.6 and 814.7 (Figure 3.1 B).
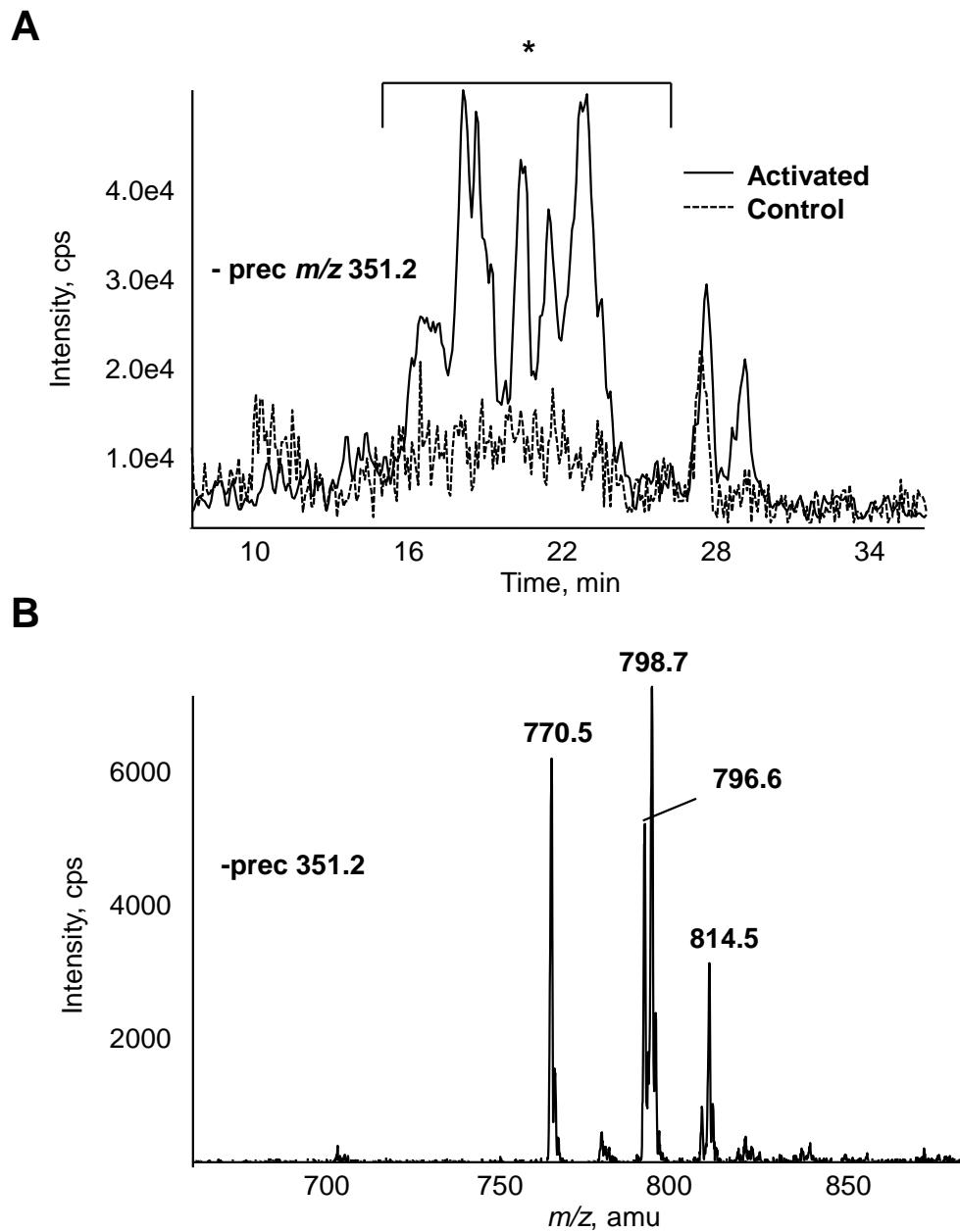
Figure 3.1: Precursor scanning LC/MS/MS of activated platelet lipid extracts identify several ions that generate daughter ions with a *m/z* of 351.2. Total lipid extracts from washed human platelets activated with 0.2 U/ml thrombin, for 30 min at 37°C, were separated using LC/MS/MS on an AB Sciex 4000 Q-Trap MS as described in Materials and Methods, Section *2.2.3.1*, with online negative precursor scanning for *m/z* 351.2. *Panel A.* * marks the region where ions appear that are elevated by thrombin stimulation. Control, dashed line; activated platelet lipid extracts, solid line. *Panel B*. Identification of ions that generate *m/z* 351.2 daughter ions. Shown is a representative negative mass spectrometry scan of region marked * in A. Scan shows ions eluting between 16 – 24 min.

3.2.2 Structural identification of phospholipid-containing esterified prostaglandin-like molecules.

Following precursor scanning, analysis of platelet lipid extracts using MRM mode, on an AB Sciex 4000 Q-Trap mass spectrometer, monitoring parent (770.6, 796.6, 798.6 and 814.7) with a *m/z* 351.2 as daughter ion, demonstrated two ions for each parent mass (Figure 3.2). This suggested the presence of two distinct prostaglandin-like structures with *m/z* 351.2 attached at the sn2 position of the glycerol backbone. Platelet lipid extracts were also analysed scanning from 620 – 900 atomic mass units (amu) using Fourier transform mass spectrometry (FTMS) on the Orbitrap Velos, which can accurately discriminate masses down to 0.1 part-per-million (ppm), giving the exact mass of the molecule. Surprisingly, the extracted ion chromatogram analysis recovered from the base peak chromatogram indicated the presence of three lipids for each *m/z* value, labelled "a – c" (Figure 3.3, solid line). Since the sensitivity of FTMS on the Orbitrap is lower compared to the MRM mode on the 4000 Q-Trap, the ions appear weaker, especially for the *m/z* 814.7 ion (Figure 3.3, D). Retention times using FTMS on Orbitrap are earlier due to the use of different high-performance liquid chromatography (HPLC) conditions (Figure 3.3).

To investigate the reason for only detecting two instead of three lipids in MRM mode on the Q-Trap platform versus FTMS, lipids were analysed using FTMS but isolating the parent (770.6, 796.6, 798.6 and 814.7) in ion trap mass mode (ITMS) and fragmenting using collision-induced dissociation (CID). Following fragmentation of parent masses, the *m/z* 351.2 daughter ion was detected using ITMS. This showed two peaks corresponding to "b" and "c" and only a small shoulder for peak "a" (Figure 3.3, dotted line). Thus, when analysing using accurate mass, three esterified prostaglandin-like molecules were detected, but when analysing on either platform (Q-trap 4000 or Orbitrap Velos) by detection of the daughter ion of *m/z* 351.2, peak "a" disappeared. This indicated that lipid "a" (*m/z* 351.2) is considerably more fragile than "b" or "c", and does not survive CID during MS/MS analysis.
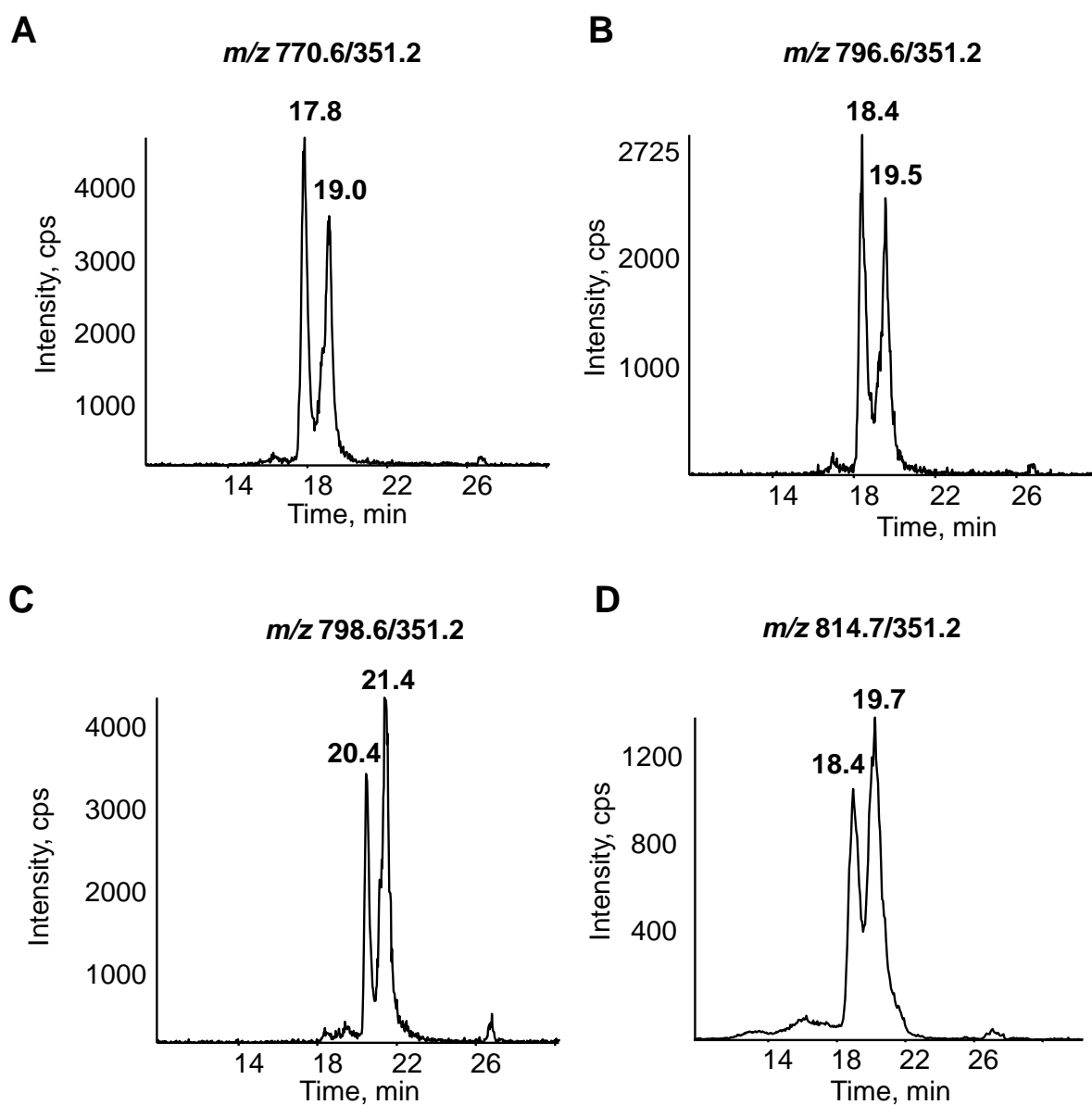
Figure 3.2: LC/MS/MS of the four putative phospholipid species with a mass of *m/z* 351.2 attached shows the presence of two species for each *m/z* value. Platelet lipid extracts were separated and analysed using reverse-phase LC/MS/MS on the Q-trap platform, monitoring parent [M-H]⁻ → *m/z* 351.2, as described in Materials and Methods, Section *2.2.3.2*.
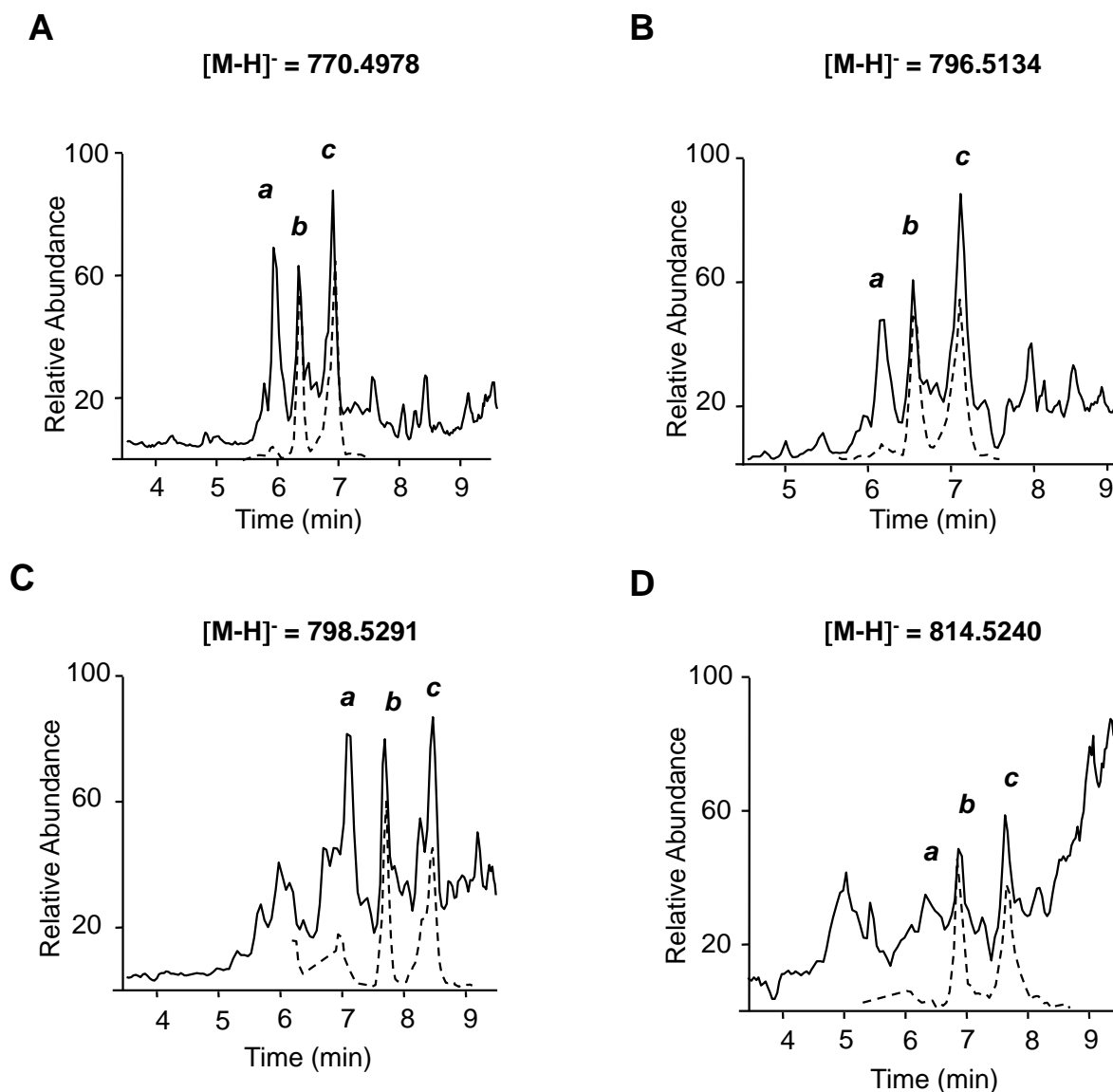
Figure 3.3: Reverse-phase LC/MS/MS separation of parent ions with and without fragmentation on the Orbitrap platform. High resolution LC/MS/MS indicates three distinct esterified eicosanoids for each phospholipid species. Platelet lipid extracts were analysed using LC/MS/MS on the Orbitrap platform, as described in Materials and Methods, Section *2.2.3.5*, monitored either using accurate mass (solid line), or by fragmentation of parent [M-H]⁻ to generate the *m/z* 351.2 daughter ion (dashed line).

In summary, a total of 12 unique lipids were detected in lipid extracts from thrombin-activated platelets, comprising four phospholipid species with three structurally distinct eicosanoids attached, and designated "a, b and c".

3.2.3 Characterisation of the phospholipid species of esterified prostaglandin-like molecules.

Phospholipid species were initially identified using the Handbook of Molecular and Product Ions, which aids characterisation of phospholipid molecular species (e.g. PC, PE or PS) and subspecies (plasmalogen and acyl) whilst also suggesting the number of carbons and double bonds (Murphy, 2002).

Prostaglandins with a *m/z* of 351.2 contain three oxygens, which are equivalent to a molecular weight of 48 amu. Each individual phospholipid species was calculated by subtracting the molecular mass of three oxygens (48 amu) from its total parent mass value (770.6, 796.6, 798.6 and 814.7) and the phospholipid mass (722, 748, 750 and 766) compared to phospholipids described in the handbook. The headgoup was suggested as PE and phospholipid species (722, 748 and 750) as plasmalogens containing 36:4p-PE, 38:5p-PE and 38:4p-PE, while *m/z* 766 was proposed as a diacyl 38:4a-PE. Thus *m/z* 770.6, 796.6, 798.6 were suggested as plasmalogens containing a 16:0p, 18:1p and 18:0p fatty acid at sn1, respectively, and the ion at *m/z* 814.7 as a diacyl assigned as 18:0a, where the first and second number indicates the number of carbons and double bonds, respectively, and the letter the phospholipid species.

This was then confirmed using MS analysis as follows: accurate mass MS/MS of all four phospholipid-containing esterified *m/z* 351.2 species was undertaken using the Orbitrap Velos, in FTMS mode, with higher-energy collisional dissociation (HCD) fragmentation, during online separation of the lipids at the apex of elution for each lipid a, b and c. Spectra of all four parent masses demonstrate fragments at *m/z* 351.2 and 271.2.

The negative MS/MS spectrum of *m/z* 770.6 (for peak a, b, and c) shows ions arising from neutral loss of the daughter ion *m/z* 351.2 (*m/z* 436.2) and from neutral loss of *m/z* 351.2

and H_2O at *m/z* 418.2, but no sn1 daughter ions (Figures 3.4). These neutral loss values are consistent with *m/z* 351.2 attached at the sn2. The absence of sn1 ions indicates a more stable bond linking the fatty acid to the glycerol backbone, such as a vinyl ether linkage, characteristic of a plasmalogen. Similarly, the parent mass *m/z* 796.6 has ions at *m/z* 462.2 and 444.2 but no sn1 ions (Figure 3.5). The MS spectrum of *m/z* 798.6 contains ions at *m/z* 464.3 and 446.3 but no sn1 daughter ions (Figure 3.6). The parent mass *m/z* 814.7 shows a neutral loss of *m/z* 351.2 and H_2O at *m/z* 480.3 and a prominent ion at *m/z* 283, which corresponds to stearic acid, indicating an acyl-linked 18:0 at sn1 (Figure 3.7). Furthermore, MS/MS of the majority of the 12 lipid species yielded a minor ion of *m/z* 196 that arises from the ethanolamine headgroup fragmentation, indicating a PE phospholipid (Balgoma *et al*., 2010).

3.2.4 Confirmation of phospholipid headgroups of esterified prostaglandin-like molecules as PE.

To confirm PE as the headgroup for each phospholipid, lipid extracts from thrombin-activated platelets were separated into PE and PC fractions using normal phase HPLC as described in Materials and Methods, Section *2.2.3.6*. Fractions were then analysed by direct flow injection (no column attached) into the mass spectrometer for detection of specific negative ion parent [M-H]⁻→ *m/z* 351.2 MRM transitions. The phospholipid headgroup for each ion was identified based on retention time comparison with phospholipid standards. All four ions (770.6, 796.6, 798.6 and 814.7) co-eluted with the same retention time as a PE standard, in the 7-9 minutes (Figure 3.8). PC eluted after 17 minutes. Figure 3.8 shows an overlay of the PE and PC fractions run for the four transitions. The data suggest that PE is the predominant phospholipid headgroup containing esterified prostaglandin-like molecules (*m/z* 351.2).

Based on the information provided above, parent masses (*m/z* 770.6, 796.6, 798.6 and 814.7) are proposed as PEs containing 16:0p, 18:1p, 18:0p and 18:0a at sn1, and a prostaglandin-like mass at sn2, which, for simplicity, are from now on termed prostaglandin-PEs (PG-PEs).
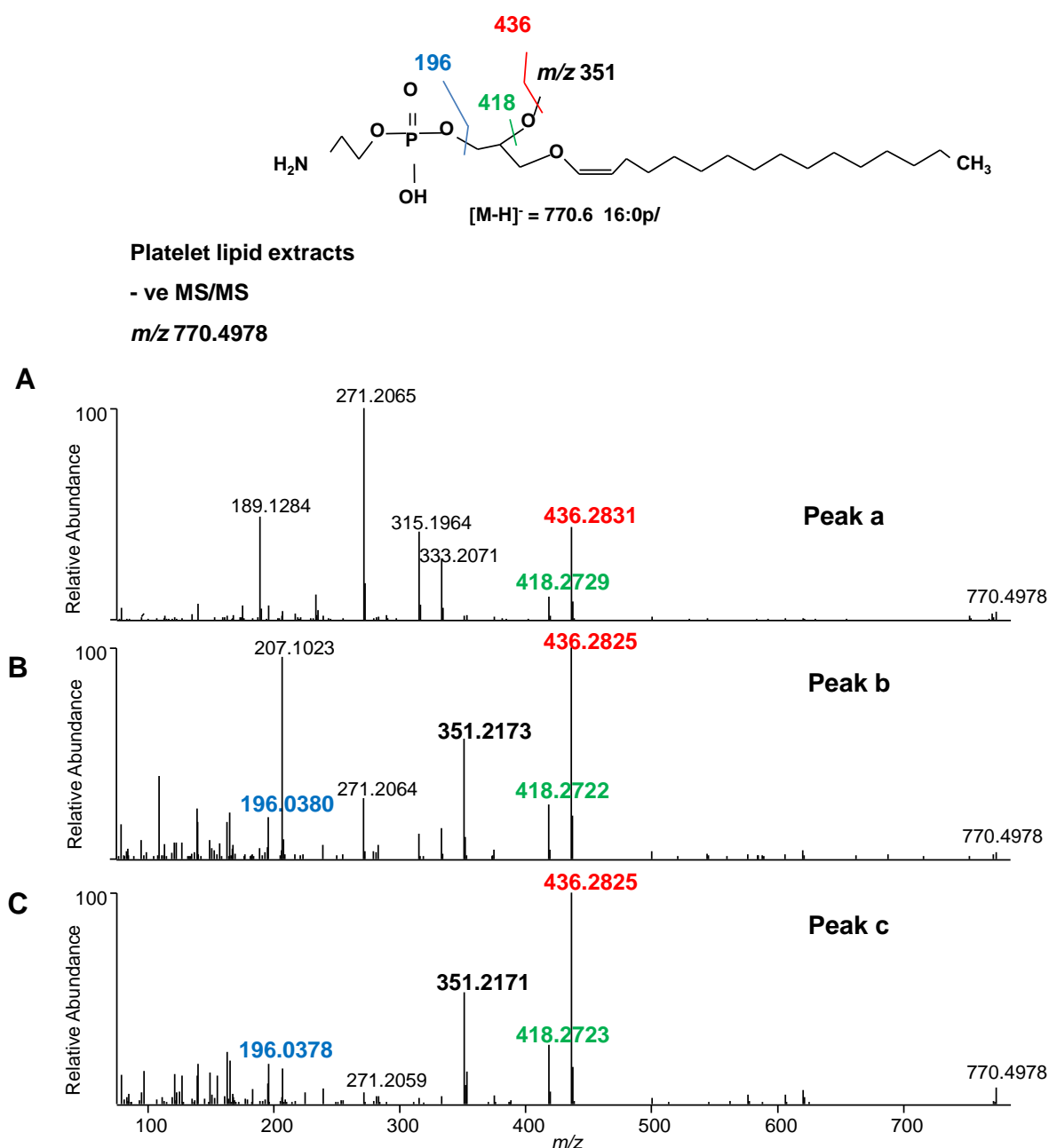
Figure 3.4: Structural identification of *m/z* 770 of peak "a", "b" and "c" as plasmalogen PEs, using MS/MS. Lipid extracts from thrombin-activated platelets were separated using LC/MS/MS and analysed using MS/MS in FTMS mode on the Orbitrap platform as described in Materials and Methods, Section *2.2.3.5*. *Panel A*. Negative MS/MS spectrum of peak "a" from thrombin-activated platelet lipid extracts. *Panel B*. Negative MS/MS spectrum of peak "b" from thrombin-activated platelet lipid extracts. *Panel C*. Negative MS/MS spectrum of peak "c" from thrombin-activated platelet lipid extracts.
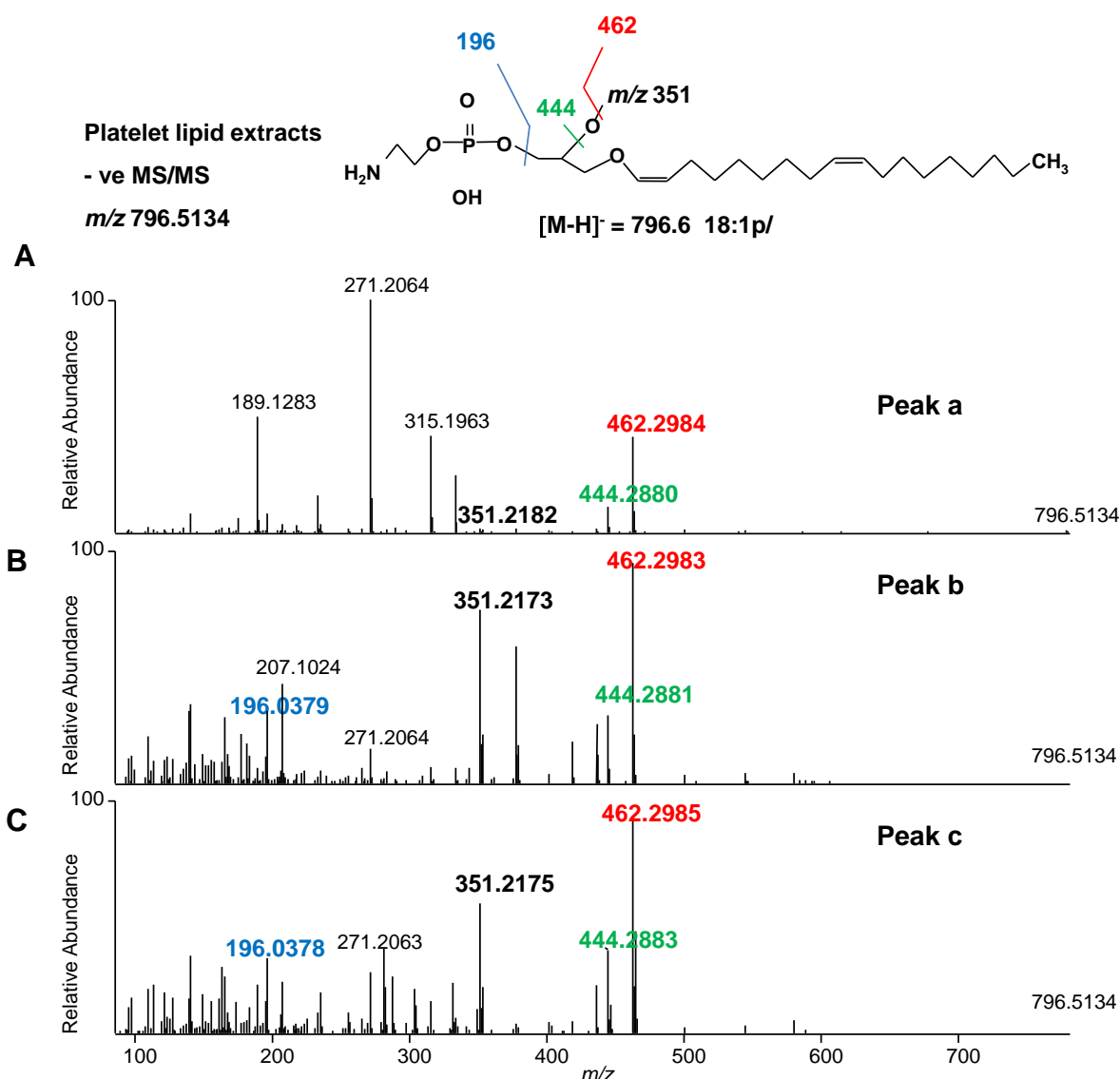
Figure 3.5: Structural identification of *m/z* 796 of peak "a", "b" and "c" as plasmalogen PEs, using MS/MS. Lipid extracts from thrombin-activated platelets were separated using LC/MS/MS and analysed using MS/MS in FTMS mode on the Orbitrap platform as described in Materials and Methods, Section *2.2.3.5*. *Panel A*. Negative MS/MS spectrum of peak "a" from thrombin-activated platelet lipid extracts. *Panel B*. Negative MS/MS spectrum of peak "b" from thrombin-activated platelet lipid extracts. *Panel C*. Negative MS/MS spectrum of peak "c" from thrombin-activated platelet lipid extracts.
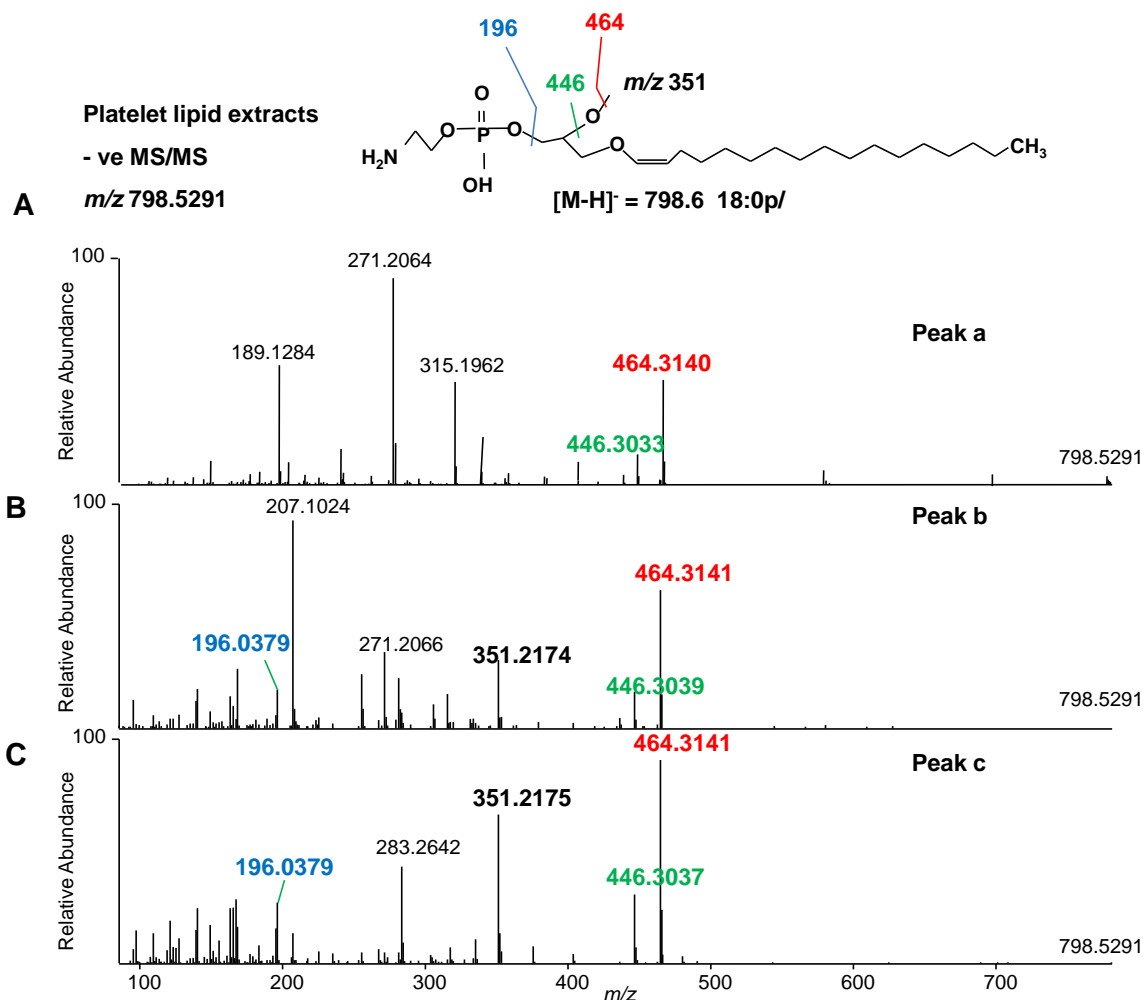
Figure 3.6: Structural identification of *m/z* 798 of peak "a", "b" and "c" as plasmalogen PEs, using MS/MS. Lipid extracts from thrombin-activated platelets were separated using LC/MS/MS and analysed using MS/MS in FTMS mode on the Orbitrap platform as described in Materials and Methods, Section *2.2.3.5*. *Panel A*. Negative MS/MS spectrum of peak "a" from thrombin-activated platelet lipid extracts. *Panel B*. Negative MS/MS spectrum of peak "b" from thrombin-activated platelet lipid extracts. *Panel C*. Negative MS/MS spectrum of peak "c" from thrombin-activated platelet lipid extracts.
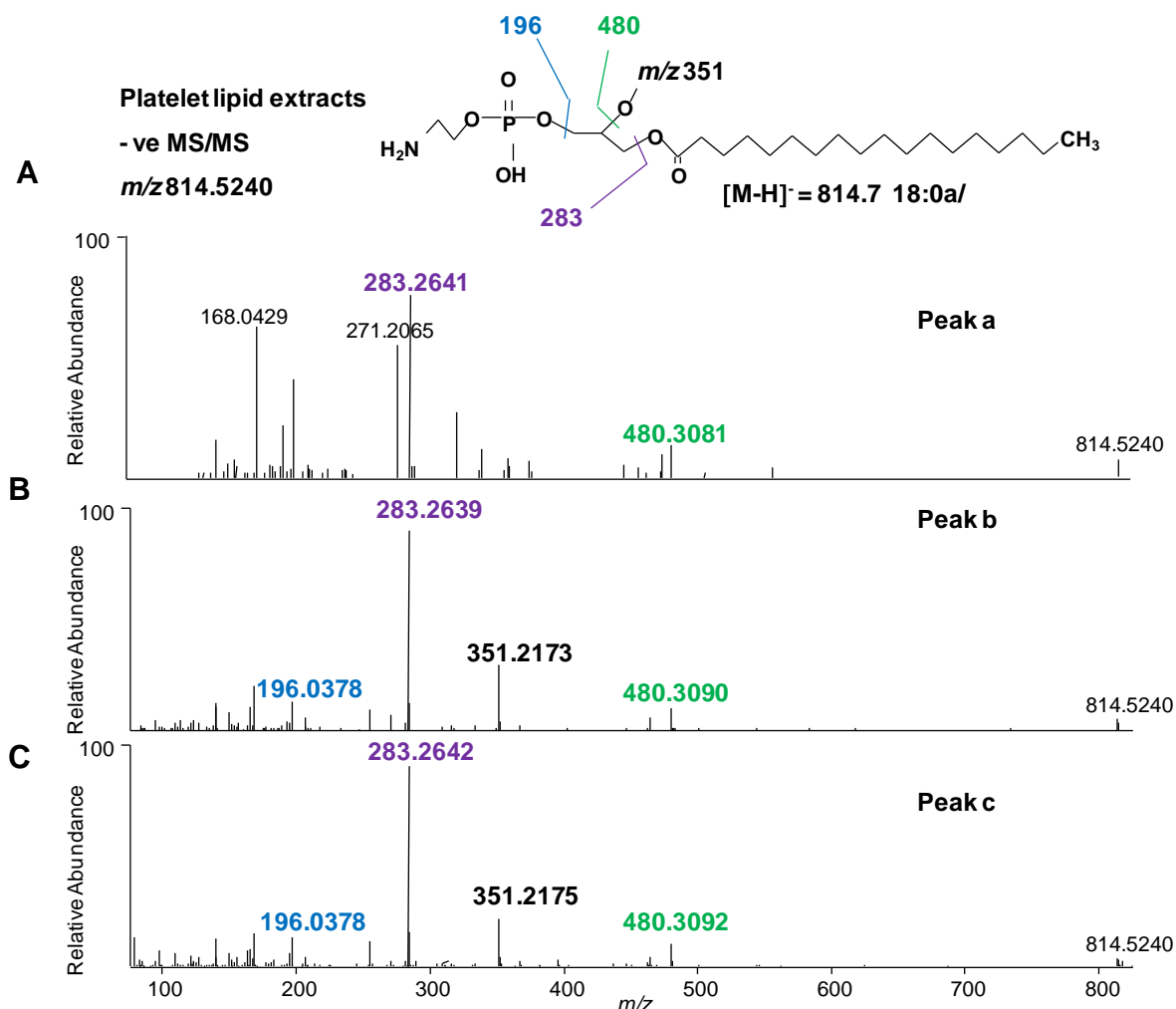
Figure 3.7: Structural identification of *m/z* 814 of peak "a", "b" and "c" as acyl-linked PEs, using MS/MS. Lipid extracts from thrombin-activated platelets were separated using LC/MS/MS and analysed using MS/MS in FTMS mode on the Orbitrap platform as described in Materials and Methods, Section *2.2.3.5*. *Panel A*. Negative MS/MS spectrum of peak "a" from thrombin-activated platelet lipid extracts. *Panel B*. Negative MS/MS spectrum of peak "b" from thrombin-activated platelet lipid extracts. *Panel C*. Negative MS/MS spectrum of peak "c" from thrombin-activated platelet lipid extracts.
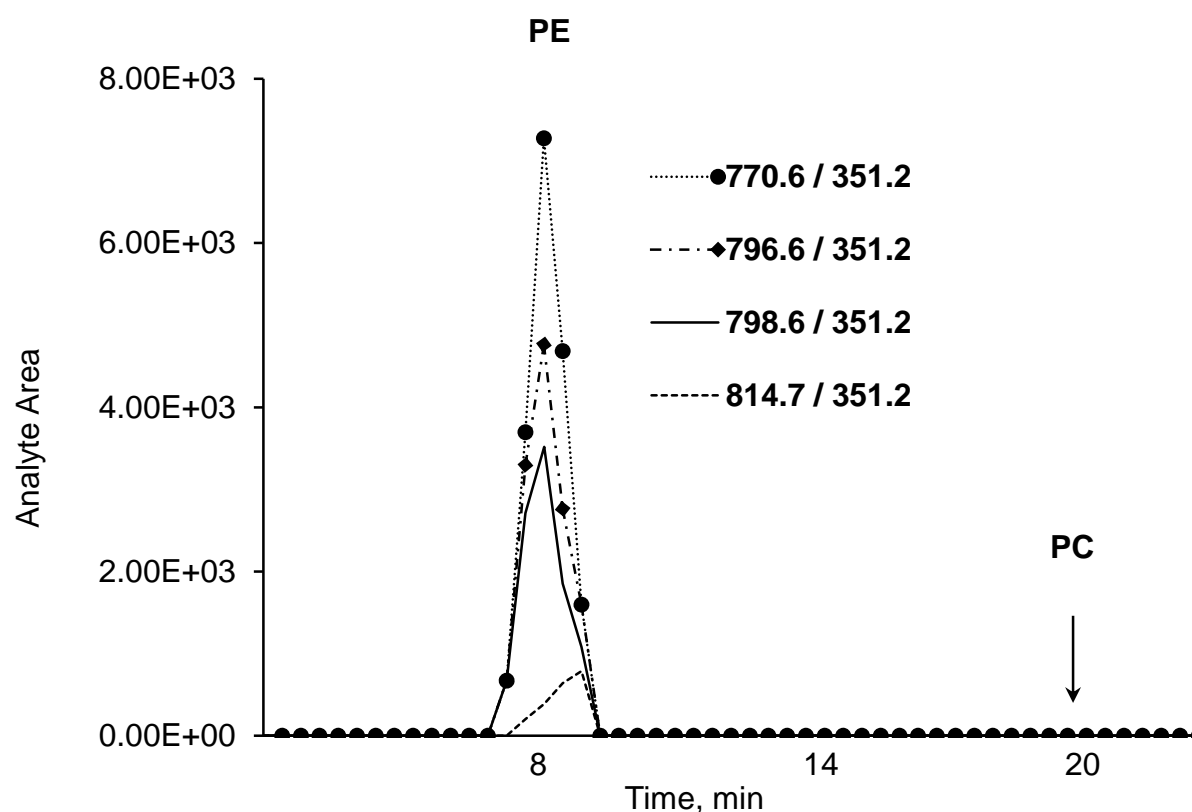
Figure 3.8: Characterisation of phospholipid headgroups of esterified prostaglandin-like molecules. Lipid extracts from thrombin-activated platelets were separated on normal phase HPLC as described in Materials and Methods, Section *2.2.3.6*, with fractions collected at 30 sec interval. 20 µl of each fraction was analysed by direct flow injection into the mass spectrometer for levels of specific negative ion parent $[M-H]^- \rightarrow$ *m/z* 351.2 MRM transitions. Phospholipid class elution was determined using commercial phospholipid standards. All four ions 770.6 $\rightarrow$ 351.2, 796.6 $\rightarrow$ 351.2, 798.6 $\rightarrow$ 351.2 and 814.7 $\rightarrow$ 351.2 co-eluted with PE (7 - 9 min). PC eluted after 17 min.

3.3 Discussion

In the present chapter, a targeted lipidomic approach was used to identify novel families of lipids with a *m/z* 351.2 attached that are generated by thrombin-activated human platelets. Using precursor scanning on a 4000 Q-trap tandem MS, lipid extracts from activated human platelets were found to generate four ions that, upon fragmentation, generate a daughter ion with *m/z* 351.2, common to prostaglandin-like molecules. Based on their *m/z,* I suggest these are likely to be PE phospholipids.

Initial results using LC/MS/MS on the 4000 Q-trap platform showed two ions for each individual parent mass, suggesting that two distinct prostaglandin-like structures with similar mass were attached to four PE molecular species (Figure 3.2). However, scanning using high resolution accurate mass on the Orbitrap mass spectrometer, in FTMS mode and monitoring parent masses with no fragmentation, instead demonstrated three molecules for each PE parent mass (Figure 3.3). Thus, a total of twelve unique lipids were detected in lipid extracts from thrombin-activated platelets, comprising three structurally distinct eicosanoids (with a *m/z* 351.2) attached to four PE species (16:0p/, 18:1p/, 18:0p/ and 18:0a/), which were named PGa-PE, PGb-PE and PGc-PE.

The PE species characterised herein is consistent with previous reports showing that, in mammals, the sn1 position is typically derived from C16:0, C18:0 or C18:1 with ethanolamine or choline as the most common headgroups (Nagan & Zoeller, 2001; Braverman & Moser, 2012). Furthermore, previous studies describing the structure of esterified HETEs in platelets showed saturated fatty acids at the sn1, with the majority of phospholipid species corresponding to plasmalogen containing 16:0, 18:1 and 18:0 alkyl chains (Thomas *et al*., 2010).

Phosphatidylcholine is the most abundant phospholipid species in eukaryotic cell membranes (40 – 50 %) and, as a result, the vast proportion of non-enzymatically-formed OxPLs detected in mammalian tissues contains the choline headgroup (Chaurio *et al*., 2009). However, previous reports showed ethanolamine as the prominent phospholipid headgroup modified via enzymatic oxidation in activated immune cells, including human

neutrophils, human monocytes and platelets (Maskrey *et al.*, 2007; Morgan *et al.*, 2009; Morgan *et al.*, 2010; Thomas *et al.*, 2010; Clark *et al.*, 2011; Hammond *et al.*, 2012). The identification of these novel lipids as plasmalogen PEs is fully consistent with previous reports.

Comparisons across ion trap and triple quadrupole platforms revealed that, during CID, peak "a" did not effectively generate a *m/z* 351.2 due to internal daughter ion fragmentation (Figures 3.4 – 3.7) and, therefore, identification of a more stable daughter ion will be required for monitoring PGa-PEs using MRM methods. This will be addressed in the next chapter.

In summary, the present study represents a new family of OxPLs that form by activated platelets in response to a physiological agonist. Their generation embodies new families of lipids that may be of importance in platelet function in health and disease. In the next chapter, characterisation of PGa structure will be performed using a targeted lipidomic approach and the identity of lipid "a" determined.

Chapter 4

4 Structural Characterisation of PGa-PE Generated by Activated Human Platelets

4.1 Introduction

Studies conducted during Chapter 3 demonstrated that agonist-activated human platelets generate families of phospholipids that fragment to generate daughter ions with a m/z 351.2. In this case, m/z 351.2 represents arachidonate with three additional oxygens characteristic of several prostaglandins or isoprostanes. Due to their unknown structure, phospholipids containing m/z 351.2 were simply named PGa-PEs, PGb-PEs and PGc-PEs.

The studies described herein aim to fully characterise PGa-PEs. Analysis of lipid extracts from activated human platelets will be performed using the LTQ Orbitrap Velos, in full scan mode. This will determine accurate mass, and allow isolation of PGa-PEs for fragmentation and structural analysis. This will be followed by data dependent MS^3, fragmenting PGa-PEs to generate daughter ions with a m/z 351.2, which can be selectively isolated and fragmented for further analysis. Accurate mass fragmentation of PGa-PE will then be compared to prostaglandin standards to identify PGa attached to PEs.

Based on the MS/MS spectra of PGa-PEs (detailed in Chapter 3), exhibiting fragments at m/z 315, 271 and 189, it was hypothesised that PGa can be either PGE_2 or PGE_2-like molecules. To test this hypothesis, PGa-PEs will be purified from platelet lipid extracts and saponified using PLA_2 (Maskrey *et al.*, 2007). PGa released from PEs will then be analysed by LC/MS/MS, on the 4000 Q-trap platform, and MS/MS spectra compared to eicosanoid standards.

Quantification of lipids is crucial to enable their bioactivity to be fully investigated, however this is not always possible as standards may not be commercially available. As a result, alternative methods for lipid quantification have been developed. For example, Thomas et al., (2010) used 18:0a/20:4-PE to synthesise 12-HETE-PE via air oxidation. The

synthesised 12-HETE-PE was subsequently purified by reverse-phase HPLC, quantified by UV absorbance and used to analyse 12-HETE-PE in platelet samples. An alternative to this approach was utilised by Maskrey et al., (2007) whereby 15-HETE-PE was indirectly quantified by calculating the amount of 15-HETE, following its release from phospholipids through saponification. Similarly, PGa-PEs generated by agonist-activated human platelets will be quantified using this approach, if their structure is successfully determined.

4.1.1   *Aims*

Studies described in this chapter aim to:

- Determine the identity of PGa attached at the sn2 position of PE species.
- Investigate the generation of PGa as a free eicosanoid formed by activated human platelets.
- Generate biogenic standards to enable quantification of PGa-PEs in human platelet samples.

4.2 Results

4.2.1   *Structural characterisation of PGa-PE generated by activated human platelets.*

4.2.1.1 Accurate mass of phospholipids containing *m/z* 351.2.

In this section, the accurate mass of individual parent ions (770.6, 796.6, 798.6 and 814.7) will be determined, using the LTQ Orbitrap Velos, in full scan mode, to enable structural analysis of PGa-PE. The accurate mass is a mass measurement acquired with sufficient accuracy (resolving power) to determine the elemental composition of an ion (Brenton &

Godfrey, 2010). The accurate mass is commonly expressed in ppm and 5 ppm or less is often sufficient to predict the elemental composition of a compound (Gross, 1994).

Lipid extracts from thrombin-activated platelets were analysed using the Orbitrap platform, with resolution set at 30,000, scanning ions from *m/z* 620 – 900 amu, in FTMS mode, discriminating masses down to 0.1 ppm. Using the Orbitrap analyser, the accurate mass of PE-containing PGa was determined at the apex of elution of each PGa-PE species. The accurate mass along with the elemental composition of individual parent ions is shown in Figures 4.1 and 4.2. The mass accuracy was determined with a mass error ≤ 0.4 ppm, which is the difference between the theoretical and observed mass. The elemental composition of PGa-PE for *m/z* 770.4977, 796.5132, 798.5292 and 814.5243 were assigned as $C_{41}H_{73}O_{10}NP$, $C_{43}H_{75}O_{10}NP$, $C_{43}H_{77}O_{10}NP$ and $C_{43}H_{77}O_{11}NP$, respectively. The elemental composition of PGa-PE species minus *m/z* 351.2 ($C_{20}H_{32}O_5$) is consistent with the proposed PE structures described in Chapter 3, comprising 16:0p-PE ($C_{21}H_{41}O_5NP$), 18:1p-PE ($C_{23}H_{43}O_5NP$), 18:0p-PE ($C_{23}H_{45}O_5NP$) and 18:0a-PE ($C_{23}H_{45}O_6NP$). Note the presence of isotope peaks (containing one or more ^{13}C), characteristic of singly-charged species, in all four lipids.
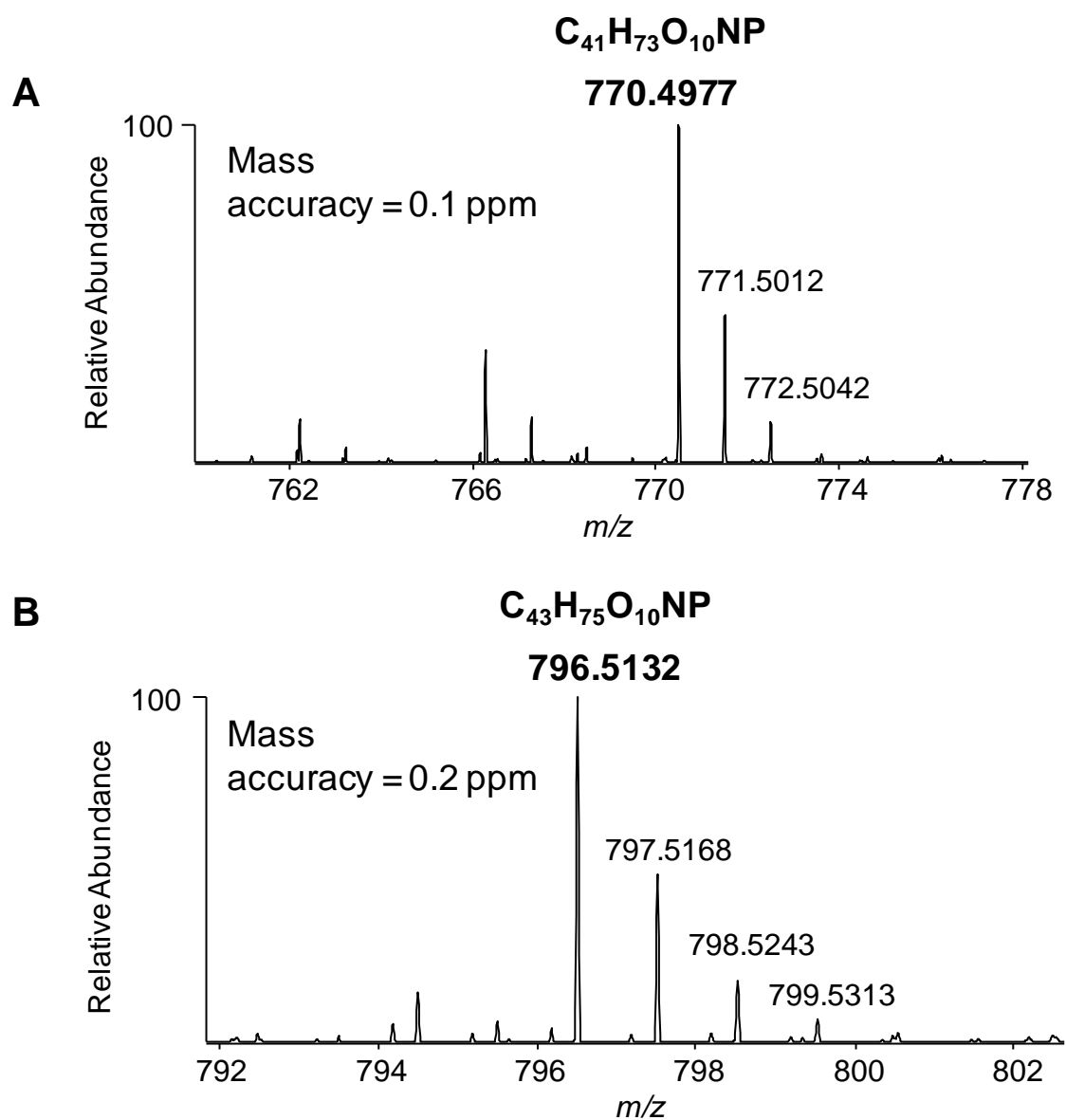
Figure 4.1: MS analysis monitoring the exact mass of *m/z* 770.4977 and 796.5132 showed isotope peaks characteristic of singly-charged species. Platelet lipid extracts were analysed in full scan mode, from 620 – 900 amu on the Orbitrap in FTMS mode at high resolution. *Panel A.* MS analysis showing exact mass of *m/z* 770.4977 and its isotope variants. *Panel B.* MS analysis showing exact mass of *m/z* 796.5132 and its isotope variants.
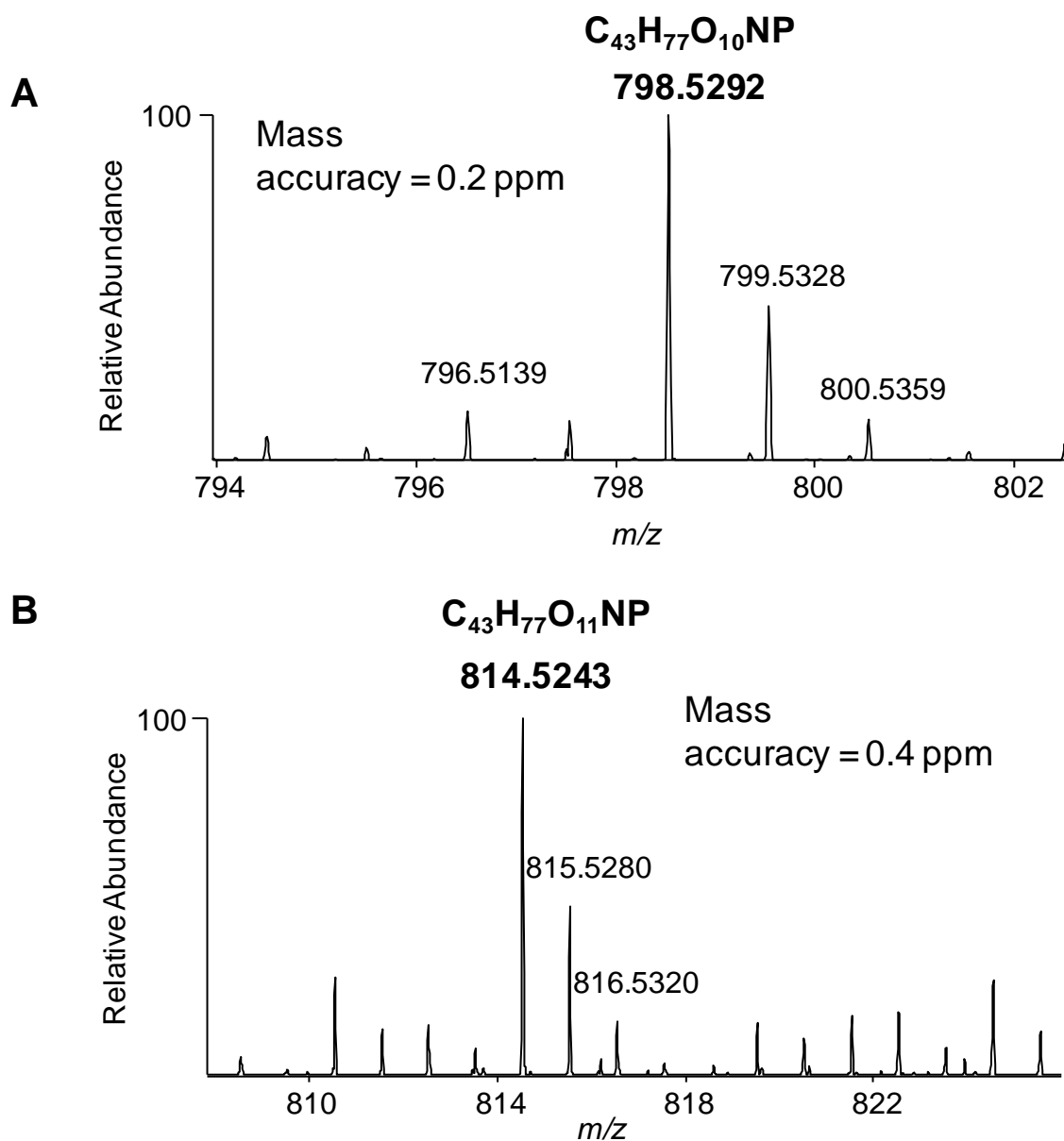
Figure 4.2: MS analysis monitoring the exact mass of *m/z* 798.5292 and 814.5243 showed isotope peaks characteristic of singly-charged species. Platelet lipid extracts were analysed in full scan mode, from 620 – 900 amu on the Orbitrap in FTMS mode at high resolution. *Panel A.* MS analysis showing exact mass of *m/z* 798.5292 and its isotope variants. *Panel B.* MS analysis showing exact mass of *m/z* 814.5243 and its isotope variants.

4.2.1.2 Targeted MS/MS analysis of PGa-PE species.

In this section, the structural characterisation of PGa attached to PEs will be performed using MS/MS of parent ions to obtain spectra of individual lipid species.

Targeted MS/MS was undertaken in FTMS mode, monitoring parent ions with accurate mass and fragmentation with higher collision dissociation (HCD). Spectra of parent ions were then compared to each other to confirm the presence of PGa attached at the sn2 position in all four PE species. Indeed, MS/MS spectra of PGa-PEs (770.6, 796.6, 798.6 and 814.7) yielded very similar fragmentation, with several daughter ions characteristic of either PGE_2 or PGD_2 (m/z 333, 315, 271, 233 and 189) present in all four PEs (Figures 4.3 and 4.4). The spectrum and fragmentation pattern of PGE_2 is shown for comparison in Figure 4.5. Note that upon HCD fragmentation, parent ions generate very small daughter ions of m/z 351.2, which can only be observed when the spectrum is enlarged using the zoom feature within the software. Although targeted MS/MS of parent ions showed product ions characteristic of PGE_2, further analysis was undertaken to confirm that m/z 333, 315, 271, 233 and 189 fragments did indeed originate from the fragmentation of the esterified m/z 351.2.
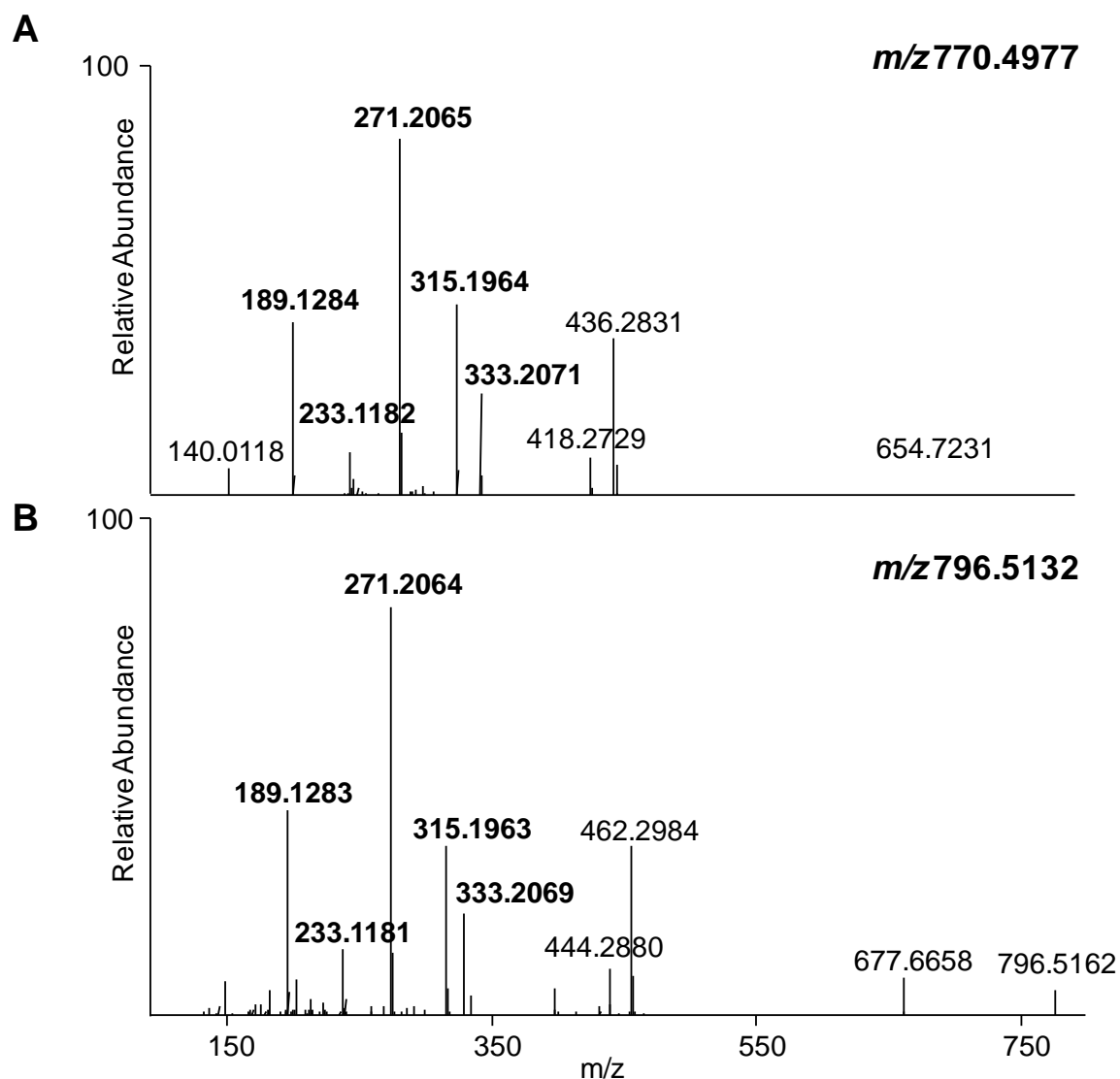
Figure 4.3: Targeted MS/MS analysis of PGa-PE shows daughter ions characteristic of PGE$_2$ and PGD$_2$. Platelet lipid extracts were separated using high resolution LC/MS/MS on the Orbitrap Velos, in FTMS mode, monitoring the exact mass, followed by targeted MS/MS using HCD. *Panel A*. LC/MS/MS spectrum acquired at the apex of elution of PGa-PE at 5.85 min, monitoring *m/z* 770.4977, generated fragments (shown in bold) representative of PGE$_2$ and PGD$_2$. *Panel B.* Negative LC/MS/MS spectrum acquired at the apex of elution of PGa-PE at 6.07 min, monitoring *m/z* 796.5132, generated fragments (shown in bold) characteristic of PGE$_2$ and PGD$_2$.
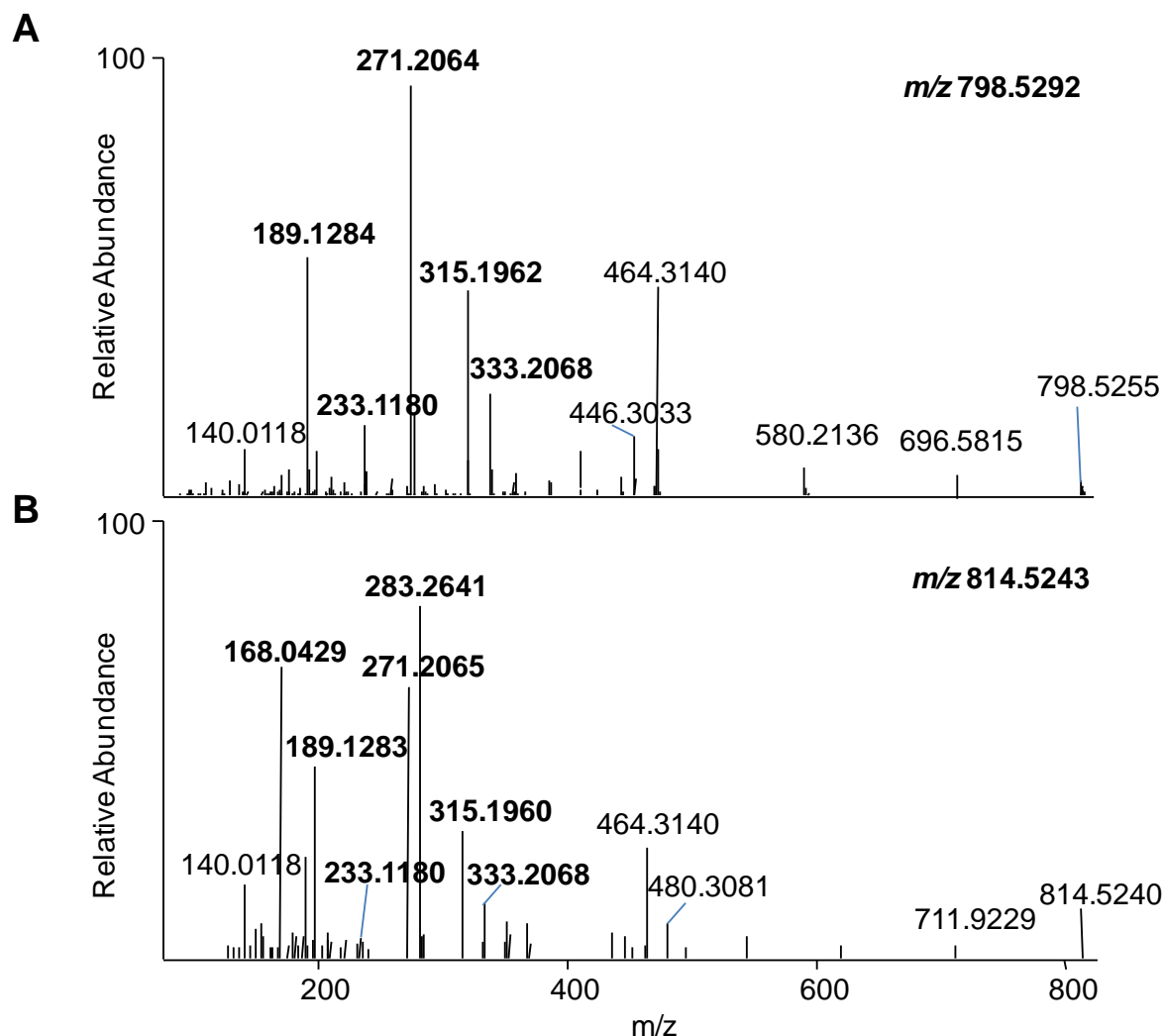
Figure 4.4: Targeted MS/MS analysis of PGa-PE shows daughter ions characteristic of PGE$_2$ and PGD$_2$. Platelet lipid extracts were separated using high resolution LC/MS/MS on the Orbitrap Velos, in FTMS mode, monitoring the exact mass, followed by targeted MS/MS using HCD. *Panel A*. LC/MS/MS spectrum acquired at the apex of elution of PGa-PE at 7.16 min, monitoring *m/z* 798.5292, generated fragments (shown in bold) representative of PGE$_2$ and PGD$_2$. *Panel B.* Negative LC/MS/MS spectrum acquired at the apex of elution of PGa-PE at 7.07 min, monitoring *m/z* 814.5243, generated fragments (shown in bold) characteristic of PGE$_2$ and PGD$_2$.
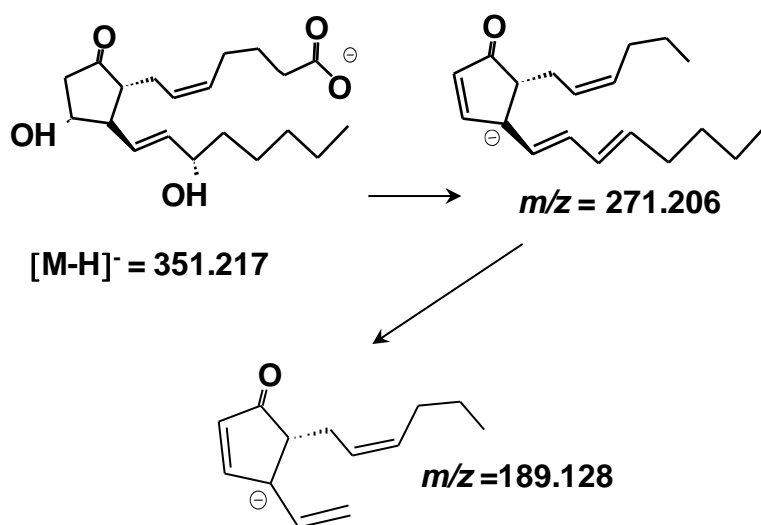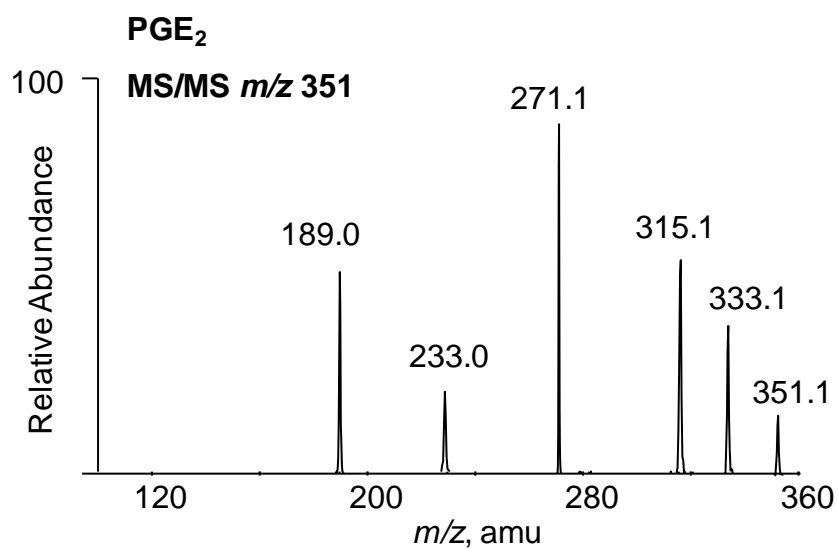
Figure 4.5: MS/MS spectrum of PGE₂. An MS/MS spectrum of PGE₂ standard was acquired using the Q-Trap 4000. Fragmentation shows the origin of daughter ions at *m/z* 271.2 and 189.1 (Murphy *et al.*, 2005).

4.2.1.3 Data dependent MS^3 analysis.

To confirm that fragments characteristic of PGE$_2$ or PGD$_2$ originated from the fragmentation of the *m/z* 351.2, data dependent MS^3 was performed on the Orbitrap platform. In these studies, ions with a *m/z* 351.2 originating from CID of individual precursor ions (770.6, 796.6, 798.6 and 814.7), in ion trap mode, were selectively isolated, fragmented and analysed, thus confirming that the characteristic PGE$_2$ and PGD$_2$ daughter ions originated from *m/z* 351.2 (Figures 4.6 and 4.7). This observation further suggested the presence of PGE$_2$ or PGD$_2$ attached to PE species (16:0p/, 18:1p/, 18:0p/ and 18:0a/). However, additional studies were required to exclude the possibility of other eicosanoids, such as isoprostanes, contributing to the MS/MS spectra, as described below.

4.2.1.4 Confirmation of esterified PGa as PGE$_2$ and PGD$_2$.

As described in detail in Section 4.2.1.2, MS^3 data suggested that esterified PGa was either PGE$_2$, PGD$_2$ or isoprostanes attached to PE, since these will all exhibit an identical molecular weight (*m/z* 351.2) and similar MS/MS fragmentation pattern. Stereoisomers such as PGE$_2$ and PGD$_2$, which differ only in the positioning of functional groups, cannot be discriminated simply by product ion spectra, but can be distinguished by HPLC separation. Thus, using the reverse-phase LC/MS/MS method described in Materials and Methods, Section *2.2.6*, lipid samples from activated platelets were analysed for prostaglandins with a *m/z* 351.2, both before and after hydrolysis of phospholipids.

Initially, generation of free prostaglandins and isoprostanes by thrombin-activated platelets was determined. Analysis using reverse-phase LC/MS/MS, monitoring *m/z* 351.2 → 271.2, revealed that activated platelets generated both PGE$_2$ and PGD$_2$, but not other E$_2$ isomers, including 8-iso-PGE$_2$ and 11β-PGE$_2$ (Figure 4.8).
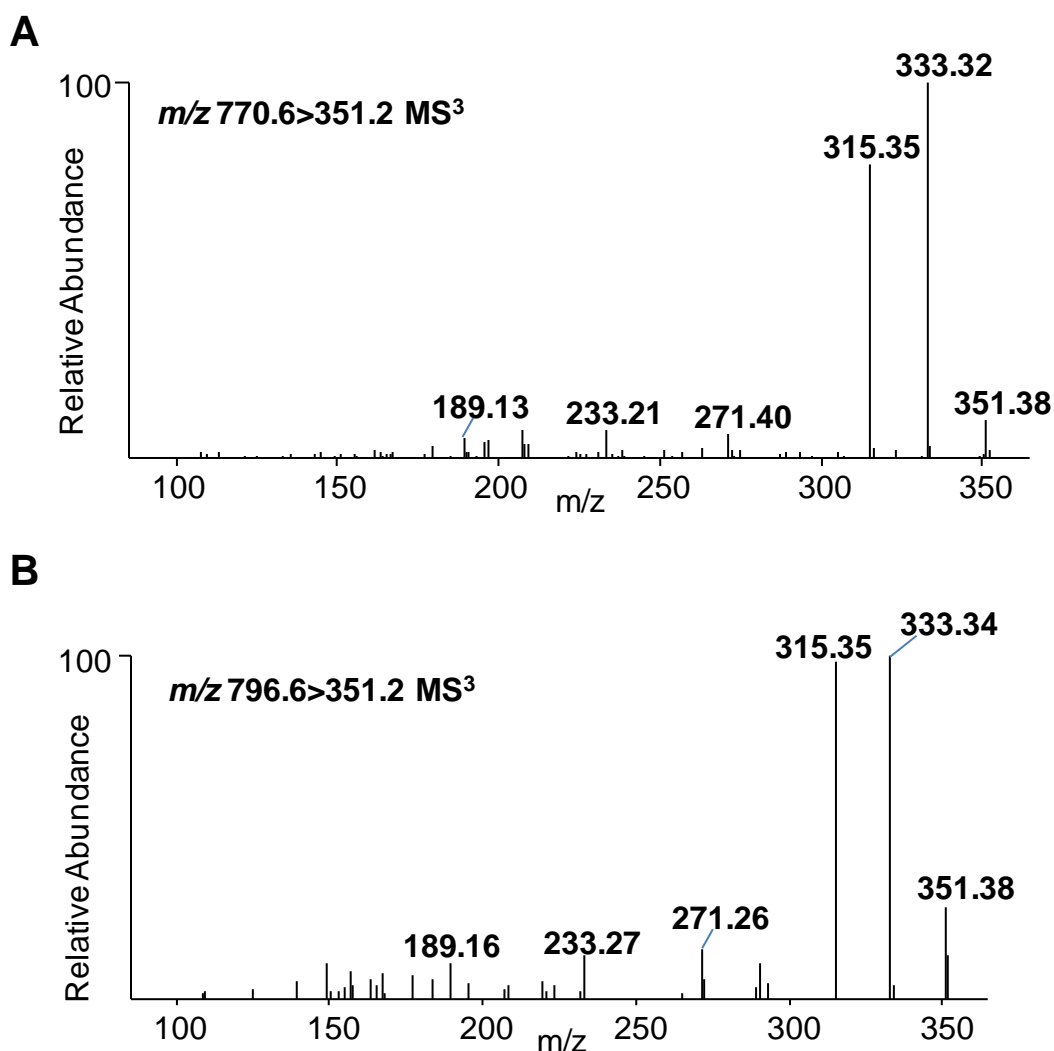
Figure 4.6: Confirmation that PGa-PE contains ions that belong to either PGE$_2$ or PGD$_2$.
MS[3] of parent PE lipids, by secondary fragmentation of daughter ion *m/z* 351.2, shows ions consistent with either PGE$_2$ or PGD$_2$. Platelet lipid extracts were separated using high resolution LC/MS/MS on the Orbitrap, with ITMS detection and targeted MS/MS of the parent mass, followed by data dependent fragmentation of the daughter ion *m/z* 351.2, using CID. *Panel A.* Targeted MS/MS of *m/z* 770.6 followed by data dependent fragmentation of *m/z* 351.2. *Panel B.* Targeted MS/MS of *m/z* 796.6 followed by data dependent fragmentation of *m/z* 351.2.
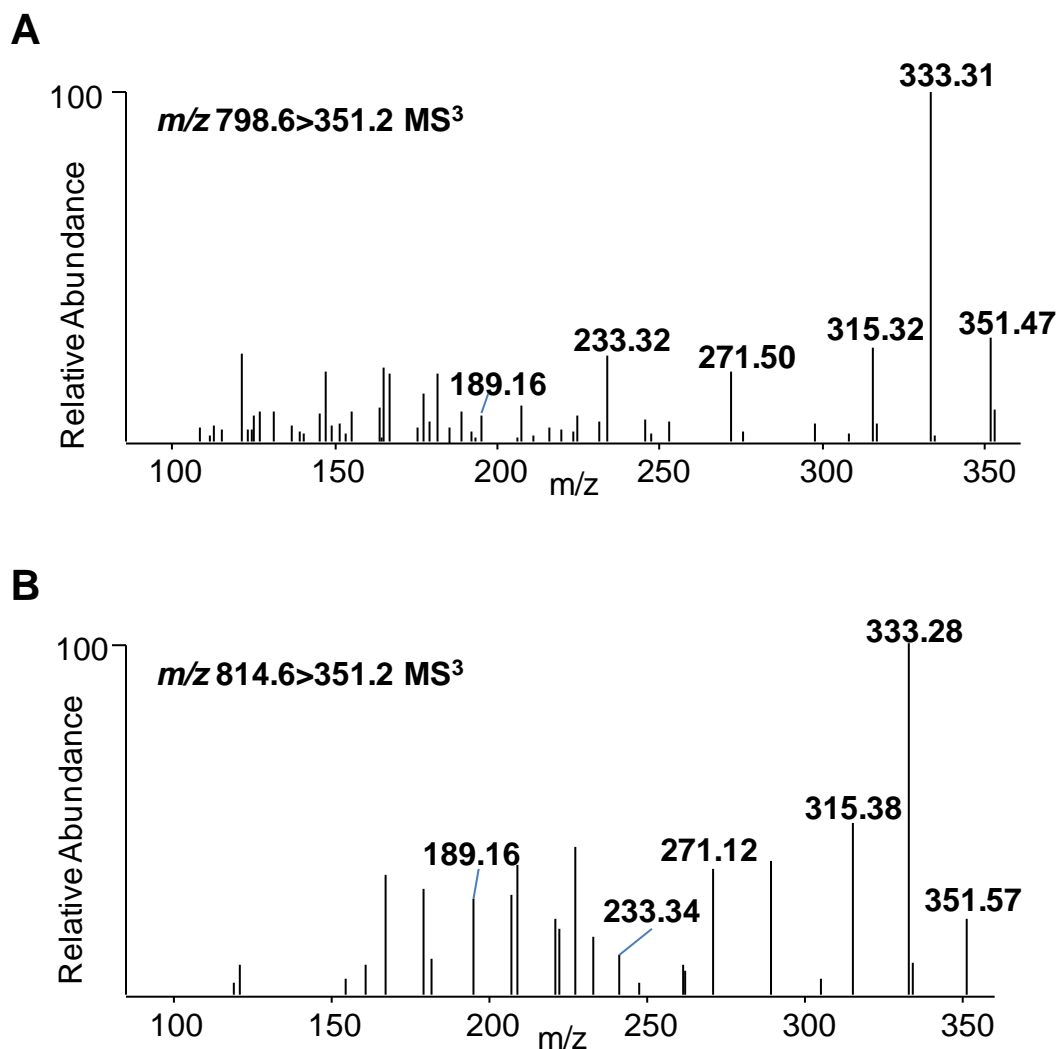
Figure 4.7: Confirmation that PGa-PE contains ions that belong to either PGE$_2$ or PGD$_2$.
MS^3 of parent PE lipids, by secondary fragmentation of daughter ion m/z 351.2, shows ions consistent with either PGE$_2$ or PGD$_2$. Lipid extracts were separated using high resolution LC/MS/MS on the Orbitrap platform, with ITMS detection and targeted MS/MS of the parent mass, followed by data dependent MS/MS of daughter ion m/z 351.2, using CID fragmentation. *Panel A.* Targeted MS/MS of m/z 798.6 followed by data dependent fragmentation of m/z 351.2. *Panel B.* Targeted MS/MS of m/z 814.7 followed by data dependent fragmentation of m/z 351.2.
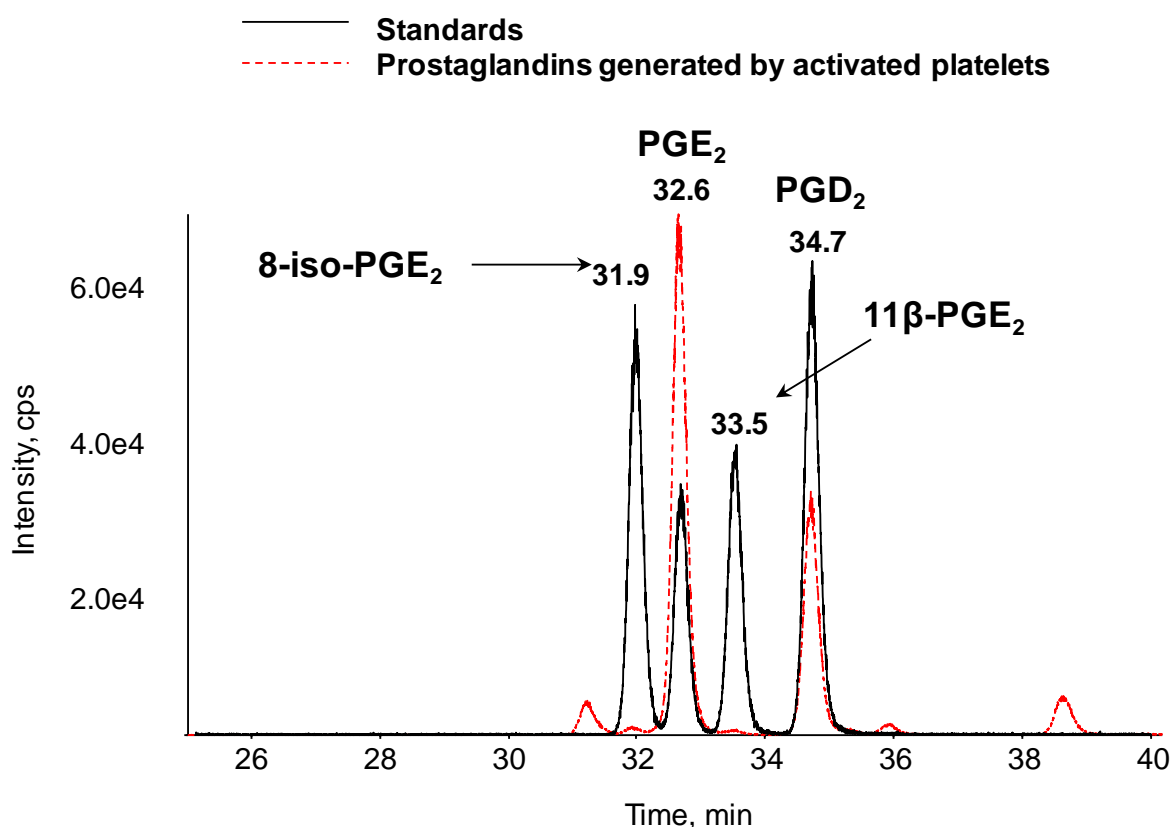
Figure 4.8: Analysis of free prostaglandins generated by activated human platelets demonstrates both PGE$_2$ and PGD$_2$ formation. Washed human platelets were activated with thrombin (0.2 U/ml) for 30 min at 37°C followed by lipid extraction. Free PGE$_2$ and PGD$_2$ isomer composition was determined by comparison with prostaglandin standards. Black solid line, prostaglandin standards. Red dashed line, oxidised fatty acids generated by activated platelets.

To establish whether PGa was PGE$_2$, PGD$_2$ or another isoprostane, platelets were activated with 10 µM of calcium ionophore, which induces higher levels of phospholipid-esterified eicosanoids than thrombin, for 30 min at 37°C (Thomas *et al.*, 2010). PE-containing esterified *m/z* 351.2 molecules were then purified from platelet lipid extracts using HPLC-UV, as described in Materials and Methods, Section *2.2.4*. Purified PGa-PEs were hydrolysed using snake venom PLA$_2$ and analysed using reverse-phase LC/MS/MS, as described in Material and Methods, Sections *2.2.5* and *2.2.6*.

For identification of prostaglandin isomers, the retention time of prostaglandins released from saponified PGa-PEs was compared to that of 8-iso-PGE$_2$, 11β-PGE$_2$, PGE$_2$ and PGD$_2$ standards. As with free platelet prostaglandins, primarily PGE$_2$ and PGD$_2$ were detected (Figure 4.9). However, smaller peaks with *m/z* 351.2 $\rightarrow$ 271.2, which could originate from different isoprostanes, were observed to elute later in the chromatogram. This indicates that PGa-PE comprises a mix of PEs with predominantly PGE$_2$ or PGD$_2$ attached (Scheme 4.1 and 4.2).

As described during Chapter 3, the detection of PGa-PE (PGE$_2$-PE and PGD$_2$-PE) by MRM mode using *m/z* 351.2 as a product ion was not possible, as the ion *m/z* 351.2 did not survive CID fragmentation. This problem was resolved by using *m/z* 271.2 instead as product ion, which allowed monitoring of all four PEs (Figures 4.10). Furthermore, since PGE$_2$-PE and PGD$_2$-PE co-elute and could not be separated using reverse-phase HPLC, each PGE$_2$ and PGD$_2$ pair, such as 16:0p/PGE$_2$-PE and 16:0p/PGD$_2$-PE, is reported as a single species (e.g. 16:0p/PGE$_2$/D$_2$-PE) in later studies.
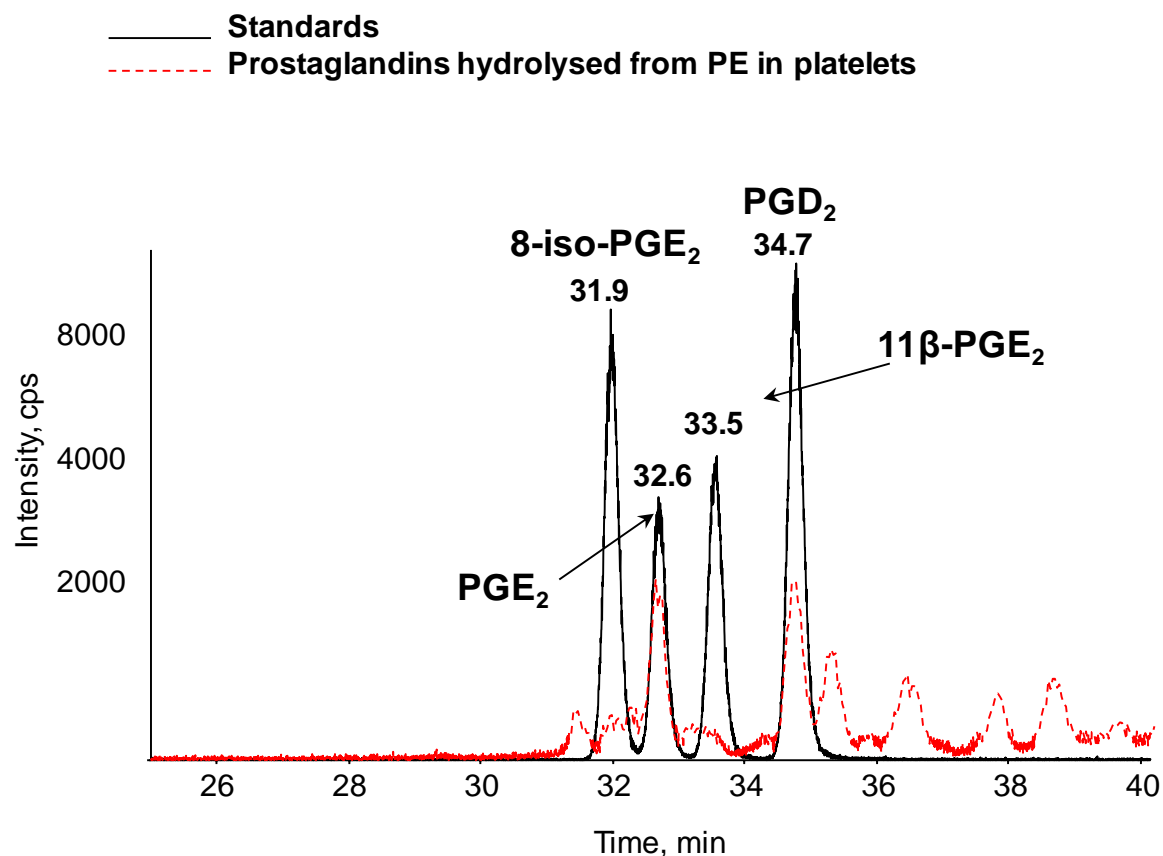
Figure 4.9: Analysis of hydrolysed PGa-PE generated by activated human platelets demonstrates both PGE₂ and PGD₂. Washed human platelets were activated with calcium ionophore (10 µM) for 30 min at 37°C followed by lipid extraction. Phospholipid-containing esterified *m/z* 351.2 molecules were purified using normal-phase HPLC-UV, where fractions were collected every 60 sec and analysed using the Q-trap with no column attached for prostaglandin-PEs. Following purification, PGa-PE species were saponified with 200 µg of snake venom (PLA₂). Hydrolysed fatty acids were then analysed for prostaglandins using reverse-phase LC/MS/MS. Black solid line, prostaglandin standards. Red dashed line, oxidised fatty acids released from platelet PE.

A

$[M-H]^- = 770.6$ 16:0p/PGE$_2$-PE

B

$[M-H]^- = 796.6$ 18:1p/PGE$_2$-PE

C

$[M-H]^- = 798.6$ 18:0p/PGE$_2$-PE

D
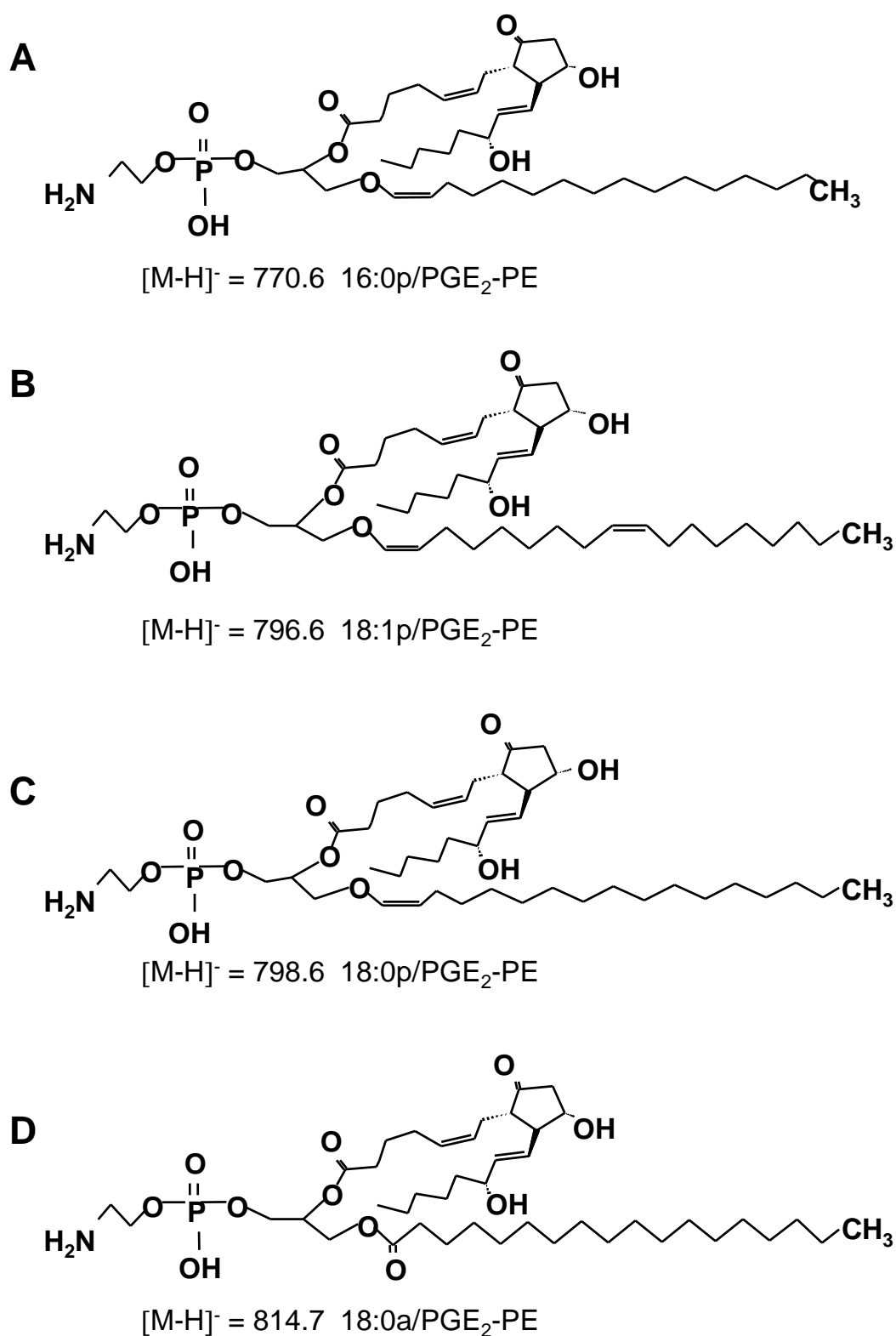
$[M-H]^- = 814.7$ 18:0a/PGE$_2$-PE

Scheme 4.1: Structures of PGE$_2$-PEs identified in activated human platelets.

A
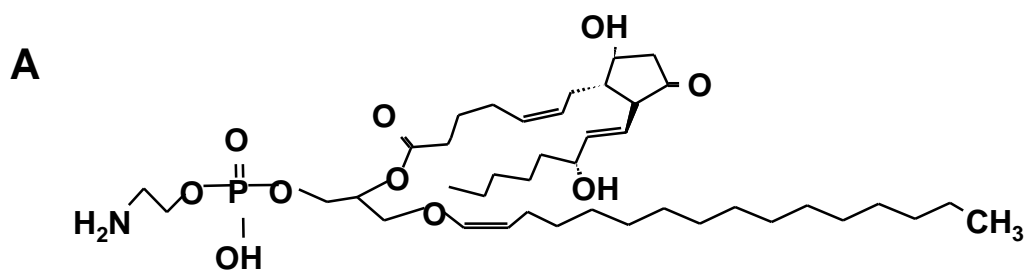
[M-H]⁻ = 770.6   16:0p/PGD$_2$-PE

B
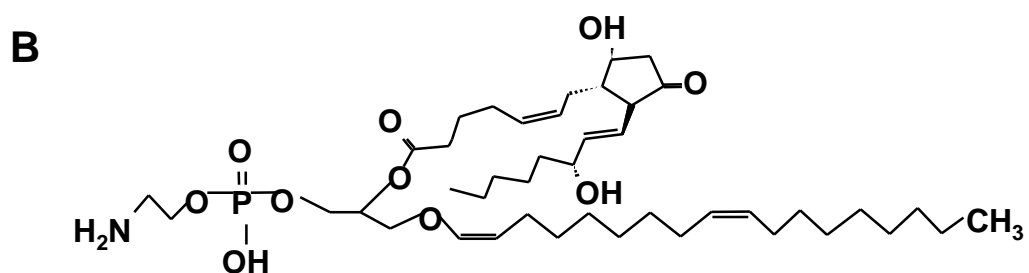
[M-H]⁻ = 796.6   18:1p/PGD$_2$-PE

C
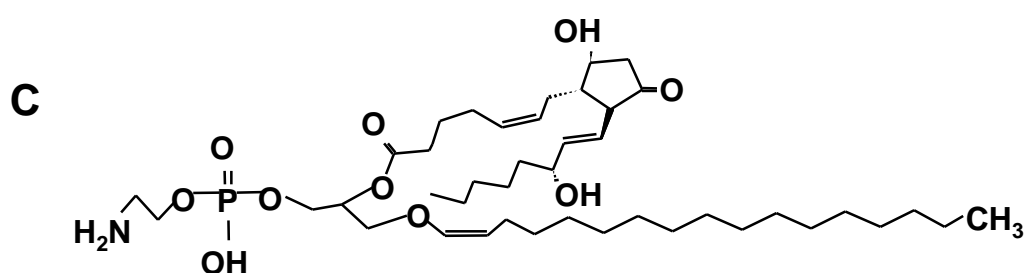
[M-H]⁻ = 798.6   18:0p/PGD$_2$-PE

D
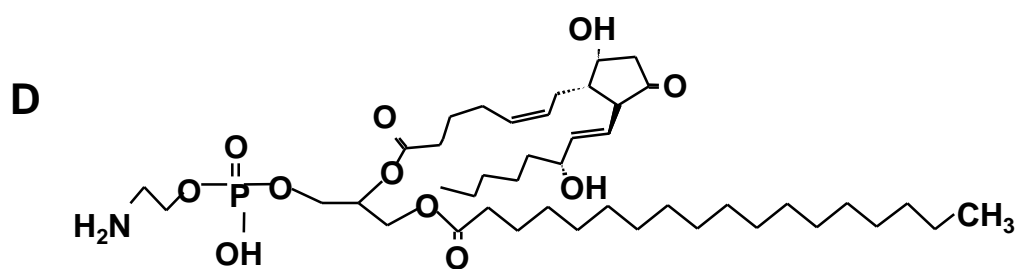
[M-H]⁻ = 814.7   18:0a/PGD$_2$-PE

Scheme 4.2: Structures of PGD$_2$-PEs identified in activated human platelets.

A 16:0p/PGE$_2$/D$_2$-PE

m/z = 770.6/271.2

B 18:1p/PGE$_2$/D$_2$-PE

m/z = 796.6/271.2

C 18:0p/PGE$_2$/D$_2$-PE

m/z = 798.6/271.2

D 18:0a/PGE$_2$/D$_2$-PE

m/z = 814.7/271.2
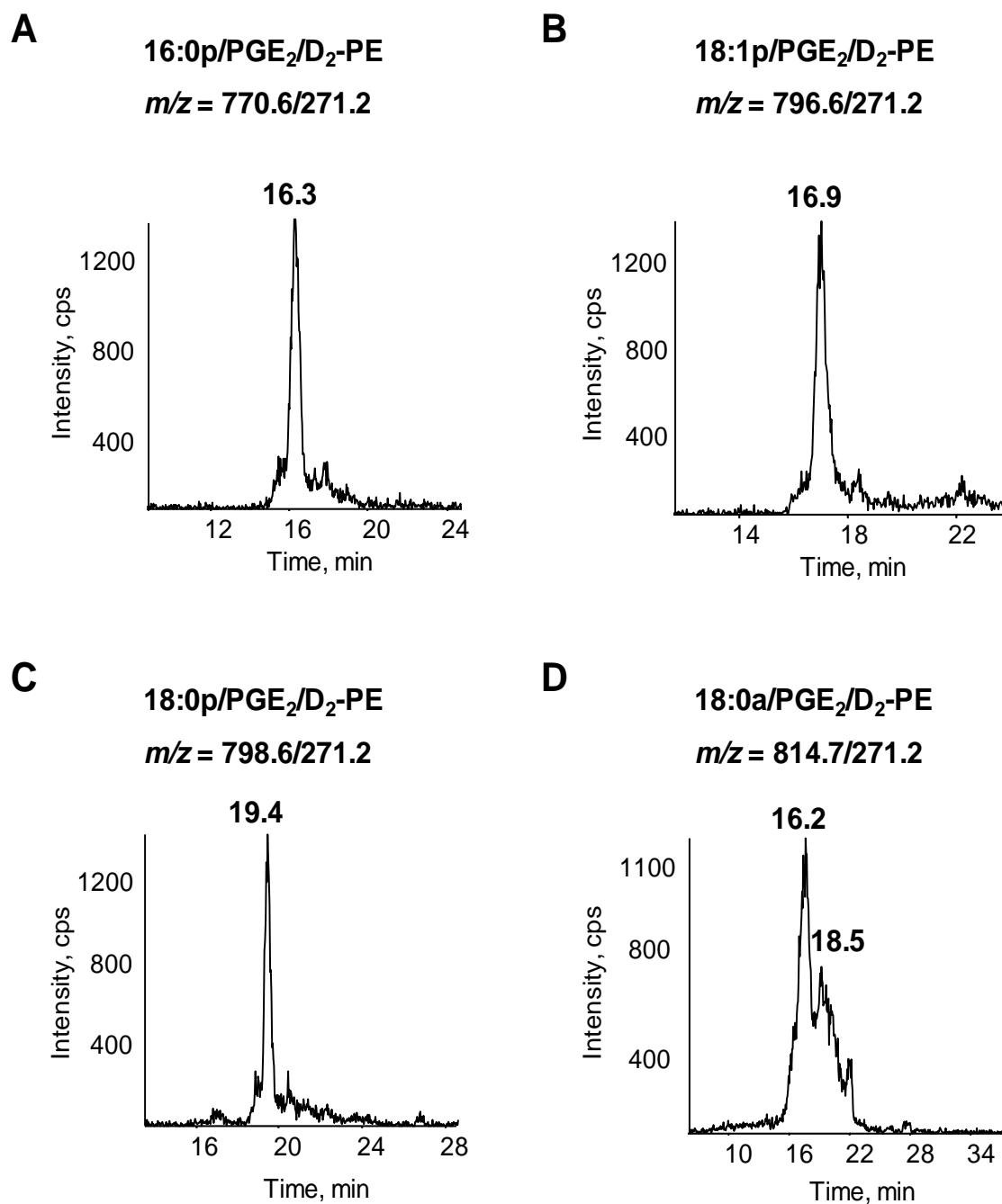
Figure 4.10: Analysis of PGE$_2$/D$_2$-PEs using LC/MS/MS. Platelet lipid extracts were separated using LC/MS/MS as described in Methods and Materials, section *2.2.3.2*, and detected on the Q-Trap platform by parent [M-H]$^-$ → *m/z* 271.2.

4.2.2   Synthesis of biogenic standards for PGE$_2$/D$_2$-PE quantification in platelet samples.

Quantification of new families of OxPLs is crucial to enable investigation of their biological activity. Due to the absence of commercial PGE$_2$/D$_2$-PE standards, routine quantification of PGE$_2$/D$_2$-PEs in platelet samples was not possible. To overcome this, I generated PGE$_2$/D$_2$-PE standards through activating platelets, isolating PGE$_2$/D$_2$-PEs and then measuring PGE$_2$ and PGD$_2$ attached to PEs following hydrolysis, as described in Materials and Methods, Section *2.2.7*.

Briefly, washed human platelets were activated with calcium ionophore and lipids extracted. Platelet lipid extracts containing PGE$_2$/D$_2$-PEs were then resuspended in 400 μl methanol. From this, 200 μl was used to quantify PGE$_2$/D$_2$-PEs in the biogenic standard and the remaining 200 μl aliquot later used to construct PGE$_2$/D$_2$-PE standard curves. To quantify PGE$_2$/D$_2$-PEs in the biogenic standard a 100 μl aliquot was hydrolysed with PLA$_2$ and the other 100 μl incubated with hydrolysis buffer only, as control. PGE$_2$ was quantified by direct comparison of its integrated peak area, in counts per second (cps), to that generated by 2 ng of PGE$_2$-d$_4$, added prior to lipid extraction. Similarly, PGD$_2$ was quantified. The amount of PGE$_2$ detected in the hydrolysed and control (non-hydrolysed) samples was calculated using the following equation:

$$PGE_{2\ (ng)} = \frac{PGE_{2(cps)}}{PGE_2-d_{4(cps)}} \cdot 2 \text{ ng (PGE}_2\text{-d}_4)$$

The amount of free PGE$_2$ and PGD$_2$ detected in the hydrolysed sample minus the amount detected in the control (non-hydrolysed) sample represented the total PGE$_2$ and PGD$_2$ in nanograms (ng) released from saponified PGE$_2$/D$_2$-PEs. Thus, 0.519 ng of PGE$_2$ and 0.28 ng of PGD$_2$ were released from PGE$_2$/D$_2$-PEs, giving a total of 0.799 ng.

However, PLA$_2$ hydrolysis was less than 100 % and some esterified prostaglandins remained attached to PE. To determine the hydrolysis efficiency the integrated peak areas of all four PGE$_2$/D$_2$-PE species in the control sample were summed, which was defined as the total amount of PGE$_2$/D$_2$-PE (in cps) before hydrolysis. The integrated peak

areas of all four PGE$_2$/D$_2$-PE species in the hydrolysed sample were also summed and defined as the total amount of PGE$_2$/D$_2$-PE (in cps) remaining after hydrolysis. Finally, the overall efficiency of the enzyme hydrolysis could then be calculated using the following equation:

$$PGE_2D_{2^h\ (\%)} = \frac{PL:PGE_2/D_{2^t\ (cps)} - PL:PGE_2/D_{2^h\ (cps)}}{PL:PGE_2/D_{2^t\ (cps)}}$$

Where:

$PGE_2D_{2^h\ (\%)}$ is the fraction of the total PGE$_2$/D$_2$ released from PEs by hydrolysis.

$PL:PGE_2/D_{2^t\ (cps)}$ is the total amount observed for all four PGE$_2$/D$_2$-PE species before hydrolysis.

$PL:PGE_2/D_{2^h\ (cps)}$ is the total amount remaining for all four PGE$_2$/D$_2$-PE species after hydrolysis.

In this equation, it is assumed that each of the four phospholipids involved give the same value (in cps) for the integrated area of the mass peak when at the same concentration. From this, I established that 69.5 % of PGE$_2$ and PGD$_2$ were released from esterified PGE$_2$/D$_2$-PEs in the standard sample.

To determine the amount (in nanograms) of each PGE$_2$/D$_2$-PE species in the biogenic standard, the relative contribution of each PGE$_2$/D$_2$-PE species to the total PGE$_2$/D$_2$-PE in the control sample was calculated using the following equation:

$$PL:PGE_2D_{2(\%)} = \frac{PL:PGE_2D_{2(cps)}}{PL:PGE_2/D_{2^t\ (cps)}}$$

Where:

$PL{:}PGE_2D_{2(\%)}$ is the relative contribution of each PGE$_2$/D$_2$-PE species to the total PGE$_2$/D$_2$-PE in the control sample.

$PL{:}PGE_2D_{2(cps)}$ is the integrated area of each PGE$_2$/D$_2$-PE mass peak in the control sample.

$PL{:}PGE_2/D_{2^t\,(cps)}$ is the total integrated peak area of all four PGE$_2$/D$_2$-PE species in the control sample.

In summary, the contribution of each PGE$_2$/D$_2$-PE species in the control sample equated to 24 % (16:0p/PGE$_2$/D$_2$-PE), 24 % (18:1p/PGE$_2$/D$_2$-PE), 42 % (18:0p/PGE$_2$/D$_2$-PE) and 10 % (18:0a/PGE$_2$/D$_2$-PE). Last, the total amount of PGE$_2$ ($PGE_{2^t\,(ng)}$) attached to PEs before hydrolysis was calculated.

$$PGE_2D_{2^t\,(ng)} \; = \; \frac{PGE_2D_{2^h\,(ng)}.\,100}{PL{:}PGE_2/D_{2^h\,(\%)}}$$

Where:

$PGE_2D_{2^t\,(ng)}$ is the total PGE$_2$ and PGD$_2$ in nanograms attached to PE before hydrolysis.

$PGE_2D_{2^h\,(ng)}$ is the amount of PGE$_2$ and PGD$_2$ (0.799 ng) released after hydrolysis.

$PL{:}PGE_2/D_{2^h\,(\%)}$ is the overall hydrolysis efficiency (69.5 %) of total PGE$_2$ and PGD$_2$ released from esterified PGE$_2$/D$_2$-PEs.

Based on the equation described above, a total of 1.15 ng of PGE$_2$ and PGD$_2$ were attached to PE before hydrolysis. Next, the amount of PGE$_2$/D$_2$ attached to each phospholipid PE species before hydrolysis was calculated using the following equation:

$$PGE_2D_{2(ng)} = \frac{PGE_2D_{2^t\,(ng)}.PL{:}PGE_2/D_{2(\%)}}{100}$$

Where:

$PGE_2D_{2\,(ng)}$ is the amount PGE$_2$ and PGD$_2$ in nanograms attached to each PE species before hydrolysis.

$PGE_2D_{2^t\,(ng)}$ is the total PGE$_2$ and PGD$_2$ (1.15 ng) attached to PE before hydrolysis.

$PL{:}PGE_2/D_{2\,(\%)}$ is the contribution of individual PGE$_2$/D$_2$-PE species to the total PGE$_2$/D$_2$-PE in the control sample.

Before hydrolysis, 0.276 ng of PGE$_2$/D$_2$ was attached to each of 16:0p/PGE$_2$/D$_2$-PE and 18:1p/PGE$_2$/D$_2$-PE species. Similarly, 0.488 and 0.111 ng of PGE$_2$/D$_2$ was esterified to 18:0p/PGE$_2$/D$_2$-PE and of 18:0a/PGE$_2$/D$_2$-PE, respectively. The nanogram amount of each PGE$_2$/D$_2$-PE species in the original biogenic standard was then calculated using the following equation:

$$PL{:}PGE_2/D_{2\,(ng)} = \frac{PGE_2D_{2(ng)}.PL{:}PGE_2/D_{2\,(MW)}}{351.2}$$

Where:

$PL{:}PGE_2/D_{2\,(ng)}$ represents individual PGE$_2$/D$_2$-PE species in nanograms.

$PGE_2/D_{2\,(ng)}$ is the amount of PGE_2 and PGD_2 in nanograms attached to each PE species before hydrolysis.

$PL{:}PGE_2/D_{2\,(MW)}$ is the molecular weight (MW) of each PGE_2/D_2-PE species.

351.2 is the molecular weight of PGE_2 and PGD_2.

The total amount of PGE_2/D_2-PEs found in 400 µl of biogenic standard, generated from activated platelets, corresponded to 10.39 ng. Comparison of integrated areas of PGE_2/D_2-PEs indicated that this corresponded to 3.18, 2.64, 3.93 and 0.64 ng of 16:0p/PGE_2/D_2-PE, 18:1p/PGE_2/D_2-PE, 18:0p/PGE_2/D_2-PE and 18:0a/PGE_2/D_2-PE, respectively.

To quantify PGE_2/D_2-PE species in platelet samples, seven serial dilutions of the biogenic standard in methanol were initially prepared to give a final amount of 70, 140, 280, 360, 1,130, 2,260 and 4,520 pg per 200 µl volume. Subsequently, a standard curve was constructed by adding a 100 µl aliquot of each serial dilution (35 – 2,260 pg of total PGE_2/D_2-PEs) to 500 pg DMPE (in 100 µl methanol), comprising a total final volume of 200 µl, of which 20 µl was injected into the column (50 pg DMPE and 3.5 – 226 pg of total PGE_2/D_2-PEs). The specific amounts of each PGE_2/D_2-PE species injected into the column were as follows: 0 - 67.3 pg (16:0p/PGE_2/D_2-PE), 0 - 57.8 pg (18:1p/PGE_2/D_2-PE), 0 - 86.2 pg (18:0p/PGE_2/D_2-PE) and 0 - 14.4 pg (18:0a/PGE_2/D_2-PE).

Before quantification in platelet samples, the analytical limit of detection of each PGE_2/D_2-PE species in the biogenic standard curve was estimated using the lowest concentration in the standard (Table 4.1). A signal was judged to be above the limit of detection if the peak area was three times the signal of the noise above baseline. The limit of detection of each individual PGE_2/D_2-PE species was found to be between 2.35 - 3.7 pg on the column, as listed in Table 4.1.

Analysed Transition [M-H]⁻	Phospholipids	Limit of detection (pg)
770.6/271.2	16:0p/PGE$_2$/D$_2$-PE	3.7
796.6/271.2	18:1p/PGE$_2$/D$_2$-PE	2.35
798.6/271.2	18:0p/PGE$_2$/D$_2$-PE	3.53
814.7/271.2	18:0a/PGE$_2$/D$_2$-PE	3.05

Table 4.1: Estimated limit of detection for PGE$_2$/D$_2$-PEs. The limit of detection was estimated for each PGE$_2$/D$_2$-PE species using reverse-phase LC/MS/MS, monitoring parent [M-H]⁻ → *m/z* 271.2, as described in Materials and Methods, Section *2.2.3.2*.

Quantification of PGE$_2$/D$_2$-PEs in platelet samples is fundamental for elucidation of their biological activity, as functional assays using inaccurate amounts could lead to misleading results. For example, underestimating quantity of PGE$_2$/D$_2$-PEs could result in lack of perceived effect, while overestimating amounts could lead to non-biological effects or toxicity. To determine the amounts of PGE$_2$/D$_2$-PEs generated by platelets, I isolated and activated washed platelets from five unrelated healthy volunteers, as described in Materials and Methods, Section *2.2.1* and *2.2.2*. Platelets were activated using 0.2 U/ml of thrombin for 30 min at 37°C, and lipids extracted. To account for differences in PGE$_2$/D$_2$-PE recovery during extraction, DMPE was added to the samples prior to lipid extraction. DMPE was used as an internal standard as it represents a phospholipid PE in structure to PGE$_2$/D$_2$-PEs, which is not present in platelets. Following extraction, platelet lipid extracts were analysed using reverse-phase LC-MS/MS.

For lipid quantification, the ratio of analyte to internal standard is calculated for both the standard curve and the analyte (e.g. PGE$_2$/D$_2$-PE) to account for lipid losses during lipid extraction. However, analysis of the DMPE in PGE$_2$/D$_2$-PE standard curves demonstrated

that the assay sensitivity was compromised by ion suppression of DMPE, caused by co-elution of endogenous components. Note that PGE_2/D_2-PE standard curves were generated from non-purified platelet lipid extracts (to avoid lipid losses) and, therefore, other phospholipids were co-eluting with DMPE, resulting in unwanted ion suppression. This meant that the ratio of analyte to internal standard (PGE_2/D_2-PE:DMPE) for the standard curve could not be calculated and, consequently, DMPE values in platelet samples could not be taken into account. As the problem of ion suppression could not be solved, each PGE_2/D_2-PE species in platelet samples was quantified by directly comparing its integrated peak area (in cps) to that of the standard curve. Furthermore, standard curve samples were subjected to the same lipid extraction procedure applied to the platelet samples to account for similar losses during lipid extraction. Analysis of the standard curves showed some abnormalities (not linear at low concentrations) (Figures 4.11 and 4.12). This was likely due to lower lipid recovery at low concentrations of PGE_2/D_2-PEs.

A

[M-H]⁻= 770.6/271.2
16:0p/PGE₂/D₂-PE

y-axis: 16:0p/PGE₂/D₂-PE (cps)
x-axis: 16:0p/PGE₂/D₂-PE (pg)

B

[M-H]⁻= 796.6/271.2
18:1p/PGE₂/D₂-PE

y-axis: 18:1p/PGE₂/D₂-PE (cps)
x-axis: 18:1p/PGE₂/D₂-PE (pg)
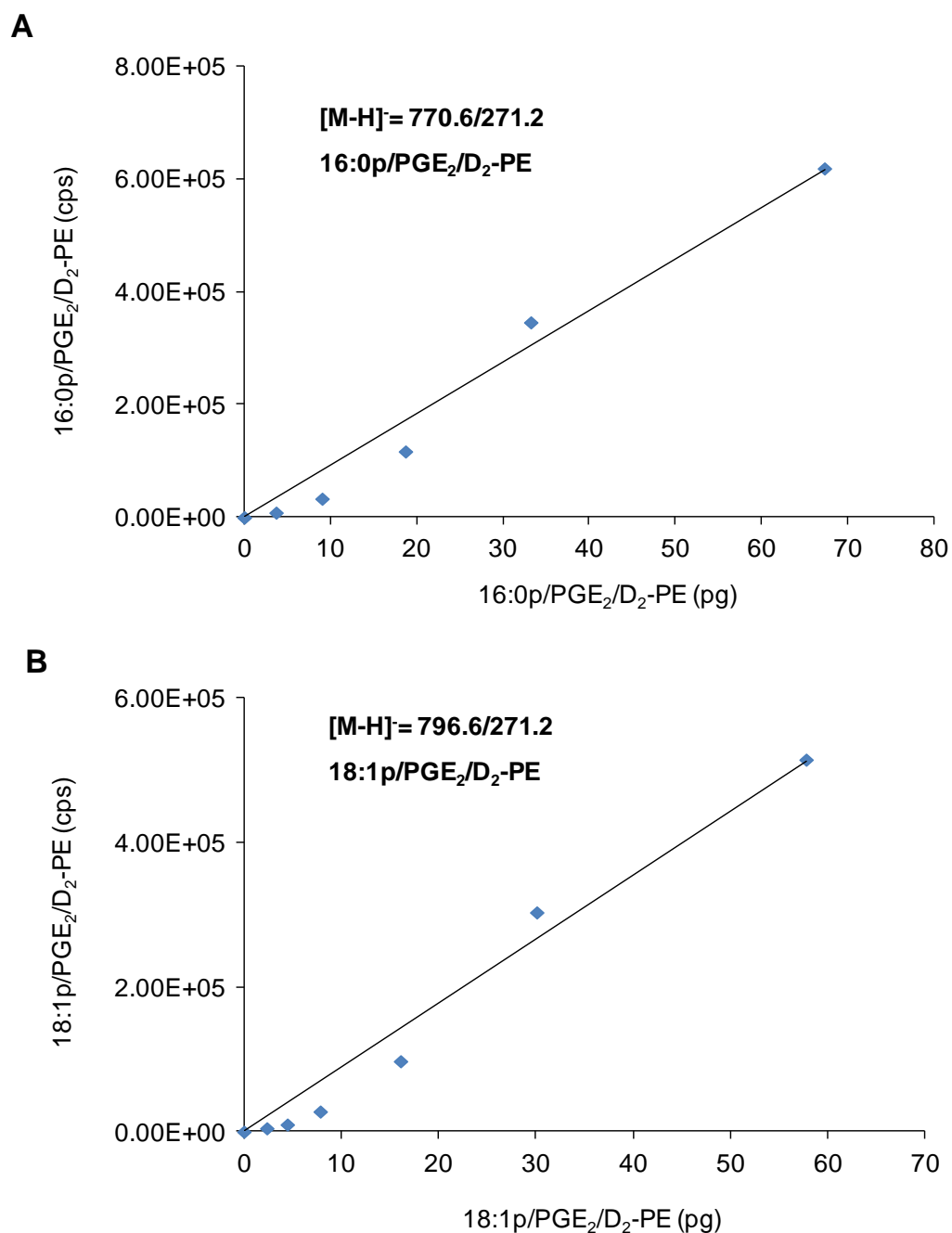
Figure 4.11: Standard curves for 16:0p/PGE₂/D₂-PE and 18:1p/PGE₂/D₂-PE biogenic standards. Biogenic standard curves were analysed by LC/MS/MS as described in Material and Methods, Section *2.2.3.2*. The integrated peak area of each PGE₂/D₂-PEs was plotted against the amount injected into the column. *Panel A*. Standard curve for 16:0p/PGE₂/D₂-PE biogenic standard. *Panel B*. Standard curve for 18:1p/PGE₂/D₂-PE biogenic standard.
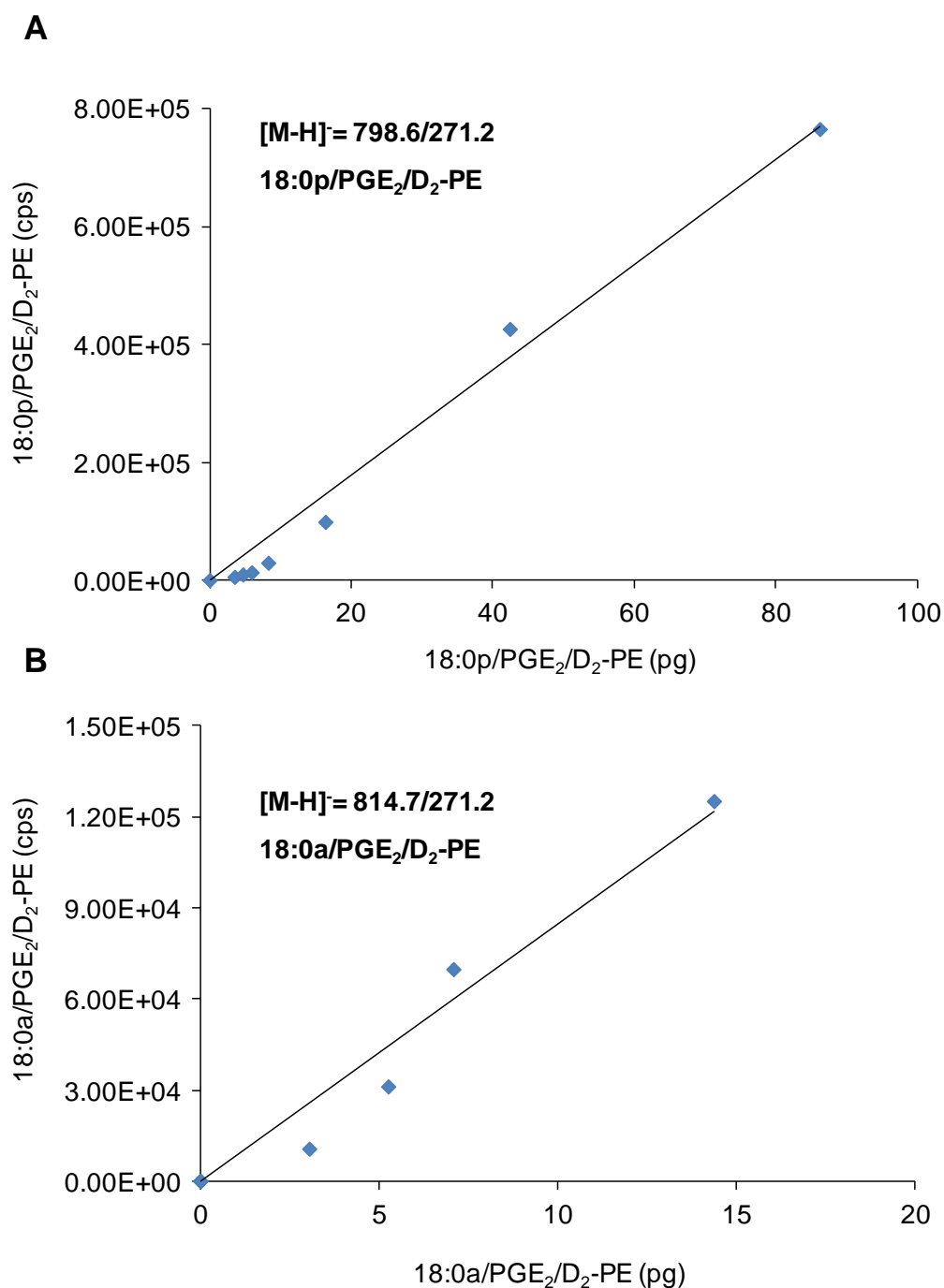
Figure 4.12: Standard curves for 18:0p/PGE₂/D₂-PE and 18:0a/PGE₂/D₂-PE biogenic standards. Biogenic standard curves were analysed by LC/MS/MS as described in Material and Methods, Section *2.2.3.2*. The integrated peak area of each PGE₂/D₂-PEs was plotted against the amount injected into the column. *Panel A*. Standard curve for 18:0p/PGE₂/D₂-PE biogenic standard. *Panel B*. Standard curve for 18:0a/PGE₂/D₂-PE biogenic standard.

To quantify PGE$_2$/D$_2$-PEs in platelet samples, the peak area (cps) of each PGE$_2$/D$_2$-PEs in platelet samples was initially integrated and compared to the standard curve. Next, the slope was calculated by finding the ratio of the "vertical change (in cps)" divided by the "horizontal change (in pg)" between the two closest points on the standard curve to the PGE$_2$/D$_2$-PE sample. This was done because the curve was not linear across all amounts of standard, as follows:

$$Slope: m = \frac{Y_2 - Y_1}{X_2 - X_1}$$

Last, the amount of each PGE$_2$/D$_2$-PEs in platelet samples was calculated using the following linear equation:

$$Y = mX \quad \text{This can be rearranged to:} \quad X = \frac{Y}{m}$$

Where:

X is the amount of PGE$_2$/D$_2$-PE in pg.

Y is the integrated peak area of PGE$_2$/D$_2$-PEs.

m is the slope.

Following quantification of each PGE$_2$/D$_2$-PE species, the total amount of PGE$_2$/D$_2$-PEs generated in response to thrombin was 28.1 ± 2.3 pg/2 × 10^8 platelets, whereas free PGE$_2$ and PGD$_2$ was 6.21 ± 0.312 ng/2 × 10^8 platelets (mean ± SEM, five genetically unrelated healthy donors), Table 4.2 and 4.3.

Analysed Transition $[M-H]^-$	Phospholipids	Mean pg/2x 10^8 platelets	SEM	N
770.6/271.2	16:0p/PGE$_2$/D$_2$-PE	7.051	± 0.711	5
796.6/271.2	18:1p/PGE$_2$/D$_2$-PE	8.178	± 0.913	5
798.6/271.2	18:0p/PGE$_2$/D$_2$-PE	9.54	± 0.523	5
814.7/271.2	18:0a/PGE$_2$/D$_2$-PE	3.302	± 0.155	5
Total	PGE$_2$/D$_2$-PEs	28.1	± 2.3	5

Table 4.2: PGE$_2$/D$_2$-PE quantification by LC/MS/MS. Washed human platelets were activated with 0.2 U/ml thrombin for 30 min at 37°C, in the presence of 1 mM CaCl$_2$. Lipids were then extracted and analysed using reverse-phase LC/MS/MS, monitoring parent $[M-H]^- \rightarrow$ *m/z* 271.2, as described in Materials and Methods, Section *2.2.3.2*. Levels of PGE$_2$/D$_2$-PEs are expressed as pg/2 x 10^8 platelets. Data is representative of five genetically unrelated healthy donors (n = 5, mean ± SEM).

Analysed Transition [M-H]$^-$	Prostaglandin	Mean ng/2x 10^8 platelets	SEM	N
351.2/271.2	PGE$_2$	3.828	± 0.216	5
351.2/271.2	PGD$_2$	2.387	± 0.096	5
Total	PGE$_2$/D$_2$	6.21	± 0.312	5

Table 4.3: PGE$_2$ and PGD$_2$ quantification by LC/MS/MS. Washed human platelets were activated with 0.2 U/ml thrombin for 30 min at 37°C, in the presence of 1 mM CaCl$_2$. Lipids were then extracted and analysed using reverse-phase LC/MS/MS, monitoring *m/z* 351.2 → *m/z* 271.2, as described in Materials and Methods, Section *2.2.3.3*. Levels of free PGE$_2$ and PGD$_2$ are expressed as ng/2 x 10^8 platelets. Data is representative of five genetically unrelated healthy donors (n = 5, mean ± SEM).

4.3 Discussion

In this chapter PGa-PEs were identified as a family of lipids that contain either PGE$_2$ or PGD$_2$ attached at the sn2 position of PEs. In light of the studies conducted in Chapter 3 where fatty acids at the sn1 position were described, PGa-PE ions (*m/z* 770.6, 796.6, 798.6 and 814.7) are now proposed as PEs containing 16:0p, 18:1p, 18:0p and 18:0a at sn1 and either PGE$_2$ or PGD$_2$ at sn2, and are termed PGE$_2$-PEs and PGD$_2$-PEs as shown in Scheme 4.1 and 4.2. The majority of PGE$_2$/D$_2$-PEs are plasmalogens with a fatty acid attached to the glycerol at the sn1 position via a vinyl-ether linkage, *m/z* 770.6, 796.6 and 798.6 (16:0p, 18:1p and 18:0p, respectively), as shown in Scheme 4.1 A-C and Scheme 4.2 A-C. The lipid with a *m/z* 814.7 represents an 18:0 fatty acid bonded to PE via a diacyl linkage (Scheme 4.1 D and Scheme 4.2 D). PGE$_2$-PE and PGD$_2$-PE are very similar in structure, differing only by the position of the ketone and the hydroxyl moiety on the prostane ring. Although free PGE$_2$ and PGD$_2$ could be separated by LC/MS/MS (Figure 4.8), HPLC separation of PGE$_2$-PEs and PGD$_2$-PEs was not possible and, therefore, the same PE species will be measured as single peaks in the following chapters.

Finally, PGE$_2$/D$_2$-PEs were quantified in platelet samples using biogenic standards. As described in this chapter, the biogenic standard was generated from total platelet lipid extracts, and this led to problems with ion suppression, both the internal standard DMPE and the PGE$_2$/D$_2$-PEs themselves. Ion suppression occurs due to competition for charge, between the analyte of interest and other contaminating lipids in a sample (Annesley, 2003). As the problem of ion suppression could not be solved, quantification was by direct comparison between samples and standards. To account for losses during extraction, the standard curve was subject to the same lipid extraction procedure as the samples. Furthermore, as the standard curve was not linear (likely due to low lipid recovery at lower concentrations of PGE$_2$/D$_2$-PEs), slopes were separately calculated for each PGE$_2$/D$_2$-PE species measured in platelet samples. Thus, the calculated amounts of PGE$_2$/D$_2$-PEs generated by activated platelets, shown in Table 4.2, represent the best estimate possible using our method. However, values measured in platelet samples are

probably underestimated. It is hoped that in future, generation of pure PGE$_2$/D$_2$-PE standards will allow more precise quantification of these OxPLs to be achieved.

Considerable variability in PGE$_2$/D$_2$-PE levels was noted between genetically unrelated donors (Table 4.2). Furthermore, it is assumed that PGE$_2$-PEs account for two-thirds of the total PGE$_2$/D$_2$-PEs, since saponification of PGE$_2$/D$_2$-PEs generated PGE$_2$ (0.519 ng) and PGD$_2$ (0.28 ng) with an approximately 2:1 predominance of PGE$_2$ over PGD$_2$. The amount of esterified PGE$_2$ and PGD$_2$ (28.1 ± 2.3 pg/2 × 10^8 platelets) corresponded to less than 1 % of the total free PGE$_2$ and PGD$_2$ (6.21 ± 0.312 ng/2 × 10^8 platelets). In contrast to this, activated platelets generate significantly higher levels of 12-HETE-PEs. Specifically, following platelet activation, 65.5 ± 17.6 ng/4 x 10^7 platelets of 12-HETE is generated, of which approximately 30 % is detected esterified to either PE (5.85 ± 1.4 ng/4 x 10^7 platelets) or PC species (18.35 ± 4.61 ng/4 x 10^7 platelets) (Thomas *et al.*, 2010). These OxPLs are initially formed as free 12-HETE via 12-LOX and enzymatically reincorporated into lysophospholipids, most likely via the deacylation/reacylation cycle. It is possible that PGE$_2$/D$_2$-PEs form in a similar manner and the lower amounts of PGE$_2$/D$_2$-PE compared to 12-HETE-PE/PC may be due to enzyme substrate specificity during the reacylation process, or simply because 12-HETEs are more abundant than either PGE$_2$ or PGD$_2$. Furthermore, it is possible that PGE$_2$ and PGD$_2$ are esterified into additional non-phospholipid pools that are not detectable in negative ion mode, such as diacylglycerides and triglycerides. Nevertheless, minor abundance does not necessarily equate with minor biological roles. It has been demonstrated that glyceryl prostaglandin E$_2$ (PGE$_2$-G) generated by the oxygenation of the 2-arachidonylglycerol by COX-2 triggers a rapid increase in intracellular calcium in a murine macrophage-like cell line (RAW264.7) at 1 pM (Nirodi *et al.*, 2004). Furthermore, PGE$_2$ induces platelet aggregation at 1 – 15 nM (Vezza *et al.*, 1993). To demonstrate the bioactivity of PGE$_2$/D$_2$-PE, pure standards are required for functional assays. Without these it is difficult to determine whether the generation of these products is physiologically relevant or whether they are minor side products of the robust activity of enzymes involved in membrane remodelling during cell activation.

The analytical limit of detection was also estimated for each PGE$_2$/D$_2$-PE species using the biogenic standard curves. This quantitative assay demonstrated that the amount of

18:0a/PGE$_2$/D$_2$-PE generated by 2 x 10^8 platelets (3.3 pg) was just above the limit of detection (3 pg) and, therefore, this isomer will not be measured in later chapters of this thesis.

As PGE$_2$ and PGD$_2$ are generated by activated platelets via COX-1, it is possible that PGE$_2$/D$_2$-PEs are also enzymatically generated and may exert similar biological activities to those of free PGE$_2$ and PGD$_2$. These prostaglandins have been implicated in numerous physiological processes and pathologies, including pain, fever, bone formation, parturition, arthritis, atherosclerosis and coagulation (Hikiji *et al.*, 2008; Akaogi *et al.*, 2006; Rajtar *et al.*, 1985; Murakami, 2011). Although PGE$_2$ and PGD$_2$ are structural isomers, in some systems they mediate opposing effects. For example in the brain, PGD$_2$ promotes sleep and lowers body temperature, whereas PGE$_2$ induces alertness and fever (Hayaish, 1988; Ueno *et al.*, 1982). In contrast, in haemostasis, PGE$_2$ and PGD$_2$ are reported primarily to inhibit platelet aggregation through activation of surface G protein-coupled receptors (Smith *et al.*, 2010; Song *et al.*, 2012). PGE$_2$-PEs and PGD$_2$-PEs may display similar biological activities to those of free PGE$_2$ and PGD$_2$ or signal in a complete different manner in their own right. These ideas will be tested in future studies using cell-based assay for PGE$_2$ receptor ligand binding.

Chapter 5

5 Mass Spectrometry Analysis of PGb-PE and PGc-PE Generated by Activated Human Platelets

5.1 Introduction

Studies in this chapter will describe the MS analysis of PGb and PGc attached to PEs. Initial studies performed in Chapter 3 demonstrated that PGb-PE and PGc-PE are structurally distinct as for each parent *m/z* they comprise two peaks with an oxidised fatty acid of *m/z* 351.2 attached to a lyso PE species (16:0p/, 18:1p/, 18:0p/ and 18:0a/).

Characterisation of PGb-PEs and PGc-PEs will be undertaken in lipid extracts from thrombin-activated platelets using the LTQ Orbitrap Velos, in full scan mode. This will determine accurate mass, and allow isolation and fragmentation. The lipids will then be subjected to MS^3 analysis. Accurate mass fragmentation of PGb and PGc attached at the sn2 position of PEs will be compared to the fragmentation patterns of known eicosanoid standards to facilitate structural characterisation.

Finally, the formation of PGb and PGc as free eicosanoids by activated platelets will be investigated using LC/MS/MS on the 4000 Q-trap. Free acid PGb and PGc in platelet samples will be identified based on both the MS spectra and retention time of PGb and PGc released from hydrolysed PGb-PEs and PGc-PEs, respectively.

5.1.1 Aims

Studies described in this chapter aim to:

- Determine the identity of PGb attached at sn2 position of PE species.
- Determine the identity of PGc attached at sn2 position of PE species.
- Investigate whether PGb and PGc are formed as free eicosanoids by activated human platelets.

5.2 Results

5.2.1   Structural characterisation of PGb-PE and PGc-PE generated by activated human platelets.

5.2.1.1 Targeted MS/MS analysis of PGb-PE and PGc-PE species.

Structural characterisation of PGb-PEs and PGc-PEs was performed using high resolution MS, monitoring the exact mass of parent ions (770.4977, 796.5132, 798.5292 and 814.5243), as described in Chapter 4, to obtain spectra of individual PE species.

Targeted MS/MS was carried out in FTMS mode, monitoring parent ions with accurate mass and conducting fragmentation with HCD. MS/MS spectra of PGb-PE parent ions were then compared to each other to confirm the presence of PGb attached at sn2 position in all four PE species. This analysis was then repeated for the PGc-PEs. Indeed, MS/MS spectra of all four PGb-PE species (770.6, 796.6, 798.6 and 814.7) yielded similar fragmentation patterns, with major daughter ions at *m/z* 351, 271, 207, 163 and 109 (Figures 5.1 and 5.2). Similarly, MS/MS spectra of PGc-PE species generated comparable fragmentation pattern, with main daughter ions at *m/z* 351, 271, 165, 163 and 149 (Figures 5.3 and 5.4). This confirms that all four "b" contain the same prostaglandin-like molecule, with the same also true for the four "c" type lipids.

Initial analysis of MS/MS spectra of PGb-PE and PGc-PE suggested PGb and PGc as potentially previously undescribed eicosanoids. However, further analysis was required to confirm that the daughter ions generated by targeted MS/MS did in fact originate from fragmentation of the *m/z* 351.2 attached at the sn2 of PEs.

5.2.1.2 Data dependent MS^3 analysis.

To confirm which fragments observed by targeted MS/MS originated from fragmentation of the daughter ion *m/z* 351.2, data dependent MS^3 was performed utilising the Orbitrap.
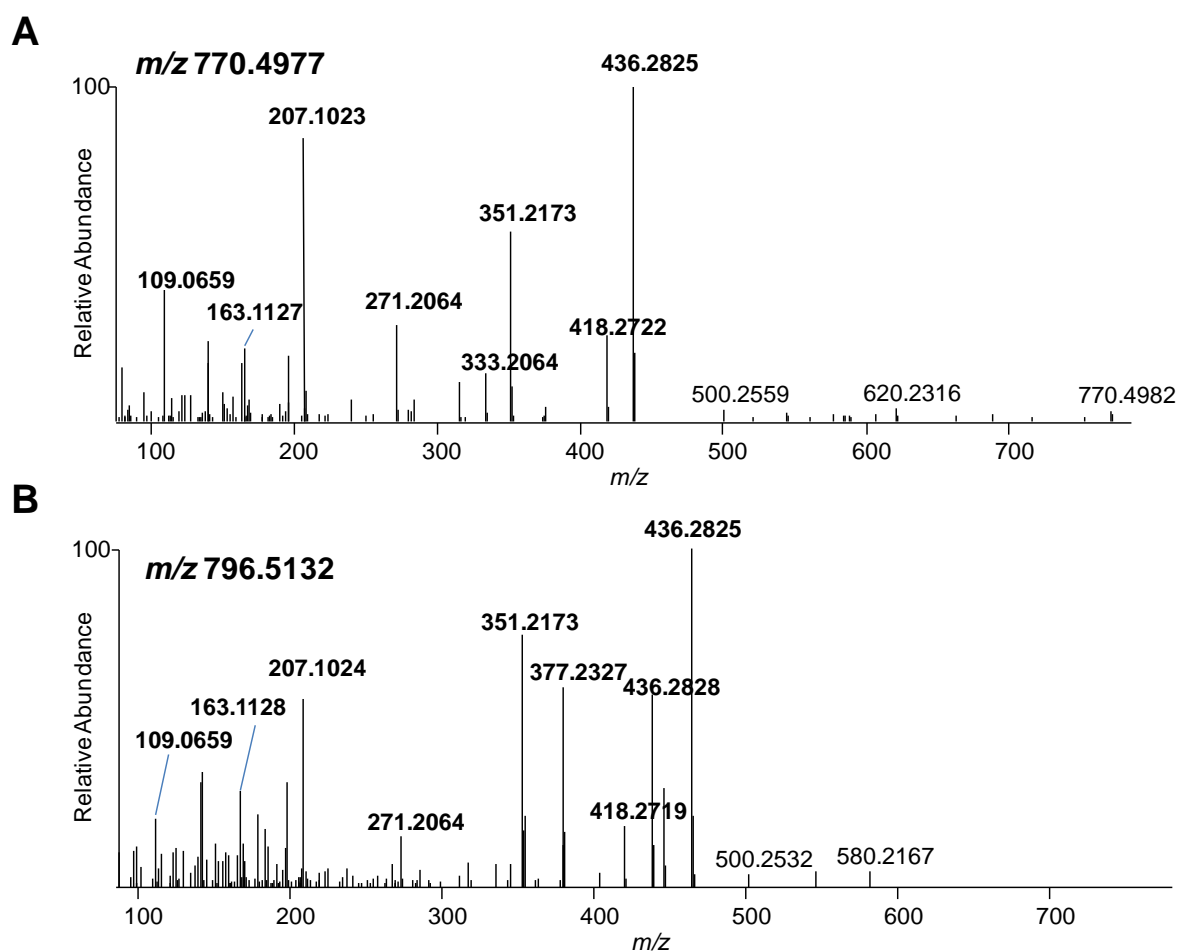
Figure 5.1: Targeted MS/MS analysis of PGb-PE demonstrated identical major daughter ions arisen from *m/z* 770.6 and 796.6 fragmentation. Platelet lipid extracts were analysed using high resolution LC/MS/MS on Orbitrap in FTMS mode, monitoring the exact mass, followed by targeted MS/MS using HCD. *Panel A*. Negative MS/MS spectrum acquired at the apex of elution of PGb-PE for *m/z* 770.4977 at 6.19 min. Major daughter ions arising from *m/z* 770.6 fragmentation are depicted in bold. *Panel B.* Negative MS/MS spectrum acquired at the apex of elution of PGb-PE for *m/z* 796.5132 at 6.43 min. Major daughter ions arising from *m/z* 796.6 fragmentation are shown in bold.
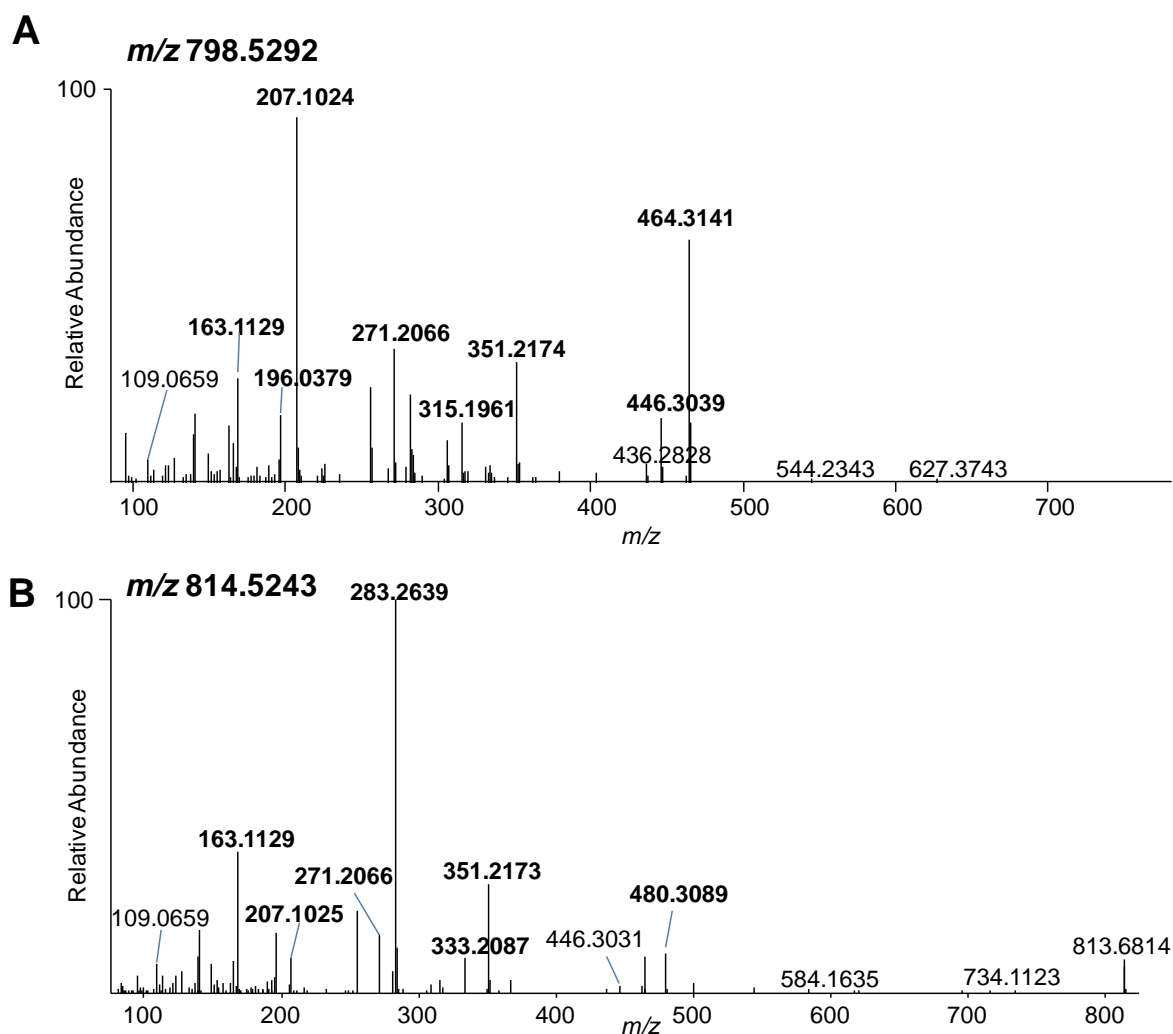
Figure 5.2: Targeted MS/MS analysis for PGb-PE showed identical major daughter ions arisen from *m/z* 798.6 and 814.7 fragmentation. Platelet lipid extracts were analysed using high resolution LC/MS/MS on Orbitrap in FTMS mode, monitoring the exact mass, followed by targeted MS/MS using HCD. *Panel A*. Negative MS/MS spectrum acquired at the apex of elution of PGb-PE for *m/z* 798.5292 at 7.69 min. Major daughter ions arising from *m/z* 798.6 fragmentation are shown in bold. *Panel B.* Negative MS/MS spectrum acquired at the apex of elution of PGb-PE for *m/z* 814.5243 at 7.1 min. Major daughter ions arising from *m/z* 814.7 fragmentation are shown in bold.
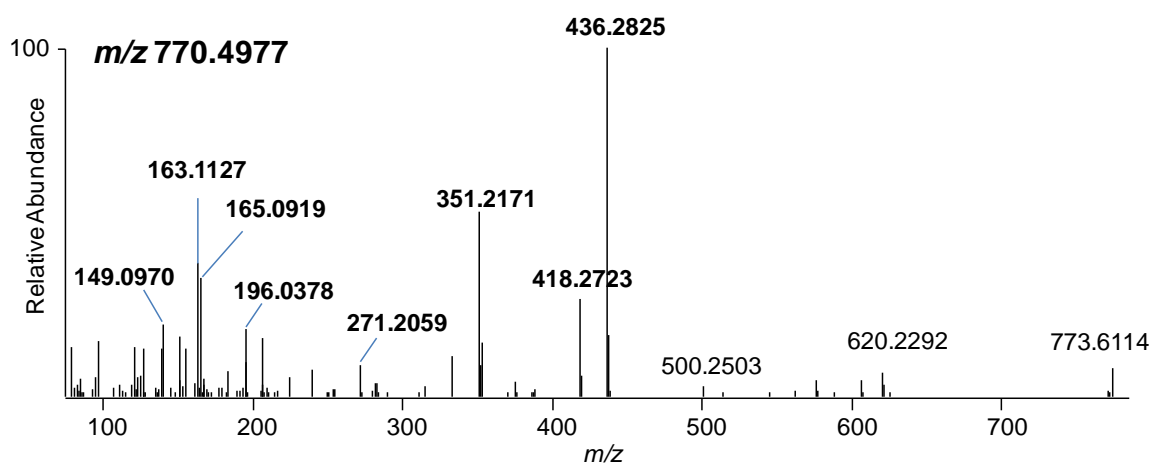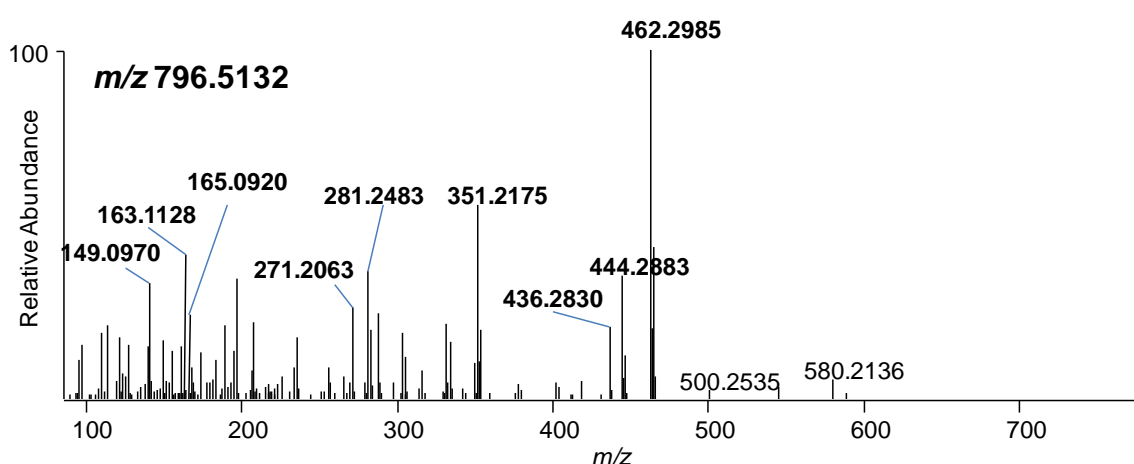
Figure 5.3: Targeted MS/MS analysis of PGc-PE showed identical major daughter ions arisen from *m/z* 770.6 and 796.6 fragmentation. Platelet lipid extracts were analysed using high resolution LC/MS/MS on Orbitrap in FTMS mode, monitoring the exact mass, followed by targeted MS/MS using HCD. *Panel A*. Negative MS/MS spectrum acquired at the apex of elution of PGc-PE for *m/z* 770.4977 at 6.72 min. Major daughter ions arising from *m/z* 770.6 fragmentation are depicted in bold. *Panel B*. Negative MS/MS spectrum acquired at the apex of elution of PGc-PE for *m/z* 796.5132 at 6.95 min. Major daughter ions arising from *m/z* 796.6 fragmentation are highlighted in bold.
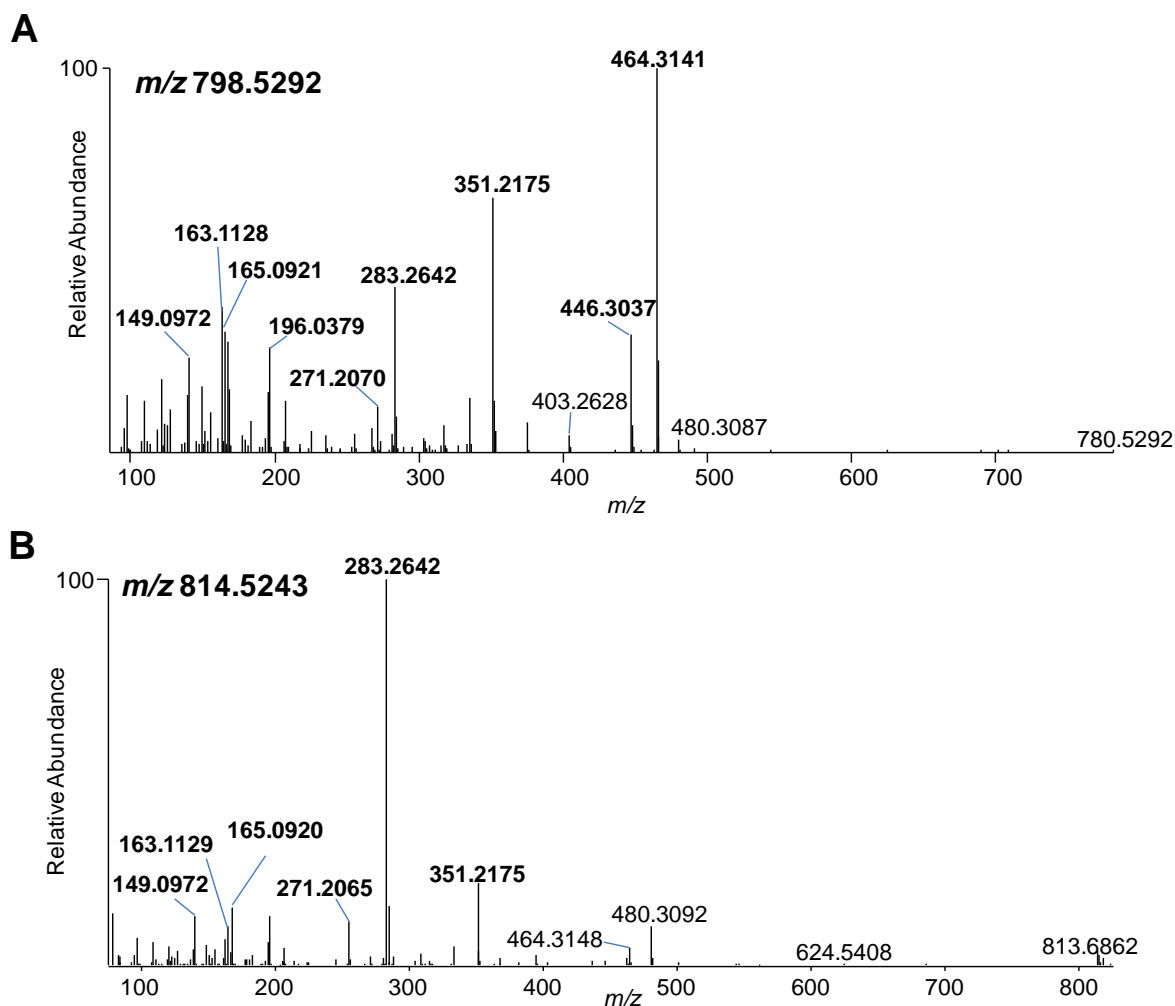
Figure 5.4: Targeted MS/MS analysis of PGc-PE identified identical major daughter ions arisen from *m/z* 798.6 and 814.7 fragmentation. Platelet lipid extracts were analysed using high resolution LC/MS/MS on the Orbitrap in FTMS mode, monitoring the exact mass, followed by targeted MS/MS using HCD. *Panel A*. Negative MS/MS spectrum acquired at the apex of elution of PGc-PE for *m/z* 798.5292 at 8.21 min. Major daughter ions arising from *m/z* 798.6 fragmentation are highlighted in bold. *Panel B.* Negative MS/MS spectrum acquired at the apex of elution of PGc-PE for *m/z* 814.5243 at 7.62 min. Major daughter ions arising from *m/z* 814.7 fragmentation are given in bold.

Here, ions with a *m/z* 351.2 arising from CID of individual parent ions (770.6, 796.6, 798.6 and 814.7) of either PGb-PE or PGc-PE, in ion trap mode, were selectively isolated, further fragmented and analysed.

Upon fragmentation, the daughter ion *m/z* 351.2 of PGb-PE generated fragments at *m/z* 271, 207, 163 and 109, similar to those observed following targeted MS/MS spectra, further confirming that these ions originate from PGb fragmentation (Figures 5.5 – 5.6). Similarly, fragments at *m/z* 271, 207, 163, 165 and 149 were confirmed as ions originating from the fragmentation of the daughter ion *m/z* 351.2 of PGc-PE (Figures 5.7 – 5.8).

To identify PGb and PGc attached to PEs, MS/MS spectra of the daughter ions for *m/z* 351.2 were compared to fully characterised eicosanoid standards. However, neither PGb nor PGc corresponded to any known prostaglandin currently listed either on LipidMaps or The Human Metabolome Database.

5.2.1.3 Detection of PGb and PGc as free eicosanoids.

Studies were performed to determine whether PGb and PGc were formed as free eicosanoids by activated platelets. Synthesis of free PGb and PGc by platelets was studied by comparing the MS spectra and retention times of free eicosanoids generated by activated platelets to those of PGb and PGc released from saponified PGb-PEs and PGc-PEs. PGb-PEs and PGc-PEs were purified from platelet lipid extracts using HPLC-UV, as described in Materials and Methods, Section *2.2.4*.

Purified PGb-PEs and PGc-PEs were then saponified with snake venom PLA_2 to release PGb and PGc and analysed using reverse-phase LC-MS/MS, on the 4000 Q-trap, as described in Material and Methods, Section *2.2.6*, with Q1 set at *m/z* 351.2 and Q3 at *m/z* 271.2, with product ion spectra acquired at the apex of lipid elution.

A

m/z 770.6 → 351.2
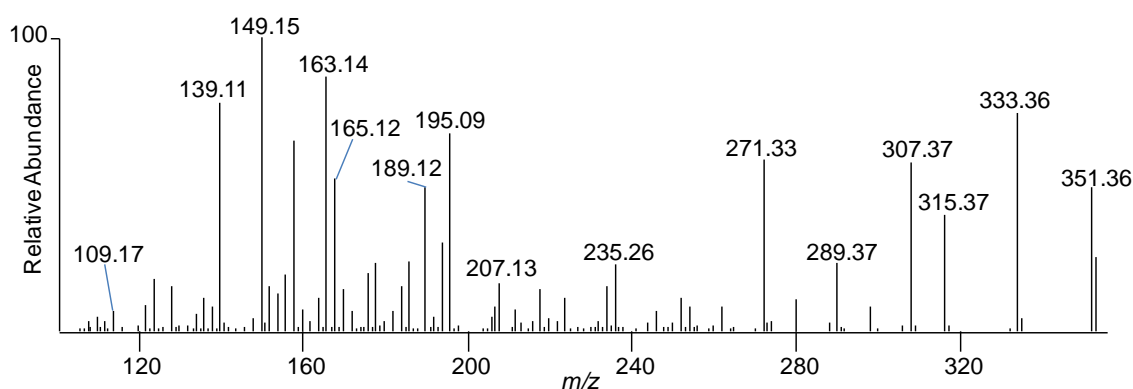
B

m/z 796.6 → 351.2
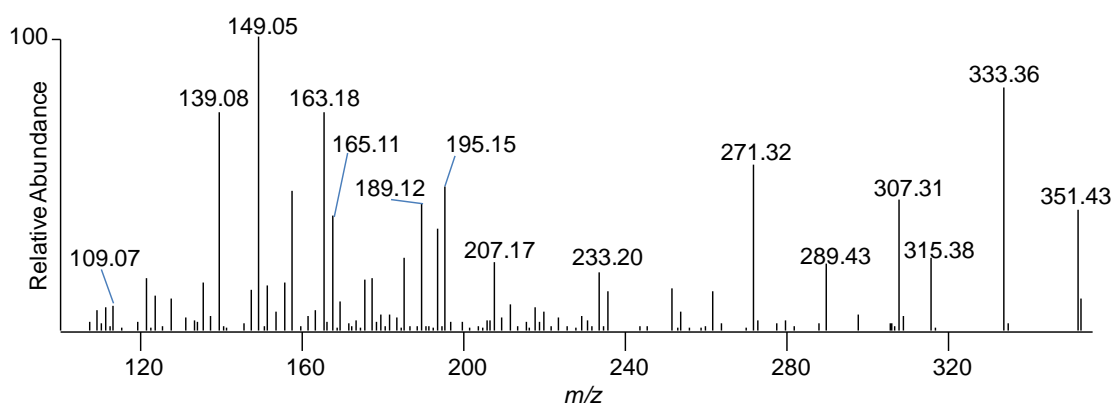
Figure 5.5: MS³ spectra of PGb-PEs confirmed the origin of product ions observed on targeted MS/MS as PGb-derived fragments. Platelet lipid extracts were separated using high resolution LC/MS/MS on Orbitrap, with ITMS detection and targeted MS/MS of the parent mass, followed by data dependent fragmentation of the daughter ion *m/z* 351.2, using CID. *Panel A*. MS³ spectrum of *m/z* 770.6 by secondary fragmentation of daughter ion *m/z* 351.2. *Panel B*. MS³ spectrum of *m/z* 796.6 by secondary fragmentation of the daughter ion *m/z* 351.2.

A   *m/z* 798.6 → 351.2

100 — Relative Abundance

149.06
163.16
165.08
189.10
139.11
271.27
333.32
351.33
307.27
315.28
109.15
207.09 233.19
289.28

120   160   200   240   280   320

m/z

B   *m/z* 814.7 → 351.2

100 — Relative Abundance

149.14
139.13
163.11
165.16
189.15
195.10
271.39
333.29
351.41
307.34
315.37
109.14
207.09 233.25
289.26

120   160   200   240   280   320

m/z
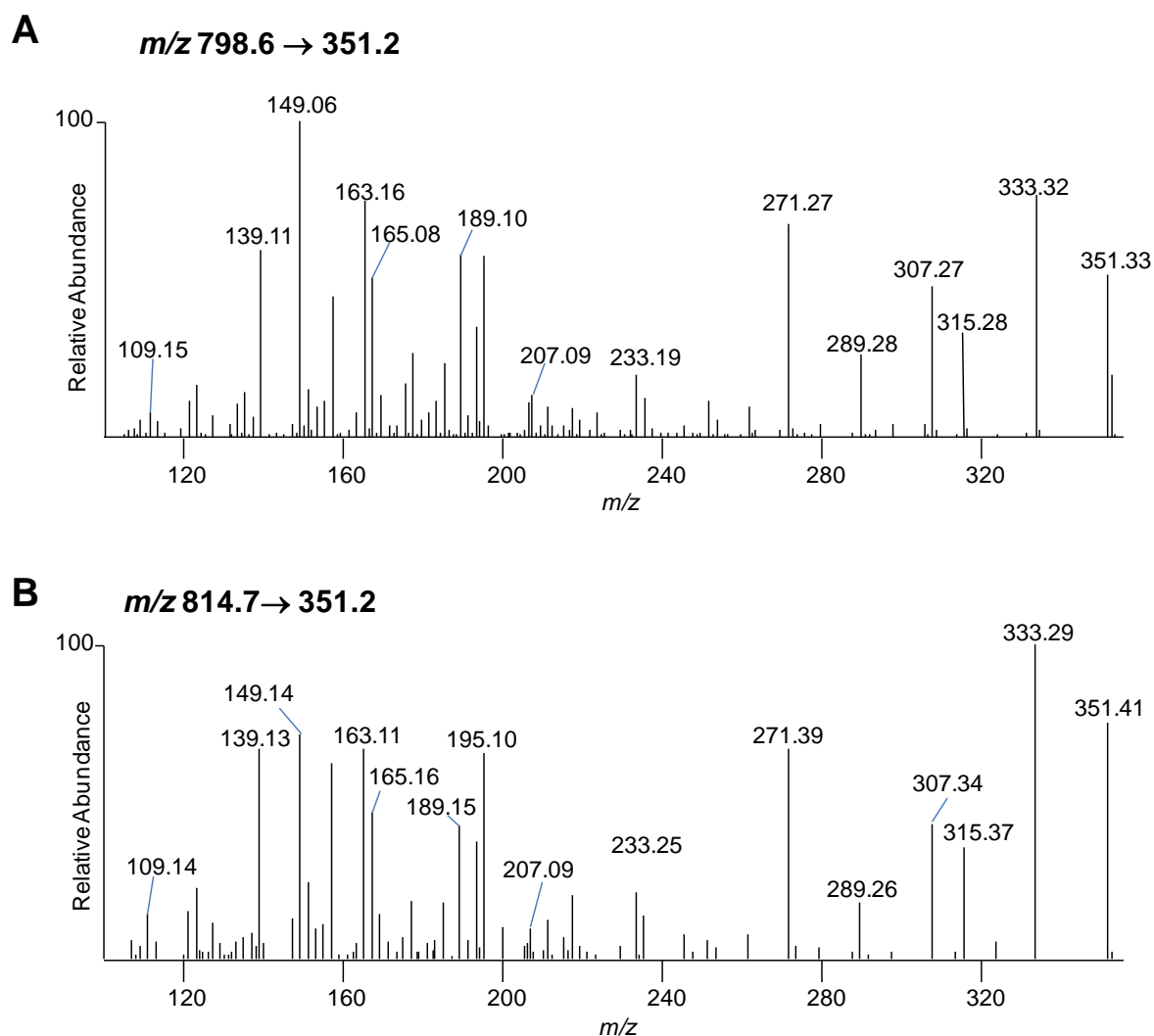
Figure 5.6: MS[3] spectra of PGb-PEs confirmed the origin of product ions observed in targeted MS/MS as PGb-derived fragments. Platelet lipid extracts were separated using high resolution LC/MS/MS on Orbitrap, with ITMS detection and targeted MS/MS of the parent mass, followed by data dependent fragmentation of the daughter ion *m/z* 351.2, using CID. *Panel A*. MS[3] spectrum of *m/z* 798.6 by secondary fragmentation of daughter ion *m/z* 351.2. *Panel B*. MS[3] spectrum of *m/z* 814.7 by secondary fragmentation of daughter ion *m/z* 351.2.
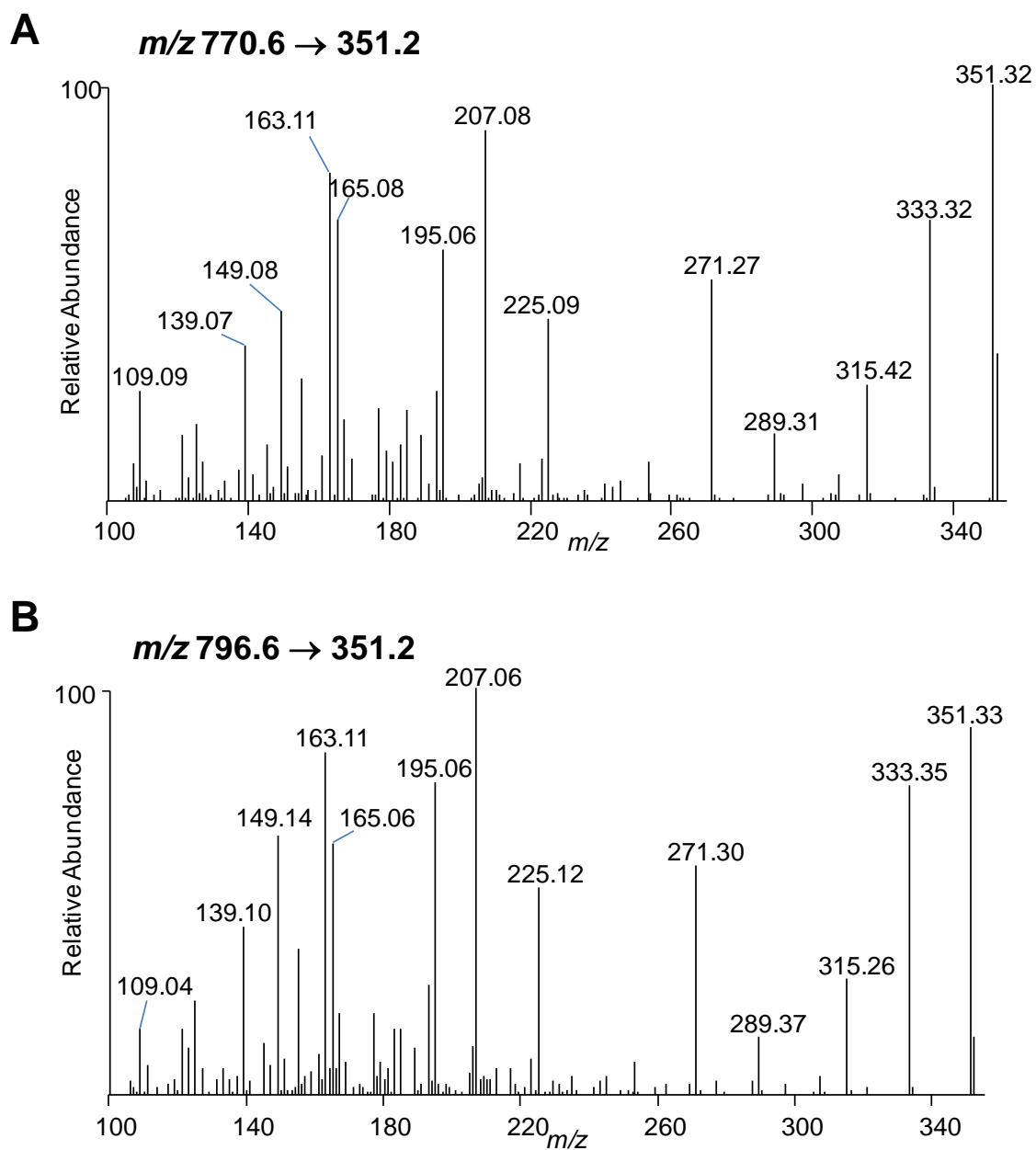
Figure 5.7: MS³ spectra of PGc-PEs confirmed the origin of product ions observed in targeted MS/MS as PGc-derived fragments. Platelet lipid extracts were separated using high resolution LC/MS/MS on Orbitrap, with ITMS detection and targeted MS/MS of the parent mass, followed by data dependent MS/MS of the daughter ion *m/z* 351.2, using CID. *Panel A*. MS³ spectrum of *m/z* 770.6 by secondary fragmentation of daughter ion *m/z* 351.2. *Panel B*. MS³ spectrum of *m/z* 796.6 by secondary fragmentation of daughter ion *m/z* 351.2.
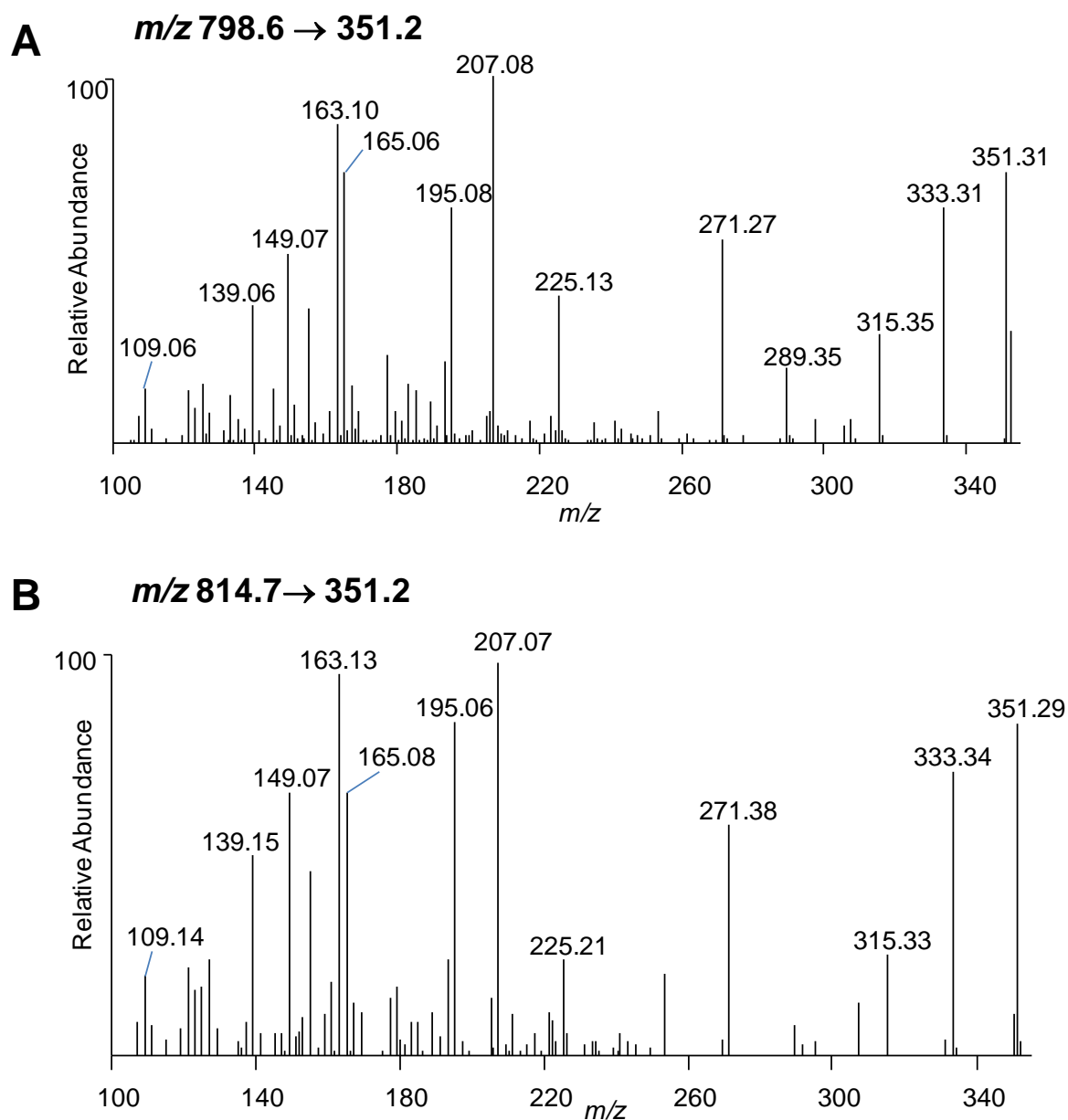
Figure 5.8: MS³ spectra of PGc-PEs confirmed the origin of product ions observed in targeted MS/MS as PGc-derived fragments. Platelet lipid extracts were separated using high resolution LC/MS/MS on Orbitrap, with ITMS detection and targeted MS/MS of the parent mass, followed by data dependent MS/MS of the daughter ion *m/z* 351.2, using CID. *Panel A*. MS³ spectrum of *m/z* 798.6 by secondary fragmentation of daughter ion *m/z* 351.2. *Panel B*. MS³ spectrum of *m/z* 814.7 by secondary fragmentation of daughter ion *m/z* 351.2.

LC-MS/MS analysis of prostaglandins released from PGb-PE and PGc-PE demonstrated a major peak from a lipid eluting at 51.5 min (Figure 5.9). Further analysis revealed that the lipid eluting at 38.6 min generated major daughter ions on MS/MS (*m/z* 351, 271, 207, 163 and 109) characteristic of esterified PGb (Figure 5.10). The MS spectrum acquired at 51.5 min demonstrated daughter ions (*m/z* 351, 271, 165, 163 and 149) characteristic of esterified PGc (Figure 5.11).

Although PGb-PE and PGc-PE were purified before hydrolysis, other esterified eicosanoids may co-elute in this system. Other peaks (with *m/z* 351.2) observed in the chromatogram may originate from isoprostanes of these lipids. This data indicates that if PGb and PGc do form as free eicosanoids, they would elute at 38 and 51.5 min, respectively.

To determine whether platelets generate free PGb and PGc, they were activated with thrombin, the lipids extracted and then analysed using reverse-phase LC/MS/MS, as described in detail in Materials and Methods, Section *2.2.6*. Based on the MS/MS spectra of PGb-PEs and PGc-PEs, distinct transitions were selected to monitor PGb (*m/z* 351.2 → 207.1) and PGc (*m/z* 351.2 → 165.1). LC/MS/MS combined with information-dependent-acquisition (IDA), monitoring *m/z* 351.2 → 207.1, demonstrated a lipid eluting at 38.6 min that, upon fragmentation, generates several ions similar to those observed for PGb hydrolysed from PGb-PEs. Similarly, the MS/MS spectrum acquired at 51.5 min showed ions similar to those observed for PGc hydrolysed from PGc-PEs.

The reverse-phase LC/MS/MS method used for the studies described thus far is both time consuming (75 minutes for a single acquisition) and also requires a considerable amount of solvent. To reduce both the analysis time and solvents consumed a shorter reverse-phase LC/MS/MS method was chosen instead. Studies detecting free PGb and PGc now employed a shorter reverse-phase LC/MS/MS method (30 minutes for a single acquisition), which is described in detail in Material and Methods, Section *2.2.3.3*. Using the shorter LC/MS/MS method PGb and PGc now eluted at 4.3 min (Figure 5.12) and 6.3 min (Figure 5.13), respectively.
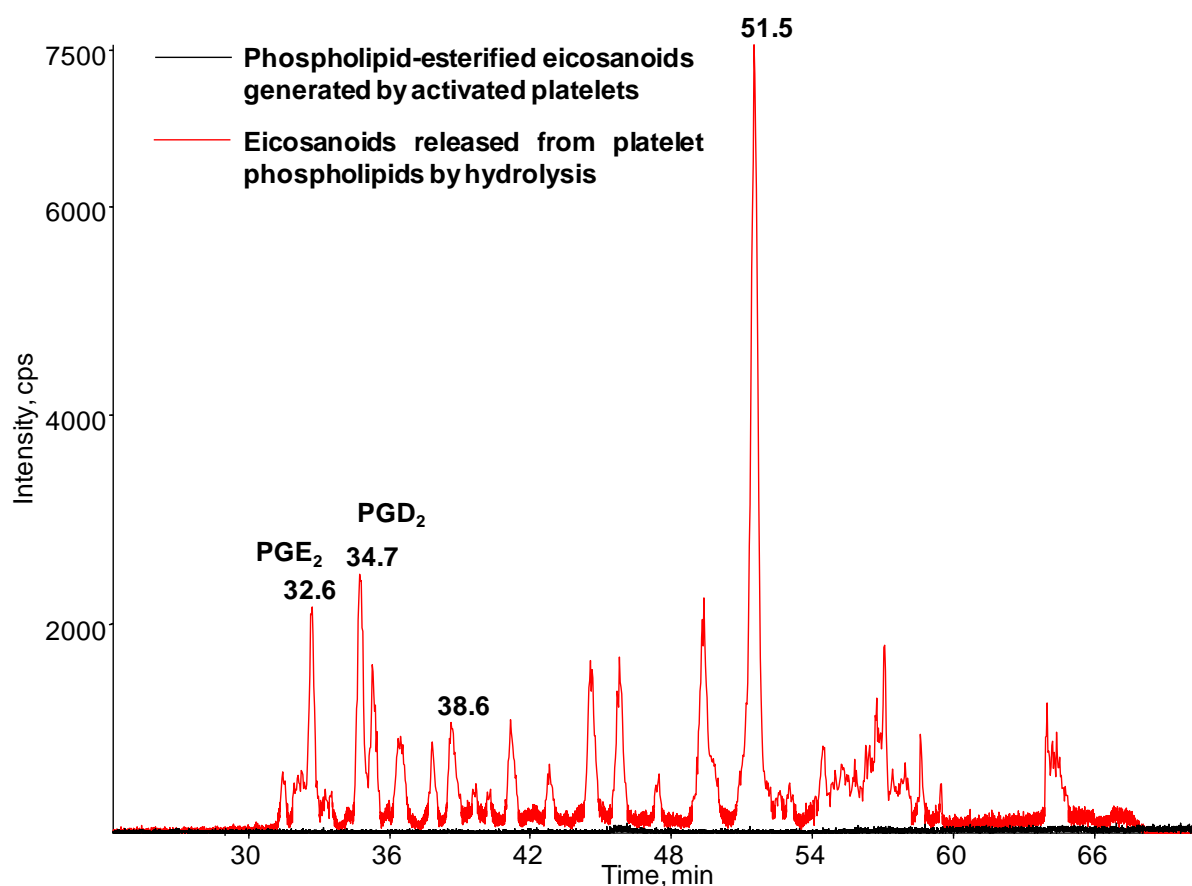
Figure 5.9: Analysis of prostaglandins released from saponified PGb-PEs and PGc-PEs. Washed human platelets were activated with calcium ionophore (10 μM) for 30 min at 37°C followed by lipid extraction. PGb-PEs and PGc-PEs were purified as described in Materials and Methods, Section *2.2.4*. Lipids were then saponified with 200 μg of snake venom (PLA$_2$). Fatty acids released from saponified PGb-PEs and PGc-PEs were analysed using reverse-phase LC/MS/MS. Black line, purified PGb-PE and PGc-PE before hydrolysis. Red line, lipids with *m/z* 351.2 released from platelet phospholipids after hydrolysis.
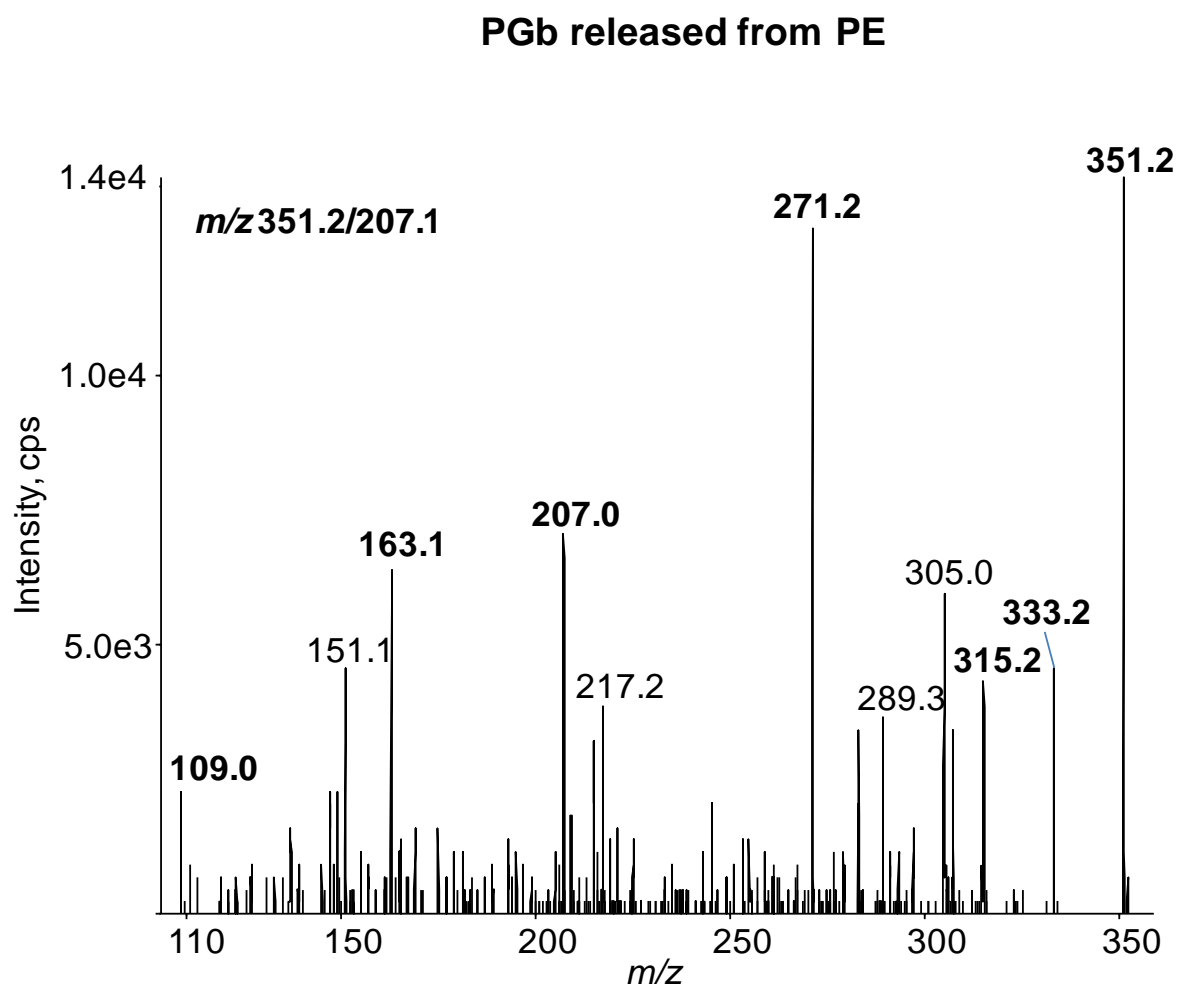
Figure 5.10: MS/MS spectrum confirming the lipid eluting at 38 min as PGb. Saponified PGb-PEs and PGc-PEs were separated using reverse-phase LC/MS/MS on Q-trap, as described in Materials and Methods, Section 2.2.6, with MS/MS spectrum acquired at the apex of elution at 38.6 min. Major daughter ions consistent with PGb attached to PEs are highlighted in bold.

PGc released from PE
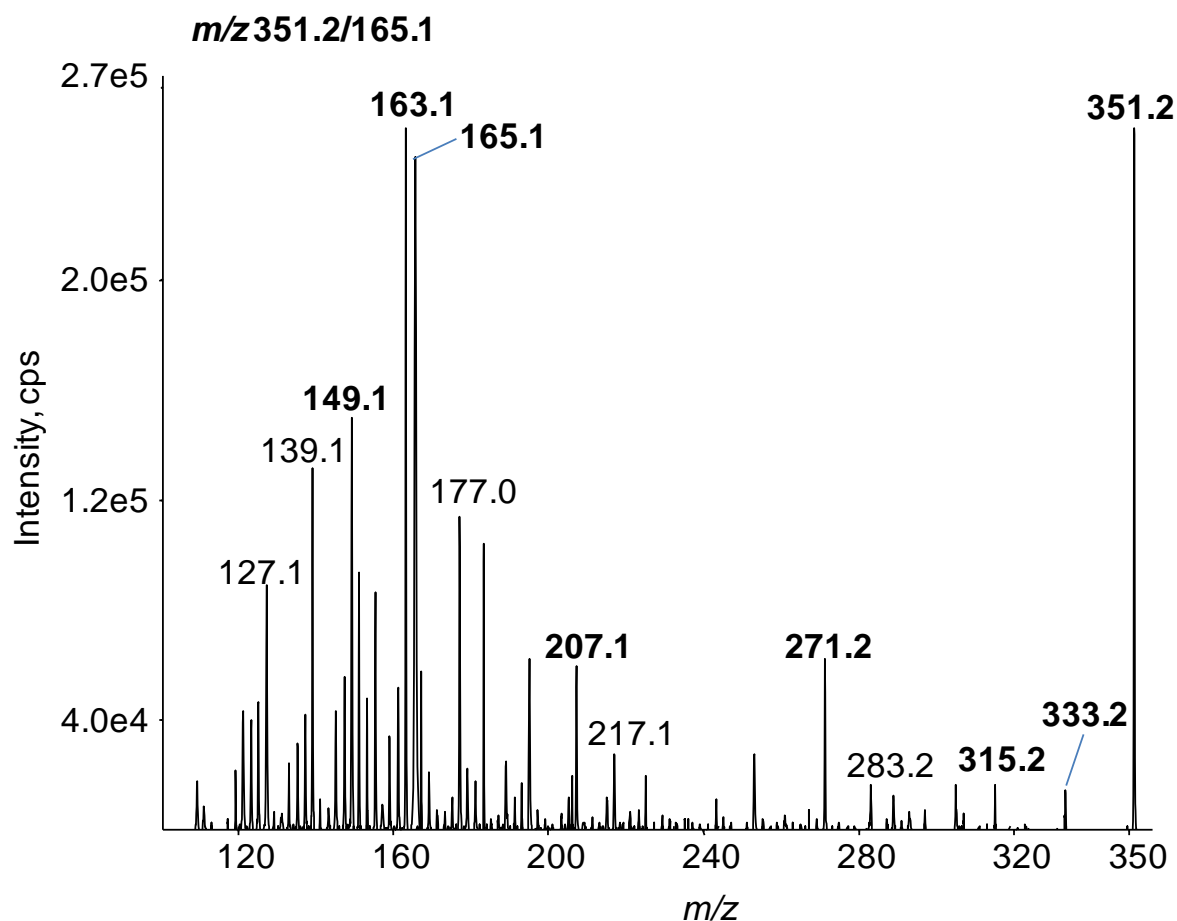
Figure 5.11: MS/MS spectrum confirming the lipid eluting at 51.5 min as PGc. Saponified PGb-PEs and PGc-PEs were separated using reverse-phase LC/MS/MS on Q-trap, as described in Materials and Methods, Section 2.2.6, with spectrum acquired at the apex of elution at 51.5 min. Major daughter ions consistent with PGc attached to PEs are highlighted in bold.
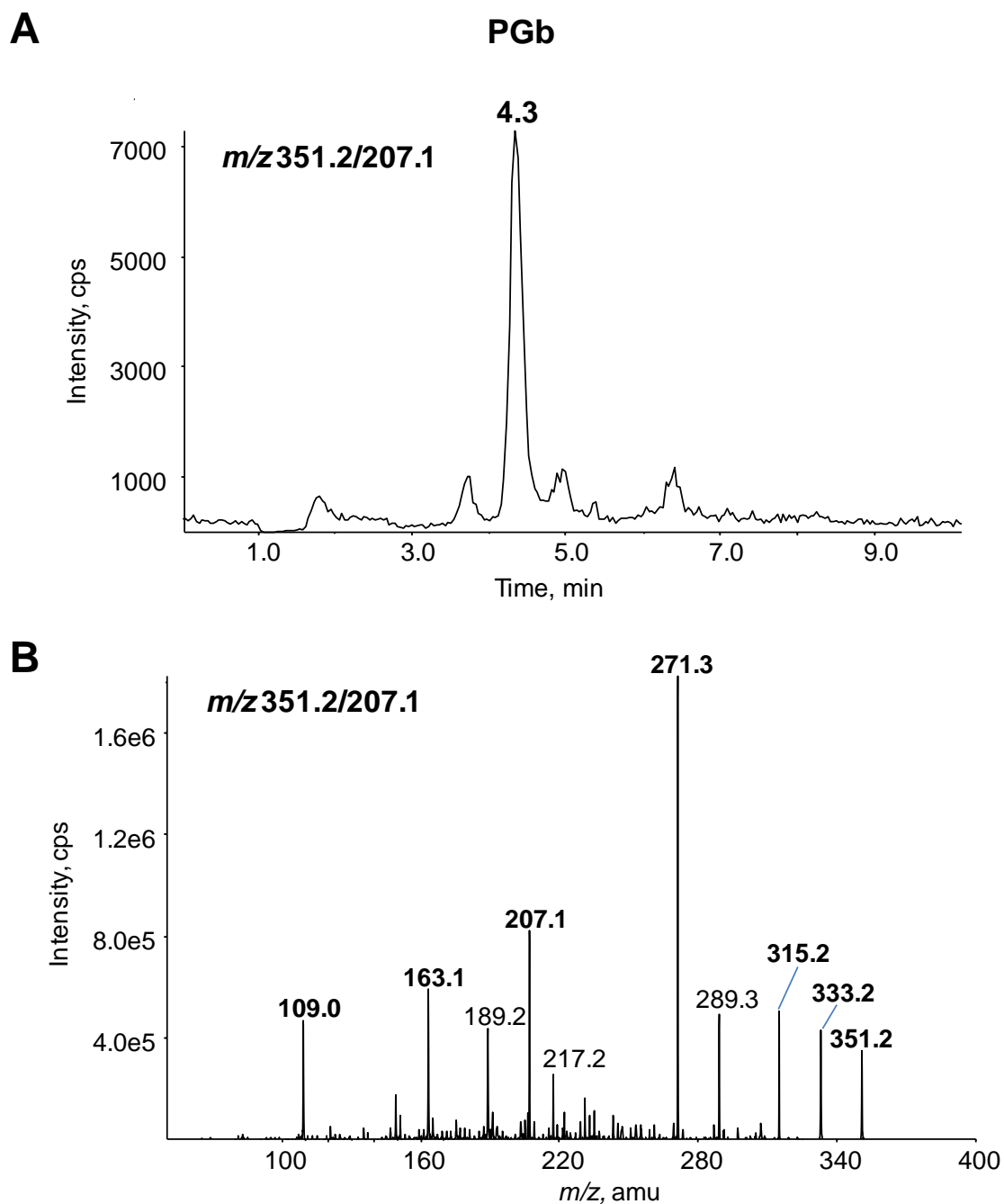
Figure 5.12: Analysis of free PGb using a shorter (30 min) reverse-phase LC/MS/MS. Lipid extracts from activated platelets were separated using a 30 min reverse-phase LC/MS/MS as described in Materials and Methods, Section *2.2.3.3*, monitoring *m/z* 351.2 → 207.1. *Panel A*. Chromatogram showing elution of free PGb at 4.3 min. *Panel B*. MS/MS spectrum of PGb acquired at the apex of elution at 4.3 min. The major daughter ions arising from free PGb fragmentation are highlighted in bold.

A

PGc

B
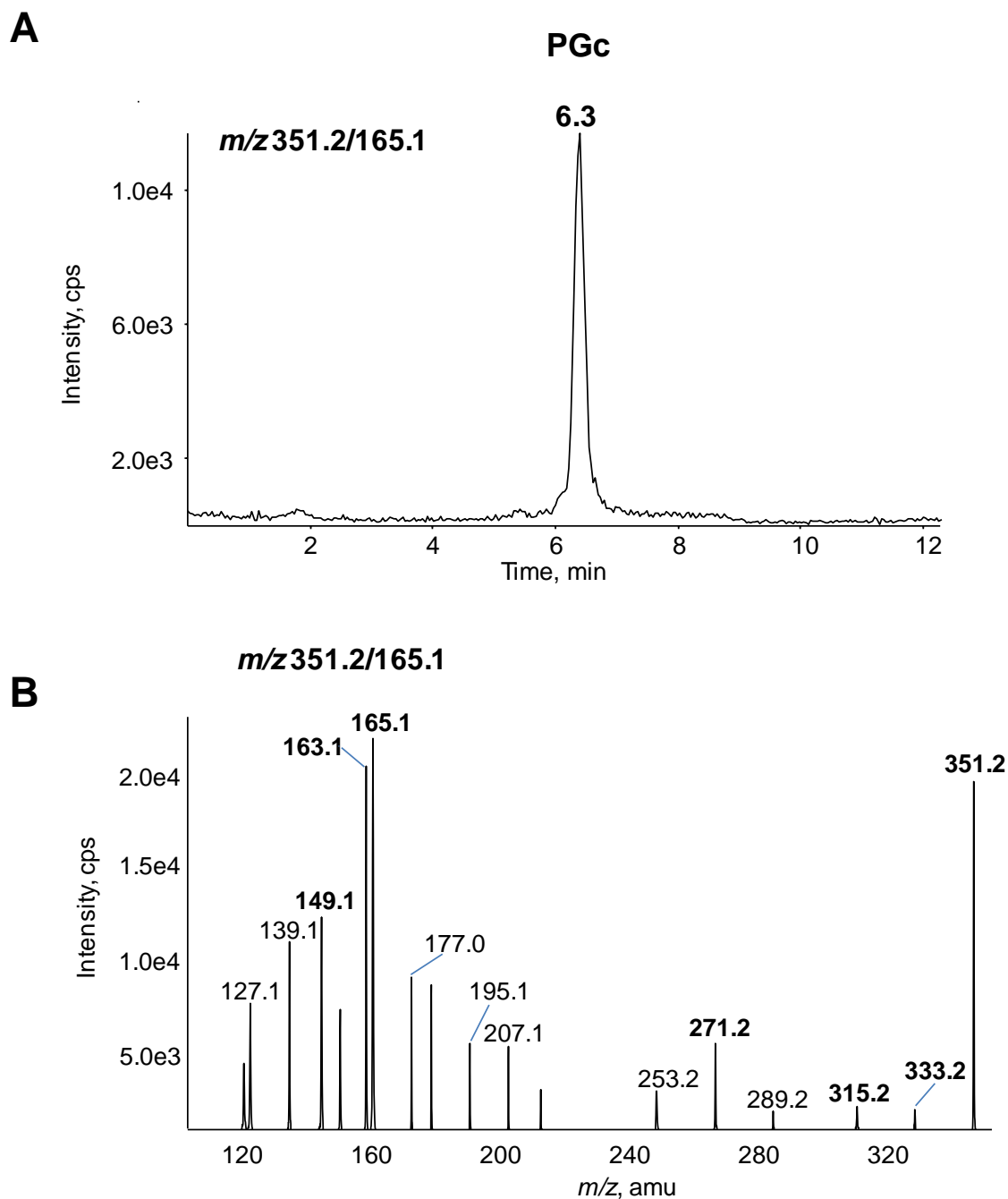
Figure 5.13: Analysis of free PGc using a shorter (30min) reverse-phase LC/MS/MS. Platelet lipid extracts were separated using a 30 min reverse-phase LC/MS/MS as described in Methods and Materials, Section *2.2.3.3*, monitoring *m/z* 351.2 → 165.1. *Panel A*. Chromatogram showing elution of free PGc at 6.3 min. *Panel B*. MS spectrum of PGc acquired at the apex of elution at 6.3 min. The major daughter ions arising from free PGc fragmentation are highlighted in bold.

5.3 Discussion

LC-MS/MS analysis revealed that PGb and PGc attached to PEs are oxidised fatty acids that have not been previously described in either platelets or other human cells. Comparison of MS^3 spectra of PGb-PEs and PGc-PEs indicates that both fatty acids at the sn2 position share a similar structure but are distinct from PGE$_2$ and PGD$_2$ (Figures 5.5 – 5.8). The presence of daughter ions at *m/z* 333, 315, 271 and 189, characteristic also of PGE$_2$ and PGD$_2$, further suggest that PGb and PGc are prostaglandin-like molecules esterified to PEs. Generation of free PGb and PGc by activated platelets was confirmed based on analysis of esterified PGb and PGc following hydrolysis and LC/MS/MS.

Where the MS fragmentation pattern of eicosanoids is already known, e.g. PGE$_2$ and PGD$_2$ (Murphy *et al*., 2005), structure characterisation is relatively straightforward. In contrast, with new lipids, elucidation represents a significant challenge. In order to determine the structures of PGb and PGc, chemical derivatization combined with either LC-MS or gas chromatography–mass spectrometry (GC-MS) would be required. Based on fragmentation, derivatization allows identification of specific functional groups. For example, the presence of hydroxyl groups (-OH) can be confirmed by silylation reactions using N,O-bis(trimethylsilyl) trifluoroacetamide (BSTFA), which reacts with active hydrogens on –OH, generating a trimethylsilyl (TMS) derivative that can be detected by a mass increase of 72 amu (Grob & Barry, 2004; Halket *et al*., 2005). Similarly, the presence of carbonyl groups can be investigated by methoximation, where methoxyamine (MOX) reacts with carbonyl groups, forming an oxime derivative that can be detected as a mass increase of 29 amu by either GC-MS or LC-MS (Halket *et al*., 2005).

Previous studies demonstrated that esterified LOX products form enzymatically in neutrophils, monocytes and platelets in a controlled manner (Maskrey *et al*., 2007; Morgan *et al*., 2009; Morgan *et al*., 2010; Thomas *et al*., 2010; Clark *et al*., 2011; Aldrovandi & O'Donnell, 2013). Formation of TxA$_2$ by COX-1 in platelets is also tightly regulated, involving activation of PLC, calcium and PLA$_2$ (Putney, 1988; Hisatsune *et al*., 2005; Levy, 2006, Nakahata, 2008). Platelet 12-HETE-PC and neutrophil 5-HETE-PEs were shown to participate in coagulation and immune responses, respectively (Thomas *et al*.,

2010; Clark *et al.*, 2011). It is possible that PGE$_2$/D$_2$-PE, PGb-PE and PGc-PE alongside free PGb and PGc also form enzymatically in a regulated manner, via activation of platelet receptors (such as PAR-1 and PAR-4) and signalling pathways, including calcium and PLA$_2$, similar to TxA$_2$. Should the enzymatic generation and bioactivity in coagulation or immune responses be confirmed, these lipids could be used as targets for drug development. For example, if they display pro-thrombotic activity they could be either synthesised *in vitro*, aiding treatment for bleeding disorders, or their *in vivo* generation inhibited to prevent thrombotic disease. The discovery of novel prostaglandins is important since known members of this lipid family play important roles in a number of biological processes *in vivo*. Prostaglandins act as autocrine and paracrine lipid mediators, maintaining local homeostasis, including in inflammation, mediating pro- or anti-inflammatory responses, and haemostasis, inhibiting/promoting platelet aggregation (Nakahata, 2008; Legler *et al.*, 2010; Sandig *et al.*, 2007). PGb and PGc may also function in an autocrine and paracrine manner in similar processes. The mechanism of formation of PGE$_2$/D$_2$-PE, PGb-PE and PGc-PE as well as free PGb and PGc will be investigated in the following chapters to determine whether these lipids are enzymatically generated, and the signal transduction pathways involved in their formation.

In summary, two novel prostaglandin-like molecules generated by activated platelets were identified. They were detected both attached to PE and as free eicosanoids. Following this work, studies in collaboration with Dr Robert Murphy (Hinz *et al.*, unpublished data 2013) are suggesting PGc as a new lipid: 8-hydroxy-9,11-dioxolane eicosatrienoic acid (Yin *et al.*, 2003; Yin *et al.*, 2004). Future studies using derivatization are expected to elucidate PGb and PGc structures in full. Until further analysis, lipid "b" will be referred to as free or esterified PGb (16:0p/PGb-PE, 18:1p/PGb-PE, 18:0p/PGb-PE and 18:0a/PGb-PE), whilst lipid "c" will be referred to as free or esterified PGc (16:0p/PGc-PE, 18:1p/PGcPE, 18:0p/PGc-PE and 18:0a/PGc-PE). For convenience, in subsequent chapters of this thesis PGE$_2$/D$_2$-PE, PGb-PE and PGc-PE will be referred to as esterified prostaglandins when described as a group. Similarly, PGE$_2$, PGD$_2$, PGb and PGc will be referred to as free prostaglandins.

Chapter 6

6 Studies on the Mechanism of Free and Esterified Prostaglandin Formation by Activated Human Platelets

6.1 Introduction

In this chapter, the temporal generation of free and esterified prostaglandins will be described. Upon thrombin stimulation of PAR-1/-4 or collagen activation of glycoprotein VI and integrin $\alpha_2\beta_1$, a cascade of intracellular signals is initiated leading to a regulated and fast generation of enzymatically formed eicosanoids, such as TxA_2, PGE_2 and PGD_2. These are subsequently released to the extracellular space, signalling in a paracrine or autocrine manner modulating platelet aggregation (Gryglewski *et al*., 1978; Rodrigues *et al*., 1994; Smith *et al*., 2010; Petrucci *et al*., 2011). On activation, platelets also acutely generate OxPLs, such as 14-HDOHE-PEs and 12-HETE-PE/PCs. 14-HDOHE-PEs are formed as early as 2 minutes by thrombin-activated platelets via 12-LOX, with levels steadily increasing up to 3 hours post-activation (Morgan *et al*., 2010). Similarly, 12-HETE-PEs and 12-HETE-PCs are rapidly synthesised (2 – 5 minutes) via 12-LOX on thrombin stimulation with approximately 100-fold increase by 15 minutes, remaining platelet-associated (Thomas *et al*., 2010). As for free eicosanoids, OxPLs generated by platelets are also proposed to play a role in coagulation, for example 12-HETE-PC enhances tissue factor-dependent thrombin generation *in vitro* (Thomas *et al*., 2010). Therefore, formation of lipids that may signal in coagulation, such as TxA_2, PGE_2, PGD_2 and 12-HETE-PLs, must be fast to ensure an effective response. In this chapter, free and esterified prostaglandin generation by activated human platelets will be determined following stimulation for various time points (0 – 180 minutes) with a range of agonists, including thrombin and collagen, using reverse-phase LC/MS/MS on 4000 Q-trap.

Following formation, lipids that remain platelet-associated are suggested to act either on the plasma membrane, regulating coagulation (e.g. 12-HETE-PCs), or intracellularly as second messengers, such as diacylglycerol (DAG) (Thomas *et al*., 2010; Stefanini *et al*., 2009). Furthermore, cell-associated lipids may alter the dynamics of plasma membrane

during platelet activation, either increasing or decreasing water permeability that could disrupt ion gradients, leading to alterations of platelet metabolic processes, such as calcium transport (Wong-Ekkabut *et al.*, 2007; Varga-Szabo *et al.*, 2009). In contrast, eicosanoids released by activated platelets, such as TxA_2, PGE_2 and PGD_2, are expected to act locally on nearby cells through activation of surface G protein-coupled receptors. Thus, it is important to determine whether free and esterified prostaglandins remain cell-associated or are released following their generation. Furthermore, since multiple agonists (e.g. thrombin and collagen) contribute to platelet activation through stimulation of specific surface receptors, it is crucial to investigate which agonists stimulate the formation of free and esterified prostaglandins.

6.1.1 Aims

The studies described in this chapter aim to:

- Investigate the temporal generation of free and esterified prostaglandins by LC/MS/MS using the 4000 Q-trap mass spectrometer.
- Compare the levels of free and esterified prostaglandins generated by human platelets stimulated with a range of different agonists.
- Determine whether free and esterified prostaglandins generated by thrombin-activated platelets are released or remain cell-associated.

6.2   Results

6.2.1   Free and esterified prostaglandins are acutely generated by agonist-activated human platelets.

To determine the formation of free and esterified prostaglandins, washed human platelets were activated with 0.2 U/ml of thrombin, 10 μg/ml of collagen, 10 μM of calcium ionophore (A23187) or co-stimulated with thrombin and collagen for 2 – 180 minutes. Lipids were extracted and analysed using reverse-phase LC-MS/MS on Q-trap, in MRM mode, as described in Materials and Methods, Sections *2.2.3.2* and *2.2.3.3*.

6.2.1.1 PGE_2/D_2-PEs are acutely generated by human platelets activated with thrombin, collagen or calcium ionophore.

As described in Chapter 4, 18:0a/PGE_2/D_2-PE generated by 2 x 10^8 platelets was just above the limit of detection and, therefore, this isomer will not be measured. LC/MS/MS analysis demonstrated that PGE_2/D_2-PEs formed immediately (2 – 5 minutes) on agonist stimulation. Levels increased up to 10 minutes and then slowly decreased (Figure 6.1 A). Collagen stimulation induced maximum formation at 60 minutes with a decrease thereafter (Figure 6.1 B). In contrast, PGE_2/D_2-PE synthesis by thrombin and collagen combined peaked at 10 minutes (Figure 6.2 A). Following calcium ionophore incubation, levels of PGE_2/D_2-PEs peaked at 30 minutes and then slowly declined (Figure 6.2 B).

Figure 6.1: Generation of PGE$_2$/D$_2$-PEs in response to thrombin or collagen stimulation of platelets. Washed platelets were activated for varying times, lipids extracted and analysed using reverse-phase LC/2MS/MS, monitoring parent [M-H]$^-$ → *m/z* 271.2, as described in Materials and Methods, Section *2.2.3.2*. Levels of PGE$_2$/D$_2$-PEs are expressed as ratio analyte to internal standard. Data presented from one experiment and representative of three (n = 3, mean ± SEM*). ***P < 0.001 versus unstimulated platelets (Control 0 min), using ANOVA and Bonferroni Post Hoc Test. *Panel A*. Platelets were activated using 0.2 U/ml thrombin. *Panel B*. Platelets were activated using 10 µg/ml collagen.

Figure 6.2: Generation of PGE$_2$/D$_2$-PEs in response to thrombin and collagen or A23187 stimulation of platelets. Washed platelets were activated for varying times, lipids extracted and analysed using reverse-phase LC/MS/MS, monitoring parent [M-H]$^-$ → m/z 271.2, as described in Materials and Methods, Section *2.2.3.2*. Levels of PGE$_2$/D$_2$-PEs are expressed as ratio analyte to internal standard. Data presented from one experiment and representative of three (n = 3, mean ± SEM). ***P < 0.001 versus unstimulated platelets (Control 0 min), using ANOVA and Bonferroni Post Hoc Test. *Panel A*. Platelets were co-stimulated with 0.2 U/ml thrombin and 10 µg/ml collagen. *Panel B*. Platelets were activated using 10 µM A23187.

6.2.1.2 Free PGE_2 and PGD_2 are acutely generated by human platelets activated with thrombin, collagen or calcium ionophore.

PGE_2 and PGD_2 formed immediately on agonist activation (2 minutes) with levels steadily increasing up to 60 – 120 minutes following thrombin stimulation (Figure 6.3 A). In contrast, on activation with either collagen alone or combined with thrombin, generation of PGE_2 and PGD_2 peaked at 10 minutes and then levelled off (Figures 6.3 B and 6.4 A). Calcium ionophore induced synthesis of PGD_2 that peaked at 5 minutes and then plateaued, while PGE_2 levels steadily increased up to 120 minutes (Figure 6.4 B).

6.2.1.3 PGb-PEs are acutely generated by human platelets activated with thrombin, collagen or calcium ionophore.

LC/MS/MS analysis demonstrated that PGb-PEs formed immediately (2 minutes) on agonist stimulation, similarly to PGE_2/D_2-PEs. Following thrombin activation, generation of PGb-PEs peaked at 10 minutes, with levels slowly declining (Figure 6.5 A). Collagen induced PGb-PE formation but seemingly at slower rate, with levels steadily rising up to 60 minutes (Figure 6.5 B). On co-stimulation with thrombin and collagen, levels increased up to 10 minutes and, after 30 minutes, gradually reduced (Figure 6.6 A). Platelets stimulated with calcium ionophore formed PGb-PEs that steadily increased up to 120 minutes (Figure 6.6 B).

Figure 6.3: Generation of PGE$_2$ and PGD$_2$ in response to thrombin or collagen stimulation of platelets. Washed platelets were activated for varying times, lipids extracted and analysed using reverse-phase LC/MS/MS, monitoring *m/z* 351.2 → *m/z* 271.2 as described in Materials and Methods, Section *2.2.3.3*. Levels of PGE$_2$ and PGD$_2$ are expressed as ng/2 x 10^8 platelets. Data presented from one experiment and representative of three (n = 3, mean ± SEM). ***P < 0.001 versus unstimulated platelets (Control 0 min), using ANOVA and Bonferroni Post Hoc Test. *Panel A*. Platelets were activated using 0.2 U/ml thrombin. *Panel B*. Platelets were activated using 10 µg/ml collagen.

Figure 6.4: Generation of PGE$_2$ and PGD$_2$ in response to collagen and thrombin or A23187 stimulation of platelets. Washed platelets were activated for varying times, lipids extracted and analysed reverse-phase LC/MS/MS, monitoring *m/z* 351.2 → 271.2 as described in Materials and Methods, Section *2.2.3.3*. Levels of PGE$_2$ and PGD$_2$ are expressed as ng/2 x 10^8 platelets. Data presented from one experiment and representative of three (n = 3, mean ± SEM). ***P < 0.001 versus unstimulated platelets (Control 0 min), using ANOVA and Bonferroni Post Hoc Test. *Panel A*. Platelets were co-stimulated with 0.2 U/ml thrombin and 10 µg/ml collagen. *Panel B*. Platelets were activated using 10 µM A23187.
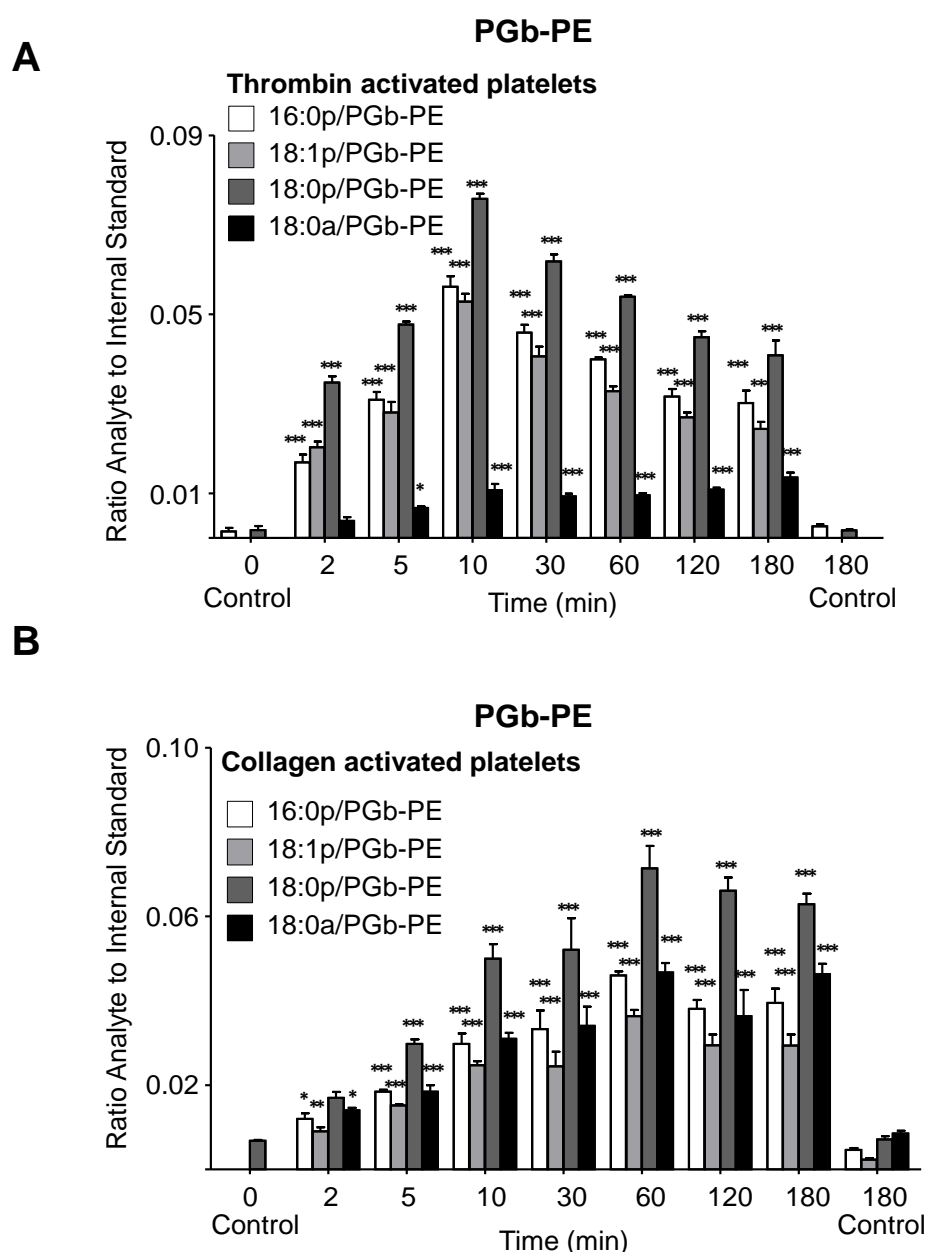
Figure 6.5: Generation of PGb-PEs in response to thrombin or collagen stimulation of platelets. Washed platelets were activated for varying times, lipids extracted and analysed using reverse-phase LC/MS/MS, monitoring parent [M-H]$^-$ → m/z 351.2, as described in Materials and Methods, Section *2.2.3.2*. Levels are expressed as ratio analyte to internal standard. Data presented from one experiment and representative of three (n = 3, mean ± SEM). *P < 0.05, **P < 0.01 and ***P < 0.001 versus unstimulated platelets (Control 0 min), using ANOVA and Bonferroni Post Hoc Test. *Panel A*. Platelets were activated using 0.2 U/ml thrombin. *Panel B*. Platelets were activated using 10 μg/ml collagen.

Figure 6.6: Generation of PGb-PEs in response to collagen and thrombin or A23187 stimulation of platelets. Washed platelets were activated for varying times, lipids extracted and analysed using reverse-phase LC/MS/MS, monitoring parent [M-H]⁻ → *m/z* 351.2 as described in Materials and Methods, Section *2.2.3.2*. Levels are expressed as ratio analyte to internal standard. Data presented from one experiment and representative of three (n = 3, mean ± SEM). *P < 0.05, **P < 0.01 and ***P < 0.001 versus unstimulated platelets (Control 0 min), using ANOVA and Bonferroni Post Hoc Test. *Panel A*. Platelets were co-stimulated with 0.2 U/ml thrombin and 10 µg/ml collagen. *Panel B*. Platelets were activated using 10 µM A23187.

6.2.1.4 Free PGb is acutely generated by human platelets activated with thrombin, collagen or calcium ionophore.

PGb formed following 2 minutes by agonist-stimulated platelets. On thrombin activation, levels increased up to 60 minutes and then reached a plateau (Figure 6.7 A). Following incubation with either collagen alone or combined with thrombin, synthesis of PGb peaked at 10 minutes, with levels gradually decreasing over time (Figure 6.7 B and 6.8 A). In contrast, on calcium ionophore stimulation, levels of PGb increased up to 120 minutes (Figure 6.8 B).

6.2.1.5 PGc-PEs are acutely generated by human platelets activated with thrombin, collagen or calcium ionophore.

PGc-PEs formed acutely on agonist stimulation (2 minutes), similarly to PGE_2/D_2-PEs and PGb-PEs. On thrombin activation, levels of PGc-PEs increased up to 10 minutes and then levelled off (Figure 6.9 A), whereas, following collagen stimulation, PGc-PE generation gradually increased up to 60 minutes (Figure 6.9 B). Addition of collagen and thrombin together induced PGc-PE formation, which levels peaked at 10 minutes and then gradually decreased (Figure 6.10 A). PGc-PEs were generated on calcium ionophore stimulation with levels increasing gradually up to 60 minutes and then plateau (Figure 6.10 B).
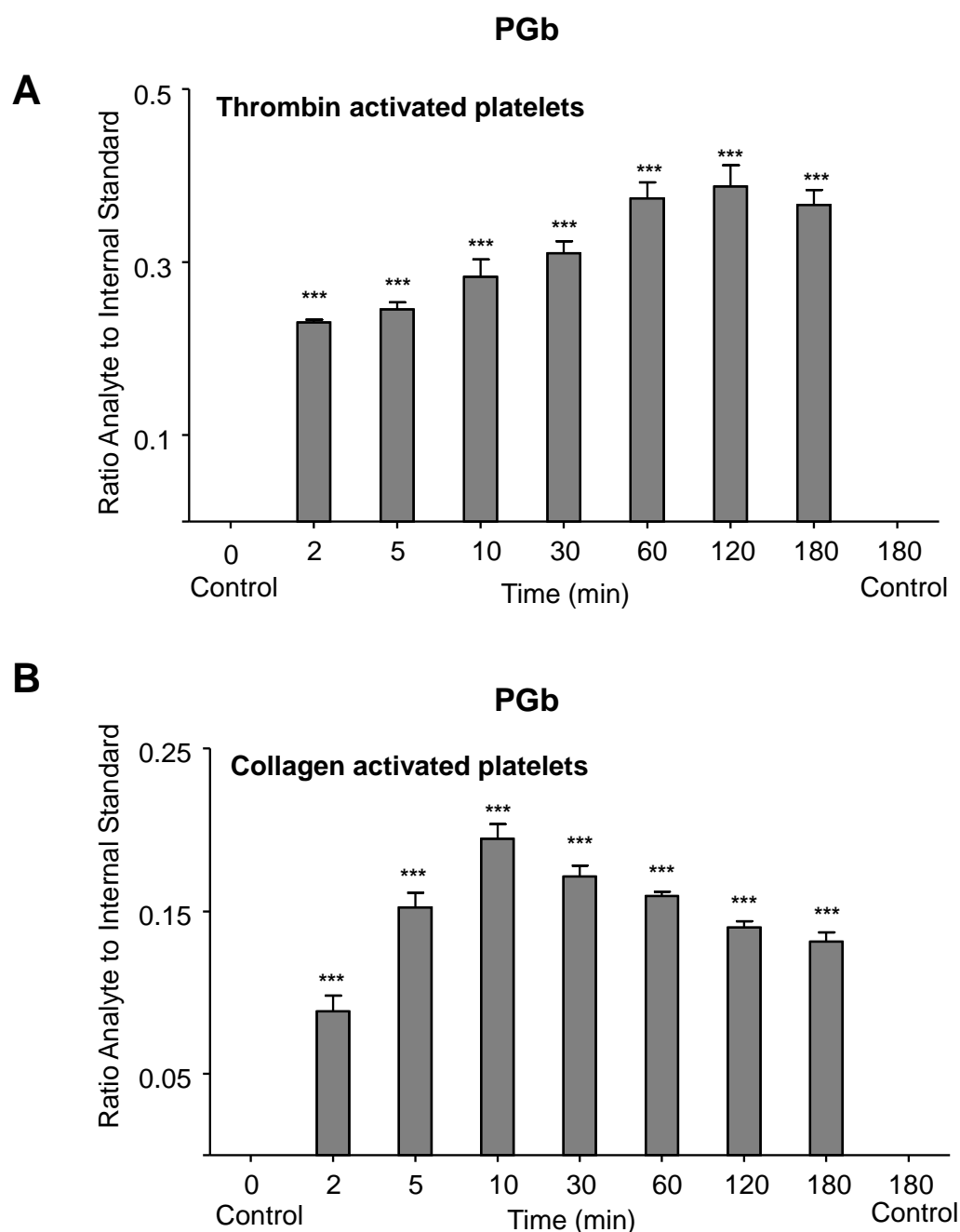
Figure 6.7: Generation of PGb in response to thrombin or collagen stimulation of platelets. Washed platelets were activated for varying times, lipids extracted and analysed using reverse-phase LC/MS/MS, monitoring *m/z* 351.2 → 207.1 as described in Materials and Methods, Section *2.2.3.3*. Levels are expressed as ratio analyte to internal standard. Data presented from one experiment and representative of three (n = 3, mean ± SEM). ***P < 0.001 versus unstimulated platelets (Control 0 min), using ANOVA and Bonferroni Post Hoc Test. *Panel A*. Platelets were activated using 0.2 U/ml thrombin. *Panel B*. Platelets were activated using 10 μg/ml collagen.
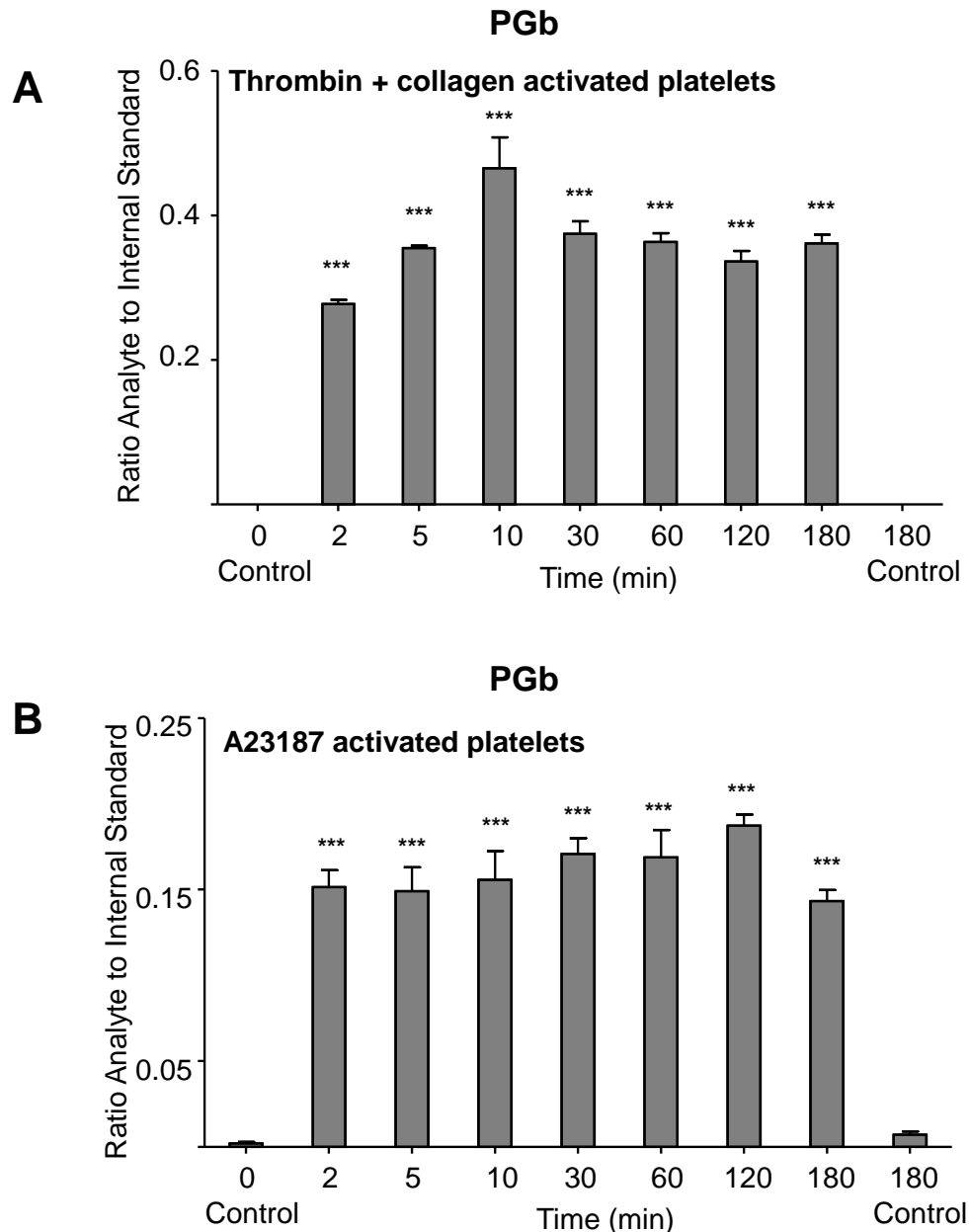
Figure 6.8: Generation of PGb in response to collagen and thrombin or A23187 stimulation of platelets. Washed platelets were activated for varying times, lipids extracted and analysed using reverse-phase LC/MS/MS, monitoring *m/z* 351.2 → 207.1 as described in Materials and Methods, Section *2.2.3.3*. Levels are expressed as ratio analyte to internal standard. Data presented from one experiment and representative of three (n = 3, mean ± SEM).). ***P < 0.001 versus unstimulated platelets (Control 0 min), using ANOVA and Bonferroni Post Hoc Test. *Panel A*. Platelets were co-stimulated with 0.2 U/ml thrombin and 10 µg/ml collagen. *Panel B*. Platelets were activated using 10 µM A23187.
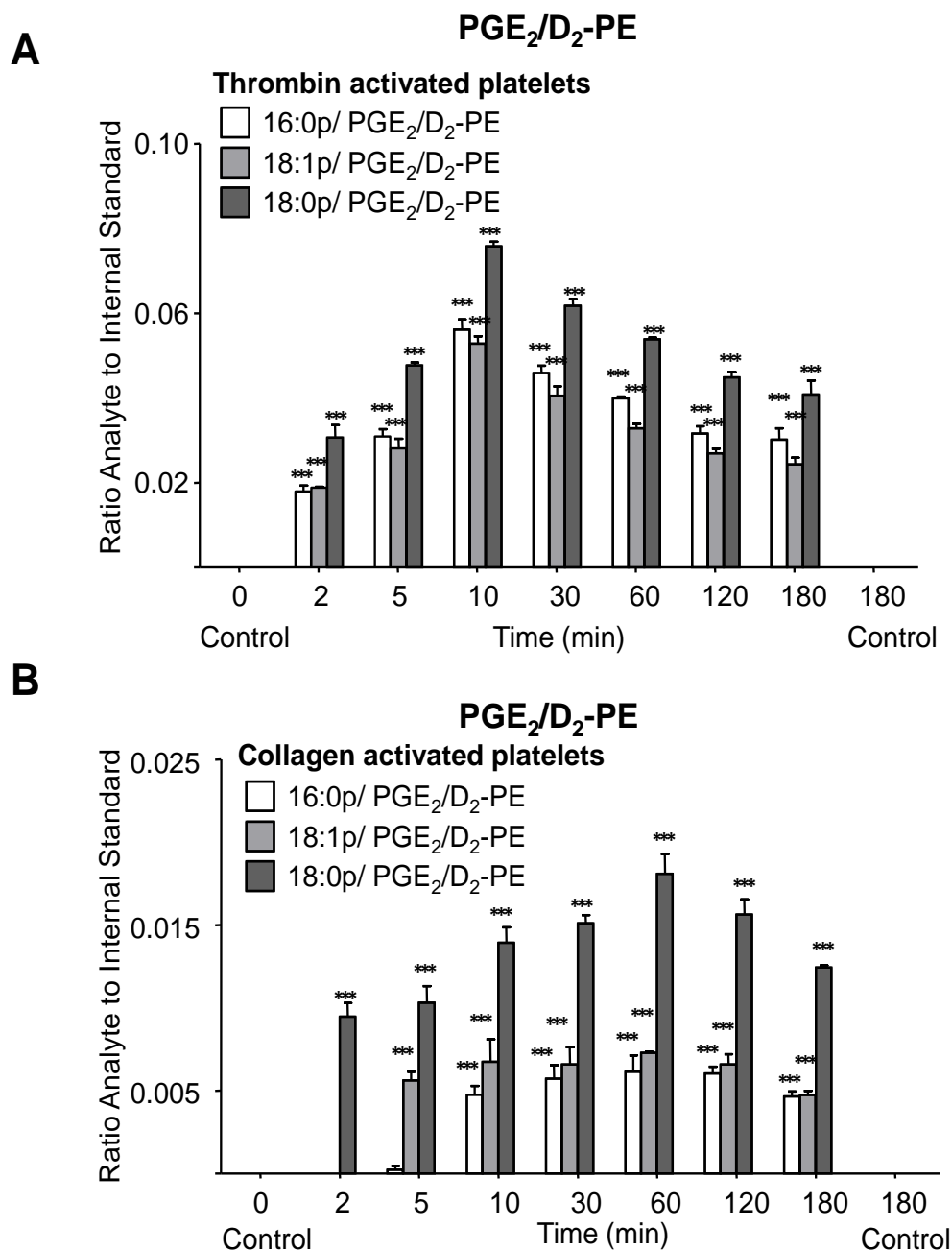
Figure 6.9: Generation of PGc-PEs in response to thrombin or collagen stimulation of platelets. Washed platelets were activated for varying times, lipids extracted and analysed using reverse-phase LC/MS/MS, monitoring parent [M-H]⁻ → *m/z* 351.2 as described in Materials and Methods, Section *2.2.3.2*. Levels are expressed as ratio analyte to internal standard. Data presented from one experiment and representative of three (n = 3, mean ± SEM). **P < 0.01 and ***P < 0.001 versus unstimulated platelets (Control 0 min), using ANOVA and Bonferroni Post Hoc Test. *Panel A*. Platelets were activated using 0.2 U/ml thrombin. *Panel B*. Platelets were activated using 10 µg/ml collagen.
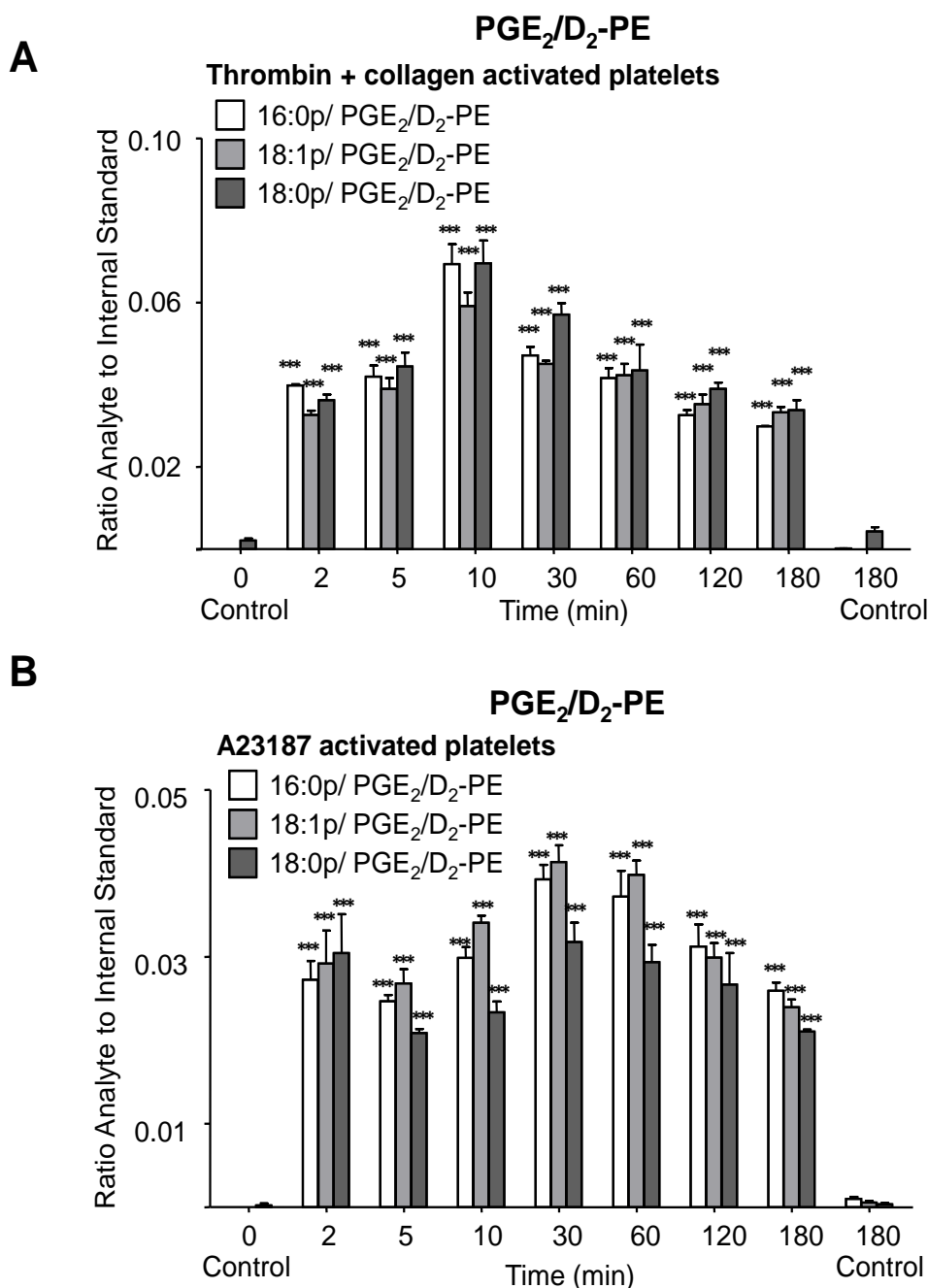
Figure 6.10: Generation of PGc-PEs in response to collagen and thrombin or A23187 stimulation of platelets. Washed platelets were activated for varying times, lipids extracted and analysed using reverse-phase LC/MS/MS, monitoring parent [M-H]⁻ → *m/z* 351.2 as described in Materials and Methods, Section *2.2.3.2*. Levels are expressed as ratio analyte to internal standard. Data presented from one experiment and representative of three (n = 3, mean ± SEM). *P < 0.05, **P < 0.01 and ***P < 0.001 versus unstimulated platelets (Control 0 min), using ANOVA and Bonferroni Post Hoc Test. *Panel A*. Platelets were co-stimulated with 0.2 U/ml thrombin and 10 µg/ml collagen. *Panel B*. Platelets were activated using 10 µM A23187.

6.2.1.6 PGc is acutely generated by human platelets activated with thrombin, collagen or calcium ionophore.

PGc formed within 2 minutes following agonist activation. On either thrombin or collagen stimulation, levels of PGc steadily increased up to 60 minutes (Figure 6.11). In contrast, on activation with collagen and thrombin combined, generation of PGc peaked at 10 minutes and, after 30 minutes, levelled off (Figures 6.12 A). Calcium ionophore induced synthesis of PGc, which levels peaked at 30 minutes and then plateau (Figure 6.12 B).

6.2.2 Different platelet agonists induce distinct levels of free and esterified prostaglandins.

Free and esterified prostaglandins were immediately formed (within 2 minutes) by agonist-activated platelets with levels increasing up to 10 – 30 minutes post stimulation, as described in Section *6.2.1*. These observations suggest that receptors on the platelet plasma membrane, such as thrombin (PAR-1/-4) and collagen receptors (glycoprotein VI) are ultimately responsible for the initiation of free and esterified prostaglandin synthesis. To determine the optimum agonist and, thus, the receptor likely to be involved in free and esterified prostaglandin formation, washed platelets derived from one donor were stimulated with a range of different agonists at the same time.

Human platelets were incubated with either 0.2 U/ml of thrombin, 10 µg/ml of collagen, thrombin and collagen combined or 10 µM of calcium ionophore (A23187), for 30 minutes at $37^{o}C$, in the presence of 1 mM $CaCl_2$. Lipids were subsequently extracted and analysed using LC/MS/MS on Q-trap as described in Materials and Methods, Sections *2.2.3.2* and *2.2.3.3*. Note that agonists were used at the given standard concentrations as described previously (Kasirer-Friede *et al.*, 1999; Chen *et al.*, 2002; Thomas *et al.*, 2010). The length of stimulation time was chosen based on the temporal generation of free and esterified prostaglandins described earlier in this chapter. At 30 minutes, all agonists induced considerable levels of free and esterified prostaglandins.
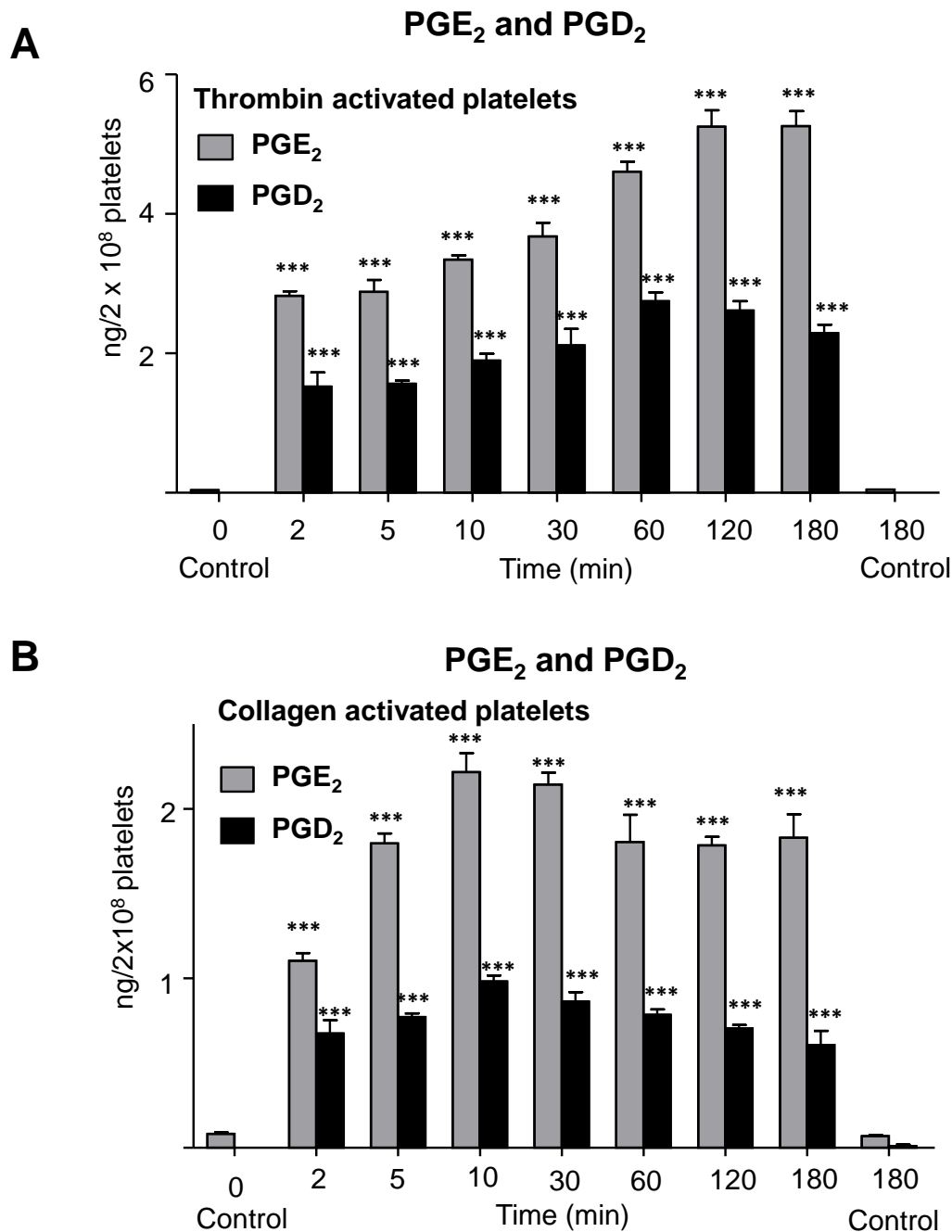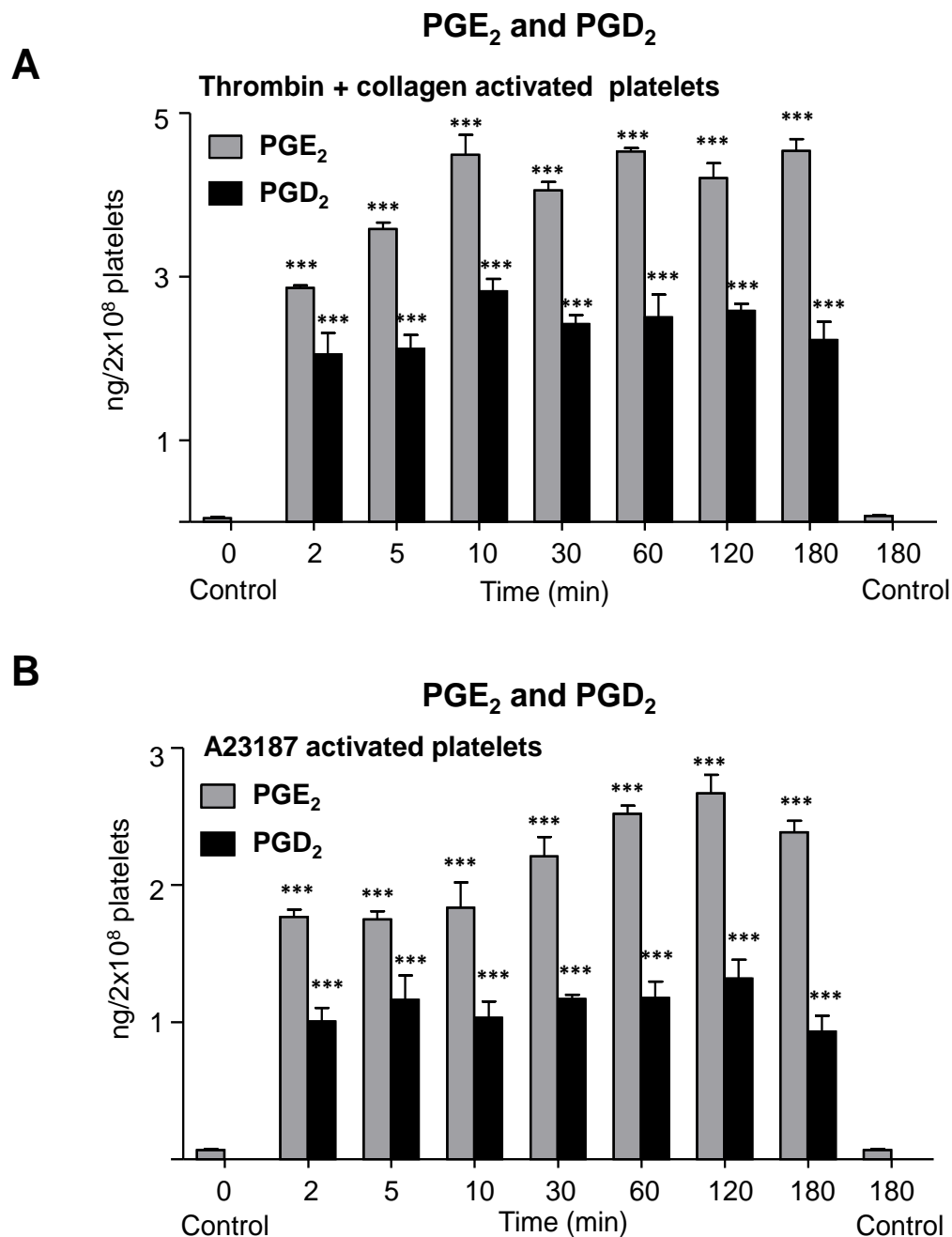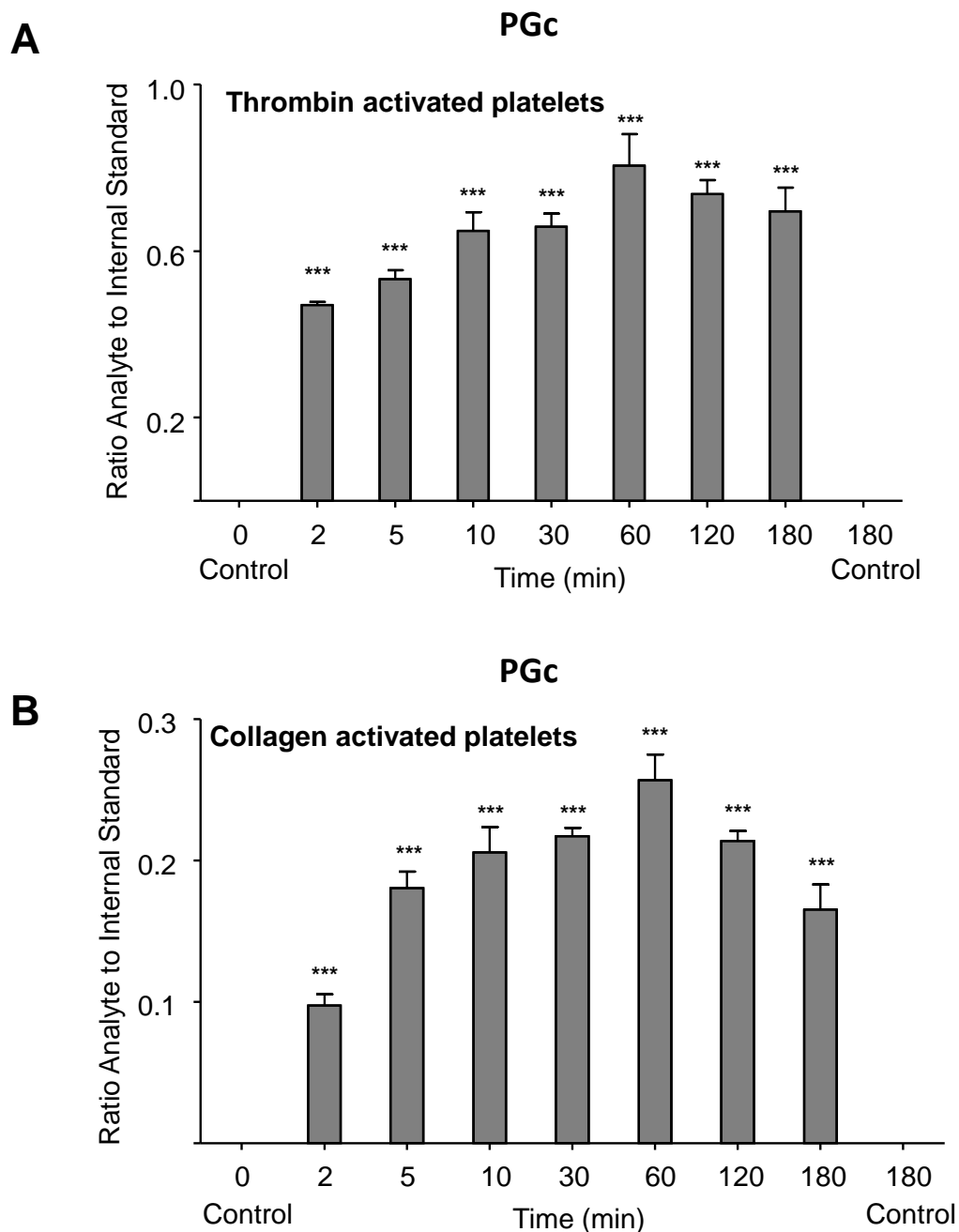
Figure 6.11: Generation of PGc in response to thrombin or collagen stimulation of platelets. Washed platelets were activated for varying times, lipids extracted and analysed using reverse-phase LC/MS/MS, monitoring *m/z* 351.2 → 165.1 as described in Materials and Methods, Section *2.2.3.3*. Levels are expressed as ratio analyte to internal standard. Data presented from one experiment and representative of three (n = 3, mean ± SEM). ***P < 0.001 versus unstimulated platelets (Control 0 min), using ANOVA and Bonferroni Post Hoc Test. *Panel A*. Platelets were activated using 0.2 U/ml thrombin. *Panel B*. Platelets were activated using 10 µg/ml collagen.
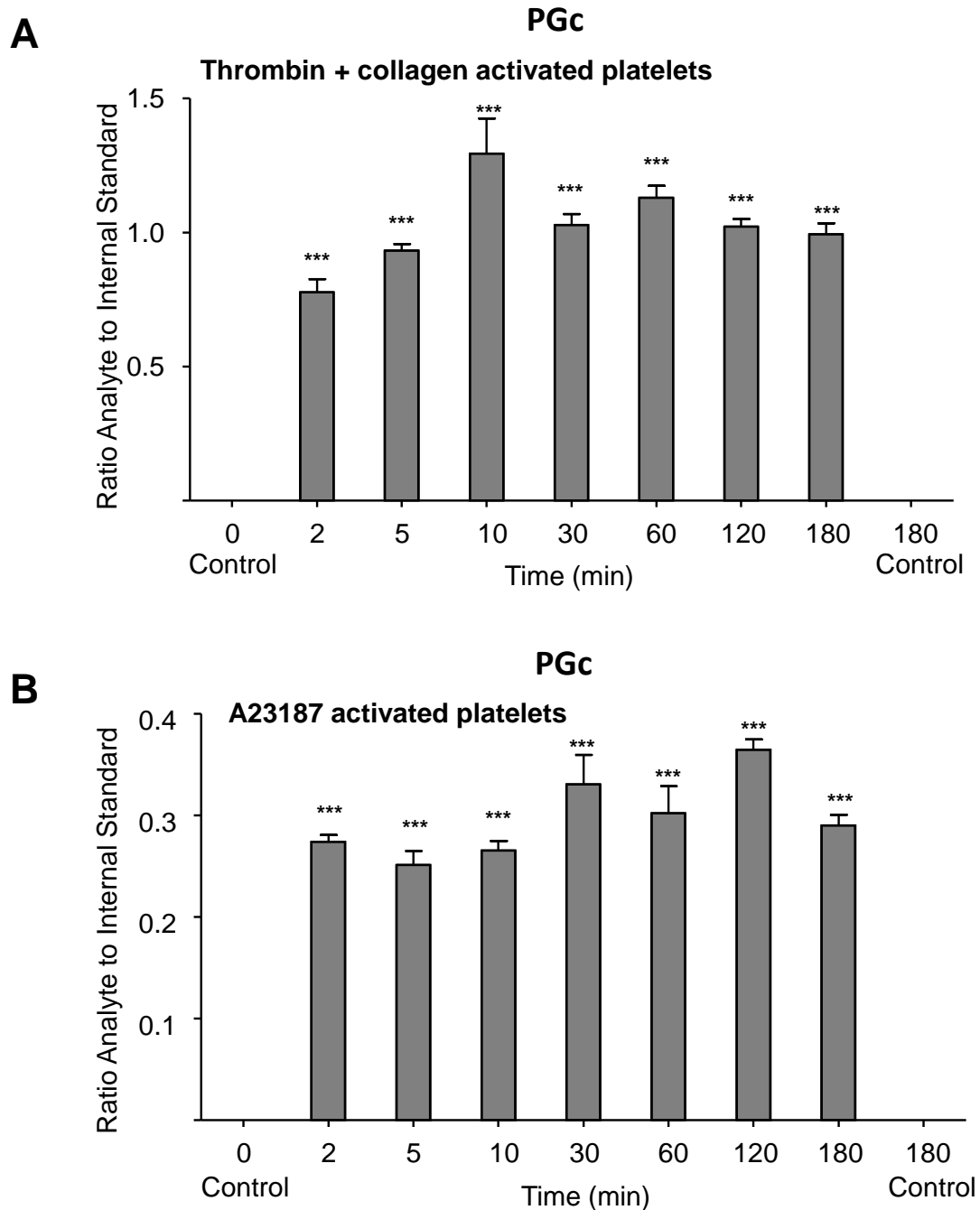
Figure 6.12: Generation of free PGc in response to collagen and thrombin or A23187 stimulation of platelets. Washed platelets were activated for varying times, lipids extracted and analysed using reverse-phase LC/MS/MS, monitoring *m/z* 351.2 → 165.1 as described in Materials and Methods, Section *2.2.3.3*. Levels are expressed as ratio analyte to internal standard. Data presented from one experiment and representative of three (n = 3, mean ± SEM).). ***P < 0.001 versus unstimulated platelets (Control 0 min), using ANOVA and Bonferroni Post Hoc Test. *Panel A*. Platelets were co-stimulated with 0.2 U/ml thrombin and 10 μg/ml collagen. *Panel B*. Platelets were activated using 10 μM A23187.

Platelets stimulated with calcium ionophore generated highest levels of esterified prostaglandins (Figure 6.13 – 6.15), whereas collagen was the least effective. Thrombin was the optimum physiological platelet agonist to induce free PGE_2 and PGD_2 formation at the concentrations and timepoints chosen (Figure 6.13 B). Co-stimulation with collagen and thrombin generated highest levels of free PGb (Figure 6.14 B) and induced an additive effect on PGc formation (Figure 6.15 B).

The agonist efficiency to induce formation of esterified prostaglandins was in the order: calcium ionophore > thrombin and collagen combined > thrombin > collagen; PGE_2 and PGD_2: thrombin ≥ thrombin and collagen combined > calcium ionophore > collagen; PGb and PGc: thrombin and collagen combined ≥ thrombin> collagen > calcium ionophore.

6.2.3 *Phospholipid-esterified prostaglandins are primarily retained by activated platelets while free prostaglandins are secreted.*

To determine whether the lipids were retained or released, washed platelets were stimulated with thrombin (0.2 U/ml for 30 min at 37°C), then pelleted by centrifugation (970 X g for 10 min) while the supernatant was aspirated and subjected to a higher spin (16,060 X g for 10 min) to pellet platelet microvesicles. Lipids were extracted and subsequently analysed using reverse-phase LC/MS/MS, as described in Materials and Methods, Section *2.2.3.2* and *2.2.3.3*.

The majority of esterified prostaglandins were predominantly retained (~ 90 %) by activated platelets, with small amounts appearing in either microparticles or supernatant (Figures 6.16 A, 6.17 A and 6.18 A). In contrast, approximately 95 % of free prostaglandins were released (Figures 6.16 B, 6.17 B and 6.18 B).
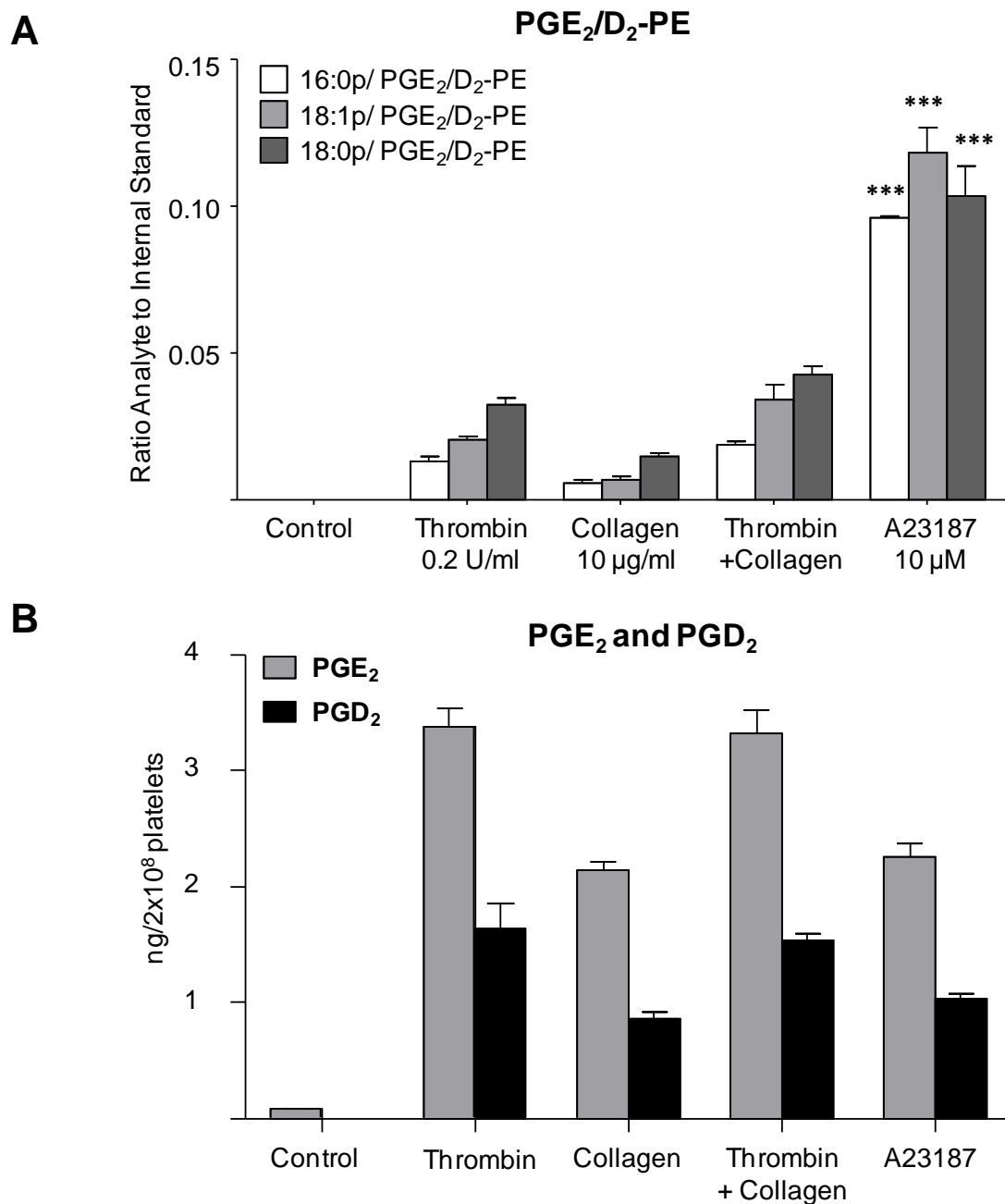
Figure 6.13: Generation of free and esterified PGE$_2$ and PGD$_2$ by human platelets in response to different agonists. Washed human platelets were activated for 30 min at 37° C in the presence of 1 mM CaCl$_2$. Lipids were then extracted and analysed using reverse-phase LC/MS/MS, as described in Materials and Methods, Section *2.2.3.2* and *2.2.3.3*. Levels of PGE$_2$/D$_2$-PEs are expressed as ratio analyte to internal standard. Levels of PGE$_2$ and PGD$_2$ are expressed as ng/2 x 10^8 platelets. Data presented from one experiment and representative of three (n = 3, mean ± SEM). ***P < 0.001 versus thrombin, using ANOVA and Bonferroni Post Hoc Test. *Panel A*. Generation of PGE$_2$/D$_2$-PEs in response to thrombin, collagen and A23187. *Panel B*. Generation of PGE$_2$ and PGD$_2$ in response to thrombin, collagen and A23187.

Figure 6.14: Generation of free and esterified PGb by human platelets in response to different agonists. Washed human platelets were activated for 30 min at 37° C in the presence of 1 mM CaCl$_2$. Lipids were then extracted and analysed using reverse-phase LC/MS/MS, as described in Materials and Methods, Section *2.2.3.2* and *2.2.3.3*. Levels of PGb-PEs and PGb are expressed as ratio analyte to internal standard. Data presented from one experiment and representative of three (n = 3, mean ± SEM). ***P < 0.001 versus thrombin, using ANOVA and Bonferroni Post Hoc Test. *Panel A*. Generation of PGb-PEs in response to thrombin, collagen and A23187. *Panel B*. Generation of PGb in response to thrombin, collagen and A23187.
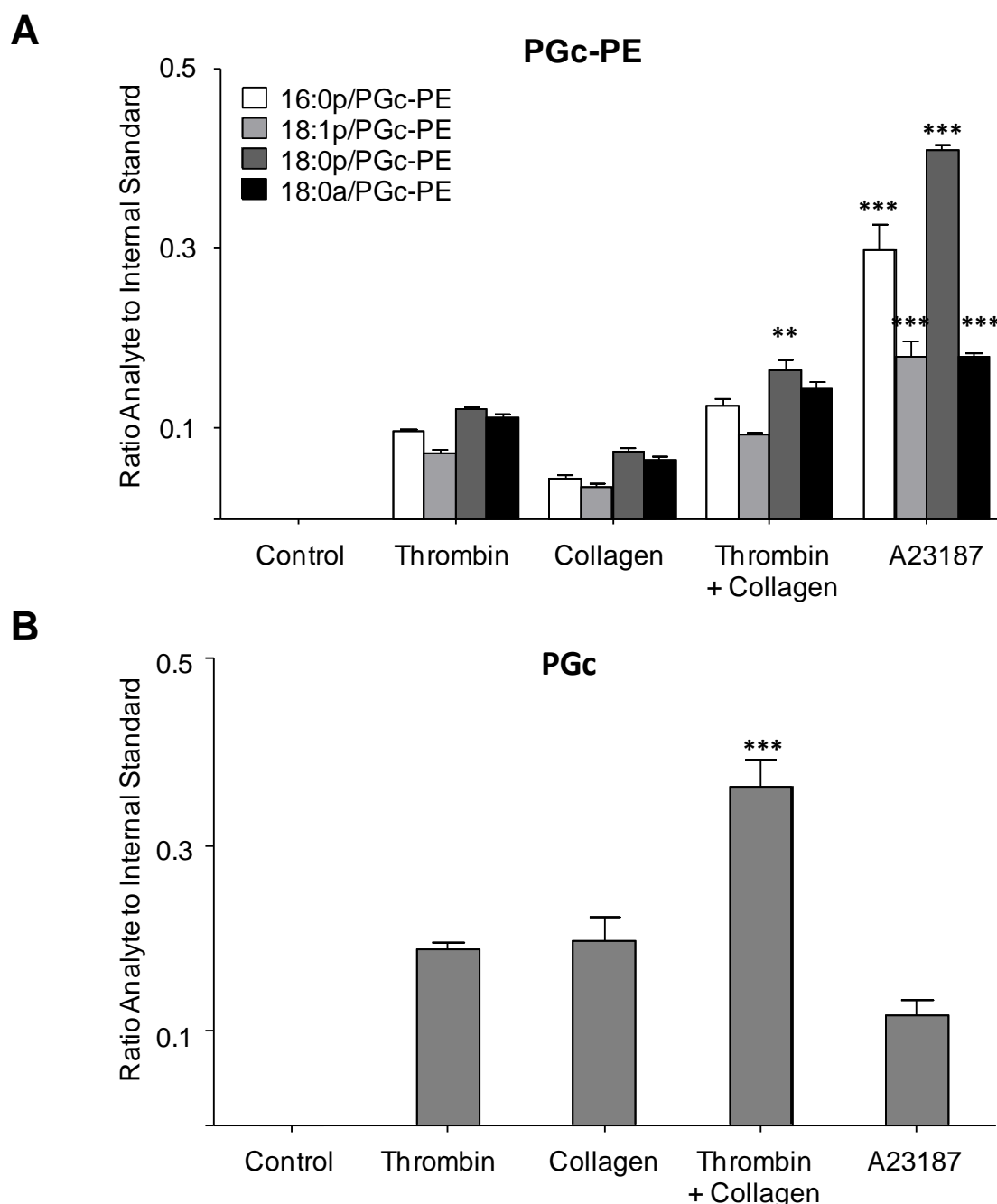
Figure 6.15: Generation of free and esterified PGc by human platelets in response to different agonists. Washed human platelets were activated for 30 min at 37° C in the presence of 1 mM CaCl$_2$. Lipids were then extracted and analysed using reverse-phase LC/MS/MS, as described in Materials and Methods, Section *2.2.3.2* and *2.2.3.3*. Levels of PGc-PEs and PGc are expressed as ratio analyte to internal standard. Data presented from one experiment and representative of three (n = 3, mean ± SEM). **P < 0.01 and ***P < 0.001 versus thrombin, using ANOVA and Bonferroni Post Hoc Test. *Panel A*. Generation of PGc-PEs in response to thrombin, collagen and A23187. *Panel B*. Generation of PGc in response to thrombin, collagen and A23187.

Figure 6.16: PGE₂/D₂-PEs are retained by platelets while PGE₂ and PGD₂ are released. Washed human platelets were activated with thrombin (0.2 U/ml for 30 min at 37°C) before centrifugation at 970 X g for 10 min. Supernatant was then centrifuged at 16,060 X g for 10 min to pellet microparticles before lipid extraction. Lipids were analysed using reverse-phase LC/MS/MS, as described in Materials and Methods, Section *2.2.3.2* and *2.2.3.3*. Levels of PGE₂/D₂-PEs are expressed as ratio analyte to internal standard. Levels of PGE₂ and PGD₂ are expressed as ng/2 x 10⁸ platelets. Data presented from one experiment and representative of three (n = 3, mean ± SEM). ***P < 0.001 versus control, using ANOVA and Bonferroni Post Hoc Test. *Panel A*. Levels of PGE₂/D₂-PEs measured in platelets, vesicles and supernatant. *Panel B*. Levels of PGE₂ and PGD₂ measured in platelets, vesicles and supernatant.
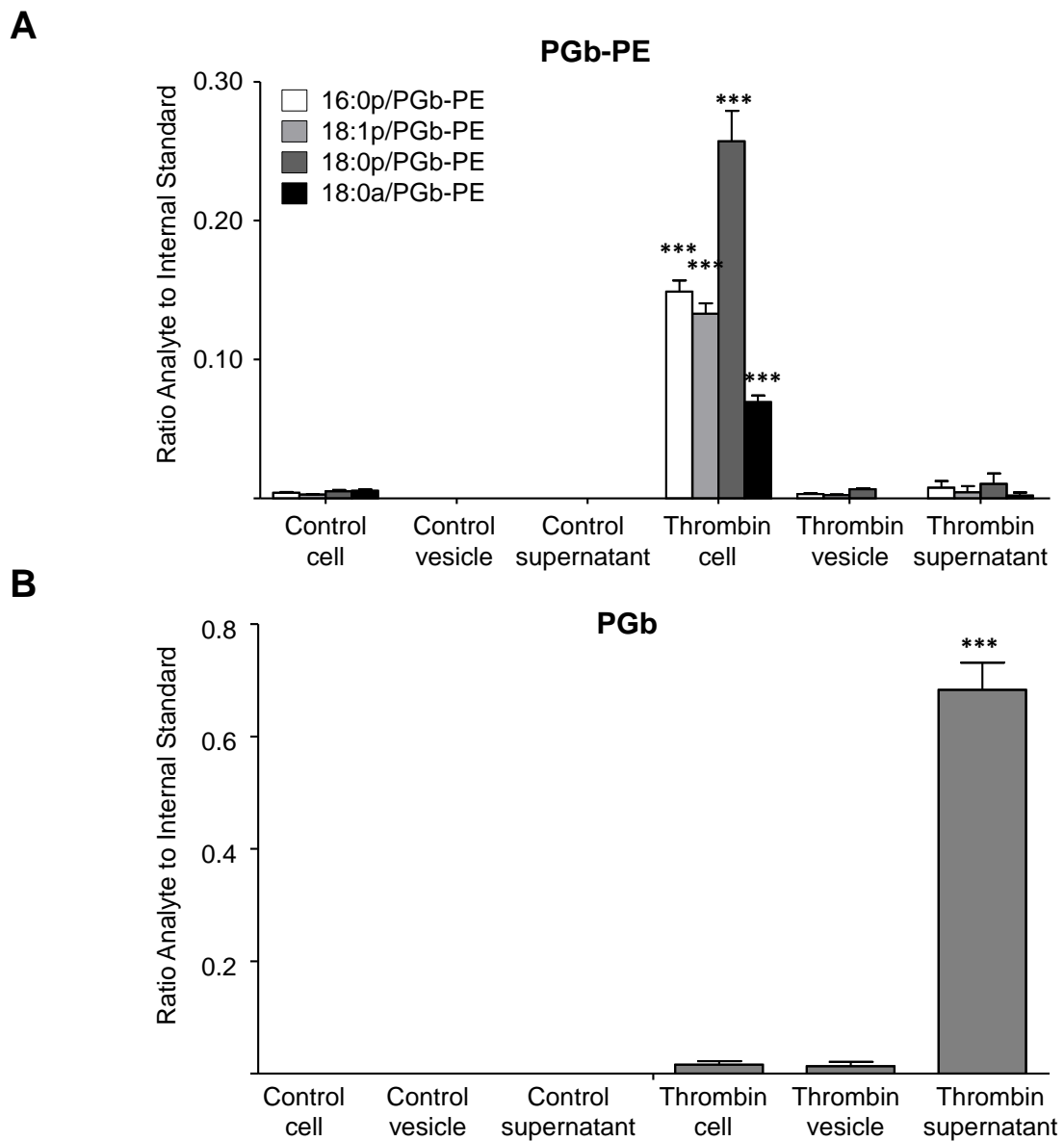
Figure 6.17: PGb-PEs are retained by platelets while PGb is released. Washed human platelets were activated with thrombin (0.2 U/ml for 30 min at 37°C) before centrifugation at 970 X g for 10 min. Supernatant was then centrifuged at 16,060 X g for 10 min to pellet microparticles before lipid extraction. Lipids were analysed using reverse-phase LC/MS/MS, as described in Materials and Methods, Section *2.2.3.2* and *2.2.3.3*. Levels of PGb-PEs and free PGb are expressed as ratio analyte to internal standard. Data presented from one experiment and representative of three (n = 3, mean ± SEM). ***P < 0.001 versus control, using ANOVA and Bonferroni Post Hoc Test. *Panel A*. Levels of PGb-PEs measured in platelets, vesicles and supernatant. *Panel B*. Levels of free PGb measured in platelets, vesicles and supernatant.
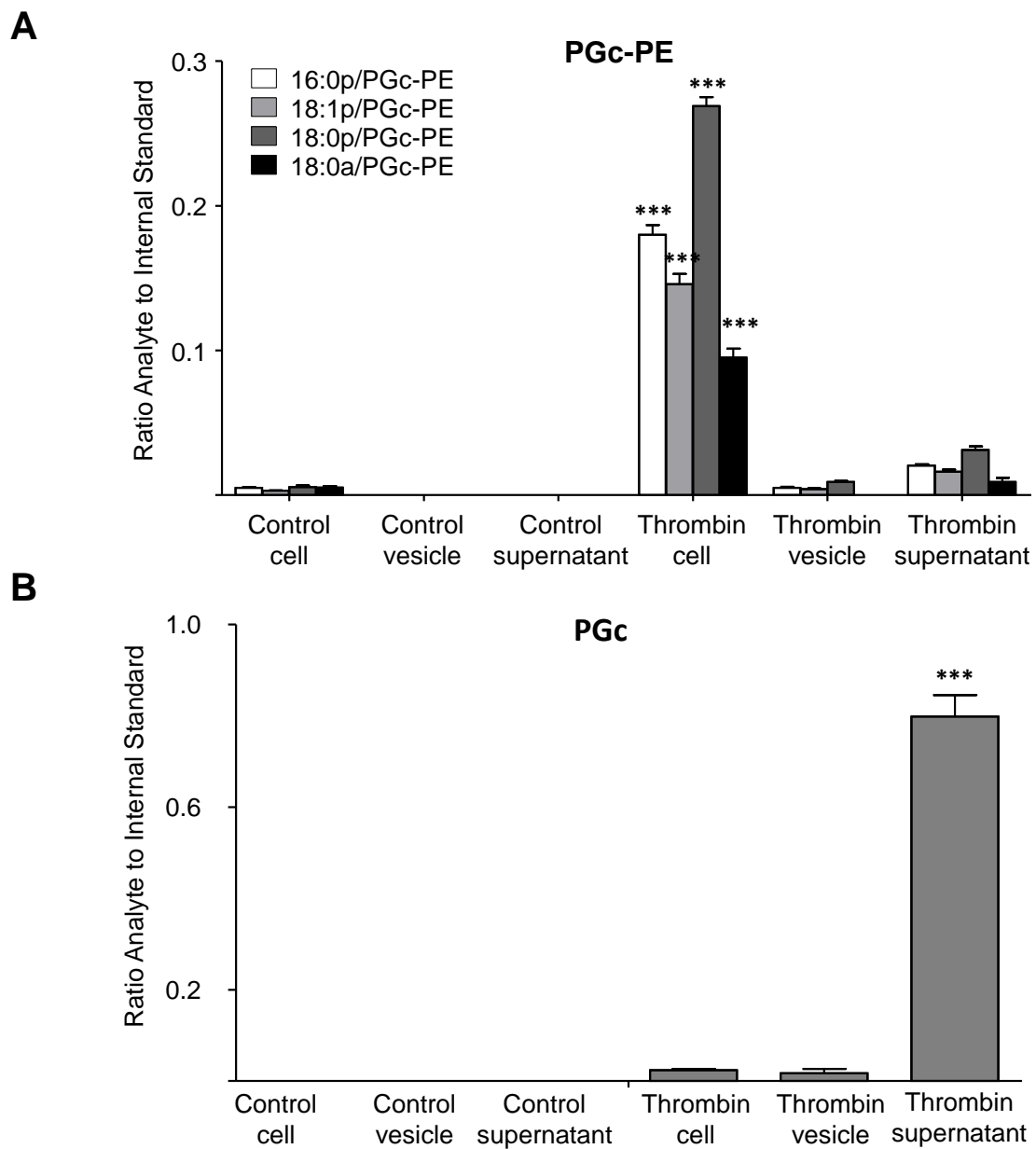
Figure 6.18: PGc-PEs are retained by platelets while PGc is released. Washed human platelets were activated with thrombin (0.2 U/ml for 30 min at 37°C) before centrifugation at 970 X g for 10 min. Supernatant was then centrifuged at 16,060 X g for 10 min to pellet microparticles before lipid extraction. Lipids were analysed using reverse-phase LC/MS/MS, as described in Materials and Methods, Section *2.2.3.2* and *2.2.3.3*. Levels of PGc-PEs and free PGc are expressed as ratio analyte to internal standard. Data presented from one experiment and representative of three (n = 3, mean ± SEM). ***P < 0.001 versus control, using ANOVA and Bonferroni Post Hoc Test. *Panel A*. Levels of PGc-PEs measured in platelets, vesicles and supernatant. *Panel B*. Levels of free PGc measured in platelets, vesicles and supernatant.

6.3 Discussion

This chapter demonstrates that esterified prostaglandins are formed within the first 2 minutes of platelet activation, comparable to the timescale for the generation of free prostaglandins. This is in line with previous studies showing acute formation (2 – 5 minutes) of 12-HETE-PE/PCs and 14-HDOHE-PEs by agonist-activated human platelets (Thomas *et al.*, 2010; Morgan *et al.*, 2010). These OxPLs are generated in a highly regulated manner via 12-LOX catalysis and require stimulation of several signalling pathways, including calcium and PLA$_2$. It is possible that free and esterified prostaglandins are also enzymatically generated and, since platelet PGE$_2$ and PGD$_2$ are formed via COX-1, it is likely that synthesis of PGE$_2$/D$_2$-PEs will involve COX-1 (Mustard *et al.*, 1980).

Levels of esterified prostaglandins peaked around 10 to 30 minutes post stimulation before starting to decline, unlike free prostaglandins, which remained stable or continue to increase up to 3 hours following platelet activation (Figures 6.1 – 6.12). This suggests that esterified prostaglandins may be further metabolised into different products over time; for example, the PE headgroup could be converted to PC by PE methyltransferase or to PS by PS synthase (Berg *et al.*, 2002). Enzymatic elongation of the sn2 fatty acid by addition of C$_2$H$_4$ may also occur (Rosenthal & Hill, 1986; Jakobsson *et al.*, 2006). Hydrolysis of phospholipid esterified prostaglandins by PLA$_2$ during platelet activation and membrane remodelling could also account for the decrease of esterified prostaglandin generation observed over time. In this case, PLA$_2$ could cleave esterified prostaglandins, such as PGE$_2$/D$_2$-PE, at the sn2 position releasing PGE$_2$ and PGD$_2$ into the extracellular space.

Furthermore, levels of esterified prostaglandins were considerably higher in platelets activated with calcium ionophore (A23187) compared to other agonists (Figure 6.13 – 6.15). This suggests that the generation of these lipids requires calcium, similar to TxA$_2$, PGE$_2$, PGD$_2$ and 12-HETE-PE/PCs (Pickett *et al.*, 1976; Knapp *et al.*, 1977; Jurk & Kehrel, 2005; Thomas *et al.*, 2010).

Similar to OxPLs generated by LOXs, esterified prostaglandins remained cell-associated (Figures 6.16 – 6.18). This suggests that PG-PEs are likely to act locally, at the platelet

surface or intracellular membranes. Furthermore, OxPLs may alter the properties of biological plasma membranes. For example, the polarity and shape of OxPLs may differ significantly from the characteristic architecture of their non-OxPLs, such that their polar groups can protrude from the plasma membrane. Addition of polar oxygen atoms to fatty acids may cause the oxidised fatty acid to protrude into the aqueous environment, facilitating direct physical access of the lipid with the cell surface. In the case of oxidised PCs, this has led to the "Lipid Whisker Hypothesis", where oxidised PCs, with protruding sn2-oxidised fatty acid acyl chains residing in the extracellular space, act as scavenger receptor ligands for macrophage scavenger receptor CD36 (Greenberg *et al.*, 2008). Greenberg suggested that receptor ligand recognition was independent of the oxidised phospholipid headgroup, but rather the sn2-oxidised fatty acid confers CD36 recognition in a membrane (Greenberg *et al.*, 2008). Due to their shape and polarity, PGE_2 and PGD_2 esterified to PEs may also protrude from the intracellular membrane surface towards the water phase where they may interact with cytosolic proteins. Furthermore, chemical oxidation of membranes can decrease bilayer thickness or enhance water permeability (Wong-Ekkabut *et al.*, 2007). Esterified prostaglandins may act in a similar manner, affecting membrane dynamics during platelet activation. These lipids may play a role in events that involve significant membrane disturbance, such as vesiculation or degranulation (Aldrovandi *et al.*, 2013).

Unlike esterified prostaglandins, free PGb and PGc were primarily secreted, suggesting an autocrine or paracrine mode of action similar to PGE_2 and PGD_2. PGE_2 is generally considered to be an inducer of inflammation, promoting activation of neutrophils, and inhibiting platelet aggregation through activation of PGE_2 receptor subtype EP2 and EP4 (Kalinski, 2012; Heptinstall *et al.*, 2008; Smith *et al.*, 2010). Whereas, PGD_2 signals as chemoattractant for immune cells, such as eosinophils, and inhibits platelet aggregation (Smith *et al.*, 1974; Hirai *et al.*, 2001). Free PGb and PGc may also participate in similar processes during innate immune events to restore and maintain homeostasis. Future studies using PGb and PGc standards will enable elucidation of their biological activity once their structures are known.

Chapter 7

7 Investigating the Requirement for COX-1 in the Generation of Esterified Prostaglandins by Activated Human Platelets

7.1 Introduction

Until recently, prostaglandins were considered to only exist as free acid mediators secreted from cells to activate G-protein coupled receptors in a paracrine manner. In 2000, Marnett and co-workers showed that PGE_2-G/PGD_2-G and PGE_2-EA/PGD_2-EA were formed in macrophage cell lines from COX-2 oxidation of endogenous arachidonyl-glycerol (2-AG) and arachidonyl-ethanolamide (AEA) (Kozak *et al.*, 2000; Kozak.*et al.*, 2002). The products signal differently to free PGE_2 and PGD_2; for example, PGE_2-G mobilises calcium rapidly in a PGE_2-independent manner. Up to now, COX-1 has not been considered as a source of complex oxidised lipids. However, since both COX isoforms catalyse the same chemical reaction (cyclooxygenase and peroxidase reaction), it is possible that COX-1 can mediate esterified prostaglandin generation.

Since the discovery of aspirin as a COX inhibitor, in 1971, this NSAID has been the most common antiplatelet drug prescribed to prevent TxA_2 formation and platelet aggregation from occurring in patients at high risk of vascular disease. At low dose (75 mg/day), aspirin irreversibly inhibits platelet's COX-1 in the pre-systemic circulation, preventing the enzymatic conversion of AA into COX-1-products, such as TxA_2, PGE_2 and PGD_2 (Rocca & Petrucci, 2012).

In this chapter, the involvement of COX-1 in the generation of esterified prostaglandins by thrombin-activated platelets will be investigated *in vitro* using selective (SC 560) and non-selective (indomethacin and aspirin) COX-1 inhibitors. Furthermore, formation of esterified prostaglandins *in vivo* will be assessed following 7 days intake of low dose (75 mg/day) aspirin. The identification of new COX-1 products in platelets would suggest additional regulatory mechanisms underpinning platelet function that may be of therapeutic relevance.

Studies described in this chapter aim to:

- Determine whether esterified prostaglandins are enzymatically generated by activated platelets via COX-1.
- Investigate the requirement of COX-1 for the generation of free PGb and PGc.
- Examine the effect of platelet COX-1 inhibition *in vivo* on formation of free and esterified prostaglandins.

7.2 Results

7.2.1   Formation of free and esterified prostaglandins is completely blocked by COX inhibitors in vitro.

To determine whether COX-1 is required for the generation of free and esterified prostaglandins by activated platelets, cells were pre-treated with 1 mM aspirin, 10 µM indomethacin or 1 µM SC-560 (the selective COX-1 inhibitor), for 10 min at room temperature prior to thrombin activation (0.2 U/ml thrombin for 30 min at 37°C). Lipids were extracted and subsequently analysed on 4000 Q-Trap, using reverse-phase LC/MS/MS, in MRM mode, as described in Materials and Methods, Section *2.2.3.2* and *2.2.3.3*. Note that inhibitors were used at the concentrations previously described (Smith *et al.*, 1998; Williams *et al.*, 2005; Seno *et al.*, 2001).

7.2.1.1 PGE$_2$/D$_2$-PE generation is inhibited by COX inhibitors *in vitro*.

Aspirin completely blocked PGE$_2$/D$_2$-PE formation by activated platelets to control levels (Figure 7.1 A). Similarly, generation of PGE$_2$/D$_2$-PEs was totally inhibited by either 1 µM SC-560 or 10 µM indomethacin (Figure 7.1 B). These results conclusively confirmed the requirement of COX-1 for the synthesis of PGE$_2$/D$_2$-PEs.
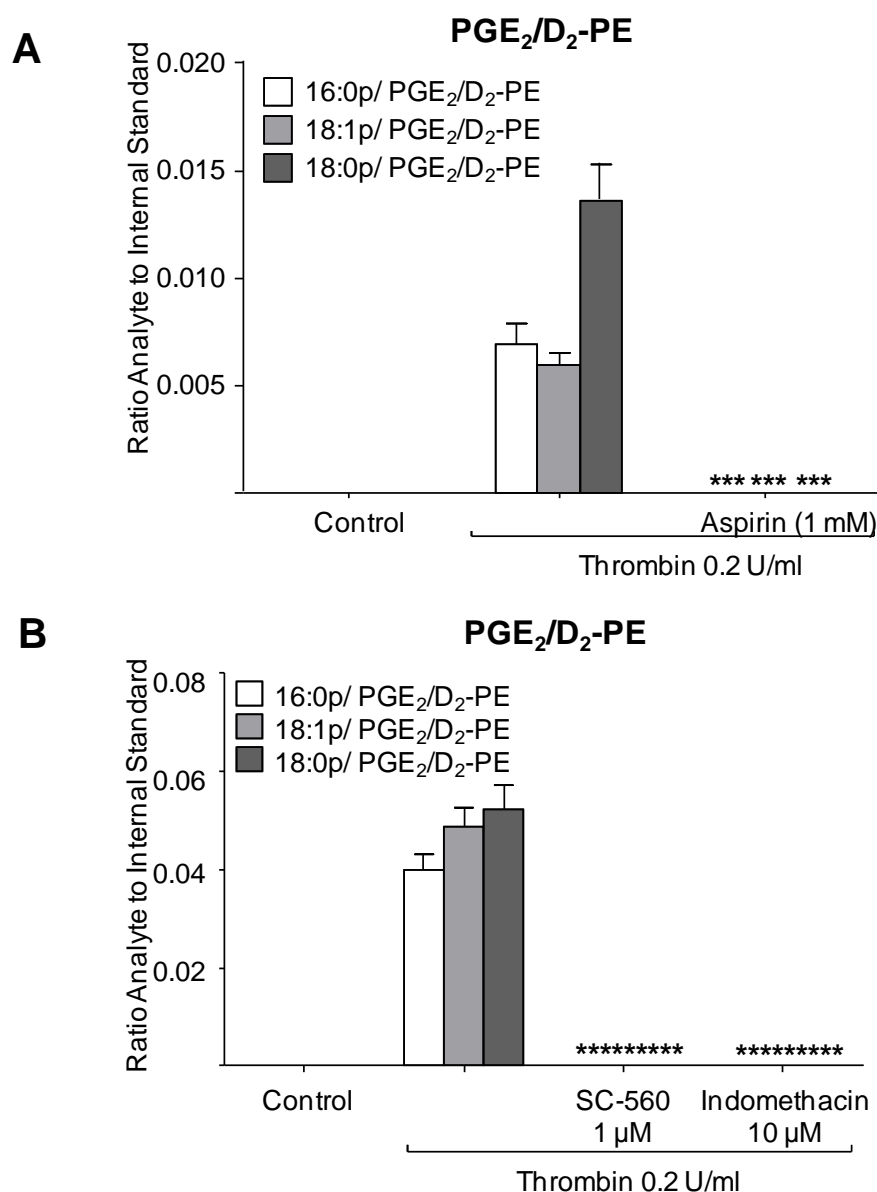
Figure 7.1: Generation of PGE$_2$/D$_2$-PEs is sensitive to aspirin *in vitro*. Platelets were incubated for 10 min at room temperature with 1 mM aspirin, 1 μM SC-560 or 10 μM indomethacin prior to thrombin activation (0.2 U/ml for 30 min at 37°C). This was followed by lipid extraction and analysis of PGE$_2$/D$_2$-PEs using reverse-phase LC/MS/MS, monitoring parent [M-H]$^-$ $\rightarrow$ *m/z* 271.2, as described in Materials and Methods, Section *2.2.3.2*. Levels of PGE$_2$/D$_2$-PEs are expressed as ratio analyte to internal standard. Data presented from one experiment and representative of three (n = 3, mean ± SEM). *** P < 0.001 versus thrombin, using ANOVA and Bonferroni Post Hoc Test. *Panel A*. PGE$_2$/D$_2$-PE formation by platelets treated with 1 mM aspirin. *Panel B*. PGE$_2$/D$_2$-PE formation by platelets treated with 1 μM SC-560 or 10 μM indomethacin.

7.2.1.2 Free PGE_2 and PGD_2 formation is inhibited by COX inhibitors *in vitro*.

Generation of free PGE_2 and PGD_2 was completely blocked by aspirin to control levels, similarly to PGE_2/D_2-PEs (Figure 7.2 A). Following treatment with 1 µM SC-560 or 10 µM indomethacin, formation of PGD_2 was decreased to undetectable levels (Figure 7.B). Furthermore, SC-560 and indomethacin reduced synthesis of PGE_2 from 3.8 ng to approximately 60 pg/2 x 10^8 platelets (Figure 7.2 B).

7.2.1.3 PGb-PE formation is significantly reduced by COX inhibitors *in vitro*.

Aspirin inhibited PGb-PE formation by thrombin-activated human platelets to undetectable levels (Figure 7.3 A). Generation of 16:0p/PGb-PE, 18:1p/PGb-PE, 18:0p/PGb-PE and 18:0a/PGb-PE by platelets treated with 1 µM SC-560 was significantly decreased (Figure 7.6). Similarly, levels of PGb-PEs were significantly reduced following treatment with 10 µM indomethacin (Figure 7.3 B).

7.2.1.4 Synthesis of free PGb is completely blocked by COX inhibitors *in vitro*.

Following aspirin treatment, generation of free PGb by thrombin-activated platelets was inhibited to control levels (Figure 7.4 A). Formation of free PGb was reduced by both 1 µM SC-560 and 10 µM indomethacin to levels below the limit of detection (Figure 7.4 B). These results conclusively confirmed that free PGb is formed in a COX-1-dependent manner.
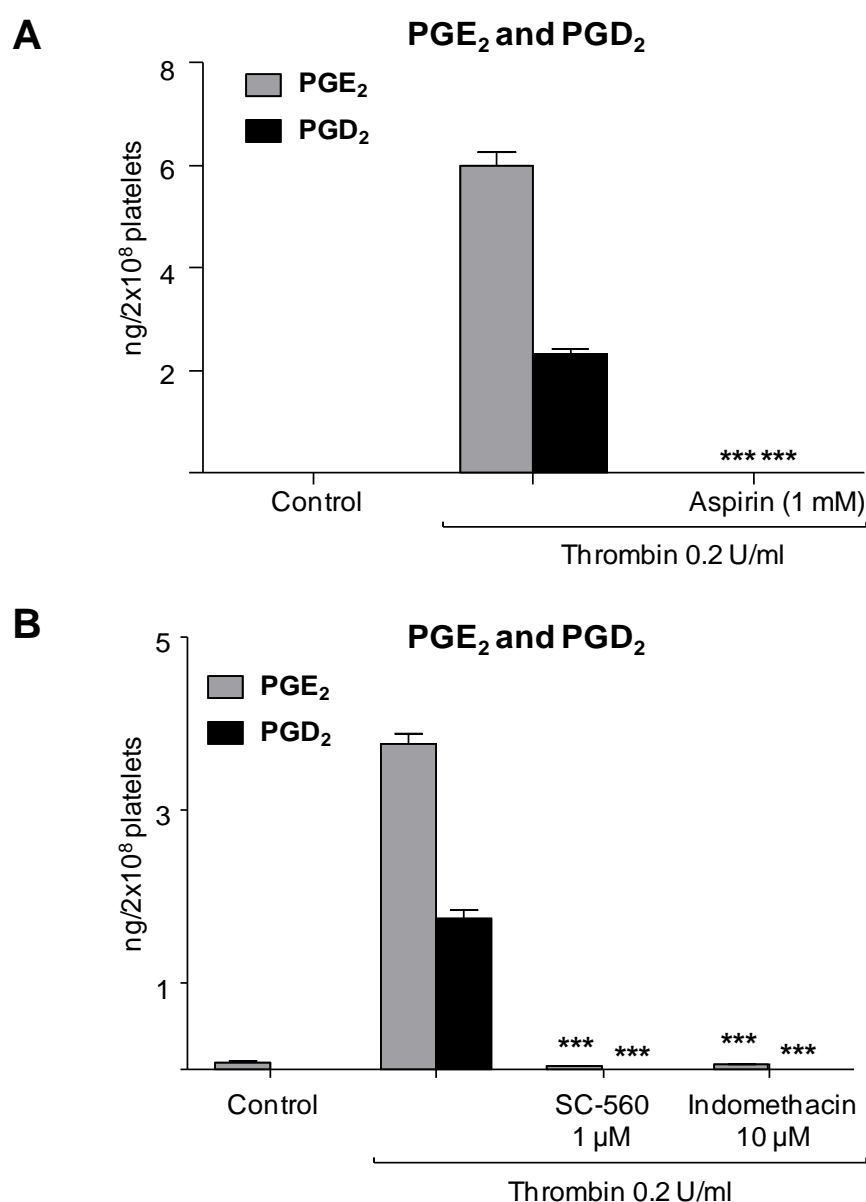
Figure 7.2: Generation of PGE$_2$ and PGD$_2$ is sensitive aspirin *in vitro*. Platelets were incubated for 10 min at room temperature with 1 mM aspirin, 1 μM SC-560 or 10 μM indomethacin prior to thrombin activation (0.2 U/ml for 30 min at 37°C). This was followed by lipid extraction and analysis of PGE$_2$ and PGD$_2$ using reverse-phase LC/MS/MS, monitoring *m/z* 351.2 → 271.2 as described in Materials and Methods, Section *2.2.3.3*. Levels of PGE$_2$ and PGD$_2$ are expressed as ng/2 x 10^8 platelets. Data presented from one experiment and representative of three (n = 3, mean ± SEM). *** P < 0.001 versus thrombin, using ANOVA and Bonferroni Post Hoc Test. *Panel A*. PGE$_2$ and PGD$_2$ formation by platelets treated with 1 mM aspirin. *Panel B*. PGE$_2$ and PGD$_2$ formation by platelets treated with 1 μM SC-560 or 10 μM indomethacin.
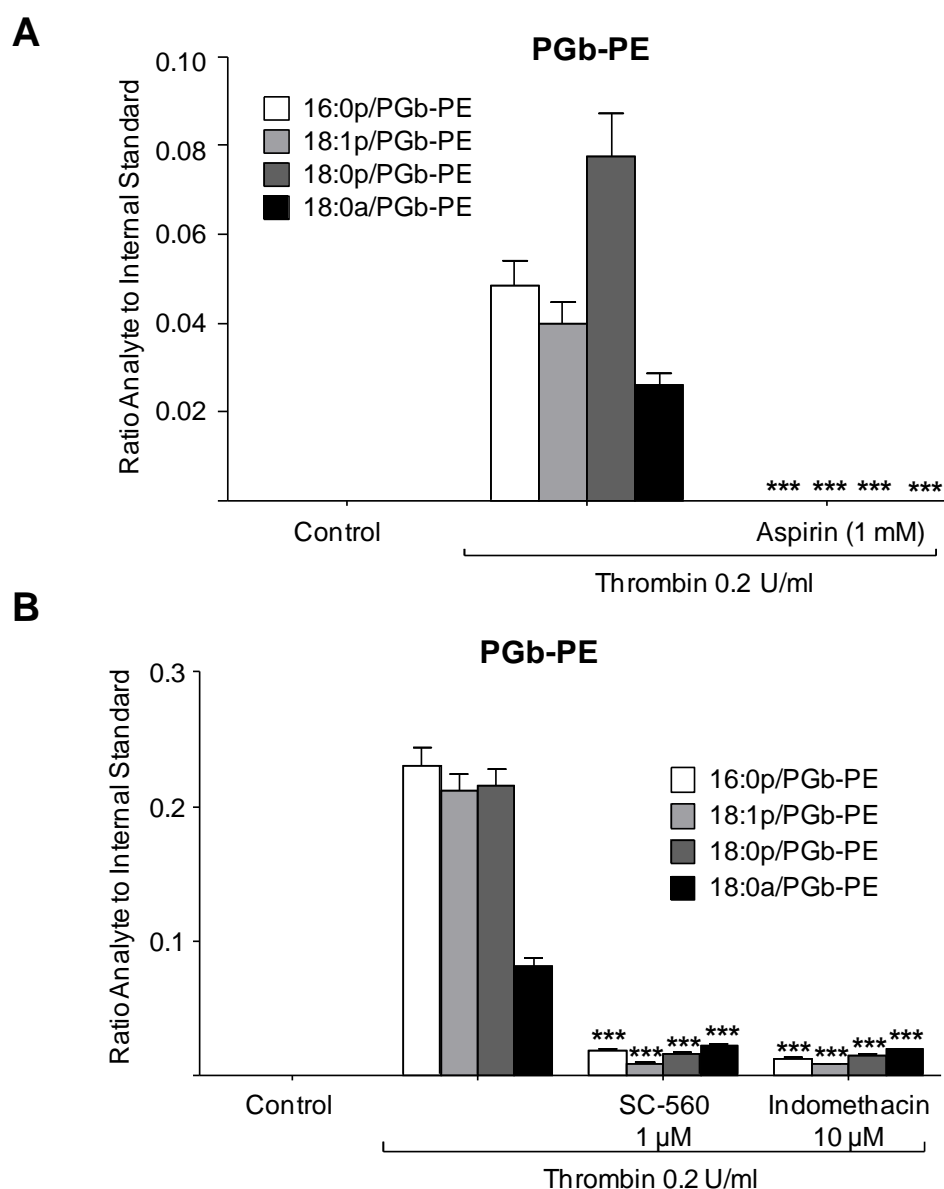
Figure 7.3: Generation of PGb-PEs is sensitive to aspirin *in vitro*. Platelets were incubated for 10 min at room temperature with 1 mM aspirin, 1 µM SC-560 or 10 µM indomethacin prior to thrombin activation (0.2 U/ml for 30 min at 37°C). This was followed by lipid extraction and analysis of PGb-PEs using reverse-phase LC/MS/MS, monitoring parent [M-H]⁻ → *m/z* 351.2, as described in Materials and Methods, Section *2.2.3.2*. Levels of PGb-PEs are expressed as ratio analyte to internal standard. Data presented from one experiment and representative of three (n = 3, mean ± SEM). *** P < 0.001 versus thrombin, using ANOVA and Bonferroni Post Hoc Test. *Panel A*. PGb-PE formation by platelets treated with 1 mM aspirin. *Panel B*. PGb-PE formation by platelets treated with 1 µM SC-560 or 10 µM indomethacin.
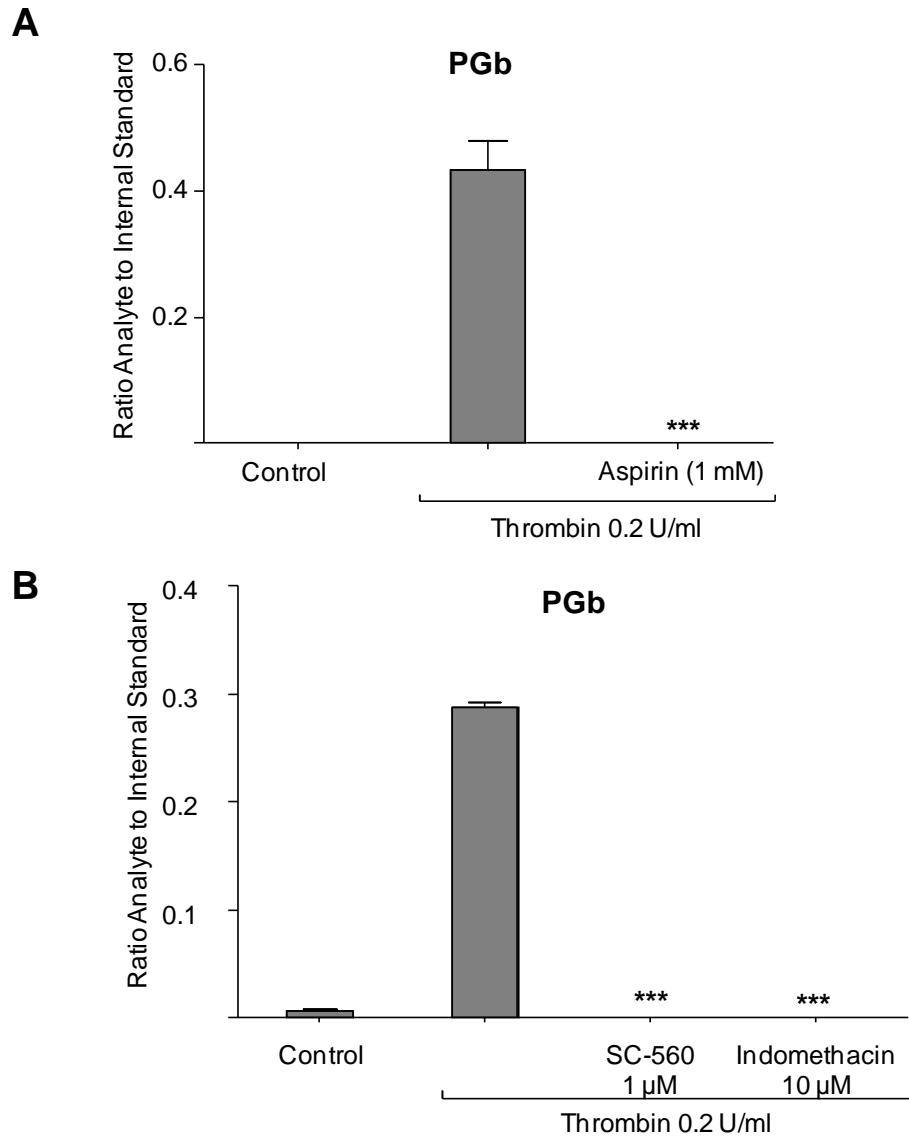
Figure 7.4: Generation of PGb is sensitive to aspirin *in vitro*. Platelets were incubated for 10 min at room temperature with 1 mM aspirin, 1 µM SC-560 or 10 µM indomethacin prior to thrombin activation (0.2 U/ml for 30 min at 37°C). This was followed by lipid extraction and analysis of PGb using reverse-phase LC/MS/MS, monitoring *m/z* 351.2 → 207.1 as described in Materials and Methods, Section *2.2.3.3*. Levels of PGb are expressed as ratio analyte to internal standard. Data presented from one experiment and representative of three (n = 3, mean ± SEM). *** $P < 0.001$ versus thrombin, using ANOVA and Bonferroni Post Hoc Test. *Panel A*. PGb formation by platelets treated with 1 mM aspirin. *Panel B*. PGb formation by platelets treated with 1 µM SC-560 or 10 µM indomethacin.

7.2.1.5 Generation of PGc-PEs is considerably reduced by COX inhibitors *in vitro*.

Aspirin completely inhibited the synthesis of PGc-PEs by thrombin-activated human platelets (Figure 7.5 A). Whereas, levels of 16:0p/PGc-PE, 18:1p/PGc-PE, 18:0p/PGc-PE and 18:0a/PGc-PE were significantly reduced following treatment with 1 μM SC-560 (Figure 7.5 B). Furthermore, SC-560 significantly decreased the formation of PGc-PEs (Figure 7.5 B).

7.2.1.6 Formation of free PGc is inhibited by COX inhibitors *in vitro*.

Synthesis of free PGc by thrombin-activated human platelets was completely blocked by 1 mM aspirin (Figure 7.6 A). Furthermore, levels of free PGc were reduced by 96.5 %, following treatment with 1 μM SC-560, whereas 10 μM indomethacin inhibited the generation of free PGc by approximately 99 % (Figure 7.6 B).
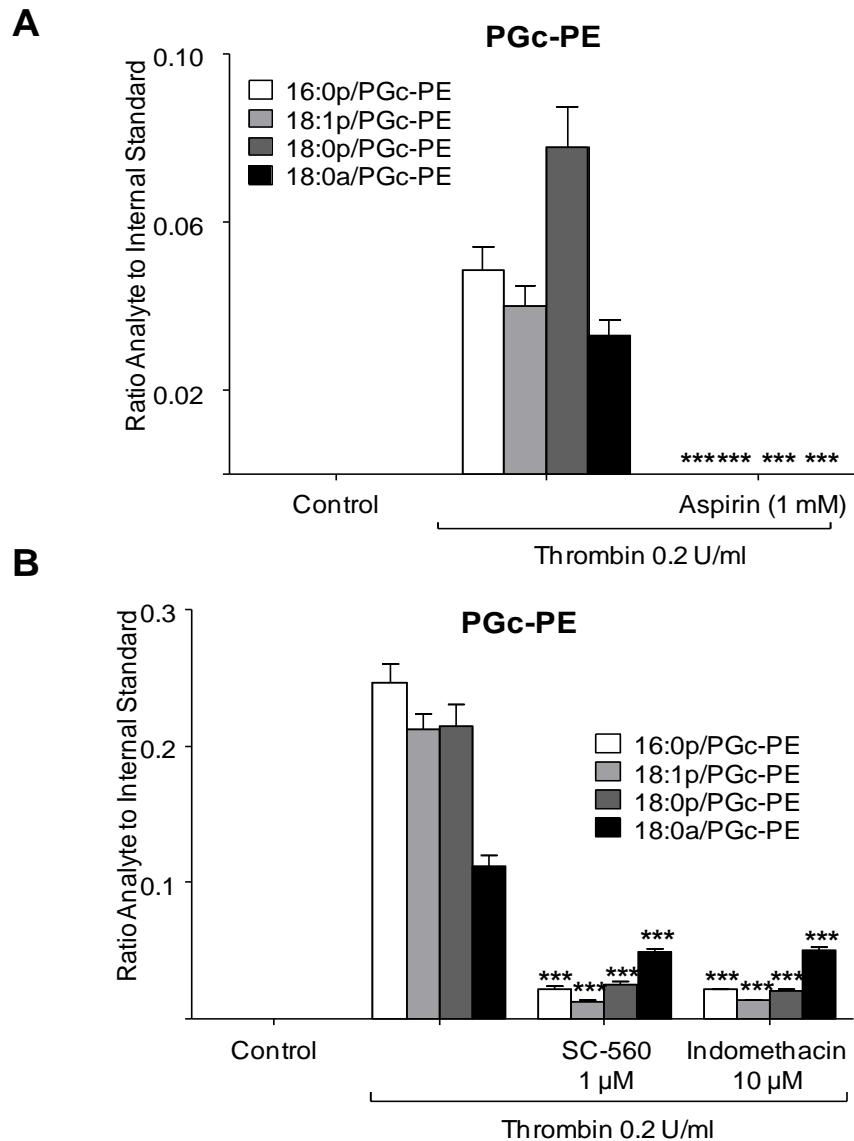
Figure 7.5: Generation of PGc-PEs is sensitive to aspirin *in vitro*. Platelets were incubated for 10 min at room temperature with 1 mM aspirin, 1 μM SC-560 or 10 μM indomethacin prior to thrombin activation (0.2 U/ml for 30 min at 37°C). This was followed by lipid extraction and analysis of PGc-PEs using reverse-phase LC/MS/MS, monitoring parent [M-H]$^{-}$ → *m/z* 351.2, as described in Materials and Methods, Section *2.2.3.2*. Levels of PGc-PEs are expressed as ratio analyte to internal standard. Data presented from one experiment and representative of three (n = 3, mean ± SEM). *** P < 0.001 versus thrombin, using ANOVA and Bonferroni Post Hoc Test. *Panel A*. PGc-PE formation by platelets treated with 1 mM aspirin. *Panel B*. PGc-PE formation by platelets treated with 1 μM SC-560 or 10 μM indomethacin.
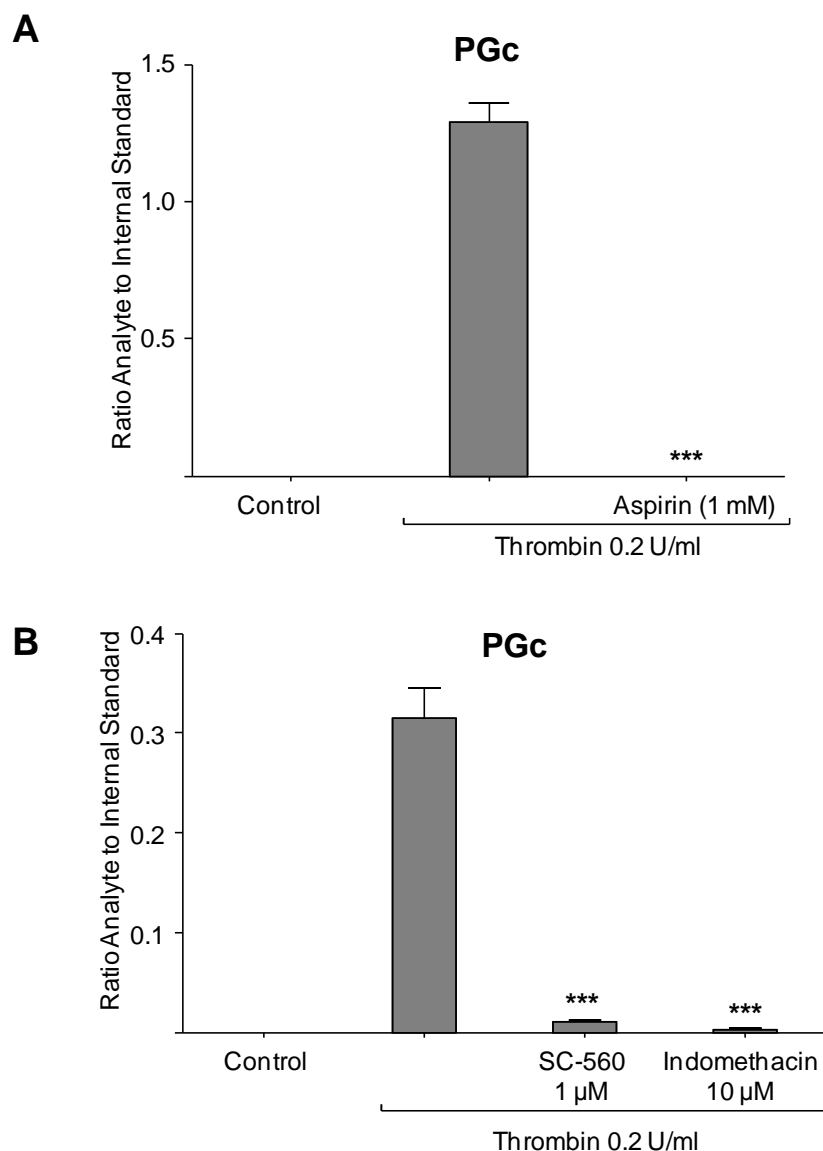
Figure 7.6: Generation of PGc is sensitive to aspirin *in vitro*. Platelets were incubated for 10 min at room temperature with 1 mM aspirin, 1 μM SC-560 or 10 μM indomethacin prior to thrombin activation (0.2 U/ml for 30 min at 37°C). This was followed by lipid extraction and analysis of PGc using reverse-phase LC/MS/MS, monitoring *m/z* 351.2 → 165.1 as described in Materials and Methods, Section *2.2.3.3*. Levels of PGc are expressed as ratio analyte to internal standard. Data presented from one experiment and representative of three (n = 3, mean ± SEM). *** P < 0.001 versus thrombin, using ANOVA and Bonferroni Post Hoc Test. *Panel A*. PGc formation by platelets treated with 1 mM aspirin. *Panel B*. PGc formation by platelets treated with 1 μM SC-560 or 10 μM indomethacin.

7.2.2   Free and esterified prostaglandin formation is blocked by low dose aspirin in vivo.

Since the discovery of aspirin as a COX inhibitor, in 1971, this NSAID has been the most common antiplatelet drug prescribed to prevent TxA_2 formation and platelet aggregation from occurring in patients at high risk of vascular disease. At low dose (75 mg/day), aspirin irreversibly inhibits platelet's COX-1 in the pre-systemic circulation, preventing the enzymatic conversion of AA into COX-1-products, such as TxA_2, PGE_2 and PGD_2 (Rocca & Petrucci, 2012).

To determine whether low dose aspirin *in vivo* could inhibit formation of free and esterified prostaglandins by thrombin-activated platelets, 75 mg was given to five healthy volunteers and lipid generation monitored in washed platelets isolated from whole blood. Following a 14-day NSAID-free washout period, blood samples were collected into acid-citrate-dextrose (ACD), platelets isolated and activated with thrombin (0.2 U/ml 30 min at 37°C) for baseline determination of free and esterified prostaglandin levels, as described in Materials and Methods, Section *2.2.10*. Subjects were then assigned to 75 mg oral aspirin daily for 7 days. Subsequently, a second blood sample was obtained on the day after the last dose and generation of free and esterified prostaglandins by thrombin-activated platelets determined.

TxA_2 is unstable in aqueous solution and rapidly converted to thromboxane B_2 (TxB_2) (Hamberg *et al*., 1975). Thus, TxB_2 formation was analysed to assess aspirin efficiency (Lordkipanidzé *et al*., 2007). Levels of 12-HETE were also monitored as a positive control for platelet activation, since 12-HETE is formed in a COX-1-independent manner (Hammond & O'Donnell, 2012). Low dose aspirin *in vivo* reduced formation of TxB_2 by approximately 98 %, confirming COX-1 inhibition (Figure 7.7 A). Furthermore, synthesis of 12-HETE by thrombin-activated platelets confirmed cell activation (Figure 7.7 B). The high standard error of the mean (SEM) values indicates a high degree of variation between genetically unrelated donors. Low dose aspirin *in vivo* inhibited the generation of free and esterified prostaglandins significantly (Figure 7.8 – 7.10).
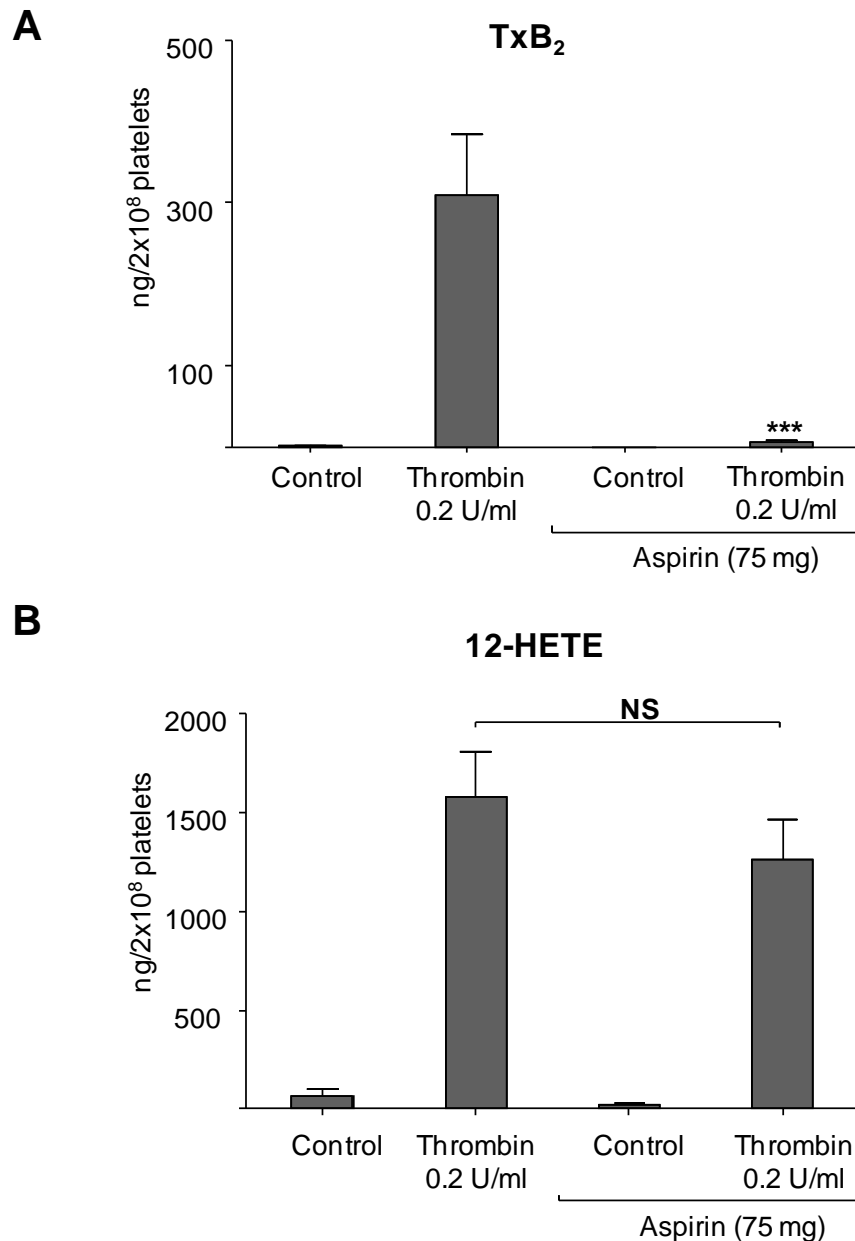
Figure 7.7: An aspirin intake of 75 mg/day inhibited TxB$_2$ formation while 12-HETE generation confirmed platelet activation. Blood was obtained following a 14-day NSAID-free washout period for baseline determination of TxB$_2$ and 12-HETE levels, following thrombin activation (0.2 U/ml for 30 min at 37°C). Subjects then received 75 mg/day aspirin for 7 days before donation of a second blood sample and repeat determination of TxB$_2$ and 12-HETE levels. Lipids were analysed using reverse-phase LC/MS/MS as described in Materials and Methods, Section *2.2.3*.3. Data is representative of five independent donors (n = 5, mean ± SEM). Levels of TxB$_2$ and 12-HETE are expressed as ng/2 x 10^8 platelets. *Panel A*. TxB$_2$ formation is inhibited following aspirin intake. ***P < 0.001 versus thrombin alone, using ANOVA and Bonferroni Post Hoc Test. *Panel B*. Generation of free 12-HETE by thrombin activated platelets following aspirin intake. NS = not significant, using ANOVA and Bonferroni Post Hoc Test.
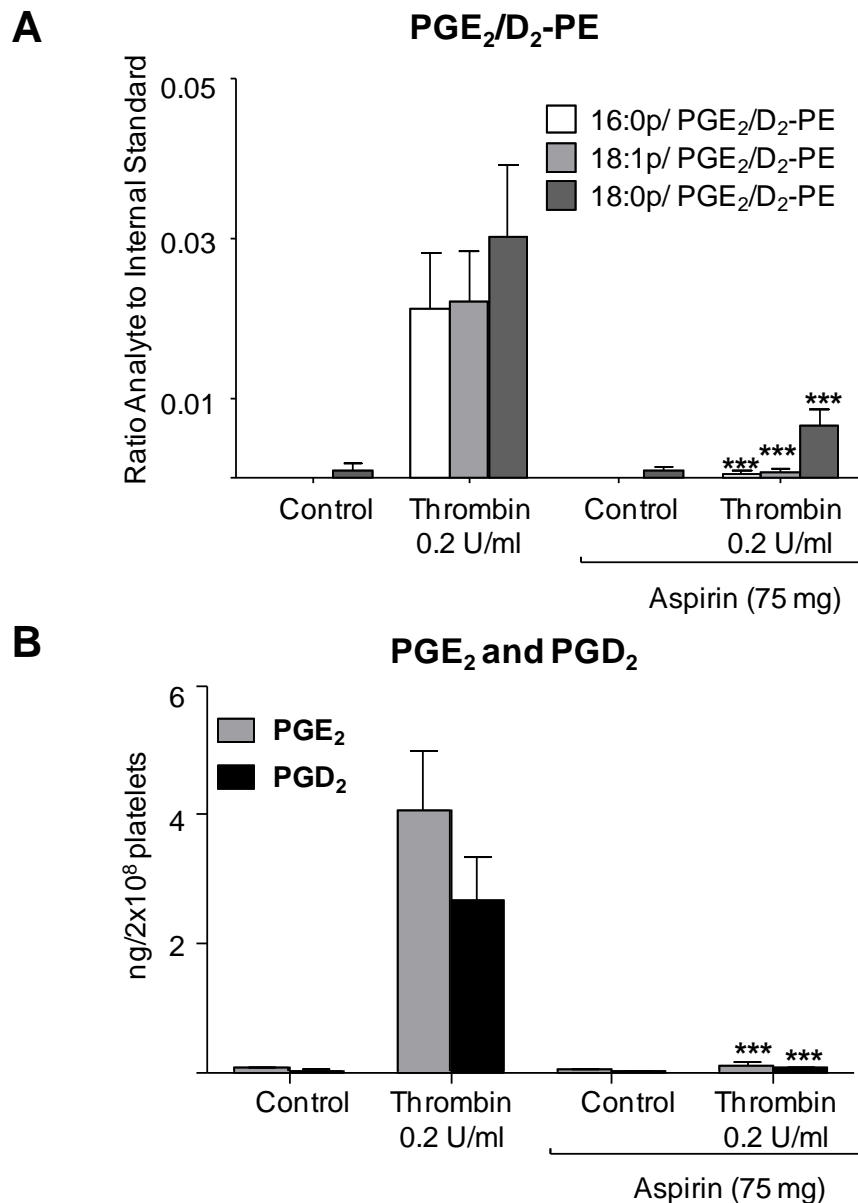
Figure 7.8: Aspirin blocks formation of PGE_2/D_2-PEs, PGE_2 and PGD_2 *in vivo*. Blood was obtained following a 14-day NSAID-free washout period for determination of PGE_2/D_2-PE, PGE_2 and PGD_2 levels, following thrombin activation (0.2 U/ml for 30 min at $37^{o}C$). Subjects then received 75 mg/day aspirin for 7 days before donation of a second blood sample and repeat determination of lipid levels. Lipids were analysed using reverse-phase LC/MS/MS as described in Materials and Methods, Sections *2.2.3.2* and *2.2.3.3*. Levels of PGE_2/D_2-PEs are expressed as ratio analyte to internal standard. PGE_2 and PGD_2 levels are expressed as ng/2 x 10^8 platelets. Data is representative of five independent donors (n = 5, mean ± SEM); ***P < 0.001 versus thrombin alone, using ANOVA and Bonferroni Post Hoc Test. *Panel A*. An aspirin intake of 75 mg/day inhibited PGE_2/D_2-PE formation by thrombin activated platelets. *Panel B*. An aspirin intake of 75 mg/day inhibited PGE_2 and PGD_2 formation by thrombin activated platelets.
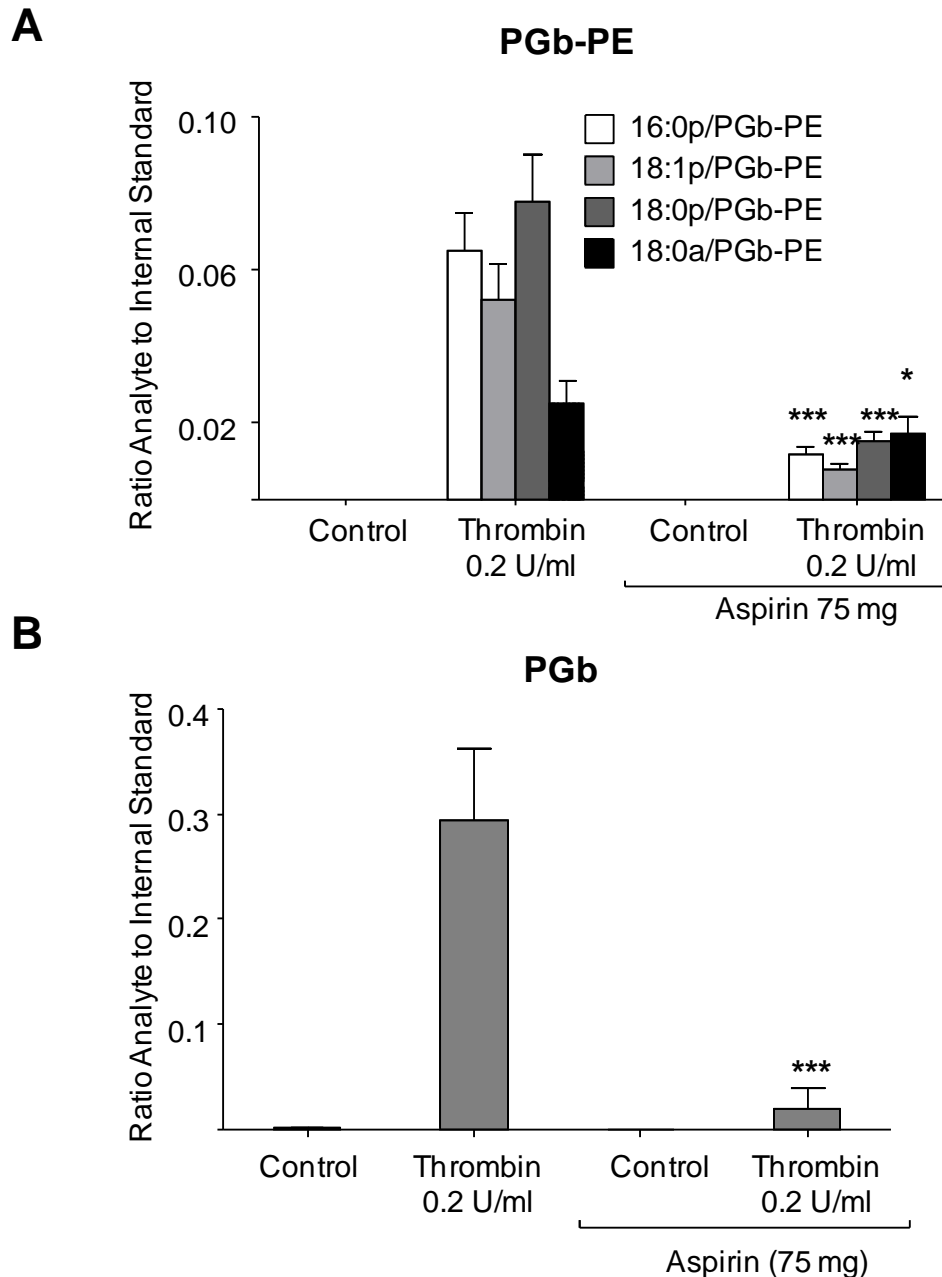
Figure 7.9: Aspirin blocks formation of PGb-PEs and free PGb *in vivo*. Blood was obtained following a 14-day NSAID-free washout period for determination of PGb-PE and PGb levels, following thrombin activation (0.2 U/ml for 30 min at 37°C). Subjects then received 75 mg/day aspirin for 7 days before donation of a second blood sample and repeat determination of lipid levels. Lipids were analysed using reverse-phase LC/MS/MS as described in Materials and Methods, Sections *2.2.3.2* and *2.2.3.3*. Levels of PGb-PE and free PGb are expressed as ratio analyte to internal standard. Data is representative of five independent donors (n = 5, mean ± SEM). *P < 0.05, **P < 0.01 and ***P < 0.001 versus thrombin alone, using ANOVA and Bonferroni Post Hoc Test. *Panel A*. An aspirin intake of 75 mg/day inhibited PGb-PE formation by thrombin activated platelets. *Panel B*. An aspirin intake of 75 mg/day inhibited free PGb formation by thrombin activated platelets.

175
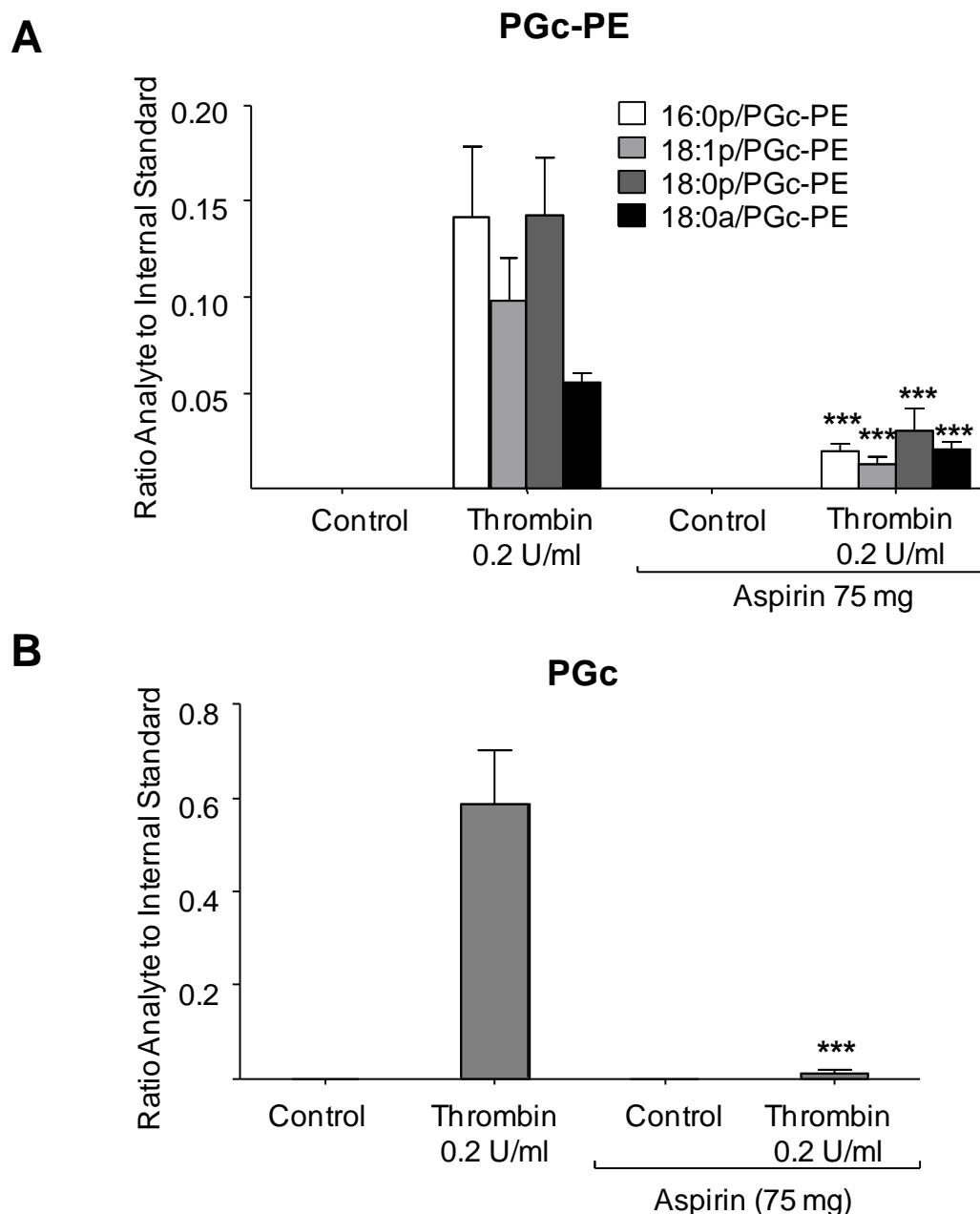
Figure 7.10: Aspirin blocks formation of PGc-PEs and free PGc *in vivo*. Blood was obtained following a 14-day NSAID-free washout period for determination of PGc-PE and PGc levels, following thrombin activation (0.2 U/ml for 30 min at 37°C). Subjects then received 75 mg/day aspirin for 7 days before donation of a second blood sample and repeat determination of lipid levels. Lipids were analysed using reverse-phase LC/MS/MS as described in Materials and Methods, Sections *2.2.3.2* and *2.2.3.3*. Levels of PGc-PE and free PGc are expressed as ratio analyte to internal standard. Data is representative of five independent donors (n = 5, mean ± SEM); ***$P < 0.001$ versus thrombin alone, using ANOVA and Bonferroni Post Hoc Test. *Panel A*. An aspirin intake of 75 mg/day inhibited PGc-PE formation by thrombin activated platelets. *Panel B*. An aspirin intake of 75 mg/day inhibited free PGc formation by thrombin activated platelets.

7.3 Discussion

Activated human platelets generate TxA_2, PGE_2 and PGD_2 enzymatically via COX-1, which is efficiently inhibited by aspirin. In this chapter, I demonstrated that esterified prostaglandins as well as free PGb and PGc originate from COX-1 turnover, since their generation is sensitive to pharmacological inhibitors of this pathway, both *in vitro* and *in vivo*. Up to now, the constitutive isoform COX-1 had not been shown to be a source of complex oxidised lipids, whereas COX-2 has been reported to oxidise AEA and 2-AG, generating PGE_2-G/PGD_2-G and PGE_2-EA/PGD_2-EA (Kozak *et al*., 2000; Kozak.*et al*., 2002). These were initially identified *in vitro* using purified COX-2 and later in murine macrophages cell lines with endogenous substrate (Kozak *et al*., 2000; Kozak *et al*., 2002; Nirodi *et al*., 2004). *In vivo* formation of PGE_2-EA and PGD_2-EA in kidneys, lungs, liver and small intestine of mice, following intravenous injection of AEA, has also been reported (Weber *et al*., 2004). In 2004, Marnett and colleagues demonstrated that PGE_2-G signals differently to classical PGE_2, mediating calcium mobilisation in a PGE_2-independent manner, indicating that PGE_2-G is not only chemically but also functionally distinct from free PGE_2 (Nirodi *et al*., 2004). It is possible that PGE_2-PEs and PGD_2-PEs also function differently to their free forms, interacting with unique specific receptors. For example, if membrane associated, the binding site of the prostaglandin part of the PGE_2-PE may only be partially exposed and, therefore, inaccessible to EP receptors. The interaction of PGE_2-PEs and PGD_2-PEs with prostaglandin receptors will be investigated in future experiments using HEK 293 cells expressing individual prostanoid receptors.

In vivo low dose aspirin (75 mg/day) inhibited free and esterified prostaglandin formation by thrombin-activated platelets (Figures 7.8 – 7.10). These results are similar to *in vitro* studies using aspirin, SC 560 or indomethacin (Figures 7.1 – 7.6). Aspirin is unique in mediating an irreversible inhibition of platelet COX-1. The mechanism triggering this long-lasting effect involves acetylation of the active site of COX, leading to irreversible inactivation of the enzyme and, consequently, inhibition of the generation of COX-1 products in platelets, such as TxA_2, PGE_2 and PGD_2 (Roth *et al*., 1975). It is likely that the antithrombotic effect of aspirin is not only due to the inhibition of TxA_2 formation but

also because of the blockade of all COX-1 products that function as pro-thrombotic and pro-inflammatory agents, including previously undescribed products, such as esterified prostaglandins, PGb and PGc. The identification of these novel metabolites suggests additional regulatory mechanisms mediating platelet function.

PGE_2 and PGD_2 are also generated via COX-2 by immune cells, such as macrophages and neutrophils (Ricciotti & FitzGerald, 2011). These prostaglandins can function either as anti- or pro-inflammatory mediators during inflammatory responses. It is possible that PGb and PGc may also form in immune cells via COX-2 during inflammation, contributing to acute inflammatory responses. Furthermore, PGb and PGc are less polar compared to PGE_2 and PGD_2 and, thus, esterified PGb and PGc are less likely to protrude from the intracellular membrane surface.

In summary, this is the first study to demonstrate formation of esterified prostaglandins by agonist-activated platelets via COX-1. These could form either by direct phospholipid oxidation or by esterification of newly formed prostaglandins into lyso PEs. In the next chapter, the formation of esterified prostaglandins by activated platelets will be investigated to determine whether this occurs via direct oxidation of PE or fast esterification of newly formed prostaglandins.

Chapter 8

8 Studies on the Mechanism of COX-1 Oxidation of Free or Esterified Arachidonic Acid in Human Platelets

8.1 Introduction

In this chapter, the process of esterified prostaglandin formation will be investigated. Enzymatically generated OxPLs can form either via esterification of oxidised fatty acids or by direct oxidation of phospholipids. In platelets, 12-HETE-PE/PCs are synthesised via AA release by PLA_2, oxidised by 12-LOX and then reincorporated into the plasma membrane (Thomas *et al.*, 2010). 12-HETE-PE/PCs are rapidly formed, on a similar time scale to free 12-HETE, suggesting that the proteins involved in their formation and re-esterification are tightly coupled in a complex, such that AA hydrolysis, oxidation, and esterification are highly regulated. This idea is supported by the inability of exogenously added 12-HETE-d_8 to become incorporated into PE or PC during platelet activation (Thomas *et al.*, 2010).

The re-esterification of free 12-HETE is likely to be orchestrated by enzymes of the Lands' cycle, such as the long chain fatty acyl-CoA synthetase (LC-FACS) and the lysophospholipid acyltransferase (Shindou *et al.*, 2013). The first enzyme catalyses the formation of fatty acyl-CoA while the second mediates the reacylation of acyl groups from acyl-CoA complexes to lysophospholipid acceptors (Scheme 8.1 and 8.2) (Hisanaga *et al.*, 2004; Shindou *et al.*, 2013). Together with PLA_2, these enzymes not only contribute to membrane asymmetry and diversity but also to the synthesis of bioactive lipids, such as platelet-activating factor (Yamashita *et al.*, 1997).
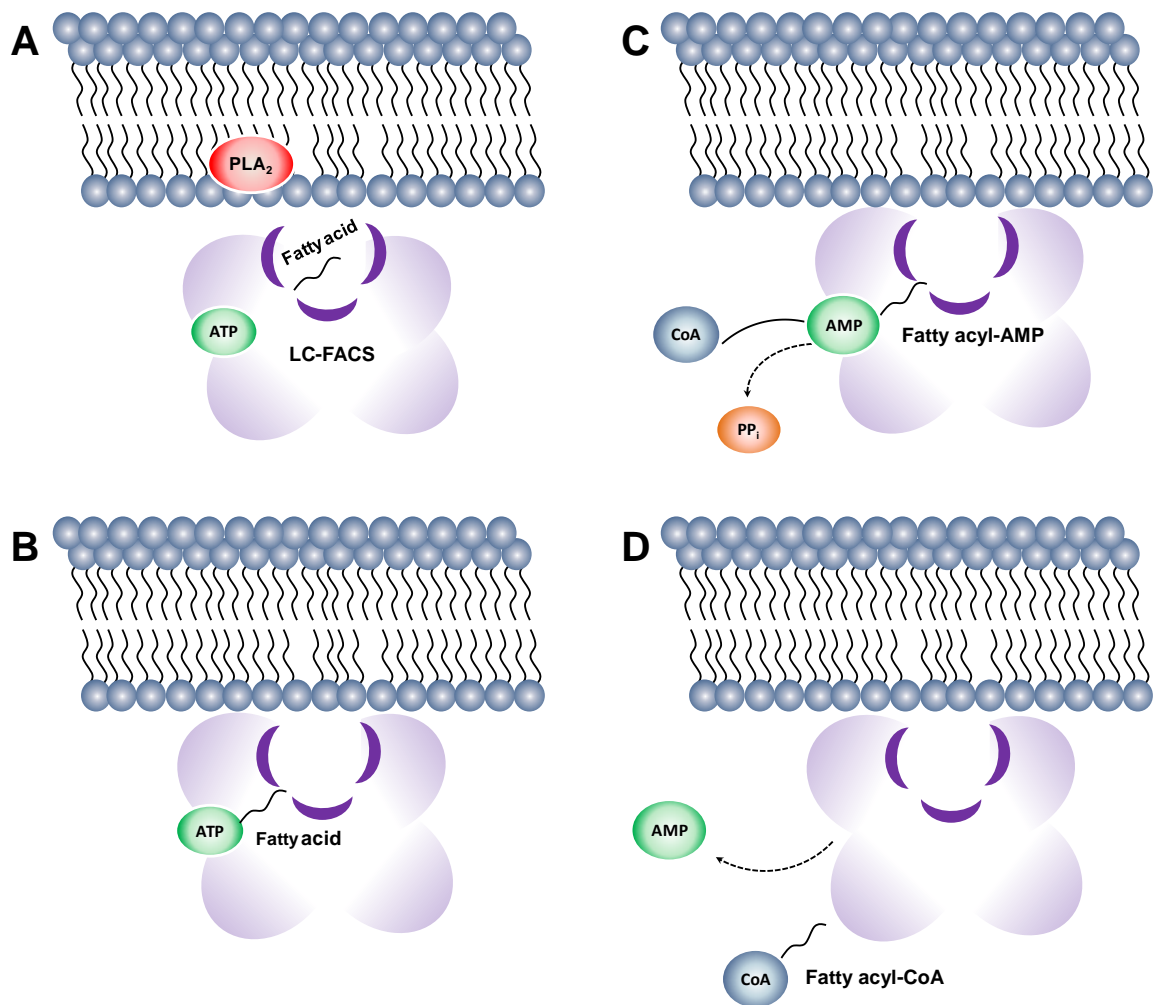
Scheme 8.1: Fatty acyl-CoA formation by LC-FACS. (A) Initially, adenosine-5'-triphosphate (ATP) binds to LC-FACS, which triggers the opening and widening of the fatty acid-binding tunnel. (B) Fatty acid released from phospholipids by PLA_2 enters the tunnel and binds to ATP. (C) Next, fatty acyl-adenosine monophosphate (AMP) complex is formed and pyrophosphate (PPi) is released. This is followed by CoA binding to the fatty acyl-AMP complex. (D) Finally, AMP dissociates and the fatty acyl-CoA complex is released. Modified from Hisanaga *et al.*, 2004.
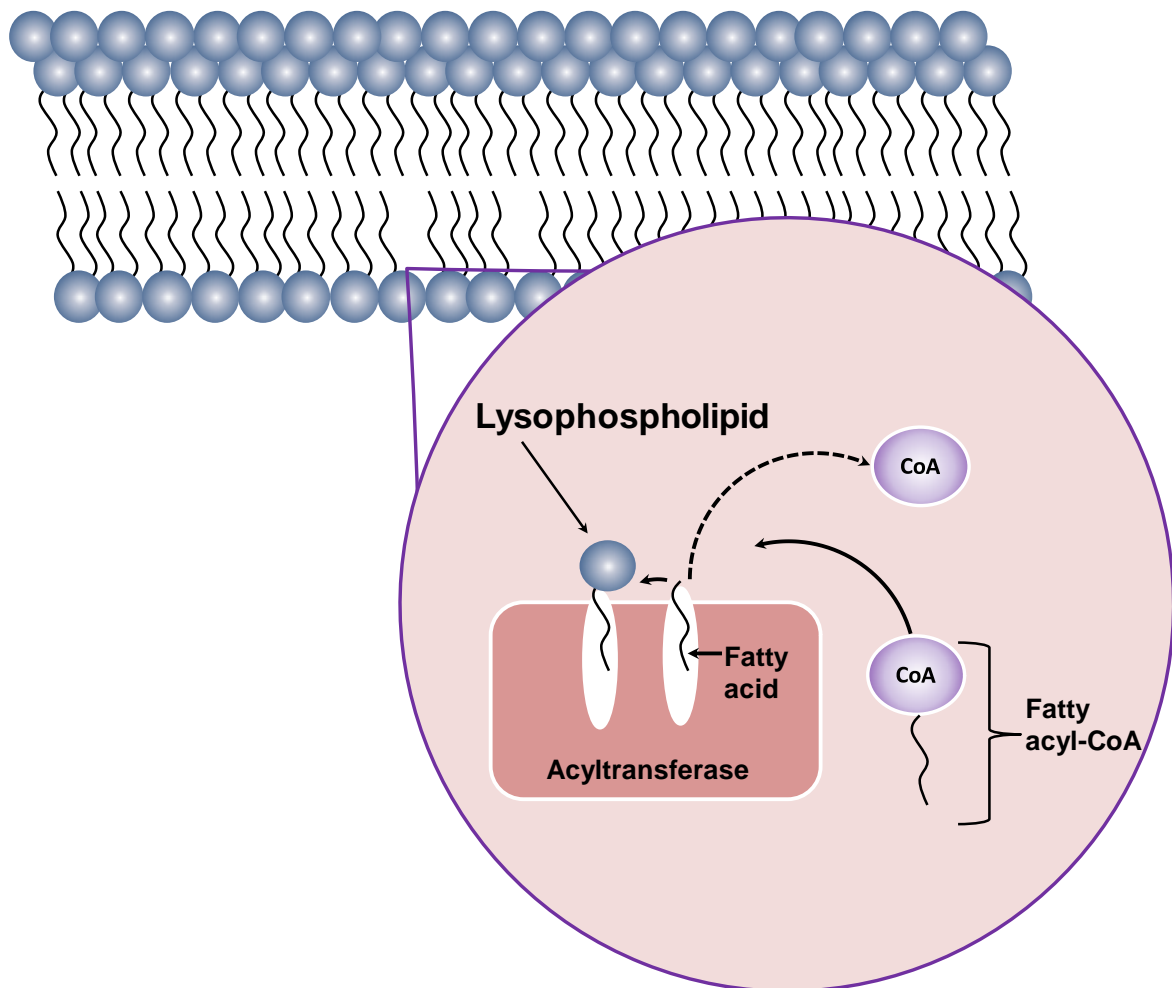
Scheme 8.2: Reacylation of fatty acids into lysophospholipids by acyltransferase.
Following formation of fatty acyl-CoA complex, the CoA dissociates and the fatty acid is
reincorporated into lysophospholipid by the acyltransferase.

While platelets generate OxPLs via fast esterification of newly formed 12-HETEs, human monocytes expressing 15-LOX can directly oxidise PEs, generating 15-HETE-PEs in a PLA_2-independent manner (Morgan *et al*., 2009; Hammond *et al*., 2012). In this chapter, I will investigate whether formation of esterified prostaglandins by platelets is via direct oxidation of PE or esterification of pre-formed prostaglandins. For this, PLA_2 isomers will be inhibited using pharmacologic inhibitors and synthesis of esterified prostaglandins assessed using reverse-phase LC/MS/MS on 4000 Q-trap. Furthermore, the requirement of LC-FACS and lysophospholipid acyltransferase for esterified prostaglandin formation will be investigated using triacsin C and thimerosal, respectively.

Separately, the requirement of prostaglandin synthases for PGE_2 and PGD_2 generation will be examined *in vitro* using purified COX isomers. Prostaglandin H_2 is unstable in aqueous milieu, and in platelets is either rapidly transformed to TxA_2 by thromboxane synthase, or undergoes enzymatic or non-enzymatic re-arrangement to PGE_2 and PGD_2 (Salomon *et al*., 1984; Boutaud *et al*., 1999). It is possible that in platelets conversion of PGH_2 to either PGE_2 or PGD_2 occurs independently of PGE synthase (PGES) or PGD synthase (PGDS). Furthermore, since both COX isoforms generate PGE_2 and PGD_2, it is likely that synthesis of PGb and PGc could also be catalysed by COX-2 (Ricciotti & FitzGerald, 2011). This will be investigated *in vitro* using recombinant COX-2.

Last, the ability of purified COX-1 to directly oxidise AA esterified into PE will be investigated. In theory, esterified prostaglandins could form not only via esterification of newly formed prostaglandins into lysophospholipids but also via direct oxidation of PE by COX-1. If observed, this would represent a new finding for COX-1, which has not been shown as a source of esterified prostaglandins before.

Studies described in this chapter aim to:

- Investigate the involvement of PLA_2 in the generation of free and esterified prostaglandins.
- Determine whether PGE_2/D_2-PE, PGb-PE and PGc-PE formation by thrombin-activated platelets is via esterification of newly formed prostaglandins or by direct oxidation of PE by COX-1.
- Examine whether PGE_2 and PGD_2 generation by activated platelets occurs via non-enzymatic re-arrangement of PGH_2.
- Investigate the ability of purified COX-1 to directly oxidise phospholipids.
- Assess PGb and PGc formation via recombinant COX-2 *in vitro*.

8.2 Results

8.2.1 Generation of free and esterified prostaglandins requires $cPLA_2$.

Human cells, such as platelets, contain structurally diverse forms of PLA_2 including cytosolic PLA_2 ($cPLA_2$), calcium-independent PLA_2 ($iPLA_2$) and secreted PLA_2 ($sPLA_2$) (Dennis, 1994; Levy, 2006). In this section, the requirement of these enzymes for the formation of free and esterified prostaglandins was determined. For this, washed human platelets were incubated with varying amounts of the $cPLA_2$ inhibitor $cPLA_{2\alpha}$i (50 – 1000 nM) at the same time (Morgan *et al*., 2010; Clark *et al*., 2011). The involvement of $sPLA_2$ and $iPLA_2$ was investigated using 2 µM of oleyloxyethyl-phosphocholine (OOEPC) and 50 nM of bromoenol lactone (BEL), respectively, which were dissolved in dimethyl sulphoxide (DMSO) (Morgan *et al*., 2010; Thomas *et al*., 2010). Platelets were incubated with each inhibitor or 0.5 % vehicle (DMSO) for 10 min at room temperature prior to thrombin activation (0.2 U/ml for 30 min at 37°C). Lipids were then extracted and analysed by reverse-phase LC/MS/MS on Q-trap, in MRM mode, as described in Materials and Methods, Sections *2.2.3.2* and *2.2.3.3*.

8.2.1.1 PGE_2/D_2-PEs are formed in a cPLA$_2$-dependent manner.

Inclusion of 50 nM cPLA$_{2\alpha}$i significantly reduced formation of PGE_2/D_2-PEs (Figure 8.1 A). In contrast, neither OOEPC nor BEL inhibited PGE_2/D_2-PE generation (Figure 8.1 B). The higher levels of PGE_2/D_2-PEs formed by platelets pre-treated with DMSO may be due to an increase in calcium influx through non-selective pores generated by DMSO (He et $al.$, 2012). The requirement of intracellular calcium will be investigated later in this thesis.

8.2.1.2 Formation of PGE$_2$ and PGD$_2$ requires cPLA$_2$

Levels of PGE$_2$ and PGD$_2$ were reduced by approximately 93 % following inhibition with 50 nM cPLA$_{2\alpha}$i (Figure 8.2 A). Generation of PGD$_2$ was not significantly affected by sPLA$_2$ (OOEPC) or iPLA$_2$ (BEL) inhibitor (Figure 8.2 B). OOEPC did not significantly decrease formation of PGE$_2$ (Figure 8.2 B), whereas, BEL partially reduced PGE$_2$ levels (Figure 8.2 B).

8.2.1.3 PGb-PEs are formed in a cPLA$_2$-dependent manner.

Generation of PGb-PEs was significantly reduced following inhibition of the cPLA$_2$ by cPLA$_{2\alpha}$i (Figure 8.3 A). In contrast, formation of PGb-PEs by thrombin-activated human platelets was not inhibited by sPLA$_2$ (OOEPC) or iPLA$_2$ (BEL) inhibitor (Figure 8.3 B).
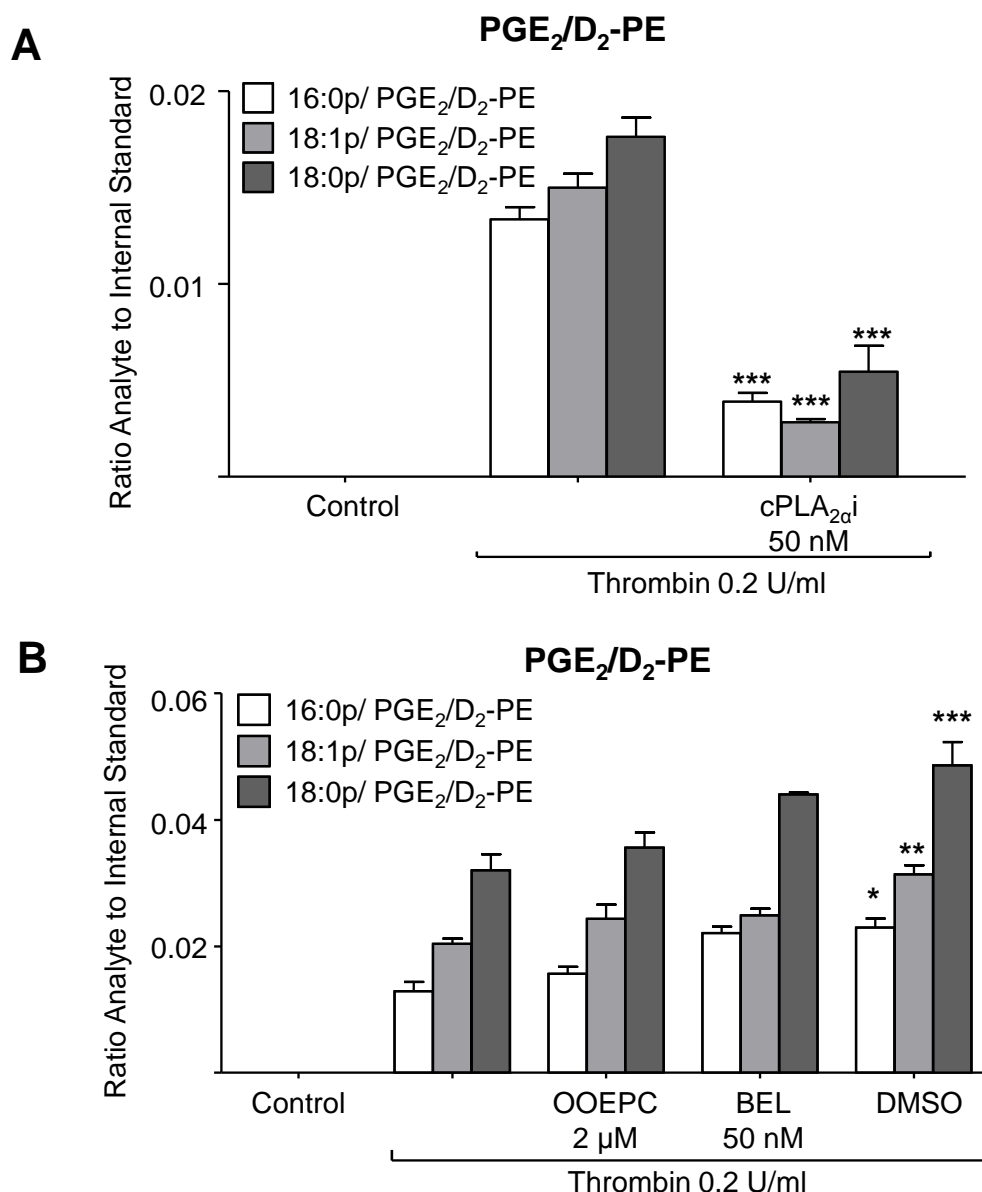
Figure 8.1: Generation of PGE₂/D₂-PEs requires cPLA₂. Washed human platelets were incubated for 10 min at room temperature with each inhibitor prior to thrombin activation (0.2 U/ml for 30 min at 37°C) before lipid extraction and analysis using reverse-phase LC/MS/MS, monitoring parent [M-H]⁻ → *m/z* 271.2, as described in Materials and Methods, Section *2.2.3.2*. Levels of PGE₂/D₂-PEs are expressed as ratio analyte to internal standard. Data presented from one experiment and representative of three (n = 3, mean ± SEM). *Panel A*. PGE₂/D₂-PE formation by platelets incubated with 50 nM cPLA₂αi. *** P < 0.001 versus thrombin, using ANOVA and Bonferroni Post Hoc Test. *Panel B*. PGE₂/D₂-PE formation by platelets incubated with 2 μM OOEPC, 50 nM BEL or vehicle (DMSO, 0.5%). * P < 0.05, ** P < 0.01 and *** P < 0.001 versus thrombin, using ANOVA and Bonferroni Post Hoc Test.
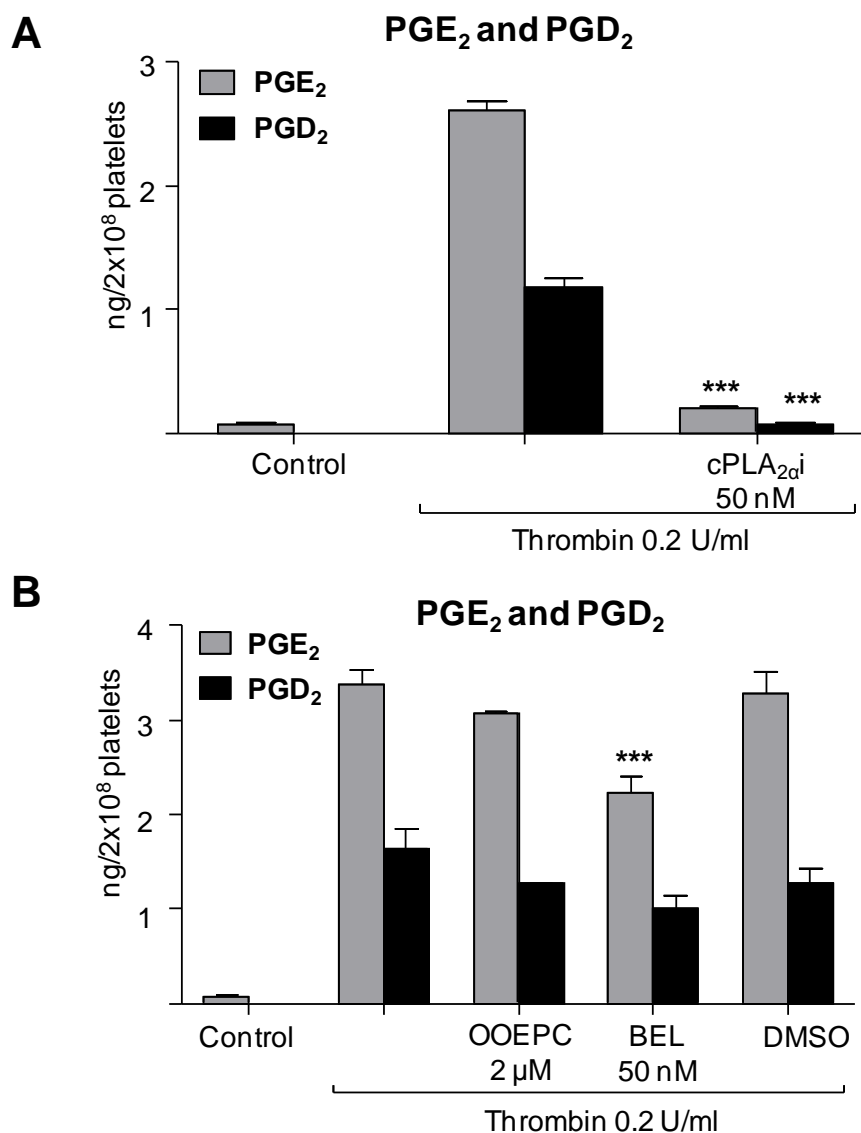
Figure 8.2: Generation of free PGE$_2$ and PGD$_2$ requires cPLA$_2$. Washed human platelets were incubated for 10 min at room temperature with each inhibitor prior to thrombin activation (0.2 U/ml for 30 min at 37°C) before lipid extraction and analysis using reverse-phase LC/MS/MS, monitoring *m/z* 351.2 → 271.2 as described in Materials and Methods, Section *2.2.3.3*. Levels of PGE$_2$ and PGD$_2$ are expressed as ng/2 x 10^8 platelets. Data presented from one experiment and representative of three (n = 3, mean ± SEM). *Panel A*. PGE$_2$ and PGD$_2$ formation by platelets incubated with 50 nM cPLA$_{2\alpha}$i. ***P < 0.001 versus thrombin, using ANOVA and Bonferroni Post Hoc Test.*Panel B*. PGE$_2$ and PGD$_2$ formation by platelets incubated with 2 μM OOEPC, 50 nM BEL or vehicle (DMSO, 0.5%). ***P < 0.001 versus thrombin in the presence of DMSO, using ANOVA and Bonferroni Post Hoc Test.
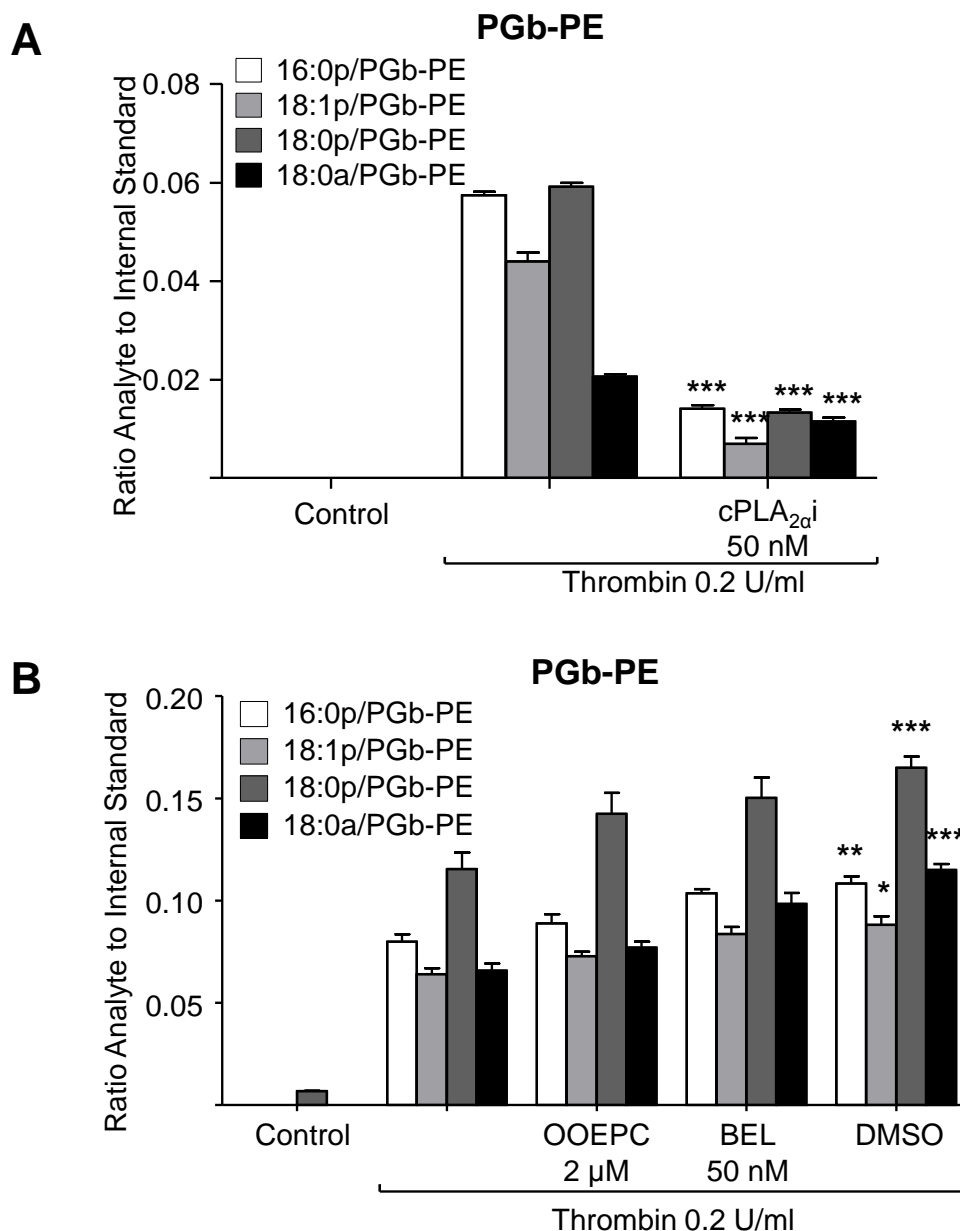
Figure 8.3: Generation of PGb-PEs requires cPLA$_2$. Washed human platelets were incubated for 10 min at room temperature with each inhibitor prior to thrombin activation (0.2 U/ml for 30 min at 37°C) before lipid extraction and analysis using reverse-phase LC/MS/MS, monitoring parent [M-H]$^-$ $\rightarrow$ *m/z* 351.2, as described in Materials and Methods, Section *2.2.3.2*. Levels of PGb-PEs are expressed as ratio analyte to internal standard. Data presented from one experiment and representative of three (n = 3, mean ± SEM). *Panel A*. PGb-PEs formation by platelets incubated with 50 nM cPLA$_{2\alpha}$i. ***P < 0.001 versus thrombin, using ANOVA and Bonferroni Post Hoc Test. *Panel B*. PGb-PEs formation by platelets incubated with 2 μM OOEPC, 50 nM BEL or vehicle (DMSO, 0.5%). * P < 0.05, ** P < 0.01 and *** P < 0.001 versus thrombin, using ANOVA and Bonferroni Post Hoc Test.

8.2.1.4 Formation of PGb requires cPLA$_2$ and is partially affected by iPLA$_2$ inhibition.

Synthesis of PGb was totally blocked by inhibition of cPLA$_2$ (Figure 8.4 A). Interestingly, PGb-PE formation was not completely abolished by cPLA$_{2\alpha}$i, suggesting that a small proportion of PGb-PEs may be formed via non-enzymatic oxidation of PEs. This hypothesis will be tested later in this chapter.

Levels of PGb were partially reduced (~ 35 %) by the iPLA$_2$ inhibitor BEL but not significantly affected by the sPLA$_2$ inhibitor OOEPC (Figure 8.4 B). This indicates that the specific pool of AA converted to PGb by COX-1 is mainly released from phospholipids by cPLA$_2$.

8.2.1.5 Synthesis of PGc-PEs requires cPLA$_2$.

Formation of PGc-PEs was reduced by approximately 80 % in response to inhibition of cPLA$_2$ (Figure 8.5 A). Whereas, synthesis of PGc-PEs by thrombin-activated human platelets was not inhibited by sPLA$_2$ (OOEPC) or iPLA$_2$ (BEL) inhibitor (Figure 8.5 B). Furthermore, levels of PGc-PEs appeared to be increased by OOEPC, BEL and DMSO compared to thrombin.

8.2.1.6 Generation of free PGc mainly requires cPLA$_2$.

Formation of free PGc by activated human platelets was reduced by 99 % following cPLA$_{2\alpha}$ inhibition (Figure 8.6 A). Levels of PGc were not affected by the sPLA$_2$ inhibitor OOEPC, while, treatment with BEL resulted in 30 % reduction (Figure 8.6 B). BEL may be a non-specific iPLA$_2$ inhibitor, affecting other pathways involved in free PGc formation.
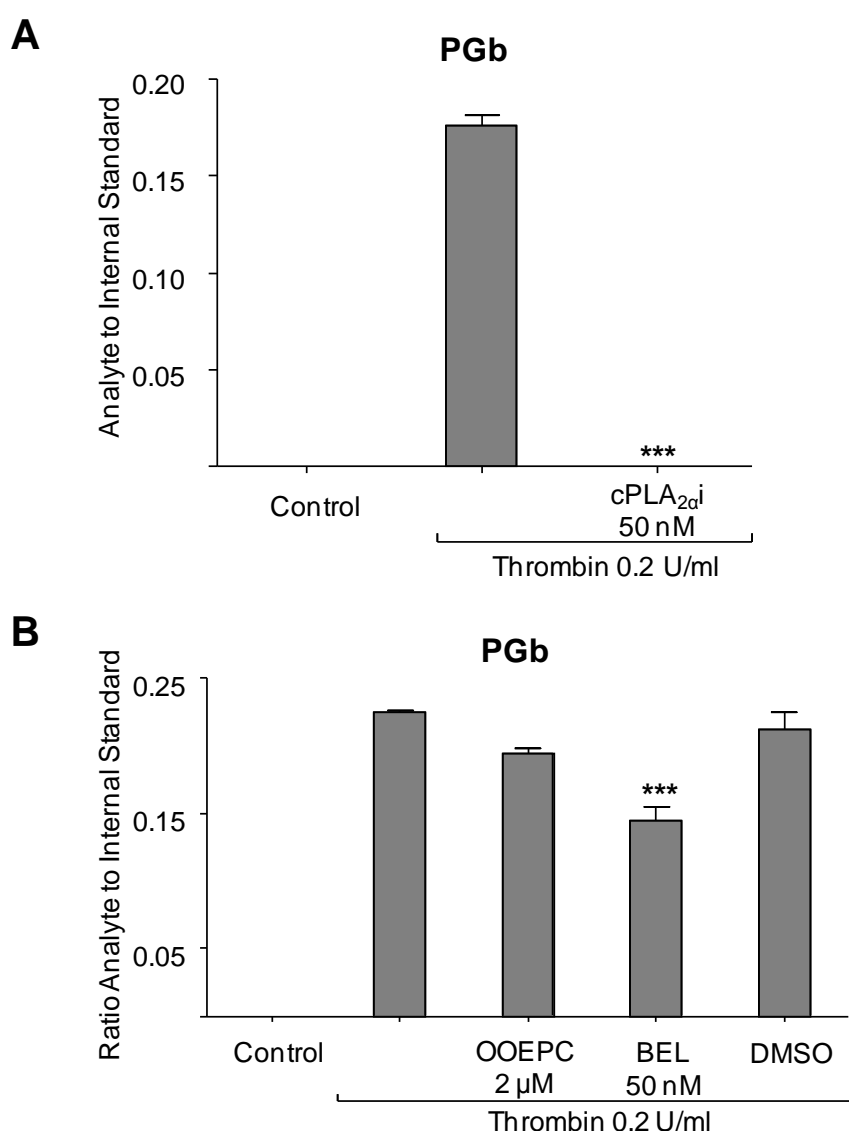
Figure 8.4: Generation of PGb is completely blocked by cPLA$_{2\alpha}$i and partially inhibited by BEL. Washed human platelets were incubated for 10 min at room temperature with each inhibitor prior to thrombin activation (0.2 U/ml for 30 min at 37°C) before lipid extraction and analysis using reverse-phase LC/MS/MS, monitoring *m/z* 351.2 $\rightarrow$ 207.1 as described in Materials and Methods, Section *2.2.3.3*. Levels of PGb are expressed as ratio analyte to internal standard. Data presented from one experiment and representative of three (n = 3, mean ± SEM). *Panel A*. PGb formation by platelets incubated with 50 nM cPLA$_{2\alpha}$i. ***P < 0.001 versus thrombin, using ANOVA and Bonferroni Post Hoc Test. *Panel B*. PGb formation by platelets incubated with 2 μM OOEPC, 50 nM BEL or vehicle (DMSO, 0.5%). ***P < 0.001 versus thrombin in the presence of DMSO, using ANOVA and Bonferroni Post Hoc Test.

Figure 8.5: Generation of PGc-PEs requires cPLA$_2$. Washed human platelets were incubated for 10 min at room temperature with each inhibitor prior to thrombin activation (0.2 U/ml for 30 min at 37°C) before lipid extraction and analysis using reverse-phase LC/MS/MS, monitoring parent [M-H]$^-$ → *m/z* 351.2, as described in Materials and Methods, Section *2.2.3.2*. Levels of PGc-PEs are expressed as ratio analyte to internal standard. Data presented from one experiment and representative of three (n = 3, mean ± SEM). *Panel A*. PGc-PE formation by platelets incubated with 50 nM cPLA$_{2\alpha}$i. ***P < 0.001 versus thrombin, using ANOVA and Bonferroni Post Hoc Test. *Panel B*. PGc-PE formation by platelets incubated with 2 μM OOEPC, 50 nM BEL or vehicle (DMSO, 0.5%). *** P < 0.001 versus thrombin, using ANOVA and Bonferroni Post Hoc Test.

Figure 8.6: Generation of free PGc is almost abolished by cPLA$_{2\alpha}$i and partially inhibited by BEL. Washed human platelets were incubated for 10 min at room temperature with each inhibitor prior to thrombin activation (0.2 U/ml for 30 min at 37°C) before lipid extraction and analysis using reverse-phase LC/MS/MS, monitoring m/z 351.2 $\rightarrow$ 165.1 as described in Materials and Methods, section *2.2.3.3*. Levels of free PGc are expressed as ratio analyte to internal standard. Data presented from one experiment and representative of three (n = 3, mean ± SEM). *Panel A*. PGc formation by platelets incubated with 50 nM cPLA$_{2\alpha}$i. ***$P < 0.001$ versus thrombin, using ANOVA and Bonferroni Post Hoc Test. *Panel B*. PGc formation by platelets incubated with 2 μM OOEPC, 50 nM BEL or vehicle (DMSO, 0.5%). *$P < 0.05$ versus thrombin in the presence of DMSO, using ANOVA and Bonferroni Post Hoc Test.

8.2.2   Formation of free and esterified prostaglandins is inhibited by triacsin C.

In this section, the requirement of LC-FACS for esterified prostaglandin formation was assessed using triacsin C (Figure 8.7). This is a polyunsaturated fatty acid analogue that competitively inhibits LC-FACS and, consequently, the first step of fatty acid reincorporation, Figure 8.8 (Kim *et al*., 2012). Platelets were treated with 7 µM triacsin C for 30 min at 37°C prior to thrombin activation (0.2 U/ml for 30 min at 37°C) (Tomoda *et al*., 1991; Igal *et al*., 1997). Lipids were then extracted and free and esterified prostaglandin formation analysed using reverse-phase LC/MS/MS, on 4000 Q-trap, as described in Materials and Methods, Sections *2.2.3.2* and *2.2.3.3*.

Figure 8.7: Chemical structure of triacsin C.
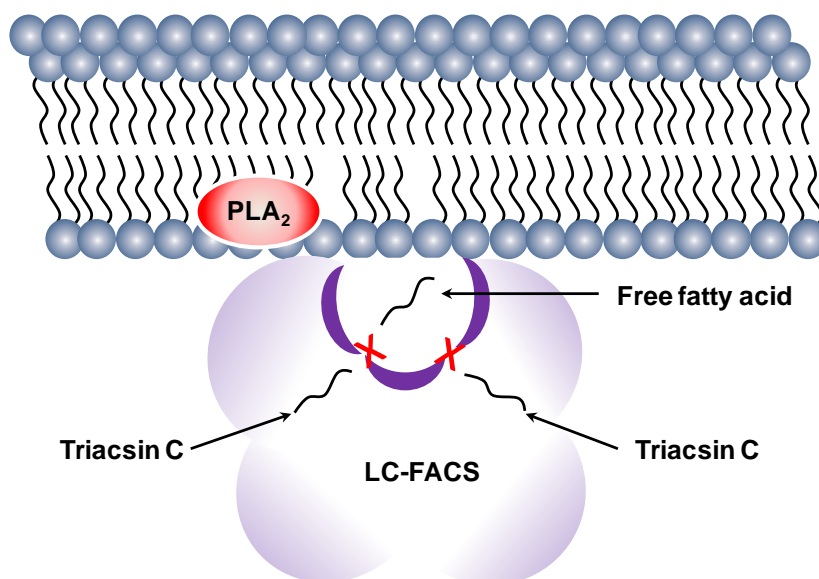
Figure 8.8: Triacsin C inhibits *de novo* synthesis of phospholipids. Following cell activation, PLA$_2$ cleaves phospholipids at the sn2 position releasing AA. Triacsin C competitively binds to LC-FACS, inhibiting fatty acyl-CoA formation and, consequently, reacylation of fatty acids into lysophospholipids.

Levels of PGE_2/D_2-PEs were reduced (~ 35 %) following inhibition of LC-FACS by triacsin C (Figure 8.9 A). Surprisingly, formation of PGE_2 and PGD_2 was also significantly inhibited (Figure 8.9 B). Generation of PGb-PEs decreased 40 % in response to triacsin C (Figure 8.10 A). Formation of PGb was partially blocked (42 %) following inhibition of LC-FACS (Figure 8.10 B). Levels of PGc-PEs were inhibited by approximately 40 % (Figure 8.11 A), similar to free PGc (Figure 8.11 B).

8.2.3 Formation of esterified prostaglandins is inhibited by thimerosal while levels of free prostaglandins are enhanced.

In this section, the requirement of lysophospholipid acyltransferases for esterified prostaglandin generation was investigated using thimerosal (Figure 8.12). This is an organomercury compound, which inhibits acyltransferases without any effect on LC-FACS activity, Figure 8.13 (Hornberger & Patscheke, 1990). To determine the requirement of lysophospholipid acyltransferases for lipid formation, washed human platelets were incubated with varying amounts of thimerosal (25 – 200 µM), at the same time, for 30 min at $37^{o}C$ prior to thrombin activation (0.2 U/ml for 30 min at $37^{o}C$). Lipids were then extracted and analysed using reverse-phase LC/MS/MS on 4000 Q-trap, in MRM mode, as described in Materials and Methods, Sections *2.2.3.2* and *2.2.3.3*.

Inclusion of 75 µM thimerosal significantly reduced formation of esterified prostaglandins. Formation of PGE_2/D_2-PEs was inhibited by 50 % in response to thimerosal (Figure 8.14 A). Levels of PGE_2 were enhanced from 3.4 to 5.7 ng/2 x 10^8 platelets, an increase of approximately 70 % (Figure 8.14 B). Similarly, synthesis of PGD_2 was increased 2-fold (Figure 8.14 B). Generation of PGb-PEs was reduced by 90 % (Figure 8.15 A), whereas levels of free PGb increased 3-fold (Figure 8.15 B). Synthesis of 16:0p/PGc-PE, 18:1p/PGc-PE and 18:0p/PGc-PE was blocked by ~ 55 %, while formation of 18:0a/PGc-PE was not affected (Figure 8.16 A). This suggests that the level of 18:0a/PGc-PE was at the limit of detection. Levels of free PGc were enhanced by ~ 60 % (Figure 8.16 B).
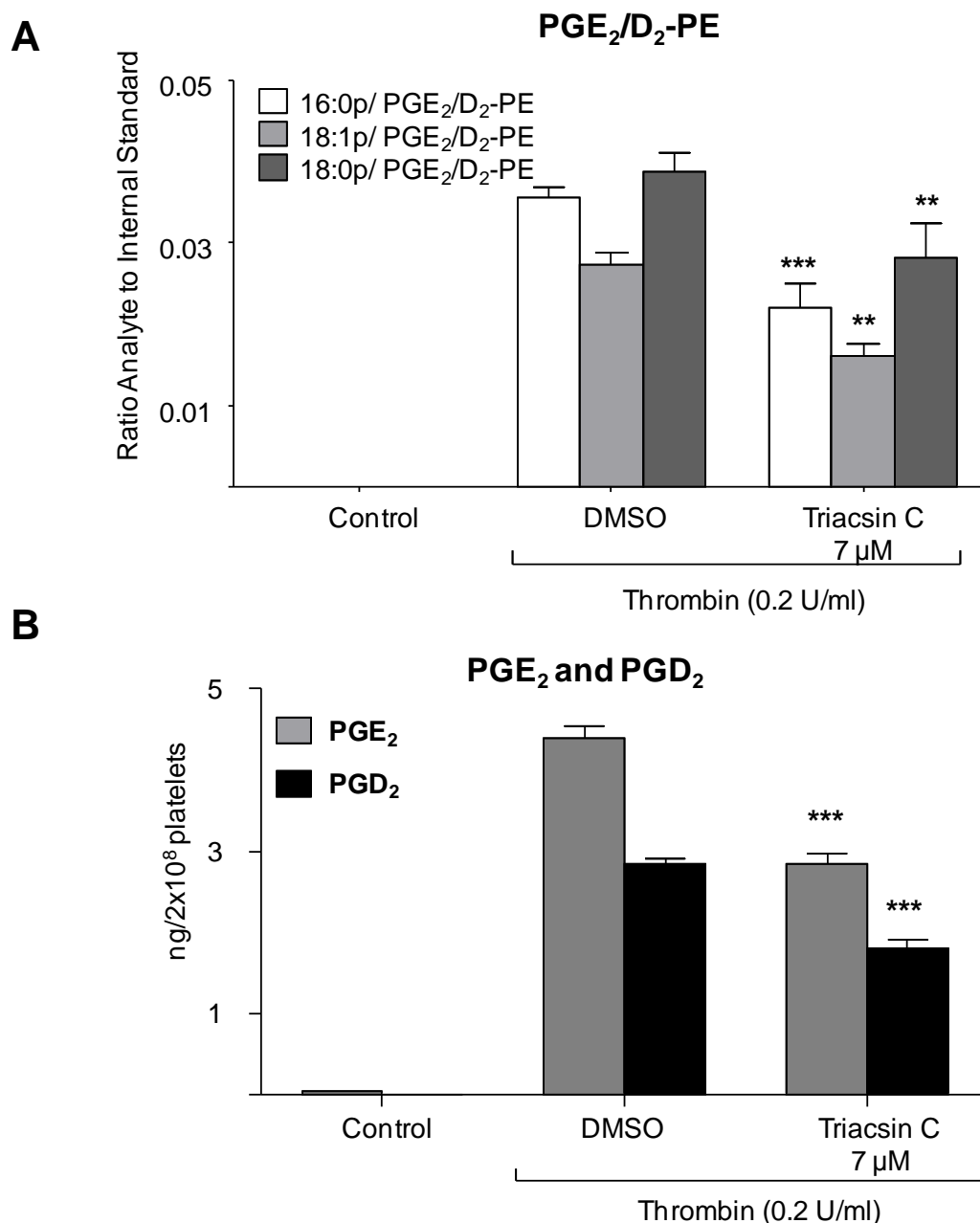
Figure 8.9: Formation of PGE$_2$/D$_2$-PEs, PGE$_2$ and PGD$_2$ are inhibited by triacsin C. Washed platelets were incubated with triacsin C for 30 min at 37°C prior to thrombin activation (0.2 U/ml for 30 min at 37°C). This was followed by lipid extraction and analysis using reverse-phase LC/MS/MS, as described in Materials and Methods, Section *2.2.3.2* and *2.2.3.3*. Levels of PGE$_2$/D$_2$-PEs are expressed as ratio analyte to internal standard while PGE$_2$ and PGD$_2$ are expressed as ng/2 x 10^8 platelets. Data presented from one experiment and representative of three (n = 3, mean ± SEM). *P < 0.05, **P < 0.01 and ***P < 0.001 versus thrombin in the presence of vehicle control (DMSO, 0.5 %), using ANOVA and Bonferroni Post Hoc Test. *Panel A*. PGE$_2$/D$_2$-PE formation by platelets incubated with 7 μM triacsin C. *Panel B*. Generation of free PGE$_2$ and PGD$_2$ by platelets incubated with 7 μM triacsin C.

Figure 8.10: Formation of PGb-PEs and PGb are inhibited by triacsin C. Washed platelets were incubated with triacsin C for 30 min at 37°C prior to thrombin activation (0.2 U/ml for 30 min at 37°C). This was followed by lipid extraction and analysis using reverse-phase LC/MS/MS, as described in Materials and Methods, Section *2.2.3.2* and *2.2.3.3*. Levels of PGb-PEs and PGb are expressed as ratio analyte to internal. Data presented from one experiment and representative of three (n = 3, mean ± SEM). *P < 0.05, **P < 0.01 and ***P < 0.001 versus thrombin in the presence of vehicle control (DMSO, 0.5 %), using ANOVA and Bonferroni Post Hoc Test. *Panel A*. PGb-PE formation by platelets incubated with 7 μM triacsin C. *Panel B*. Generation of free PGb by platelets incubated with 7 μM triacsin C.
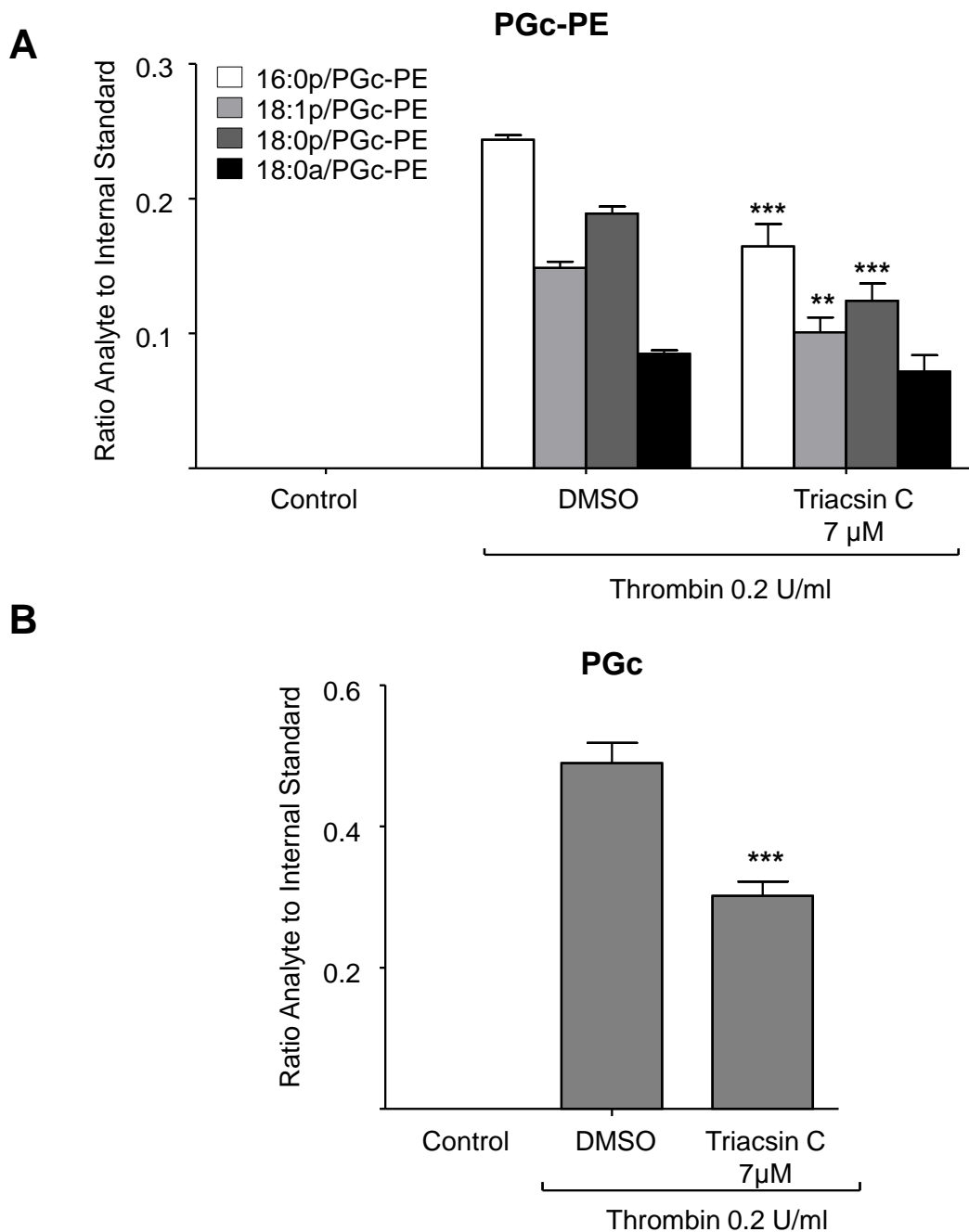
Figure 8.11: Formation of PGc-PEs and PGc are inhibited by triacsin C. Washed platelets were incubated with triacsin C for 30 min at 37°C prior to thrombin activation (0.2 U/ml for 30 min at 37°C). This was followed by lipid extraction and analysis using reverse-phase LC/MS/MS, as described in Materials and Methods, Section *2.2.3.2* and *2.2.3.3*. Levels of PGc-PEs and PGc are expressed as ratio analyte to internal. Data presented from one experiment and representative of three (n = 3, mean ± SEM). *P < 0.05, **P < 0.01 and ***P < 0.001 versus thrombin in the presence of vehicle control (DMSO, 0.5 %), using ANOVA and Bonferroni Post Hoc Test. *Panel A*. PGc-PE formation by platelets incubated with 7 µM triacsin C. *Panel B*. Generation of free PGc by platelets incubated with 7 µM triacsin C.
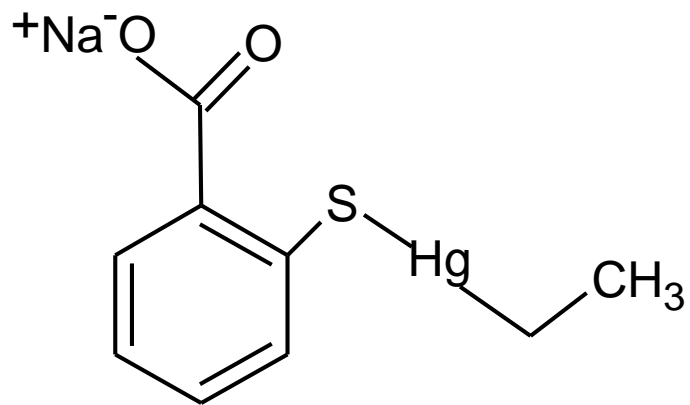
Figure 8.12: Chemical structure of thimerosal.
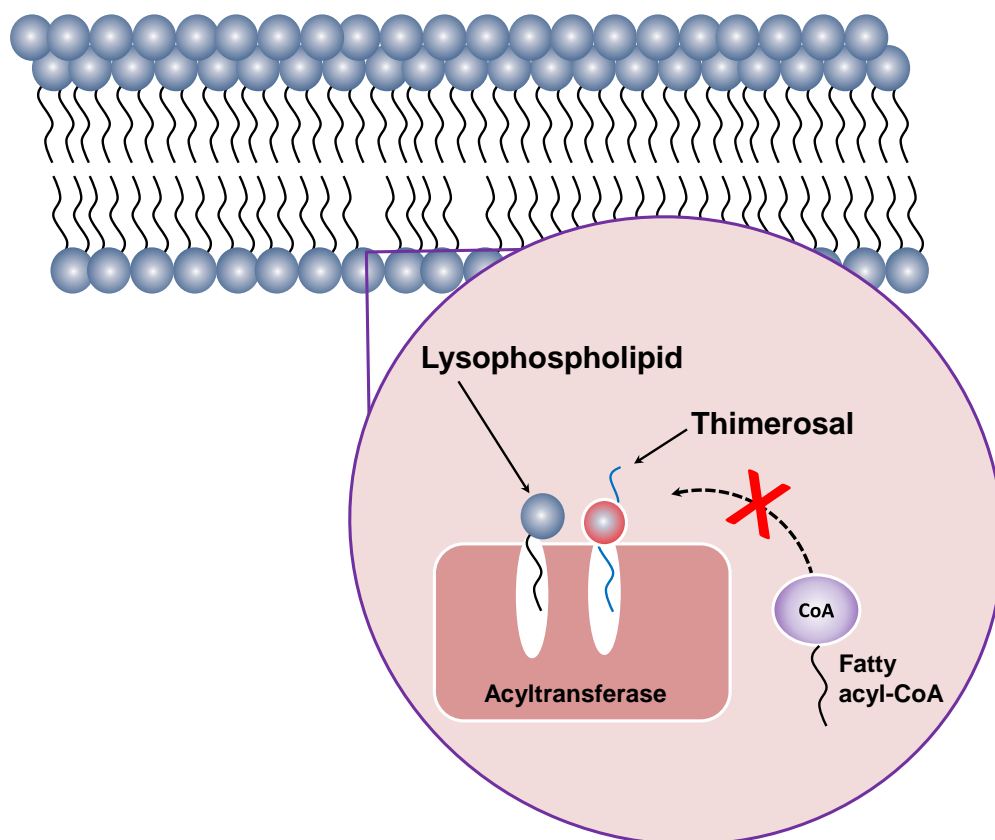
Figure 8.13: Inhibition of fatty acid reacylation by thimerosal. Thimerosal competitively binds to lysophospholipid acyltransferase, inhibiting the reacylation of fatty acids into lysophospholipids.
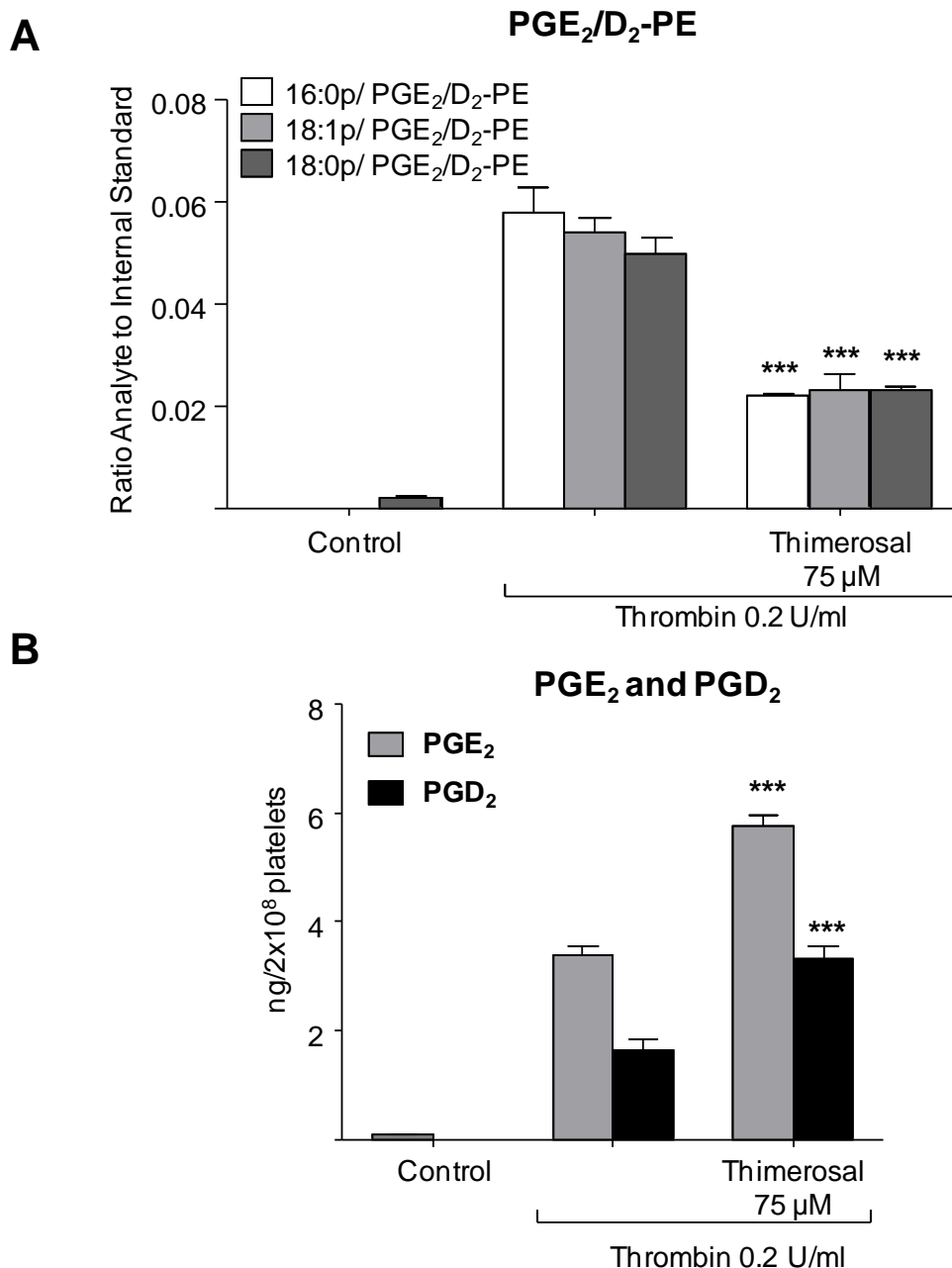
Figure 8.14: PGE$_2$/D$_2$-PEs, PGE$_2$ and PGD$_2$ are inhibited by thimerosal. Washed platelets were incubated with thimerosal for 30 min at 37°C prior to thrombin activation (0.2 U/ml for 30 min at 37°C). This was followed by lipid extraction and analysis using reverse-phase LC/MS/MS, as described in Materials and Methods, Section *2.2.3.2* and *2.2.3.3*. Levels of PGE$_2$/D$_2$-PEs are expressed as ratio analyte to internal standard while PGE$_2$ and PGD$_2$ are expressed as ng/2 x 10^8 platelets. Data presented from one experiment and representative of three (n = 3, mean ± SEM). ***P < 0.001 versus thrombin, using ANOVA and Bonferroni Post Hoc Test. *Panel A*. PGE$_2$/D$_2$-PE formation by platelets incubated with 75 μM thimerosal. *Panel B*. Generation of free PGE$_2$ and PGD$_2$ by platelets incubated with 75 μM thimerosal.
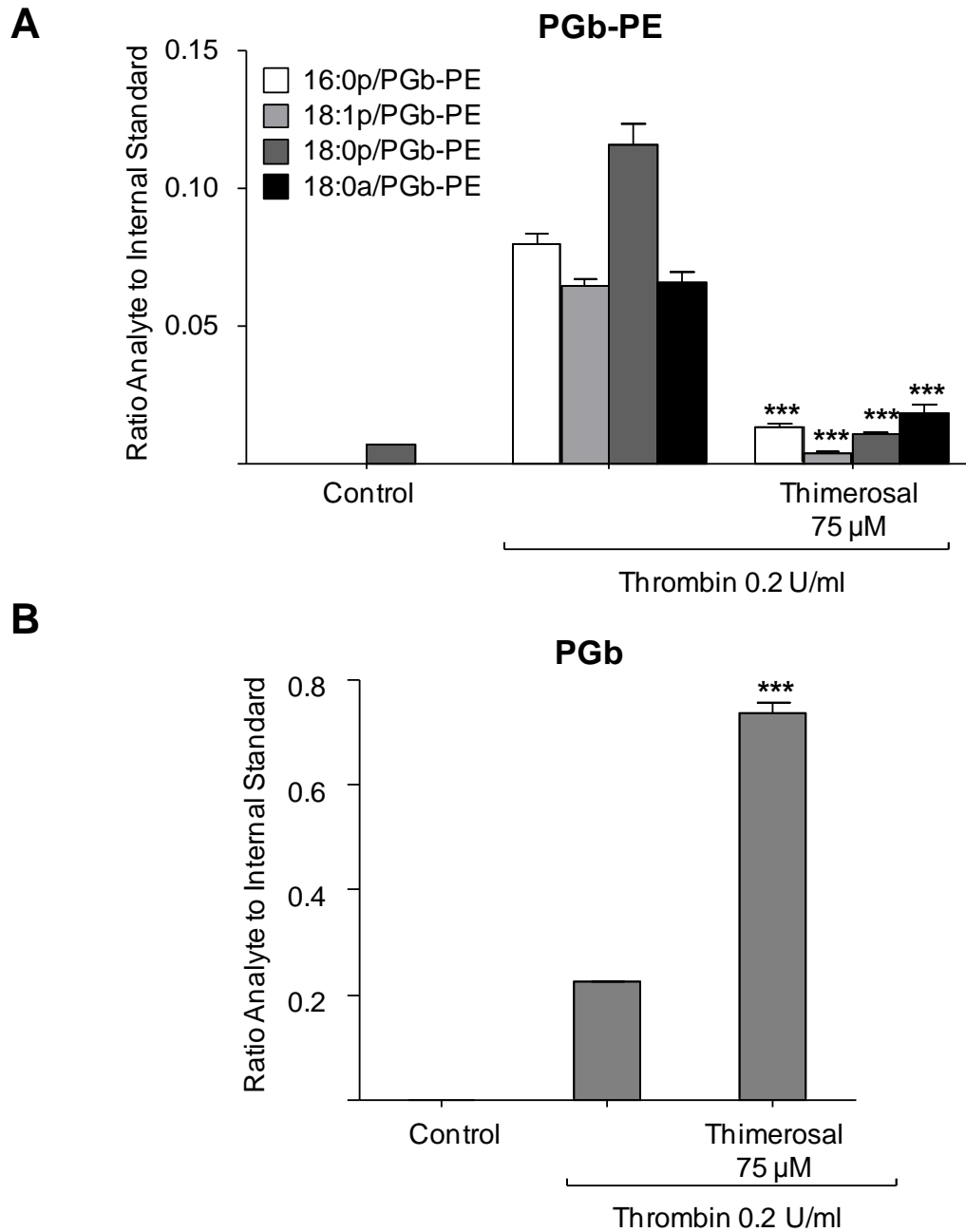
Figure 8.15: PGb-PEs and free PGb are inhibited by thimerosal. Washed platelets were incubated with thimerosal for 30 min at 37°C prior to thrombin activation (0.2 U/ml for 30 min at 37°C). This was followed by lipid extraction and analysis using reverse-phase LC/MS/MS, as described in Materials and Methods, Section *2.2.3.2* and *2.2.3.3*. Levels of PGb-PEs and PGb are expressed as ratio analyte to internal standard. Data presented from one experiment and representative of three (n = 3, mean ± SEM). ***P < 0.001 versus thrombin, using ANOVA and Bonferroni Post Hoc Test. *Panel A*. PGb-PE formation by platelets incubated with 75 μM thimerosal. *Panel B*. PGb generation by platelets incubated with 75 μM thimerosal.
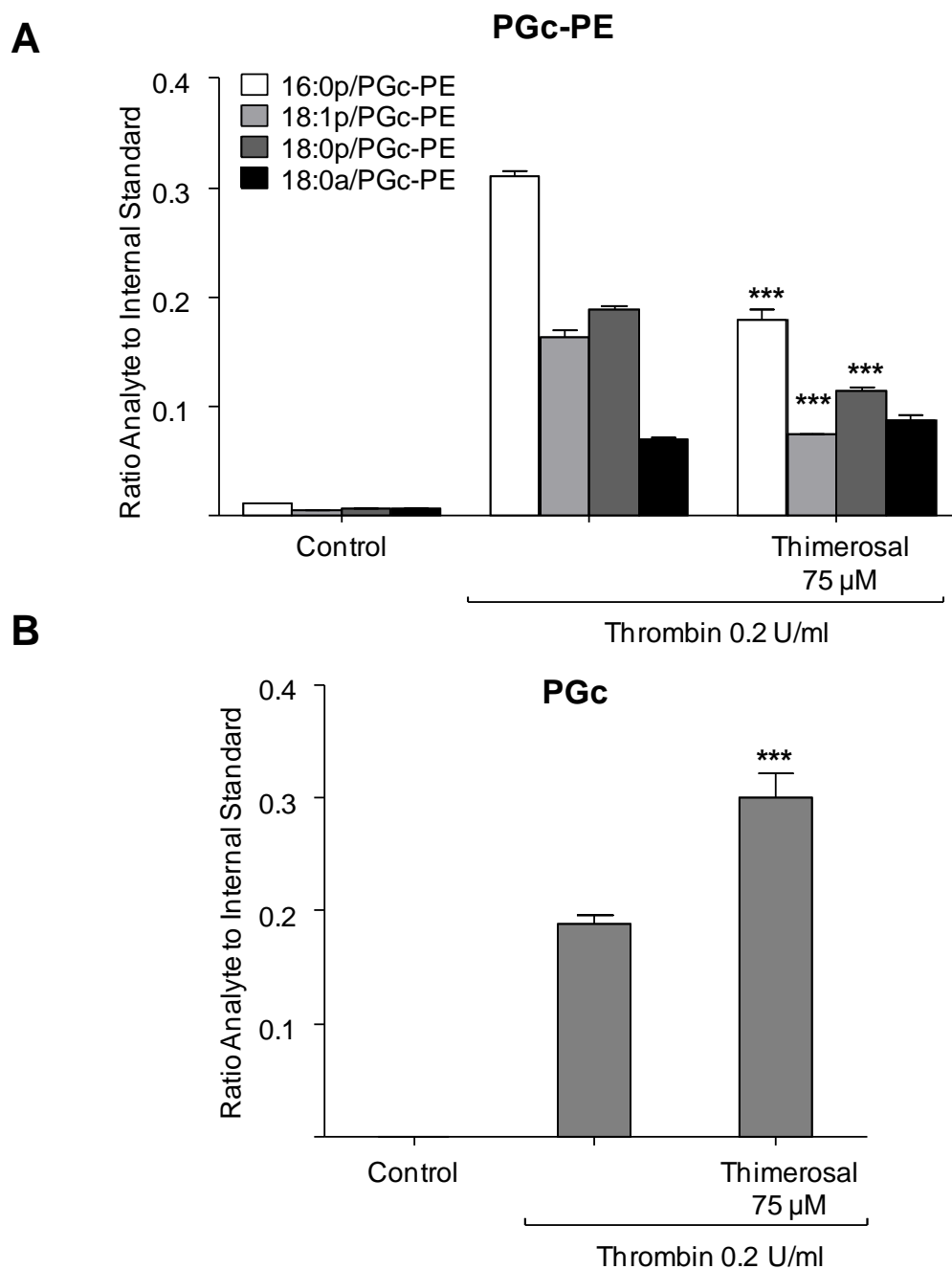
Figure 8.16: PGc-PEs and free PGc are inhibited by thimerosal. Washed platelets were incubated with thimerosal for 30 min at 37°C prior to thrombin activation (0.2 U/ml for 30 min at 37°C). This was followed by lipid extraction and analysis using reverse-phase LC/MS/MS, as described in Materials and Methods, Section *2.2.3.2* and *2.2.3.3*. Levels of PGc-PEs and PGc are expressed as ratio analyte to internal standard. Data presented from one experiment and representative of three (n = 3, mean ± SEM). ***P < 0.001 versus thrombin, using ANOVA and Bonferroni Post Hoc Test. *Panel A*. PGc-PE formation by platelets incubated with 75 μM thimerosal. *Panel B*. PGc generation by platelets incubated with 75 μM thimerosal.

8.2.4   Esterification of free prostaglandins is a controlled mechanism.

To determine whether exogenously added prostaglandins and AA could be incorporated into phospholipids, platelets were spiked with exogenous AA-d_8, PGE$_2$-d_4 or PGD$_2$-d_4 at amounts similar to that generated during platelet activation. Deuterated fatty acids (5 ng of PGE$_2$-d_4, 2.5 ng of PGD$_2$-d_4 and 2 μg of AA-d_8) were incubated with washed human platelets for 30 min at 37°C in the presence of 0.2 U/ml thrombin and 1 mM CaCl$_2$, as described in Materials and Methods, Section *2.2.9* (Smith *et al*., 1985).

Deuterated esterified prostaglandins did not form by thrombin-activated platelets supplemented with AA-d_8, although, very small amounts (at the limit of detection) of deuterated free PGs were detectable (data not shown).

8.2.5   PGE$_2$ and PGD$_2$ are formed in vitro in a PGES and PGDS-independent manner.

In platelets, COX-1 catalyses the first two steps in the biosynthesis of prostanoids. These are the oxidation of AA to the hydroperoxy endoperoxide PGG$_2$ and its subsequent reduction to the hydroxyl endoperoxide PGH$_2$. This is rapidly converted to TxA$_2$ through thromboxane synthase or undergoes enzymatic or non-enzymatic re-arrangement to PGE$_2$ and PGD$_2$ (Salomon *et al*., 1984; Boutaud *et al*., 1999).

In this section, formation of PGE$_2$ and PGD$_2$ via non-enzymatic re-arrangement of PGH$_2$ was investigated *in vitro* using purified/recombinant COX isoforms. In platelets, microsomal PGES-2 and cytosolic PGES are detectable but no PGDS (Bruno *et al*., 2010; Mahmud *et al*., 1997; Watanabe *et al*., 1982). Furthermore, as selective mPGES-2 and cPGEs inhibitors are not commercially available, the involvement of these enzymes could not be investigated. To determine whether PGE$_2$ and PGD$_2$ formation by activated platelets resulted from structural re-arrangement of PGH$_2$, COX isoforms were incubated with AA and ratios of PGE$_2$ and PGD$_2$ formed *in vitro* compared to that generated by thrombin-activated platelets.

Briefly, purified ovine COX-1 (apoCOX-1) and recombinant murine COX-2 (apoCOX-2) was reconstituted with hematin. Next, 3.5 µg of heme-reconstituted COXs (holoCOX-1 or holoCOX-2) was incubated with 150 µM of AA for 3 min at 37°C in the presence of 500 µM of phenol. Formation of PGE_2 and PGD_2 was then analysed using reverse-phase LC/MS/MS, as described in Materials and Methods, Section *2.2.6*.

Oxidation of AA by holoCOX-1 generated PGE_2 and PGD_2 with a 2:1 predominance of PGE_2 over PGD_2, due to decomposition of enzymatically-generated PGH_2, similar to that observed in platelets (Figure 8.17 A). This indicates that PGE_2 and PGD_2 formation by platelets does not require PGE or PGD synthase. Although levels of PGE_2 and PGD_2 formed by COX-2 were lower compared to those generated by COX-1, the 2:1 ratio of PGE_2:PGD_2 was maintained (Figure 8.17 B).

For identification of PGE_2 and PGD_2 formation *in vitro*, the retention time and MS/MS spectrum were compared to that generated by thrombin-activated human platelets. As for *ex vivo* formation, PGE_2 and PGD_2 generated *in vitro* eluted at 32.5 and 34.4 min with identical MS/MS spectra (Figure 8.18 – 8.19). Since PGE_2 and PGD_2 share a similar fragmentation pattern, only the MS spectrum of PGE_2 is shown for comparison (Figure 8.19).
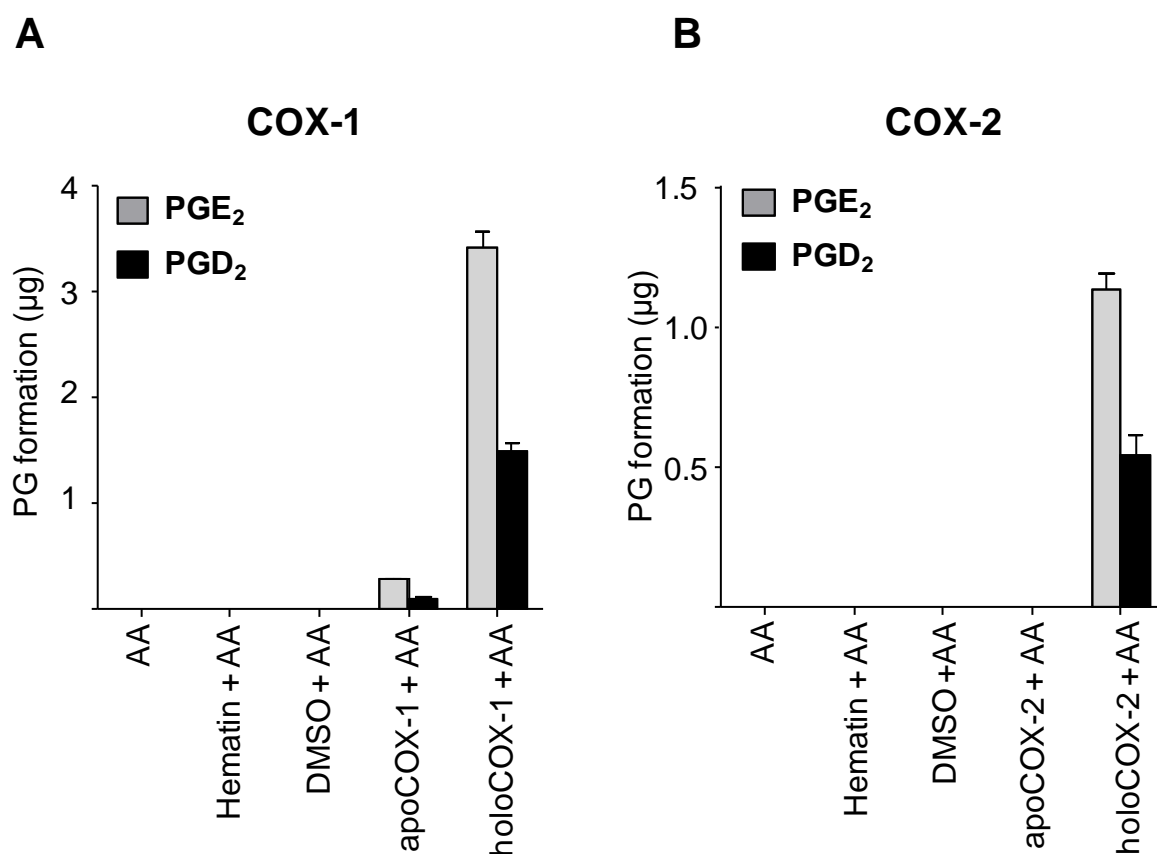
Figure 8.17: COX isoforms generate a 2:1 ratio of PGE$_2$:PGD$_2$ *in vitro*. 3.5 μg of either heme-reconstituted COX isoforms (holoCOX-1 or holoCOX-2) was incubated with 150 μM of AA for 3 min at 37°C, before lipid extraction and analysis using reverse-phase LC/MS/MS, monitoring *m/z* 351.2 → 271.2 as described in Materials and Methods, Section *2.2.6*. PGE$_2$ and PGD$_2$ are expressed as micrograms/3.5 μg enzyme generated over 3 min (n = 3, mean ± SEM). Data is presented from 1 experiment and representative of ≥ 3 separate experiments.
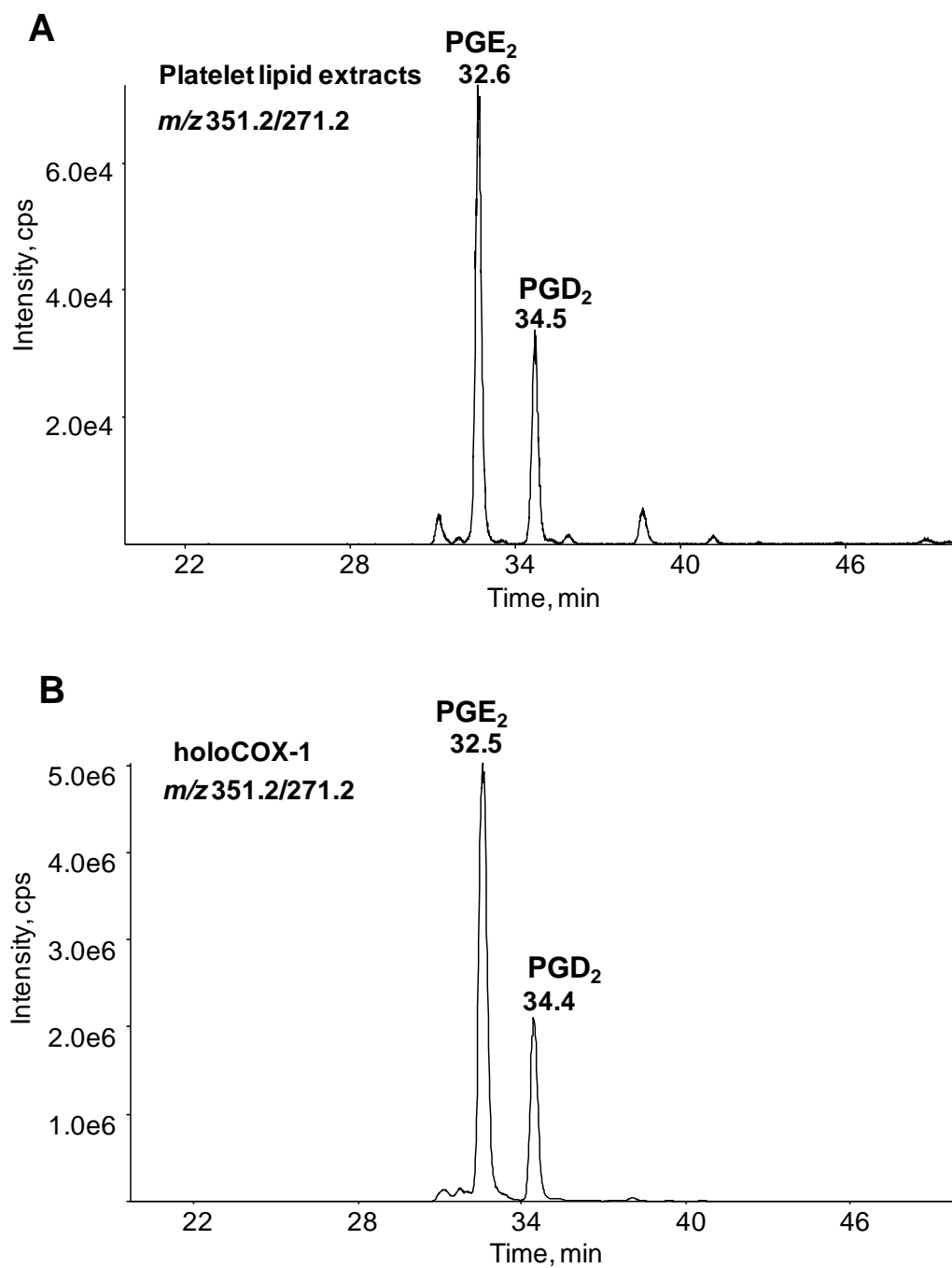
Figure 8.18: Comparison of PGE$_2$ and PGD$_2$ formed by activated platelets and *in vitro* via COX-1. Lipid extracts were separated using reverse-phase LC/MS/MS, monitoring *m/z* 351.2 → 271.2 as described in Materials and Methods, Section *2.2.6*. *Panel A*. Chromatogram showing PGE$_2$ and PGD$_2$ formed by thrombin-activated platelets. *Panel B*. Chromatogram showing PGE$_2$ and PGD$_2$ formed *in vitro* via COX-1.
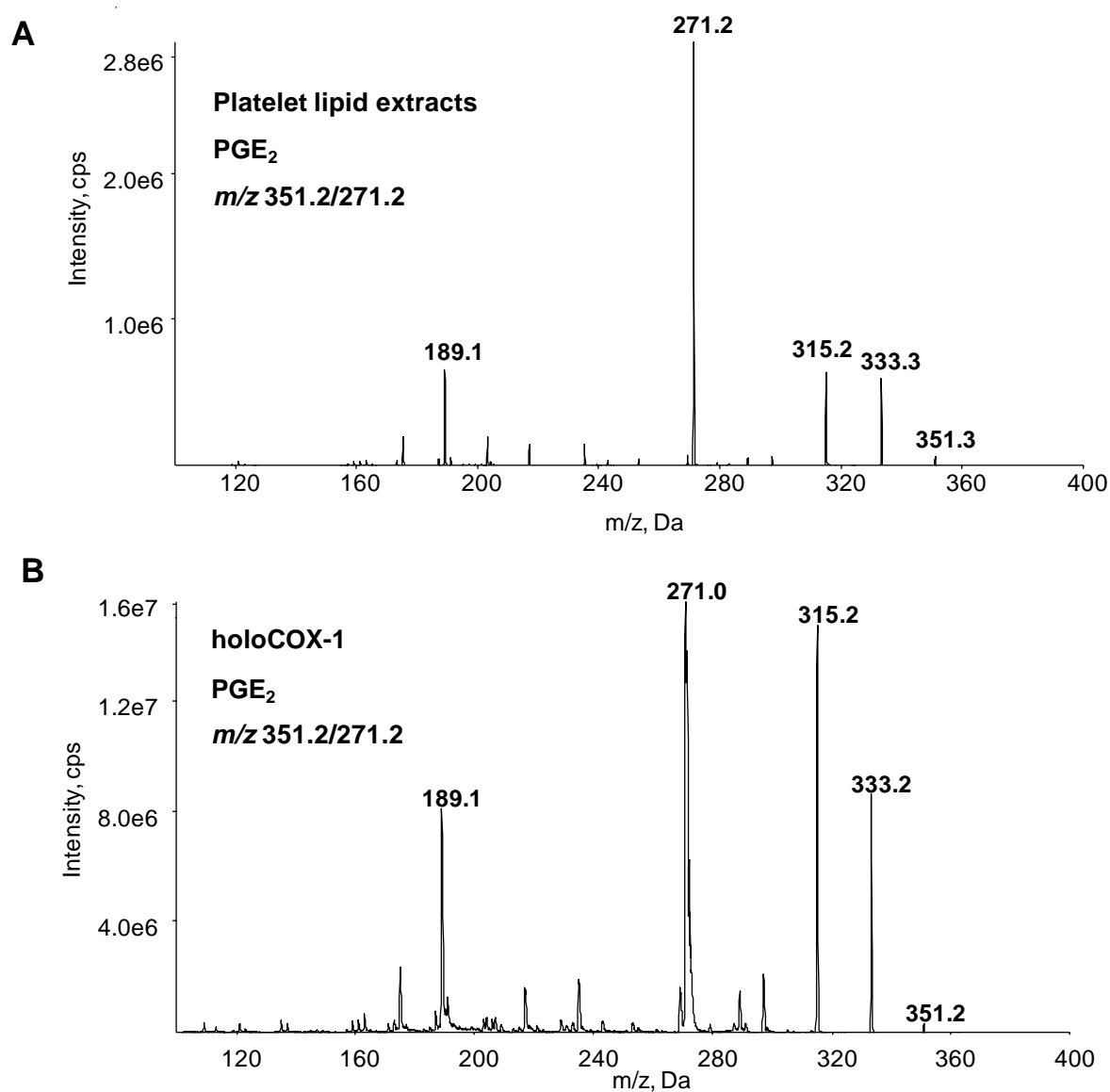
Figure 8.19: Comparison of MS spectrum of PGE$_2$ formed by thrombin-activated platelets and *in vitro* via COX-1. Lipid extracts were separated using reverse-phase LC/MS/MS, as described in Materials and Methods, Section *2.2.6*, in product ion mode, with Q1 set at *m/z* 351.2, CID at Q2 and Q3 set at *m/z* 271.2. MS spectrum was acquired at the apex of elution of PGE$_2$ at 32 min. *Panel A*. MS/MS spectrum of PGE$_2$ formed by thrombin-activated platelets. *Panel B.* MS/MS spectrum of PGE$_2$ formed *in vitro* by COX-1.

8.2.6   Free PGb is formed in vitro via COX-1 and COX-2.

To determine whether free PGb could originate from decomposition of enzymatically-generated PGH_2, 3.5 µg of either holoCOX-1 or holoCOX-2 was incubated with 150 µM of AA and formation of PGb assessed, using reverse-phase LC/MS/MS, as described in Materials and Methods, Section *2.2.6*.

In vitro formation of free PGb via COX-1 and COX-2 was confirmed (Figure 8.20). Free PGb formed *in vitro* via both COX isoforms eluted at 38 min, similarly to free PGb generated by activated platelets (Figure 8.21). The MS/MS spectrum of free PGb generated *in vitro* was identical to that formed by activated platelets (Figure 8.22).

8.2.7   Free PGc is formed in vitro via both COX-1 and COX-2.

Formation of free PGc *in vitro* via both COX-1/-2 was confirmed (Figure 8.23). Levels of free PGc generated by recombinant COX-2 were approximately 3-fold lower compared to that generated by purified COX-1. This difference could be due to lower COX-2 activity. Free PGc formed *in vitro* eluted at 51.5 min, similar to PGc generated by agonist-activated platelets (Figure 8.24). The time of elution and MS/MS spectrum of free PGc formed *in vitro* was comparable to that generated by platelets (Figure 8.25).
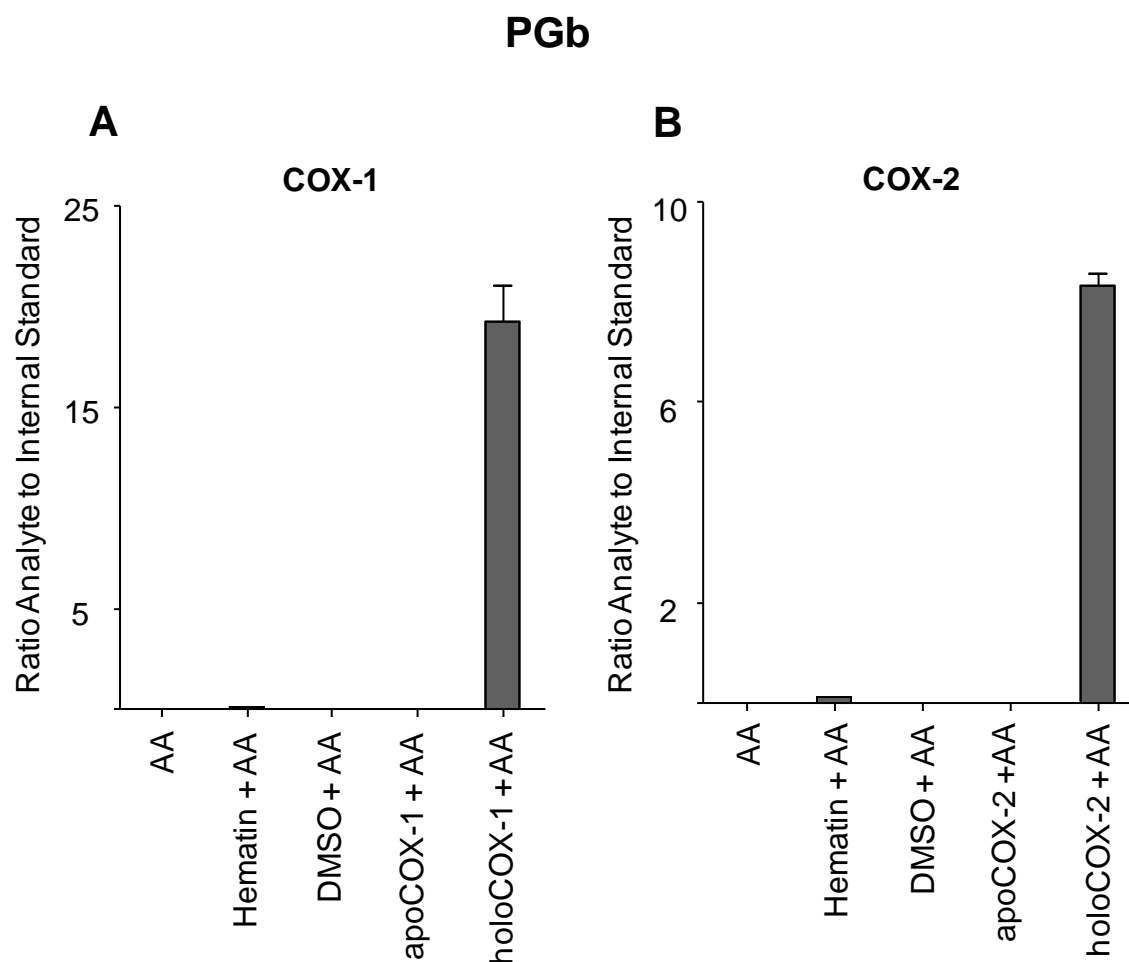
Figure 8.20: COX isoforms generate PGb *in vitro*. 3.5 µg of either holoCOX-1 or holoCOX-2 was incubated with 150 µM of AA for 3 min at 37°C, before lipid extraction and analysis using reverse-phase LC/MS/MS, monitoring *m/z* 351.2 → 207.1 as described in Materials and Methods, Section *2.2.6*. Levels of PGb are expressed as ratio analyte to internal standard/3.5 µg enzyme generated over 3 min (n = 3, mean ± SEM). Data is presented from 1 experiment and representative of ≥ 3 separate experiments.
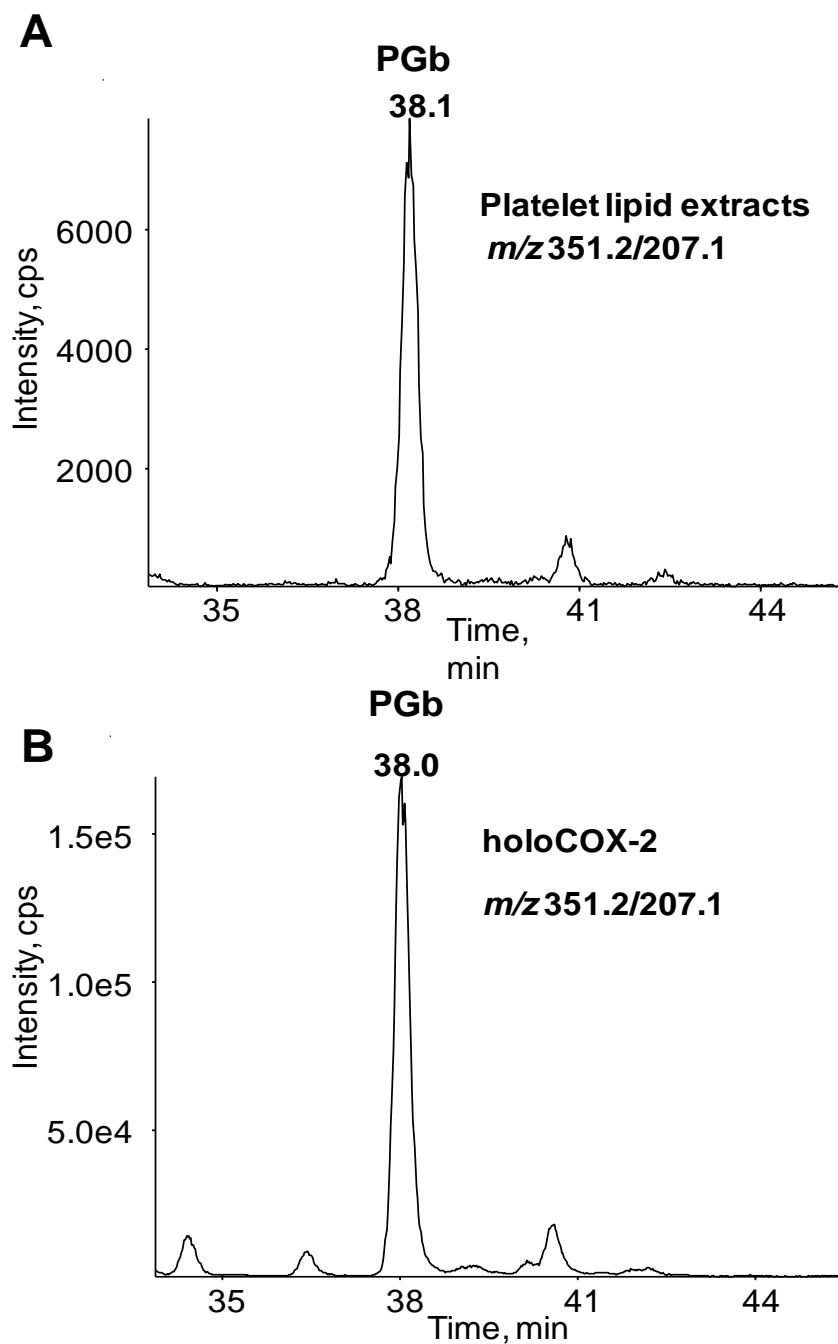
Figure 8.21: Comparison of PGb formed by activated platelets and *in vitro* via COX-2. Lipid extracts were separated using reverse-phase LC/MS/MS, monitoring *m/z* 351.2 → 207.1 as described in Materials and Methods, Section *2.2.6*. *Panel A*. Chromatogram showing PGb formed by thrombin-activated platelets. *Panel B*. Chromatogram showing PGb formed *in vitro* via COX-2.
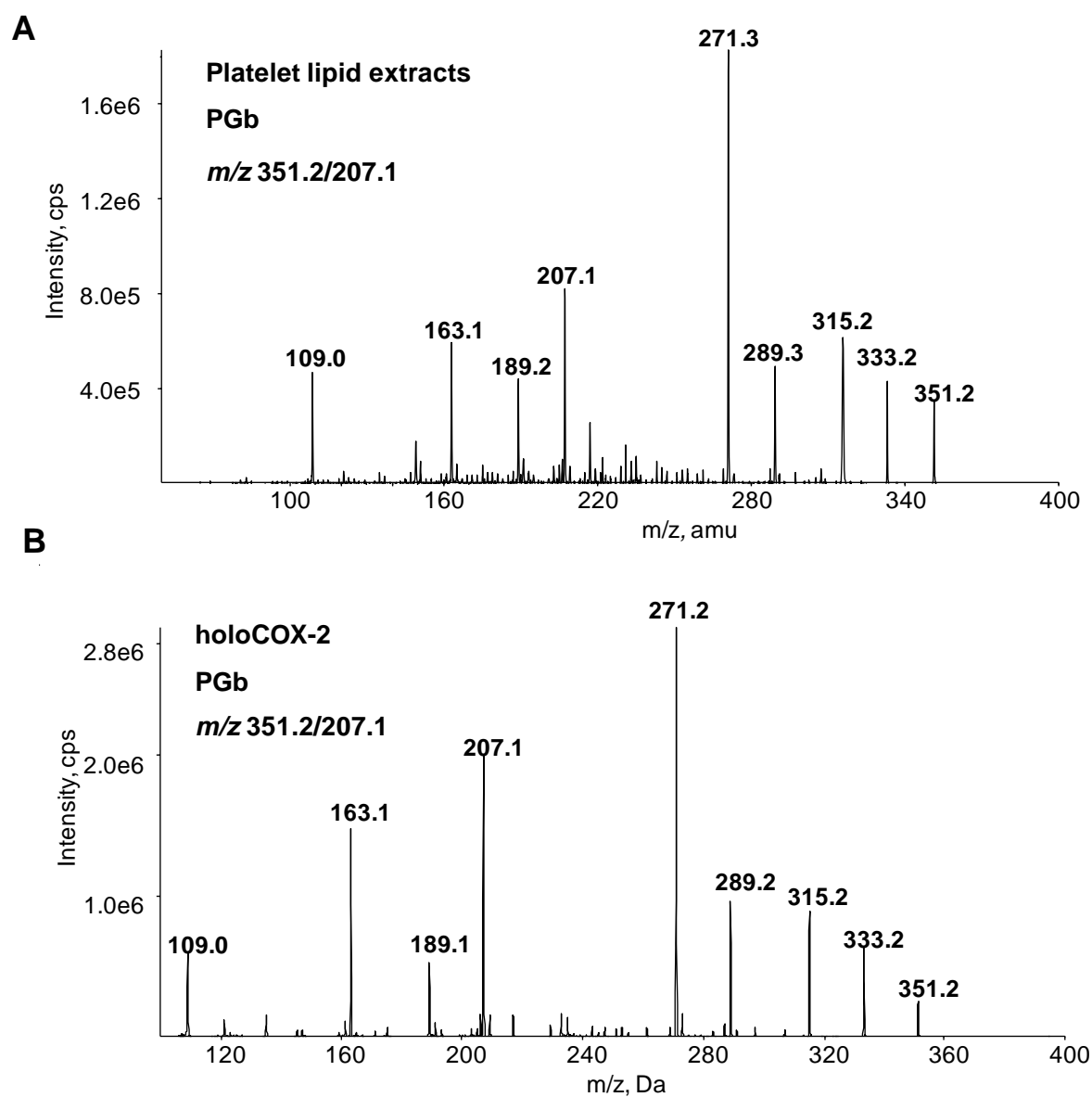
Figure 8.22: MS/MS spectra of PGb formed by activated platelets and *in vitro* via COX-2. Lipid extracts were separated using reverse phase LC/MS/MS, as described in Materials and Methods, Section *2.2.6*, in product ion mode, with Q1 set at *m/z* 351, CID at Q2 and Q3 set at *m/z* 207.1. MS spectra were acquired at the apex of elution of PGb at 38 min. *Panel A*. MS/MS spectrum of PGb formed by thrombin-activated platelets. *Panel B.* MS/MS spectrum of PGb formed *in vitro* by COX-2.

PGc
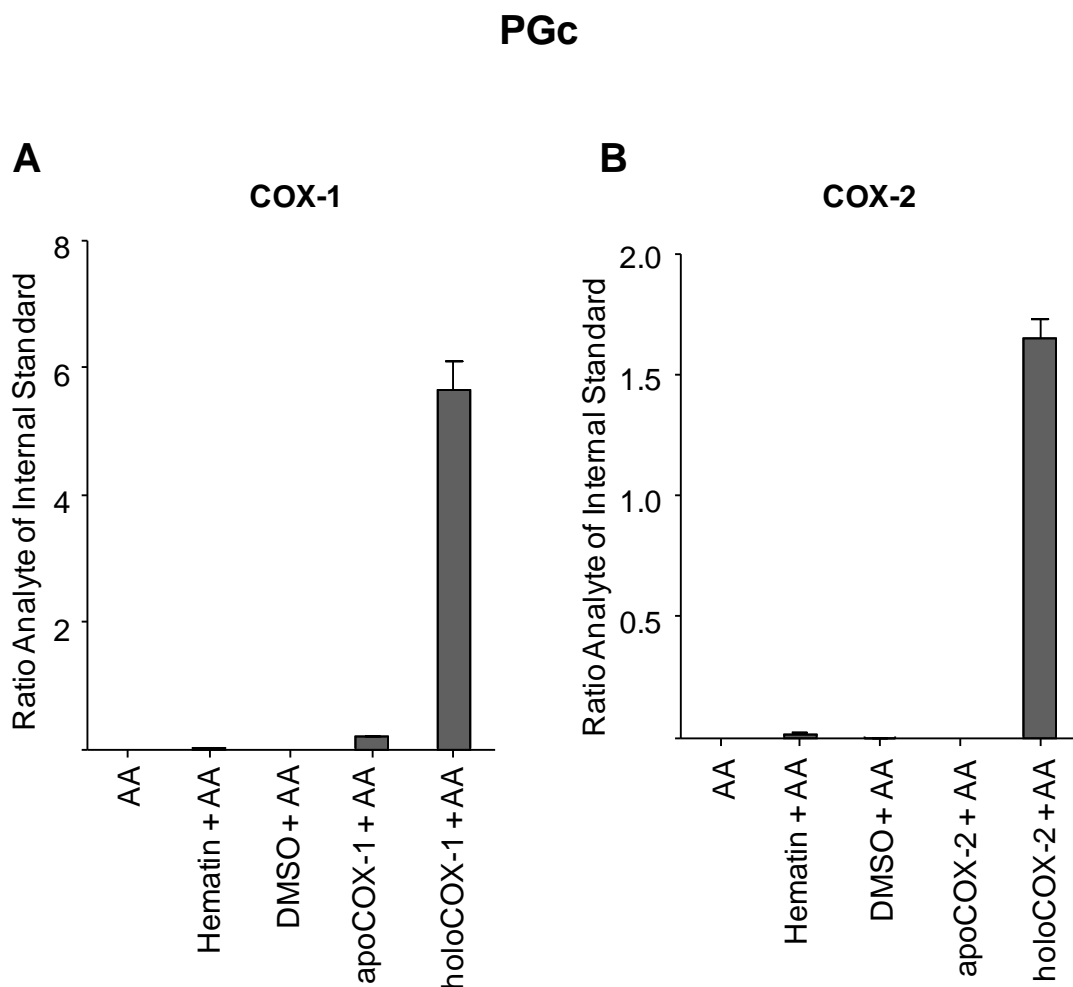
Figure 8.23: COX isoforms generate PGc *in vitro*. 3.5 µg of either holoCOX-1 or holoCOX-2 was incubated with 150 µM of AA for 3 min at 37°C, before lipid extraction and analysis using reverse-phase LC/MS/MS, monitoring *m/z* 351.2 → 165.1 as described in Materials and Methods, Section *2.2.6*. Levels of PGc are expressed as ratio analyte to internal standard/3.5 µg enzyme generated over 3 min (n = 3, mean ± SEM). Data is presented from 1 experiment and representative of ≥ 3 separate experiments.

Figure 8.24: Comparison PGc formed by activated platelets and *in vitro* via COX-2. Lipid extracts were separated using reverse-phase LC/MS/MS, monitoring *m/z* 351.2 → 165.1 as described in Materials and Methods, Section *2.2.6*. *Panel A*. Chromatogram showing PGc formed by thrombin-activated platelets. *Panel B*. Chromatogram showing PGc formed *in vitro* via COX-2.
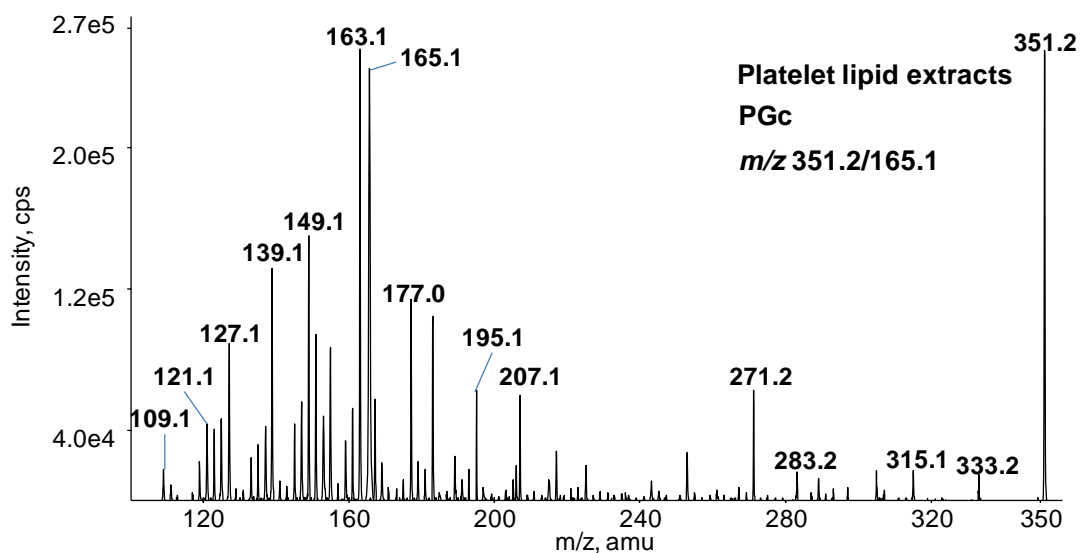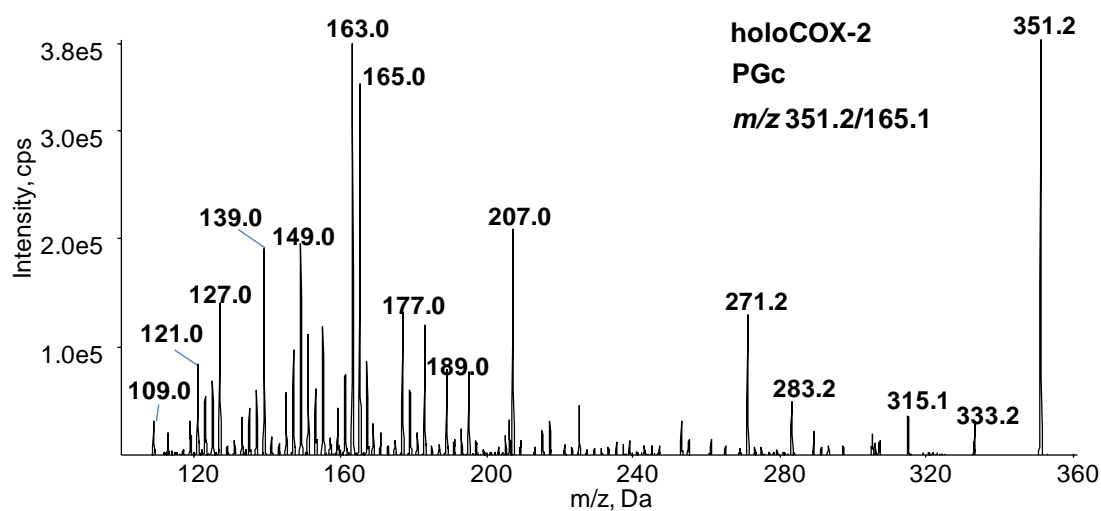
Figure 8.25: MS/MS spectra of PGc formed by thrombin-activated platelets and *in vitro* via COX-2. Lipid extracts were separated using reverse-phase LC/MS/MS, as described in Materials and Methods, Section *2.2.6*, in product ion mode, with Q1 set at *m/z* 351, CID at Q2 and Q3 set at *m/z* 165.1. MS spectra were acquired at the apex of elution of PGc at 51 min. *Panel A*. MS/MS spectrum of PGc formed by thrombin-activated platelets. *Panel B.* MS/MS spectrum of PGc formed *in vitro* by COX-2.

8.2.8 *PG-PEs may form via free radical attack on phospholipid membranes during COX-1 turnover.*

In this section, formation of esterified prostaglandins via direct oxidation of PE by COX-1 was investigated *in vitro*. For this, purified COX-1 was incubated with AA-containing PE, 1-stearoly-2-arachidonyl-PE (SAPE) and esterified prostaglandin formation assessed, using reverse-phase LC/MS/MS, as described in Materials and Methods, Section *2.2.3.2*.

Purified COX-1 was also incubated with SAPE in the presence of AA to test the hypothesis that during oxidation of AA by COX-1, radicals formed at the cyclooxygenase active site could escape, reaching intact phospholipids where they may initiate non-enzymatic oxidation of esterified AA, and lead to non-enzymatic formation of PG-PEs.

Briefly, purified ovine COX-1 (apoCOX-1) was reconstituted with hematin (an iron-containing porphyrin), as described in Materials and Methods, Section *2.2.8.2*. Next, 3.5 µg of heme-reconstituted COX-1 (holoCOX-1) was incubated with 150 µM of SAPE in the presence or absence of 150 µM of AA. In some experiments, AA was replaced with AA-d_8. In order to mimic the conformation of membrane bilayer, lipids were incorporated into liposomes, as described in Materials and Methods, Section *2.2.11*.

Fenton chemistry was also initially considered as the mechanism for esterified prostaglandin generation. In this reaction, ferrous iron is oxidised by hydrogen peroxide to ferric iron. The latter is then reduced back to iron. Radicals generated by this process could engage in secondary reactions abstracting hydrogen, inducing non-enzymatic oxidation of phospholipids. Thus, free ferric iron ions in solution could potentially stimulate lipid peroxidation by decomposing hydroperoxides present as contaminants in commercial lipid standards. To investigate whether the generation of esterified prostaglandins was induced by Fenton chemistry reactions, lipid substrates were incubated with holoCOX-1 in the presence of diethylenetriaminepentaacetic acid (DTPA), an ion metal chelator.

A small amount of PGE_2/D_2-PE (Figures 8.26), PGb-PE (Figures 8.27) and PGc-PE (Figures 8.28) was detected in 18:0a/20:4-PE (SAPE), even though it was a freshly opened vial, and this was increased by addition of hematin (the COX-1 cofactor, added alone as control) through non-enzymatic oxidation. However, incubation of holoCOX-1 and SAPE did not elevate esterified prostaglandins further, indicating that COX-1 cannot directly oxidise SAPE. However, when SAPE was added during COX-1 dependent oxidation of AA, significant higher levels of PGE_2/D_2-PE, PGb-PE and PGc-PE formation were observed (p < 0.001 versus SAPE in the presence COX-1, using ANOVA and Bonferroni Post Hoc Test), Figure 8.26 – 8.28.

In addition, where AA-d_8 was used instead of AA, deuterated free PGs but no deuterated esterified prostaglandins were detectable (data not shown). Metal chelation by DTPA did not inhibit formation of 18:0a/PGE_2/D_2-PE, demonstrating that Fenton chemistry was not involved, Figures 8.26. Whereas, generation of 18:0a/PGb-PE was slightly decreased (Figures 8.27) and 18:0a/PGc-PE increased (Figures 8.27).

For identification of esterified prostaglandin formation *in vitro*, the retention time and MS/MS spectrum were compared to that generated by thrombin-activated human platelets. As for *ex vivo* formation, 18:0a/PGE_2/D_2-PE, 18:0a/PGb-PE and 18:0a/PGc-PE generated *in vitro* eluted at 16.9, 18.5 and 18.9 minutes, respectively, with comparable MS/MS spectra (Figure 8.29 – 8.32).

18:0a/PGE$_2$/D$_2$-PE
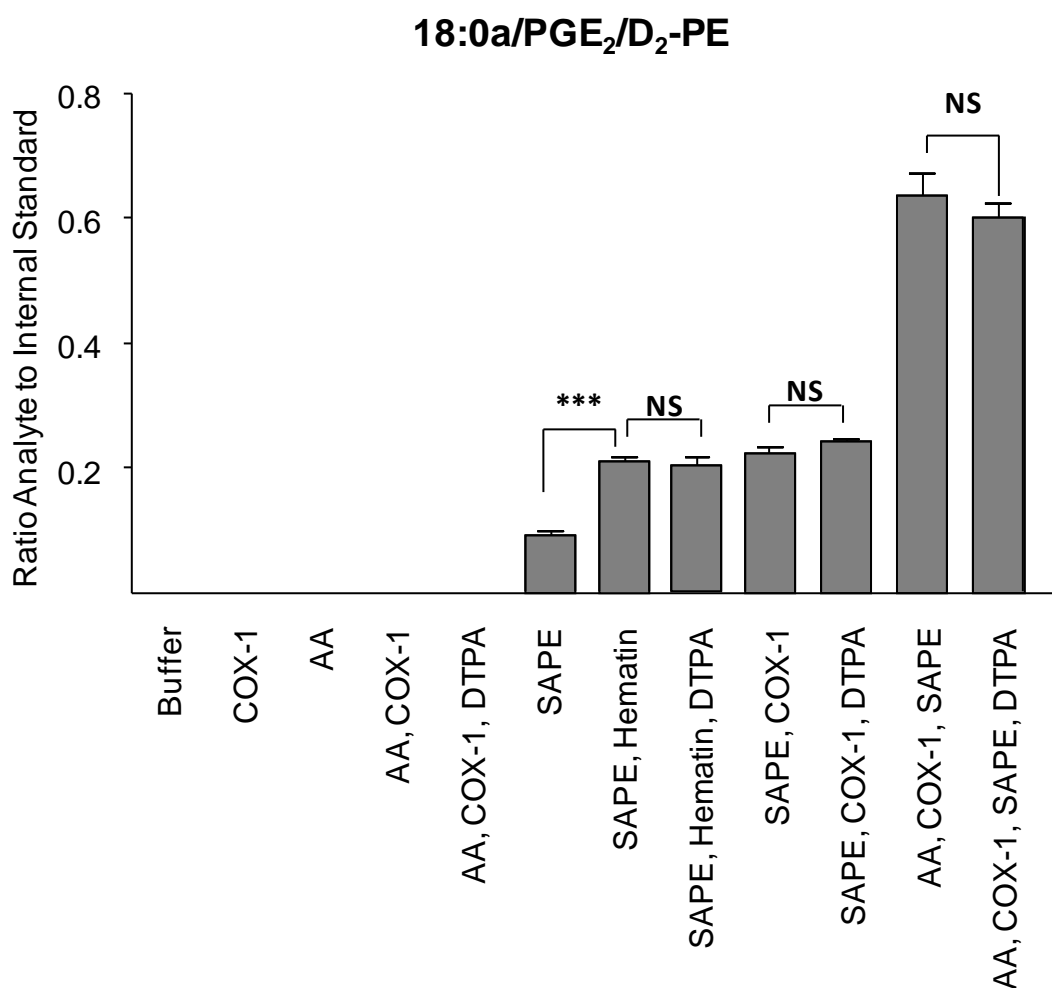
Figure 8.26: PE is oxidised to PGE$_2$/D$_2$-PE during oxidation of AA by COX-1. 3.5 μg of holoCOX-1 was incubated with either 150 μM of AA, 150 μM of SAPE or liposomes containing AA and SAPE, for 3 min at 37°C, in the presence or absence of 10 μM DTPA. This was followed by lipid extraction and analysis using reverse-phase LC/MS/MS, monitoring parent [M-H]$^-$ → *m/z* 271.2, as described in Materials and Methods, Section *2.2.3.2*. Levels of 18:0a/PGE$_2$/D$_2$-PE are expressed as ratio analyte to internal standard/3.5 μg enzyme generated over 3 min (n = 3, mean ± SEM). Data is presented from 1 experiment and representative of ≥ 3 separate experiments. NS = not significant, *** P < 0.001 versus SAPE, using ANOVA and Bonferroni Post Hoc Test.
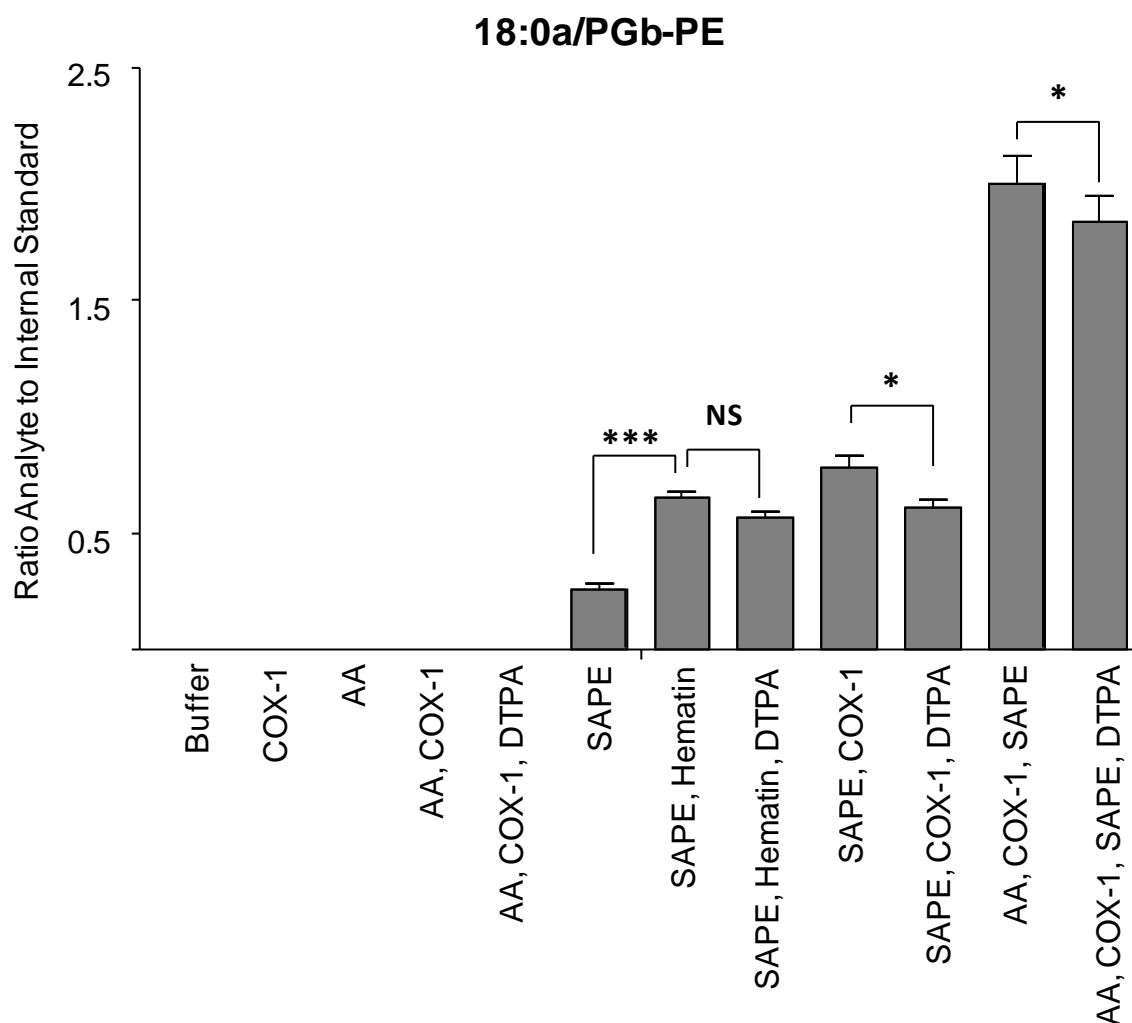
Figure 8.27: PE is oxidised to PGb-PE during oxidation of AA by COX-1. 3.5 µg of holoCOX-1 was incubated with either 150 µM of AA, 150 µM of SAPE or liposomes containing AA and SAPE, for 3 min at 37°C, in the presence or absence of 10 µM DTPA. This was followed by lipid extraction and analysis using reverse-phase LC/MS/MS, monitoring parent [M-H]$^-$ → *m/z* 351.2, as described in Materials and Methods, Section *2.2.3.2*. Levels of 18:0a/PGb-PE are expressed as ratio analyte to internal standard/3.5 µg enzyme generated over 3 min (n = 3, mean ± SEM). Data is presented from 1 experiment and representative of ≥ 3 separate experiments. NS = not significant, ***P < 0.001 versus SAPE alone, *P <0.05 versus SAPE in the presence of COX-1 or AA and COX-1, using ANOVA and Bonferroni Post Hoc Test.
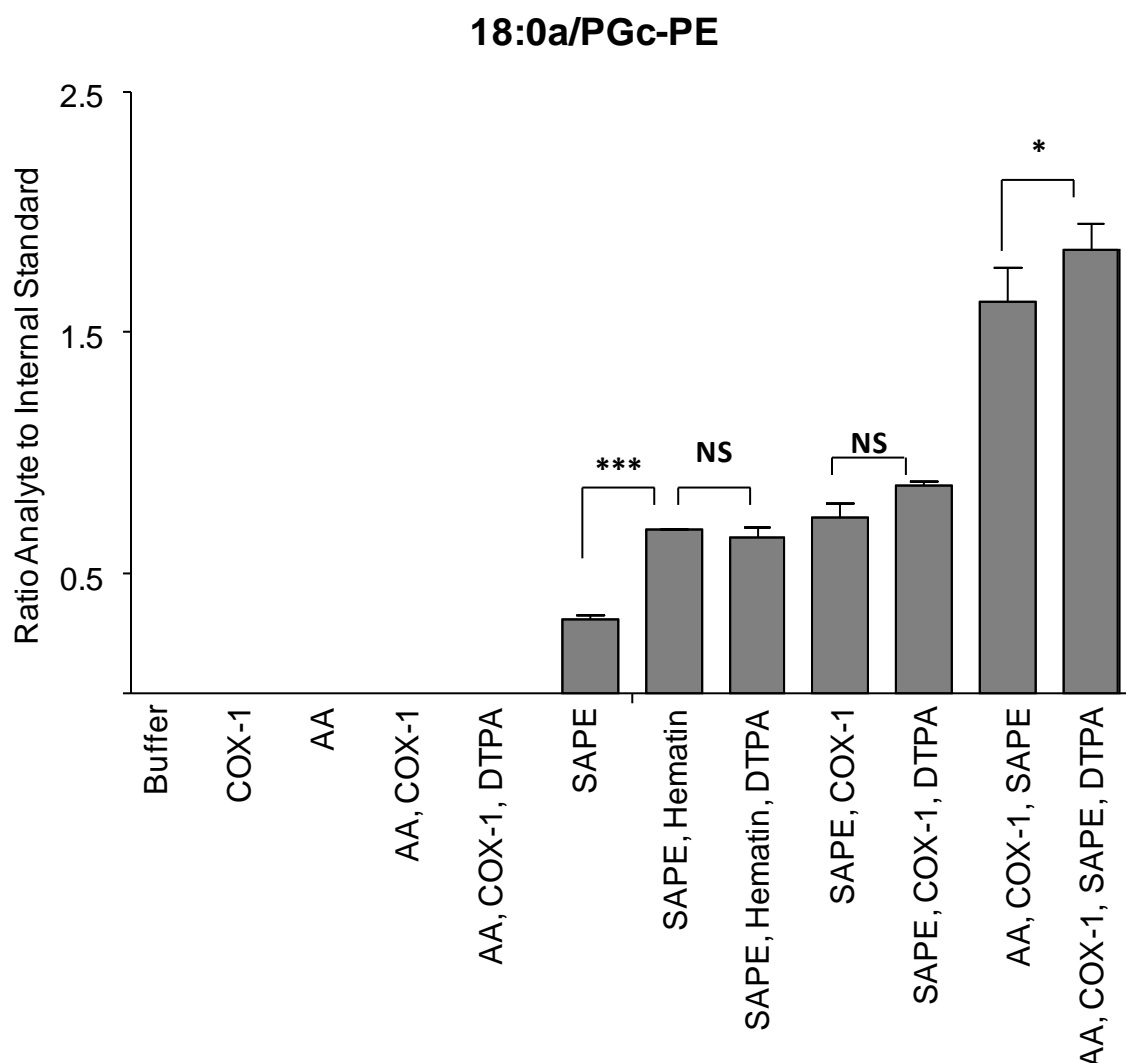
Figure 8.28: PE is oxidised to PGc-PE during oxidation of AA by COX-1. 3.5 µg of holoCOX-1 was incubated with either 150 µM of AA, 150 µM of SAPE or liposomes containing AA and SAPE, for 3 min at 37°C, in the presence or absence of 10 µM DTPA. This was followed by lipid extraction and analysis using reverse-phase LC/MS/MS, monitoring parent $[M-H]^- \rightarrow$ *m/z* 351.2, as described in Materials and Methods, Section *2.2.3.2*. Levels of 18:0a/PGc-PE are expressed as ratio analyte to internal standard/3.5 µg enzyme generated over 3 min (n = 3, mean ± SEM). Data is presented from 1 experiment and representative of $\geq$ 3 separate experiments. NS = not significant, ***P < 0.001 versus SAPE alone. *P <0.05 versus SAPE in the presence of AA and COX-1, using ANOVA and Bonferroni Post Hoc Test.

A

18:0a/PGE$_2$/D$_2$-PE

17.1

Platelet lipid extracts

***m/z* = 814.7/271.2**

18.9

Intensity, cps

2400

1800

1200

600

8   14   20   26   32
Time, min

B

18:0a/PGE$_2$/D$_2$-PE

16.9

18.5

COX-1
***m/z* 814.7/271.2**

Intensity, cps

3.0e4

2.0e4

1.0e4

8   14   20   26   32
Time, min
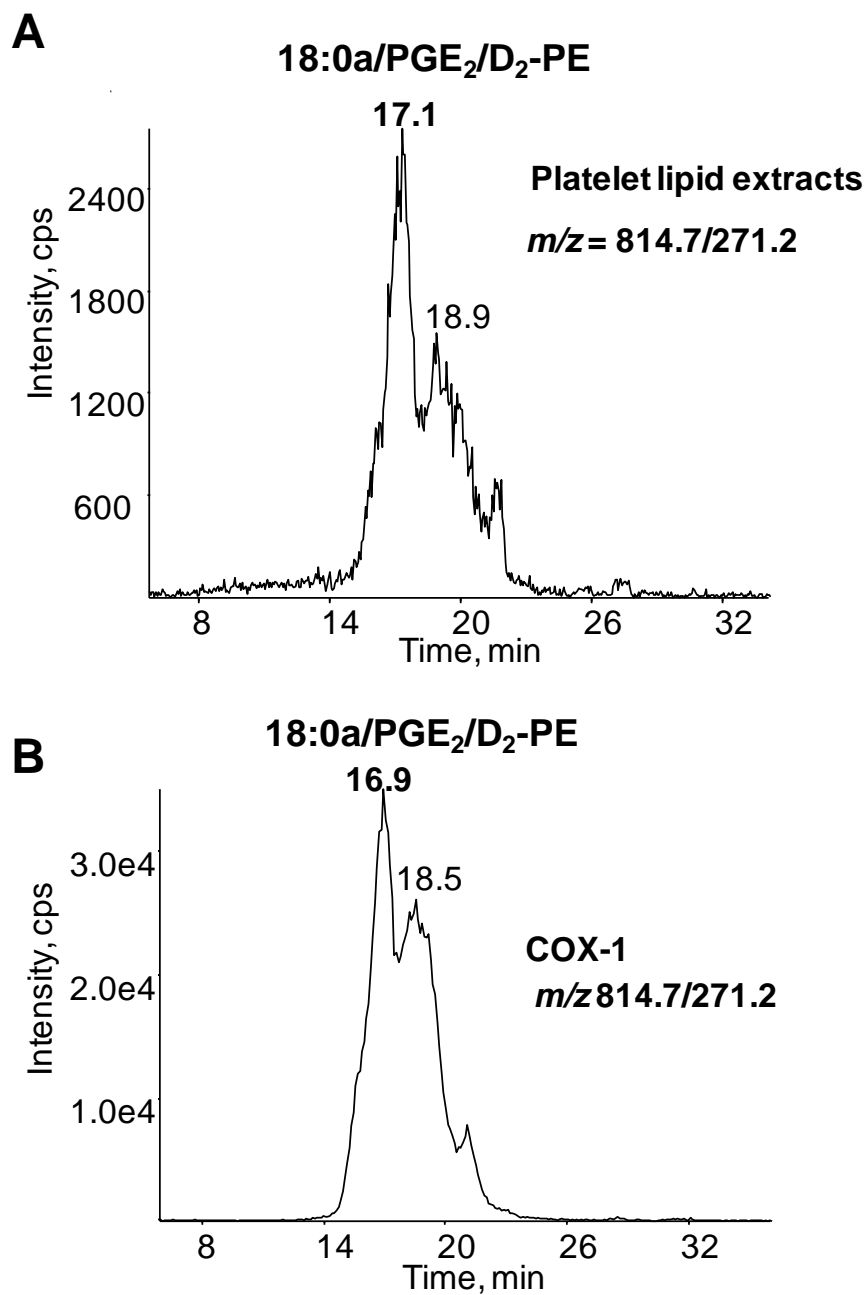
Figure 8.29: Comparison of 18:0a/PGE$_2$/D$_2$-PE formed by activated platelets and *in vitro* via COX-1. Lipids were separated using reverse-phase LC/MS/MS, monitoring *m/z* 814.7 → 271.2, as described in Materials and Methods, Section *2.2.3.2*. *Panel A*. Chromatogram of 18:0a/ PGE$_2$/D$_2$-PE formed by thrombin-activated platelets. *Panel B*. Chromatogram of 18:0a/ PGE$_2$/D$_2$-PE formed *in vitro* via COX-1.

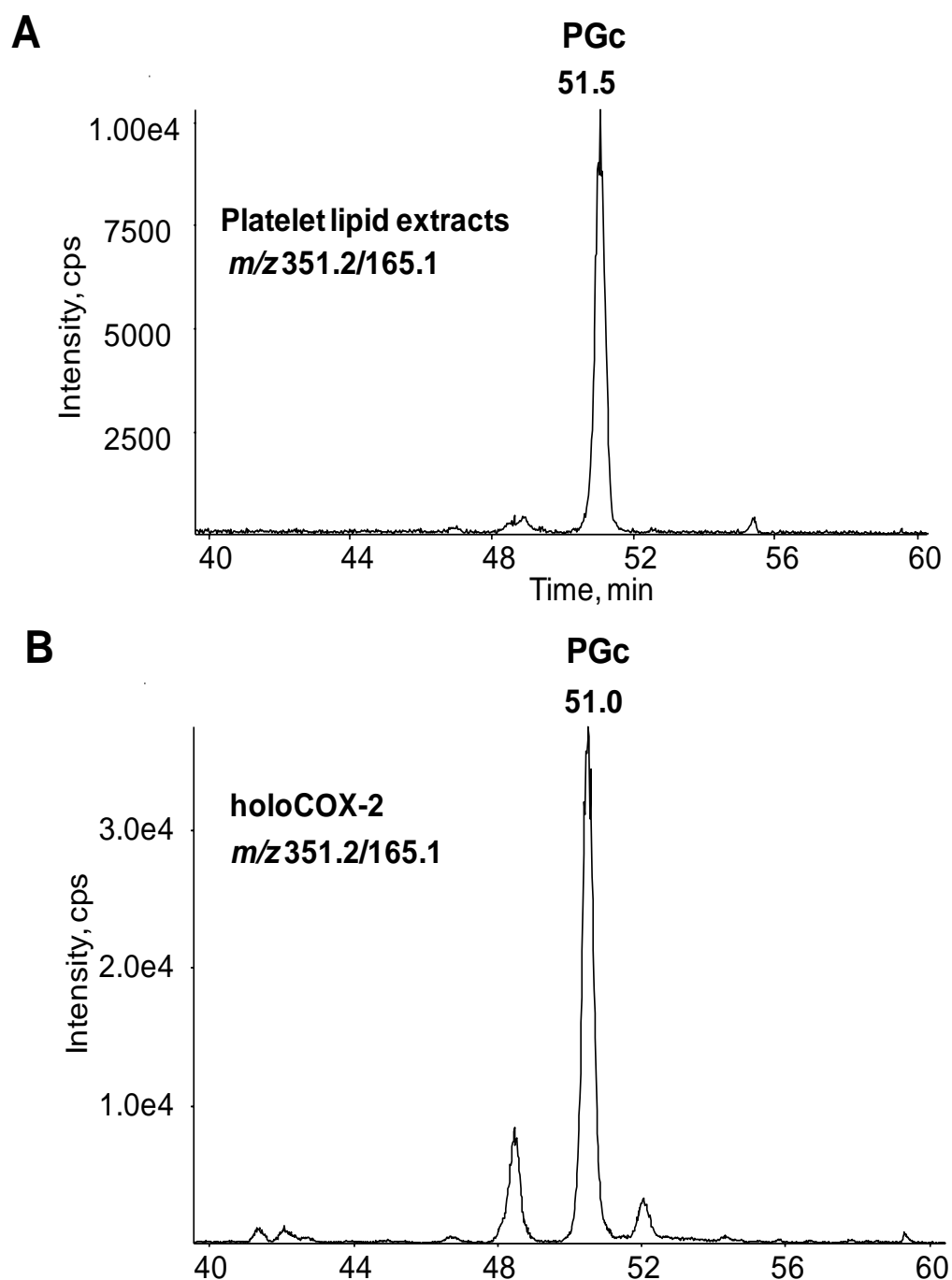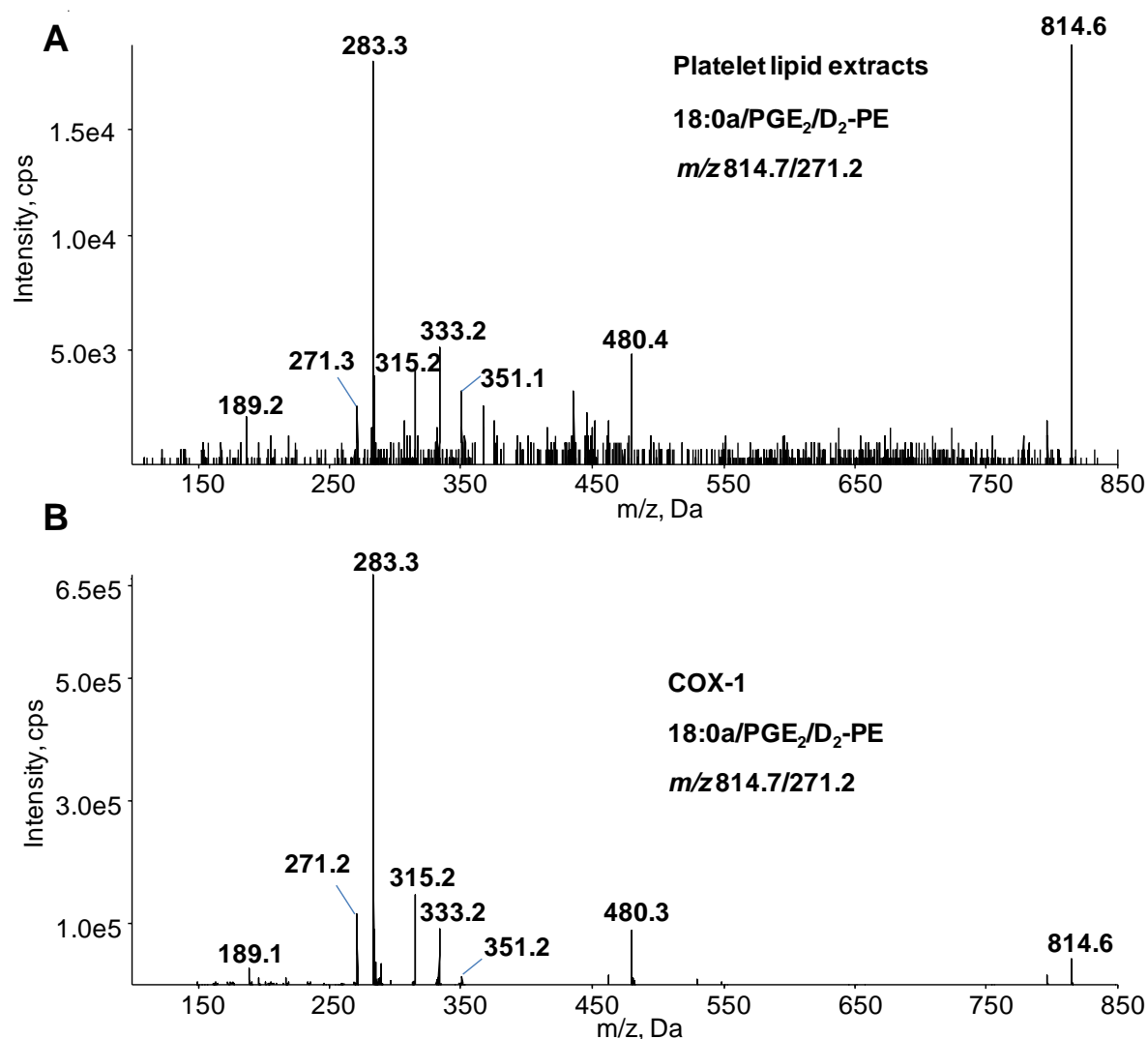**Figure 8.30: Comparison of MS spectra of 18:0a/PGE$_2$/D$_2$-PE formed by activated platelets and *in vitro* via COX-1.** Lipid extracts were separated using reverse-phase LC/MS/MS, as described in Materials and Methods, Section *2.2.3.2*, in product ion mode, with Q1 set at *m/z* 814, CID at Q2 and Q3 set at *m/z* 271.2. MS spectra were acquired at the apex of elution of 18:0a/PGE$_2$/D$_2$-PE. *Panel A*. MS/MS spectrum of 18:0a/PGE$_2$/D$_2$-PE formed by thrombin-activated platelets. *Panel B.* MS/MS spectrum of 18:0a/PGE$_2$/D$_2$-PE formed *in vitro* by COX-1.
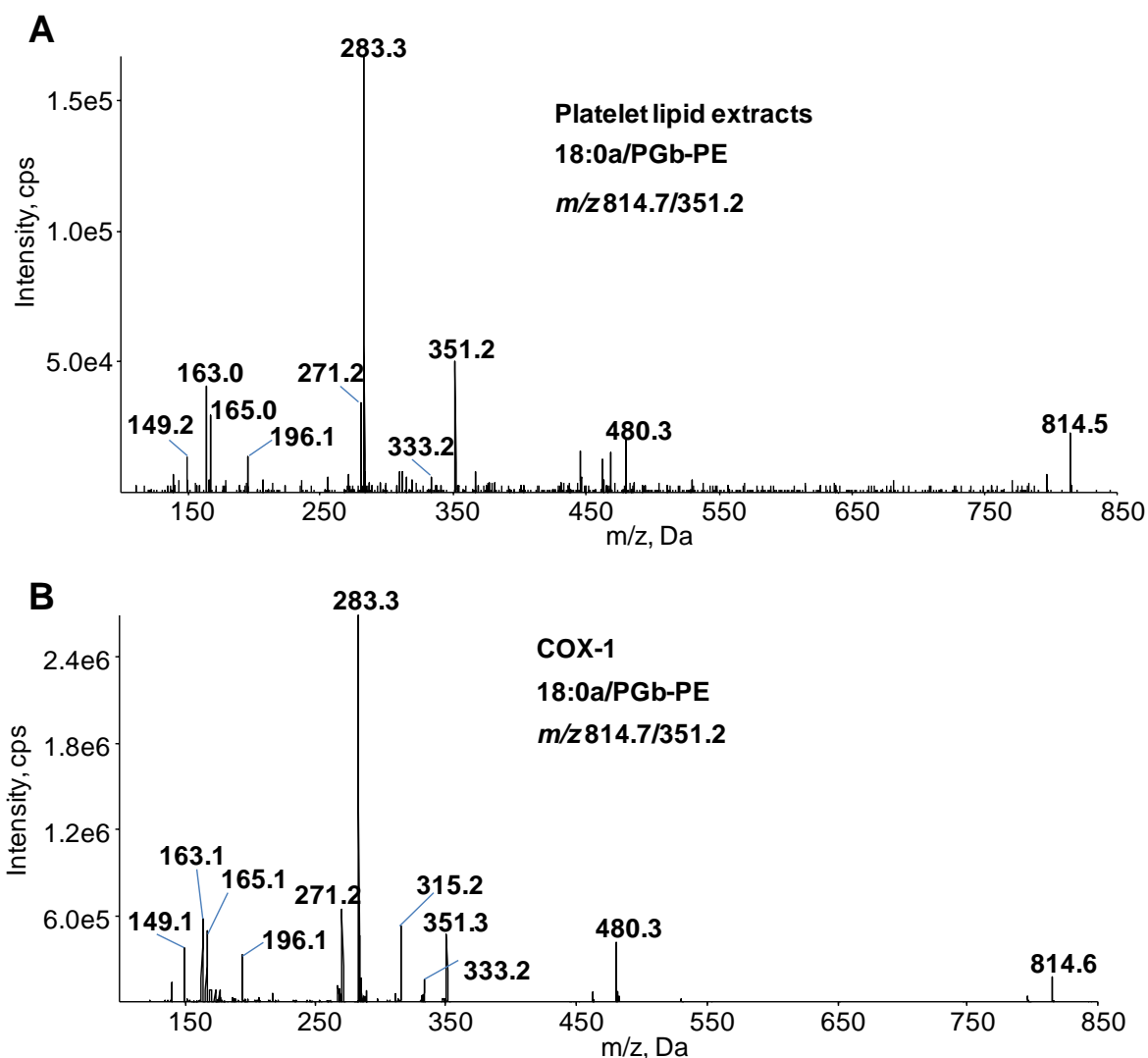
Figure 8.31: Comparison of MS spectra of 18:0a/PGb-PE formed by activated platelets and *in vitro* via COX-1. Lipid extracts were separated using reverse-phase LC/MS/MS, as described in Materials and Methods, Section *2.2.3.2*, in product ion mode, with Q1 set at *m/z* 814, CID at Q2 and Q3 set at *m/z* 351.2. MS spectra were acquired at the apex of elution of 18:0a/PGb-PE. *Panel A*. LC/MS/MS spectrum of 18:0a/PGb-PE formed by thrombin-activated platelets. *Panel B.* LC/MS/MS spectrum of 18:0a/PGb-PE formed *in vitro* by COX-1.
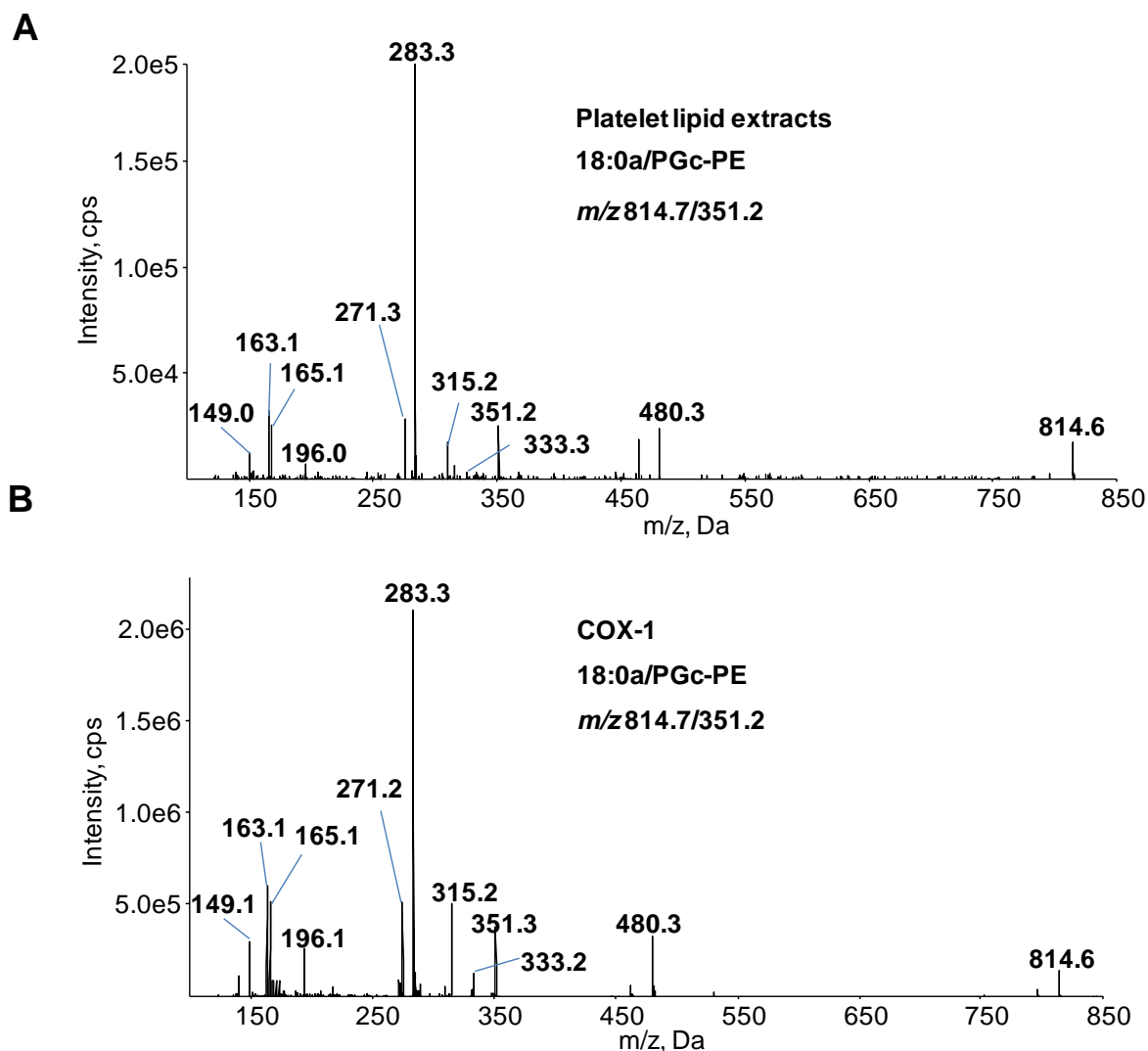
Figure 8.32: Comparison of MS spectra of 18:0a/PGc-PE formed by activated platelets and *in vitro* by COX-1. Lipid extracts were separated using reverse-phase LC/MS/MS, as described in Materials and Methods, Section *2.2.3.2*, in product ion mode, with Q1 set at *m/z* 814, CID at Q2 and Q3 set at *m/z* 351.2. MS spectra were acquired at the apex of elution of 18:0a/PGc-PE. *Panel A*. LC/MS/MS spectrum of 18:0a/PGc-PE formed by thrombin-activated platelets. *Panel B.* LC/MS/MS spectrum of 18:0a/PGc-PE formed *in vitro* by COX-1.

8.3 Discussion

In this chapter, I demonstrated that in platelets, esterified prostaglandins are synthesised via AA release by $cPLA_2$, oxidation by COX-1, and reincorporation into lysophospholipids via LC-FACS and acyltransferase. In resting platelets, as in other immune cells, a small amount of free AA is continuously being generated through the deacylation/reacylation of membrane phospholipids (Chilton *et al.*, 1996). Upon cell activation, this process is considerably amplified via activation of PLA_2. This family of enzymes is the major contributor of prostaglandin formation, releasing high amounts of AA that act as substrate for COX oxidation (Smith, 1992). Inhibition of $cPLA_2$ blocked approximately 75 % of free and esterified prostaglandin formation (Figures 8.1 – 8.6). This suggests that the AA pool that is specifically converted by COX-1 to free and esterified prostaglandins is mainly cleaved by $cPLA_2$. This is in line with previous reports showing that $cPLA_2$ is responsible for AA mobilisation for the biosynthesis of TxA_2 in platelets and prostaglandins in human monocytes and rat peritoneal macrophages (Liberty *et al.*, 2004; Kramer *et al.*, 1993). In contrast, generation of esterified 12-HETEs in platelets requires $sPLA_2$ (Thomas *et al.*, 2010). This likely reflects the different signalling pathways involved in 12-LOX versus COX-1 activation in platelets.

Separately, it was demonstrated that triacsin C partially inhibits both free and esterified prostaglandin generation (Figures 8.9 – 8.11). Although there is a body of evidence showing triacsin C as a mammalian LC-FACS inhibitor, there are controversial reports of the effects of this compound on AA reincorporation (Vessey *et al.*, 2004). For example, Beltramo and Piomelli have demonstrated significant inhibition of arachidonate esterification, while others, such as Igal and co-workers, have found little or no effect of triacsin C on the incorporation of labelled AA into phospholipids (Igal *et al.*, 1997; Hartman *et al.*, 1989; Lewin *et al.*, 2001). Thus, partial inhibition of free PGs may be due to: (1) ambiguous compound specificity, inhibiting other pathways required for both free and esterified prostaglandin formation; (2) or toxicity, leading to cell death.

In contrast, thimerosal significantly inhibited the synthesis of esterified prostaglandins while enhancing the generation of free PGs (Figures 8.14 – 8.16). This is in line with

previous reports showing that inhibition of lysophospholipid acyltransferases by thimerosal in macrophages and platelets blocked reincorporation of AA into lysophospholipids, increasing PGE_2 formation (Hunter *et al.*, 1984; Goppelt-Struebe *et al.*, 1986).

Collectively, inhibition of esterified prostaglandin formation by triacsin C and thimerosal indicates that at least 50 % of the generation of these lipids occurs via the deacylation/reacylation pathway. This suggests that, on platelet activation, $cPLA_2$ cleaves phospholipids at the sn2 position, releasing AA, which is then oxidised by COX-1, forming PGE_2, PGD_2, PGb and PGc. Newly synthesised free PGs are subsequently coupled to CoA, by LC-FACS, resulting in a PG-CoA complex. This is followed by dissociation of CoA and reincorporation of free PGs into lyso PEs by lysophospholipid acyltransferases (Scheme 8.3).

Separately, no detectable exogenously added PGE_2-d_4, PGD_2-d_4 or AA-d_8 was incorporated into platelet phospholipids during the time scale of esterified prostaglandin generation. This demonstrates that only endogenously generated prostaglandins are incorporated through the deacylation/re-acylation mechanism. It is likely that the proteins involved in the formation and reincorporation of free prostaglandins are closely associated such that AA hydrolysis, oxidation and esterification are tightly coordinated, in a manner that exogenous PGE_2-d_4 and PGD_2-d_4 cannot effectively compete (Aldrovandi *et al.*, 2013). Furthermore, as COX-1 in platelets is localised to the membranes of the dense tubular system, formation of esterified prostaglandins may occur on intracellular membranes (Gerrard *et al.*, 1976). In this case, exogenously added PGE_2 and PGD_2 must enter the platelet in order to be esterified into lysophospholipids. Therefore, the absence of reincorporation of PGE_2-d_4 and PGD_2-d_4 into PEs might also be due to the lack of prostaglandin transporters on the platelet surface and the inability of these lipids to diffuse passively through the plasma membrane (Aldrovandi *et al.*, 2013). To date, nothing is known regarding expression of these proteins by platelets or how these cells utilise oxidised fatty acids as substrates (Chi *et al.*, 2011).
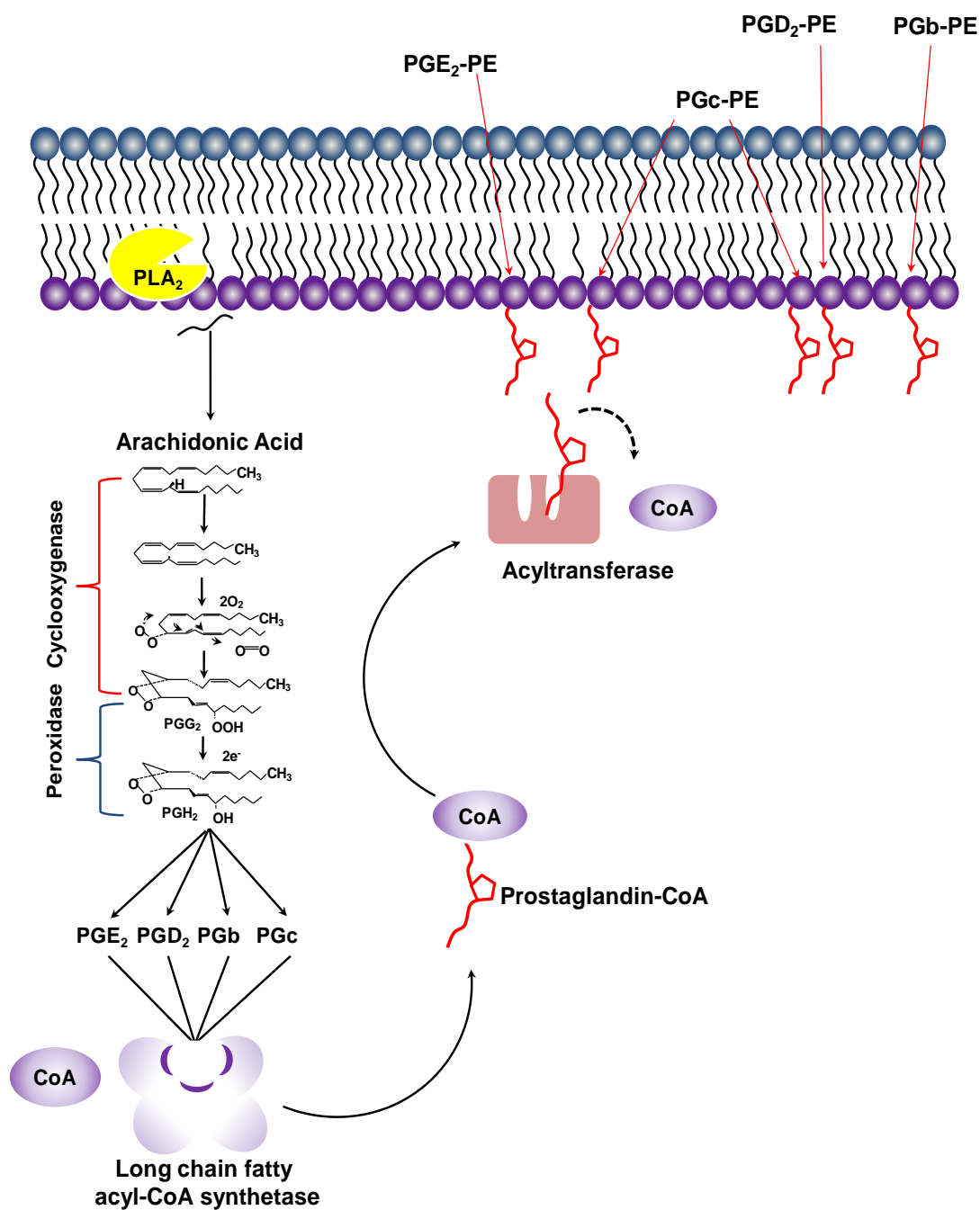
Scheme 8.3: Schematic representation of PG-PE formation via reincorporation of newly formed PGs by COX-1. On platelet activation, cPLA$_2$ cleaves phospholipids at the sn2, releasing AA, which is oxidised by COX-1. Free PGs are then coupled to CoA via LC-FACS and reincorporated into lyso PEs via acyltransferase.

Free PGE$_2$ and PGD$_2$ are formed at similar ratios by both activated human platelets and purified COX-1 (Figure 8.17), indicating that in platelets free PGE$_2$ and PGD$_2$ are likely to result from non-enzymatic rearrangement of PGH$_2$. Furthermore, *in vitro* generation of free PGb (Figure 8.20) and PGc (Figure 8.23) via both COX isoforms was demonstrated, suggesting their generation *in vivo* from PGH$_2$ prior to esterification is probably non-enzymatic.

Furthermore, the results showed that PE bound prostaglandin can form *in vitro* during oxidation of AA by COX-1 independently of free metal ions, generating isoprostane-PEs that include PGE$_2$/D$_2$-PEs and PGc-PEs. It is possible that during oxidation of AA by COX-1, radicals formed at the cyclooxygenase active site escape reaching intact phospholipids. These radicals could abstract a bisallylic hydrogen from phospholipids containing polyunsaturated fatty acids, generating a carbon-centred radical that rearranges to more stable cis,trans-pentadienyl radical, which then couples to molecular oxygen to form peroxyl radicals (Yin *et al.*, 2003; Niki, 2009). The radical could then attack neighbouring carbons containing double bonds, yielding bicyclic PGG$_2$, which is then reduced to PGH$_2$. The latter could structurally rearrange forming prostaglandin-like products (Scheme 8.4).

Formation of esterified prostaglandins *in vitro* and partial inhibition by thimerosal (~ 50 % of PGE$_2$/D$_2$-PEs) could mistakenly lead to the conclusion that the remaining 50 % of esterified prostaglandins are generated from non-enzymatic oxidation of PE. However, commercial inhibitors rarely result in 100 % effective inhibition in cells, mostly due to solubility and membrane permeability. Furthermore, *in vitro* reaction does not mimic *in vivo* conditions. Thus, non-enzymatic oxidation of PE may also occur in platelets but as a minor pathway for esterified isoprostane formation. This idea is also supported by the absence of 8-iso-PGE$_2$ and 11β-PGE$_2$ in LC-MS/MS chromatograms of prostaglandins hydrolysed from platelet PE described in Chapter 4.
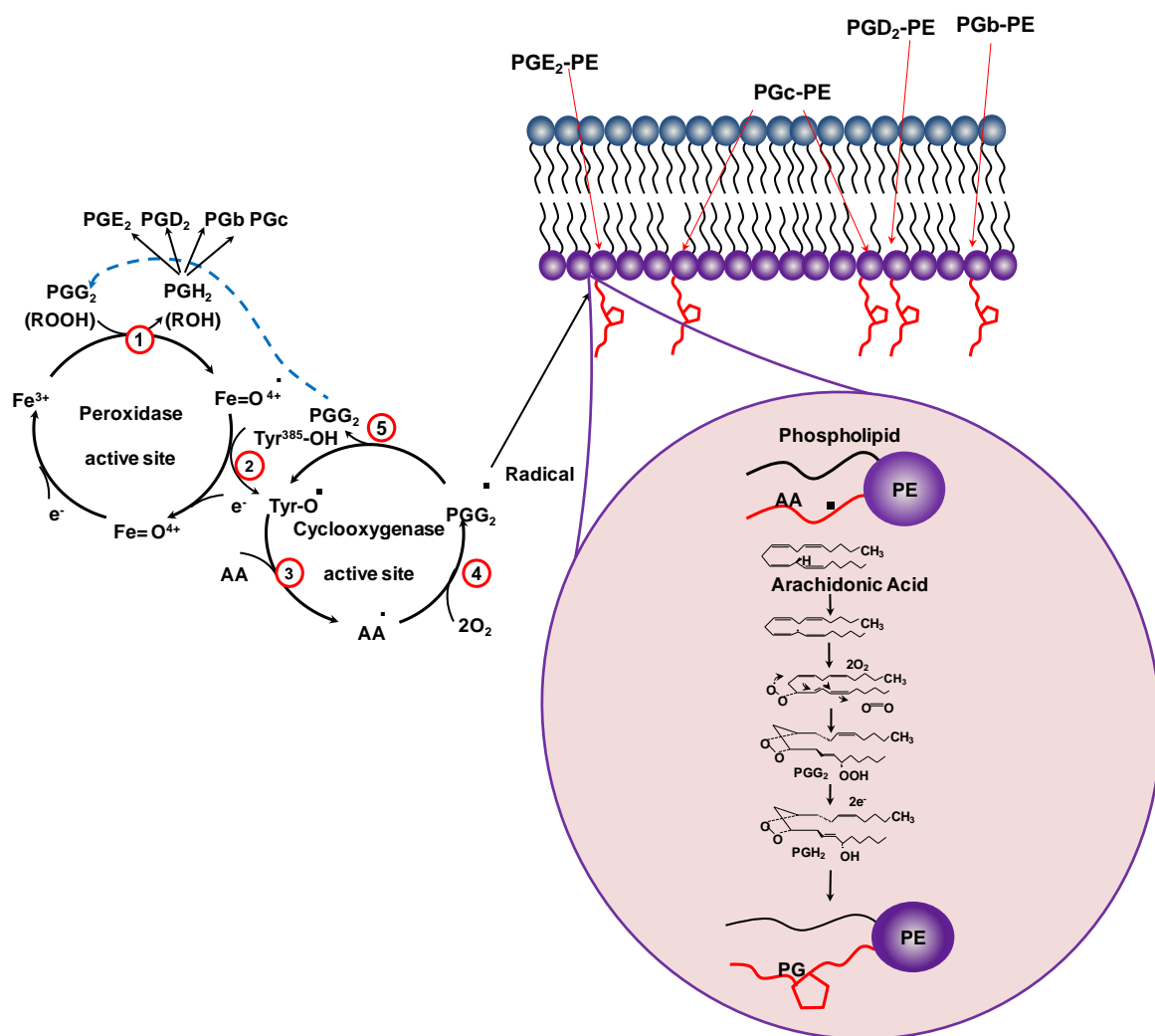
Scheme 8.4: Schematic representation of PG-PE formation by AA-derived radicals escaping from COX-1 active site. During COX-1 turnover, radicals could escape from the cyclooxygenase active site attacking intact phospholipids, leading to non-enzymatic PG-PE formation.

In these studies, it was found that COX-1 could not directly oxidise SAPE. This is in line with previous reports showing that COX-2 but not COX-1 can oxidise complex substrates such as arachidonyl-glycerol and arachidonyl-ethanolamide, forming esterified prostaglandins including PGE$_2$-G/PGD$_2$-G and PGE$_2$-EA/PGD$_2$-EA (Kozak & Marnett, 2002; Kozak *et al.*, 2002). The inability of COX-1 to direct oxidise phospholipids is likely due to substrate specificity determined by the conformation of its hydrophobic channel, which is smaller than that of COX-2, so it accepts a narrower range of structures as substrates (Kurumbail *et al.*, 1996).

In summary, I demonstrated that esterified prostaglandins are rapidly formed on platelet activation, in a cPLA$_2$-dependent manner, via COX-1, followed by esterification of newly formed free PGs into PEs. This is similar to other enzymatically-generated OxPLs, such as HETE-phospholipids generated by LOXs, which regulate coagulation and immune cell signalling (Thomas *et al.*, 2010; Clark *et al.*, 2011). It possible that free PGb and PGc as well as esterified prostaglandins may also signal during platelet activation.

Chapter 9

9 Characterisation of Receptor and Signalling Mediators Regulating Free and Esterified Prostaglandin Formation by Activated Human Platelets

9.1 Introduction

Formation of OxPLs *in vivo* has been generally considered an uncontrolled and undesirable pathological event, generating hundreds of bioactive lipid species that play deleterious roles in chronic inflammation and vascular diseases. However, in the past five years, several families of enzymatically-generated OxPLs formed by activated human monocytes (15-HETE-PE and 15-KETE-PE), neutrophils (5-HETE-PE) and platelets (14-HDOHE-PE and 12-HETE-PE/PC) have been reported (Maskrey *et al.*, 2007; Morgan *et al.*, 2009; Morgan *et al.*, 2010; Thomas *et al.*, 2010; Clark *et al.*, 2011; Hammond *et al.*, 2012). These differ from non-enzymatically-generated OxPLs because they are rapidly formed on cell activation, through controlled processes involving receptors and intracellular signalling, similar to free eicosanoids such as TxA$_2$.

The signal transduction pathways that lead to TxA$_2$ formation have been extensively characterised in human platelets. This prostanoid is formed on platelet stimulation by various physiological agonists including thrombin, which signals through thrombin receptors, PAR-1 and PAR-4. These belong to a superfamily of seven transmembrane G-protein-coupled receptors that are activated by proteolytic cleavage of part of their extracellular domain by thrombin, exposing a new amino-terminal sequence that functions as a tethered ligand activating the receptor (Vu *et al.*, 1991; Kahn *et al.*, 1998; Xu *et al.*, 1998; Coughlin, 2000; Macfarlane *et al.*, 2001). This leads to intracellular signalling, activating *src* tyrosine kinases and PLC. *Src* family kinases are non-receptor protein tyrosine kinases that transduce signals from a variety of receptors to internal signalling pathways (Corey & Anderson, 1999). In contrast, PLC catalyses the hydrolysis of phosphatidylinositol 4,5-bisphosphate (PIP$_2$) to form DAG and inositol 1,4,5-triphosphate (IP$_3$) that in turn mediates calcium mobilisation from intracellular stores (Murugappan *et al.*, 2005; Li *et al.*, 2010; Putney, 1988; Hisatsune *et al.*, 2005). All these and p38 mitogen-

activated protein (MAP) kinase stimulate $cPLA_2$ and COX-1, leading to PGH_2 formation that is then converted to TxA_2 by thromboxane-A synthase (Scheme 9.1) (Jurk & Kehrel, 2005; Levy, 2006, Nakahata, 2008, Kramer *et al.*, 1995).

In this chapter, the involvement of receptor-dependent signalling pathways regulating the generation of free and esterified prostaglandins will be investigated. The thrombin-receptor agonist peptides $TFLLRNH_2$ and $AY-NH_2$ will be used to determine the involvement of PAR-1 and PAR-4, respectively. Whereas, the involvement of *src* tyrosine kinases, PLC and p38 MAP kinase will be assessed using PP2, U-73122 and p38 inhibitor (2-(4-Chlorophenyl)-4-(4-fluorophenyl)-5-pyridin-4-yl-1,2-dihydro-pyrazol-3-one), respectively. Furthermore, phosphatidylinositide 3-kinases (PI3Ks) and protein kinase C (PKC) stimulated during platelet activation will also be examined using wortmannin and Gö 6850.

The requirement of intra and extracellular calcium will be determined using the cytosolic calcium chelator 1,2-bis-(*o*-aminophenoxy) ethane-*N,N,N',N'*-tetraacetic acid tetrakis-acetoxymethyl ester (BAPTA/AM) and the extracellular calcium chelator ethylene glycol-bis(2-aminoethylether)-N,N,N',N'-tetraacetic acid (EGTA). Lipids will then be extracted and analysed using reverse-phase LC/MS/MS on 4000 Q-trap.

The requirement for specific receptors and intracellular signalling pathways will determine whether the generation of PGb, PGc, PGE_2/D_2-PEs, PGb-PEs and PGc-PEs is a controlled event in human platelets. Furthermore, this would suggest that these lipids are of physiologic relevance and probably important in haemostasis.
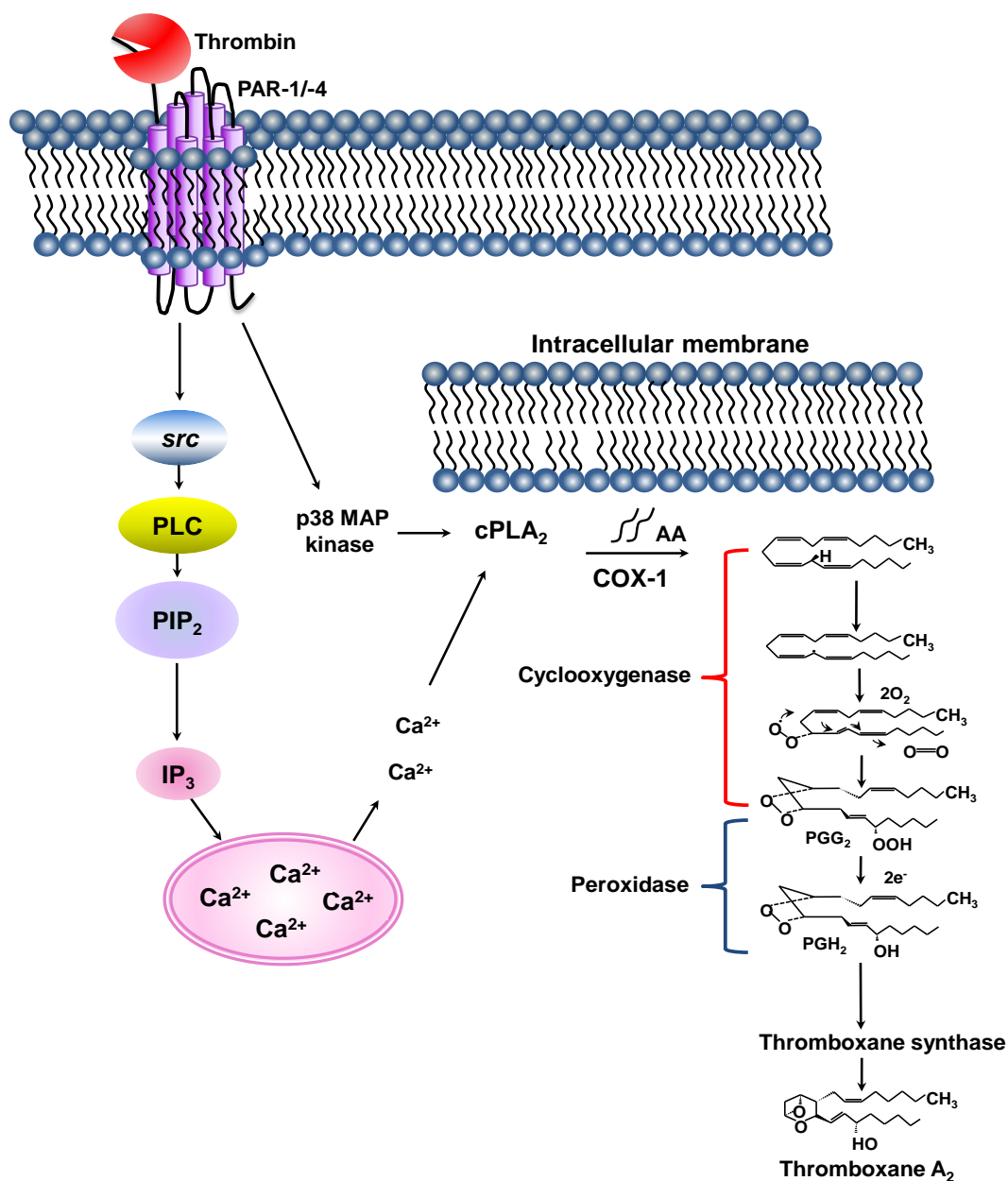
Scheme 9.1: Schematic representation of TxA$_2$ formation by thrombin-activated platelets. TxA$_2$ is synthesised via AA release by cPLA$_2$, oxidised by COX-1 and converted to TxA$_2$ by thromboxane synthase. Modified from Jurk & Kehrel, 2005.

9.1.1 Aims

The studies described in this chapter aim to:

- Investigate the requirement of PAR-1 and PAR-4 stimulation for the generation of free and esterified prostaglandins.
- Uncover the intracellular signalling pathways required for the formation of free and esterified prostaglandins.
- Examine the requirement of extra and intracellular calcium for the synthesis of these lipids.

9.2 Results

9.2.1 Platelet PAR-1 and PAR-4 receptors upregulate free and esterified prostaglandin formation.

In this section, the requirement of PAR-1/-4 activation for the generation of free and esterified prostaglandins was determined using the thrombin-receptor agonist peptides TFLLRNH$_2$ and AY-NH$_2$, respectively. These synthetic peptides are unable to cleave the receptor; instead, they mimic the human tethered ligands by interacting with the receptor extracellular domains, inducing conformational changes similar to natural ligands (Bahou *et al.*, 1993; Gerszten *et al.*, 1994).

Briefly, washed human platelets were incubated with 20 μM TFLLRNH$_2$ and/or 150 μM AY-NH$_2$, respectively, for 30 min at 37$^\text{o}$C (Thomas *et al.*, 2010). Lipids were then extracted and analysed using reverse-phase LC/MS/MS, as described in Materials and Methods, Sections *2.2.3.2* and *2.2.3.3*. Platelets stimulated with 0.2 U/ml thrombin acted as a positive control for free and esterified prostaglandin synthesis.

The thrombin-receptor agonist peptides TFLLRNH$_2$ (PAR-1) and AY-NH$_2$ (PAR-4) induced formation of free and esterified prostaglandins to a similar level, with additive effects

implicating both of the platelet thrombin receptors (Figure 9.1 – 9.3). Exception of $16:0p/PGE_2/D_2$-PE and $18:0a/PG$-PEs, co-stimulation with $TFLLRNH_2$ and $AY-NH_2$ generated significant lower levels of free and esterified prostaglandins compared to thrombin. This may be due to differences between the synthetic peptides and the natural built-in tethered ligand generated by thrombin.

9.2.2 *Free and esterified prostaglandins are formed in a phospholipase C, p38 MAP kinase and src-tyrosine kinase dependent manner.*

In this section, the requirement of *src*-tyrosine kinases, p38 MAP kinase and PLC for the synthesis of free and esterified prostaglandins was assessed using 50 µM PP2, 100 nM p38 inhibitor and 5 µM U-73122, respectively. PP2 is an inhibitor of the Src family kinases that binds tightly adjacent to the ATP-binding site interfering with the protein substrate binding (Zhu *et al*., 1999; Karni *et al*., 2003). The p38 inhibitor, also known as 2-(4-Chlorophenyl)-4-(4-fluorophenyl)-5-pyridin-4-yl-1,2-dihydro-pyrazol-3-one, is a pyridinyl imidazole inhibitor that competitively binds to the ATP binding pocket inhibiting ATP binding (Tong *et al*., 1997). U-73122 is an aminosteroid that in platelets inhibits both PLCβ and PLCγ isoforms (Bleasdale *et al*., 1990; Heemskerk *et al*., 1997).

Briefly, washed human platelets were incubated with each inhibitor or 0.5 % vehicle (DMSO) for 10 min at room temperature prior to thrombin activation (0.2 U/ml for 30 min at 37°C). Lipids were then extracted and analysed using reverse-phase LC/MS/MS, on Q-trap, in MRM mode, as described in Materials and Methods, Sections *2.2.3.2* and *2.2.3.3*.

Figure 9.1: PGE$_2$/D$_2$-PEs, PGE$_2$ and PGD$_2$ are generated via PAR-1 and PAR-4 receptor stimulation. Washed platelets were activated with each agonist for 30 min at 37° C before lipid extraction. Lipids were then analysed using reverse-phase LC/MS/MS, as described in Materials and Methods, Section *2.2.3.2* and *2.2.3.3*. Levels of PGE$_2$/D$_2$-PEs are expressed as ratio analyte to internal standard while free PGE$_2$ and PGD$_2$ are expressed as ng/2 x 10^8 platelets. Data is presented from one experiment and representative of three (n = 3, mean ± SEM). *P < 0.05, **P < 0.01 and ***P < 0.001 versus thrombin, using ANOVA and Bonferroni Post Hoc Test. *Panel A*. PGE$_2$/D$_2$-PE generation by platelets incubated with 20 μM TFLLR-NH$_2$ and/or 150 μM AY-NH$_2$. *Panel B*. PGE$_2$ and PGD$_2$ generation by platelets incubated with 20 μM TFLLR-NH$_2$ and/or 150 μM AY-NH$_2$.
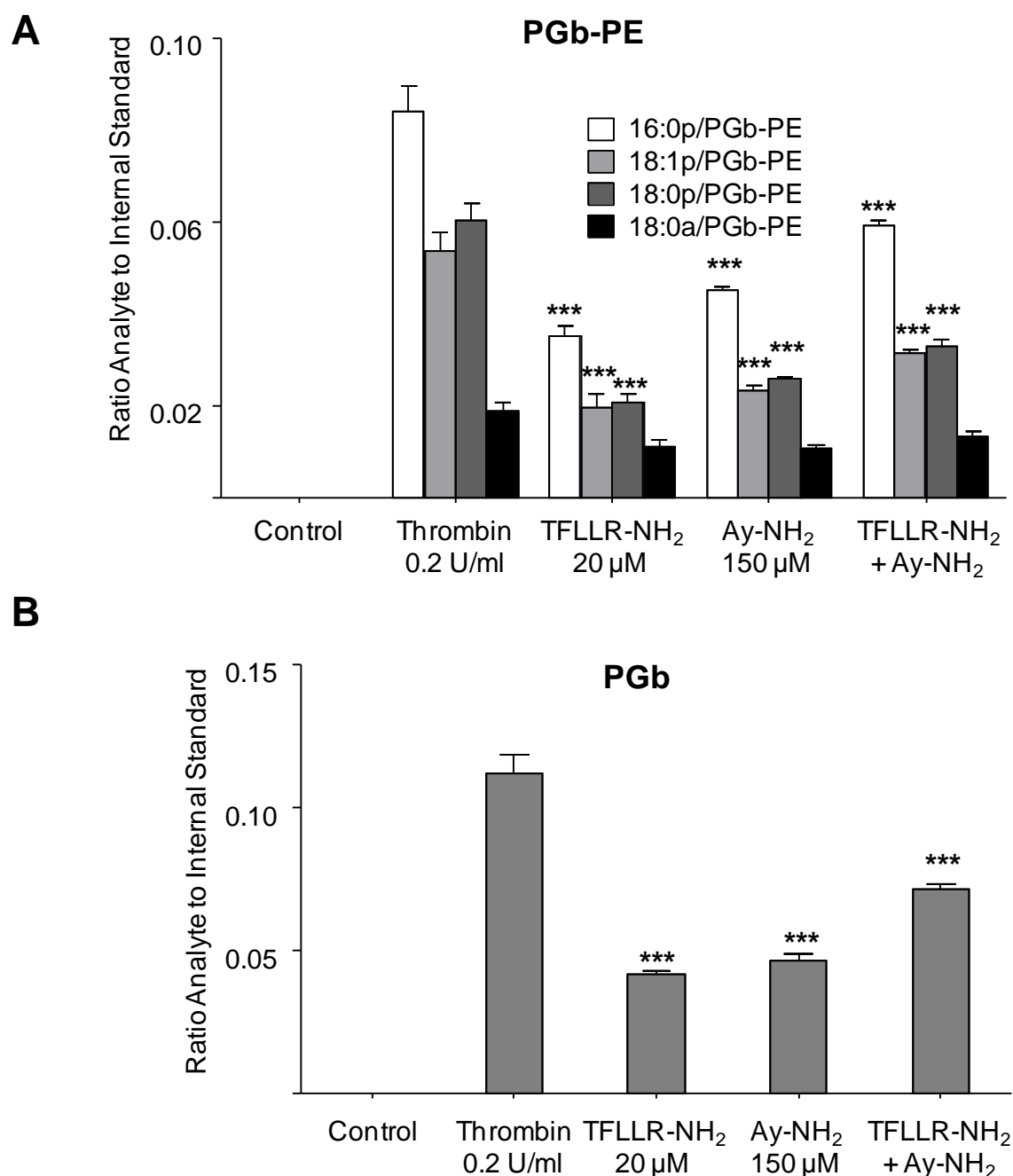
Figure 9.2: PGb-PEs and free PGb are generated via PAR-1 and PAR-4 receptor stimulation. Washed platelets were activated with each agonist for 30 min at 37° C before lipid extraction. Lipids were then analysed using reverse-phase LC/MS/MS, as described in Materials and Methods, Section *2.2.3.2* and *2.2.3.3*. Levels of PGb-PEs and PGb are expressed as ratio analyte to internal standard. Data is presented from one experiment and representative of three (n = 3, mean ± SEM). ***P < 0.001 versus thrombin, using ANOVA and Bonferroni Post Hoc Test. *Panel A*. PGb-PE generation by platelets incubated with 20 μM TFLLR-NH$_2$ and/or 150 μM AY-NH$_2$. *Panel B*. PGb generation by platelets incubated with 20 μM TFLLR-NH$_2$ and/or 150 μM AY-NH$_2$.
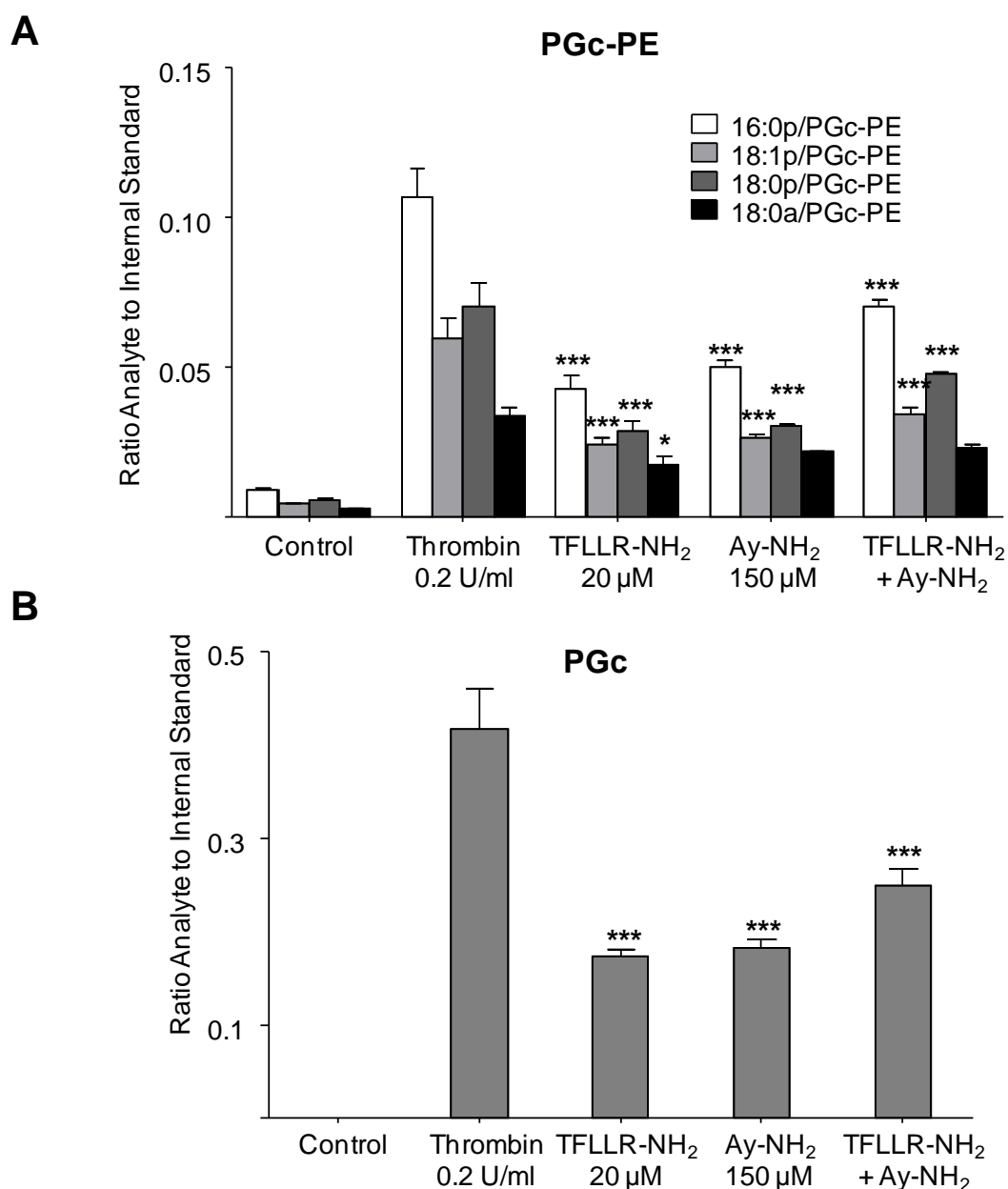
Figure 9.3: PGc-PEs and free PGc are generated via PAR-1 and PAR-4 receptor stimulation. Washed platelets were activated with each agonist for 30 min at 37° C before lipid extraction. Lipids were then analysed using reverse-phase LC/MS/MS, as described in Materials and Methods, Section *2.2.3.2* and *2.2.3.3*. Levels of PGc-PEs and PGc are expressed as ratio analyte to internal standard. Data is presented from one experiment and representative of three (n = 3, mean ± SEM). ***P < 0.001 versus thrombin, using ANOVA and Bonferroni Post Hoc Test. *Panel A*. PGc-PE generation by platelets incubated with 20 μM TFLLR-NH$_2$ and/or 150 μM AY-NH$_2$. *Panel B*. PGc generation by platelets incubated with 20 μM TFLLR-NH$_2$ and/or 150 μM AY-NH$_2$.

The *src* tyrosine kinase inhibitor PP2 completely blocked PGE_2/D_2-PE formation while the p38 inhibitor only partially reduced (Figure 9.4 A). In addition, formation of PGE_2/D_2-PEs was decreased by 80 % in response to the PLC inhibitor U-73122. Similarly, PP2 considerably inhibited formation of PGE_2, whereas inhibition of p38 MAP kinase and PLC reduced PGE_2 formation by 40 and 68 %, respectively (Figure 9.4 B). PGD_2 generation was significantly inhibited by PP2, not affected by p38 inhibitor and partially blocked by U-73122 (Figure 9.4 B). PGb-PE synthesis was nearly abolished by PP2 and significantly inhibited by p38 inhibitor and U-73122 (Figure 9.5 A), similar to free PGb (Figure 9.5 B). PGc-PE generation was blocked by PP2 (~ 95 %), p38 inhibitor (~ 65 %) and U-73122 (~ 70 %), confirming the requirement of *src*-tyrosine kinase, p38 MAP kinase and PLC, respectively (Figure 9.6 A). Levels of free PGc were reduced 85 % in response to PP2 and significantly inhibited by p38 inhibitor and U-73122 (Figure 9.6 B). These studies indicate that both free and esterified prostaglandin formation requires stimulation of *src*-tyrosine kinase, p38 MAP kinase and PLC.

9.2.3   *Inhibition of PKC enhances free and esterified prostaglandin formation.*

In this section, the participation of PI3Ks and PKC for the generation of free and esterified prostaglandins was investigated using 100 nM wortmannin and 100 nM Gö 6850, respectively (Thomas *et al*., 2010; Clark *et al*., 2010). Wortmannin is a fungal metabolite that irreversibly inhibits PI3Ks in a noncompetitive manner (Powis *et al*., 1994). Whereas, Gö 6850 is a reversible PKC inhibitor that acts as a competitive inhibitor for the ATP binding site mainly of PKCα and PKCβ but can also affect other isoforms (Toullec *et al*., 1991).

Washed human platelets were incubated with each inhibitor or 0.5 % vehicle (DMSO) for 10 min at room temperature prior to thrombin activation (0.2 U/ml for 30 min at $37^{\circ}C$). Lipids were then extracted and analysed using reverse-phase LC/MS/MS on Q-trap, in MRM mode, as described in Materials and Methods, Sections *2.2.3.2* and *2.2.3.3*.

Figure 9.4: Phospholipase C and *src* tyrosine kinase are required for PGE$_2$/D$_2$-PE, PGE$_2$ and PGD$_2$ generation while p38 MAP kinase is only necessary for PGE$_2$/D$_2$-PE and PGE$_2$. Washed human platelets were incubated for 10 min at room temperature with each inhibitor prior to thrombin activation (0.2 U/ml, 30 min at 37°C). Lipids were then extracted and analysed using reverse-phase LC/MS/MS, as described in Materials and Methods, Section *2.2.3.2* and *2.2.3.3*. Levels of PGE$_2$/D$_2$-PEs are expressed as ratio analyte to internal standard while free PGE$_2$ and PGD$_2$ are expressed as ng/2 x 10^8 platelets. Data is presented from one experiment and representative of three (n = 3, mean ± SEM). *P < 0.05, **P < 0.01 and ***P < 0.001 versus thrombin in the presence of DMSO, using ANOVA and Bonferroni Post Hoc Test. *Panel A*. PGE$_2$/D$_2$-PE generation by platelets incubated with 50 μM PP2, 100 nM p38 MAP kinase inhibitor or 5 μM U-73112. *Panel B*. PGE$_2$ and PGD$_2$ formation by platelets incubated with 50 μM PP2, 100 nM p38 MAP kinase inhibitor or 5 μM U-73112.
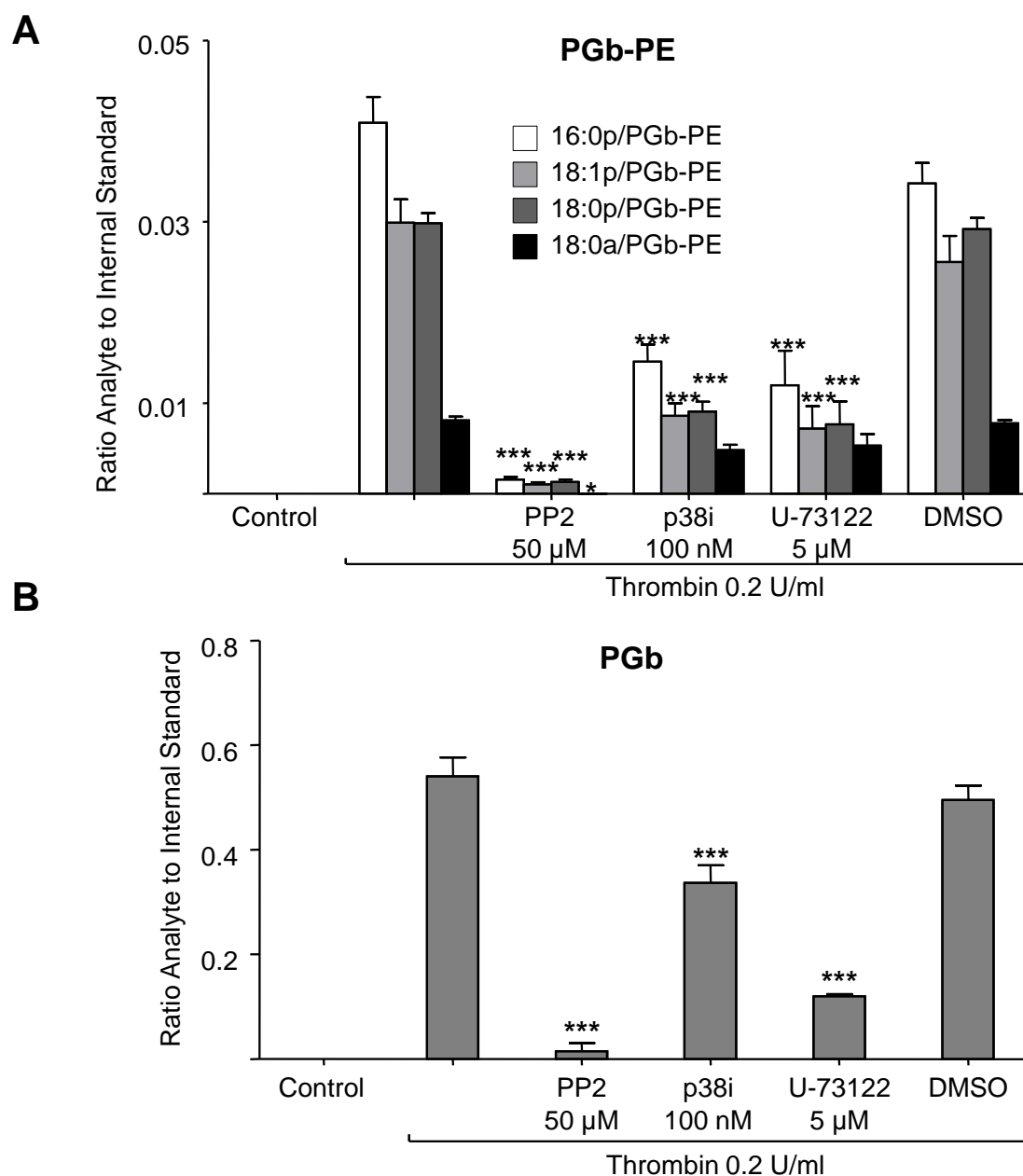
Figure 9.5: Phospholipase C, p38 MAP kinase and *src* tyrosine kinase are required for PGb-PE and PGb generation. Washed human platelets were incubated for 10 min at room temperature with each inhibitor prior to thrombin activation (0.2 U/ml, 30 min at 37°C). Lipids were then extracted and analysed using reverse-phase LC/MS/MS, as described in Materials and Methods, Section *2.2.3.2* and *2.2.3.3*. Levels of PGb-PEs and PGb are expressed as ratio analyte to internal standard. Data is presented from one experiment and representative of three (n = 3, mean ± SEM). *$P < 0.05$, **$P < 0.01$ and ***$P < 0.001$ versus thrombin in the presence of DMSO, using ANOVA and Bonferroni Post Hoc Test. *Panel A*. PGb-PE generation by platelets incubated with 50 μM PP2, 100 nM p38 MAP kinase inhibitor or 5 μM U-73112. *Panel B*. PGb formation by platelets incubated with 50 μM PP2, 100 nM p38 MAP kinase inhibitor or 5 μM U-73112.
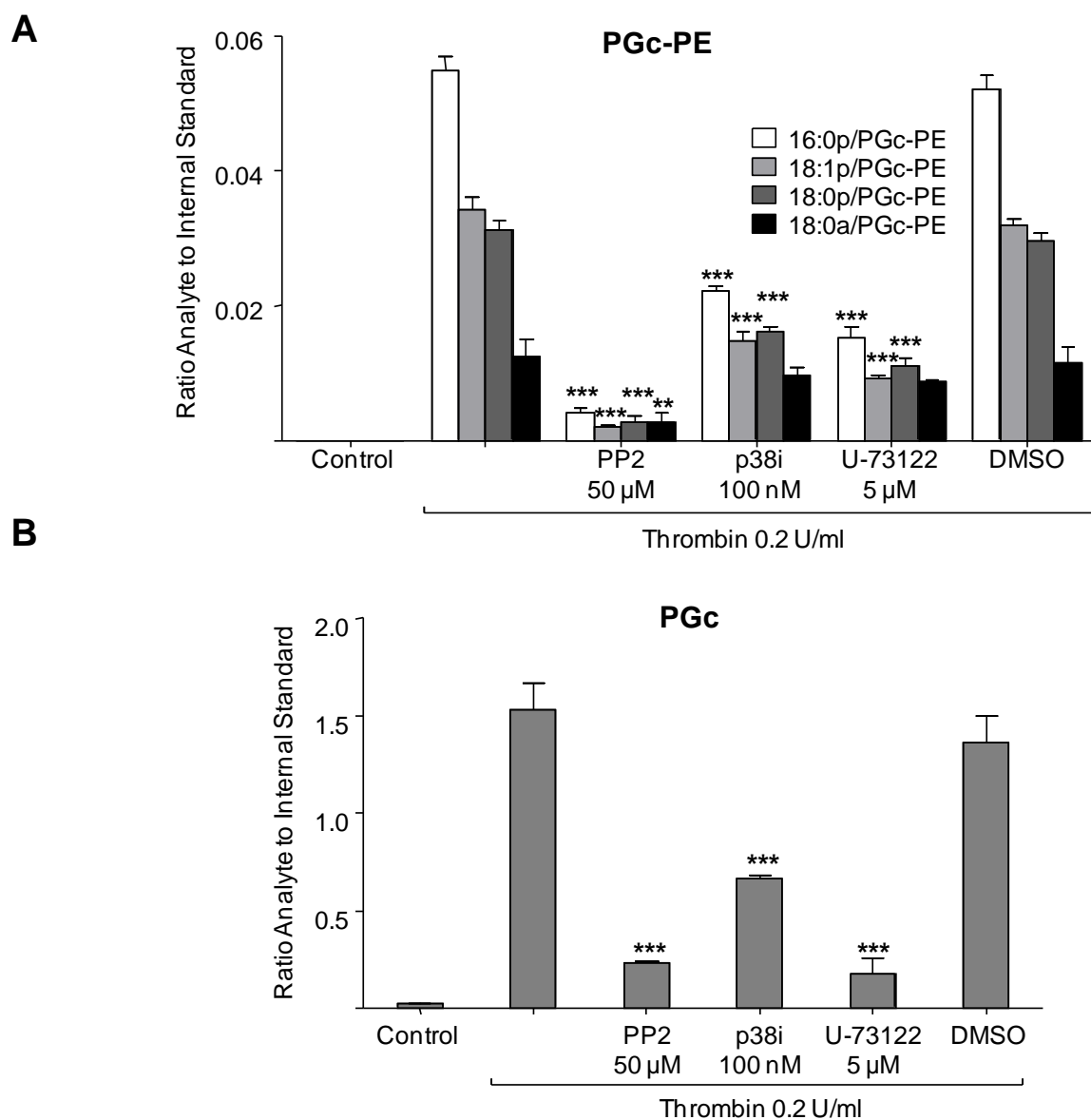
Figure 9.6: Phospholipase C, p38 MAP kinase and *src* tyrosine kinase are required for PGc-PE and PGc generation. Washed human platelets were incubated for 10 min at room temperature with each inhibitor prior to thrombin activation (0.2 U/ml, 30 min at 37°C). Lipids were then extracted and analysed using reverse-phase LC/MS/MS, as describe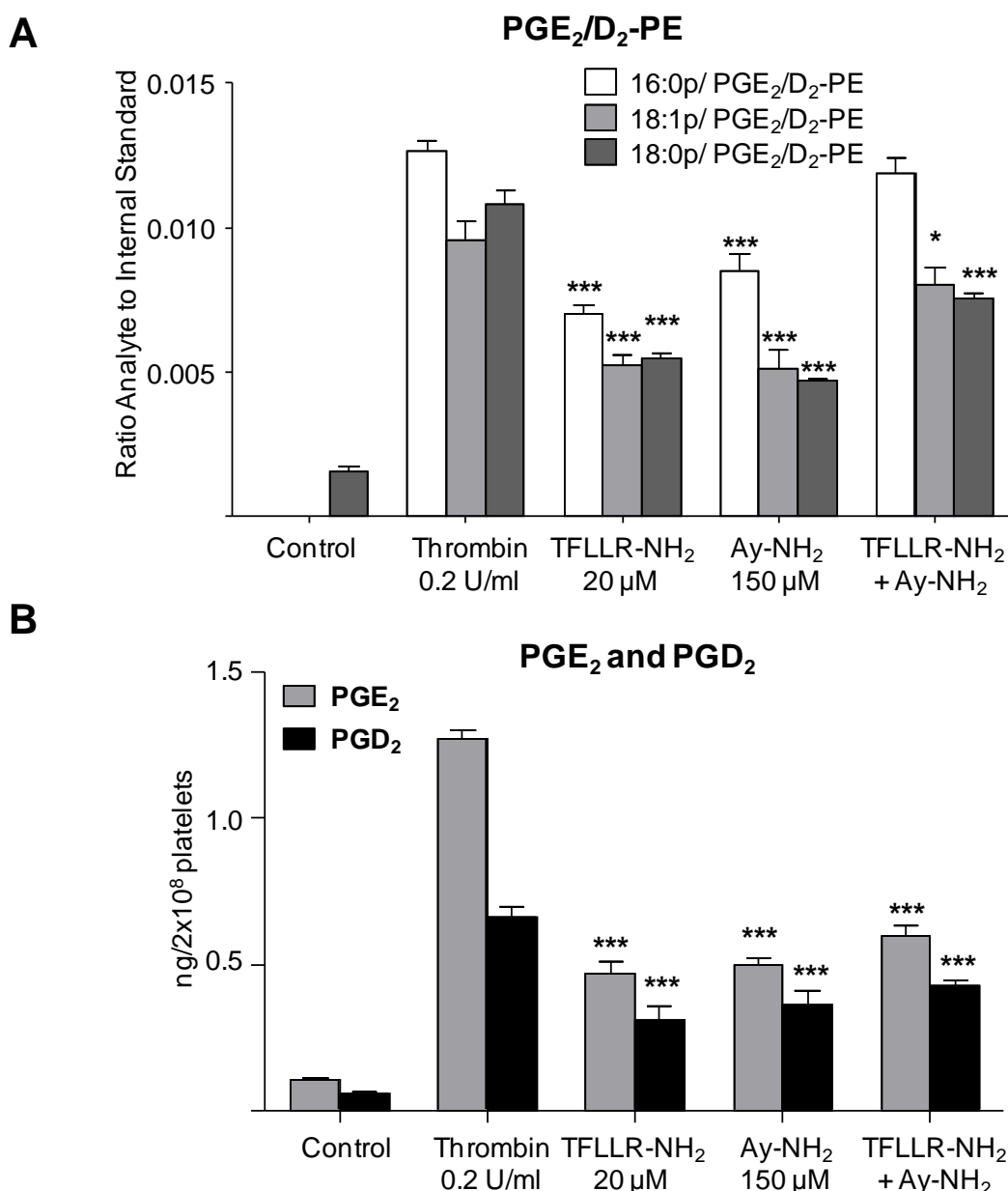d in Materials and Methods, Section *2.2.3.2* and *2.2.3.3*. Levels of PGc-PEs and PGc are expressed as ratio analyte to internal standard. Data is presented from one experiment and representative of three (n = 3, mean ± SEM). *P < 0.05, **P < 0.01 and ***P < 0.001 versus thrombin in the presence of DMSO, using ANOVA and Bonferroni Post Hoc Test. *Panel A*. PGc-PE generation by platelets incubated with 50 µM PP2, 100 nM p38 MAP kinase inhibitor or 5 µM U-73112. *Panel B*. PGc formation by platelets incubated with 50 µM PP2, 100 nM p38 MAP kinase inhibitor or 5 µM U-73112.

Formation of PGE_2/D_2-PE was not affected by the PI3k inhibitor wortmannin, whereas, inhibition of PKC by Gö 6850 induced a 2-fold increase (Figure 9.7 A). Levels of free PGE_2 and PGD_2 were also enhanced by 2-fold in response to Gö 6850 (Figure 9.7 B). Generation of PGb-PEs was not inhibited by wortmannin but considerably increased by Gö 6850 (Figure 9.8 A), similar to free PGb (Figure 9.8 B). Levels of PGc-PEs (Figure 9.9 A) and free PGc (Figure 9.9 B) were significantly enhanced by Gö 6850 but not affected by wortmannin. The data indicate that PKC exerts a negative feedback effect on the formation of free and esterified prostaglandins.

9.2.4 Generation of free and esterified prostaglandins requires intracellular calcium mobilisation.

An increase in intracellular calcium can originate from two major sources, the release of calcium from intracellular stores or the influx of extracellular calcium via the plasma membrane (Bergmeier & Stefanini, 2009). In this section, the requirement for intra and extracellular calcium was determined using the cytosolic calcium chelator BAPTA/AM and the extracellular calcium chelator EGTA. BAPTA/AM is a lipophilic compound capable of crossing cell membranes. Once inside the cell, the AM moiety is cleaved by esterases forming a calcium binding BAPTA complex, remaining intracellular (Tsien, 1981). Formation of PGE_2/D_2-PE was reduced by approximately 80 % in response to BAPTA/AM (Figure 9.10 A). In contrast, chelation of extracellular calcium by EGTA increased levels of PGE_2/D_2-PEs by 40 % (Figure 9.10 A). Similarly, PGE_2 and PGD_2 synthesis was inhibited (85 %) by BAPTA/AM and significantly enhanced in response to EGTA (Figure 9.10 B). Formation of PGb-PEs was reduced 84 % by BAPTA/AM but not affected by EGTA (Figure 9.11 A), similar to free PGb (Figure 9.11 B). Generation of PGc-PEs (Figure 9.12 A) and free PGc (Figure 9.12 B) was significantly reduced in response to BAPTA/AM. This indicates that free and esterified prostaglandin formation requires calcium mobilisation from intracellular stores.
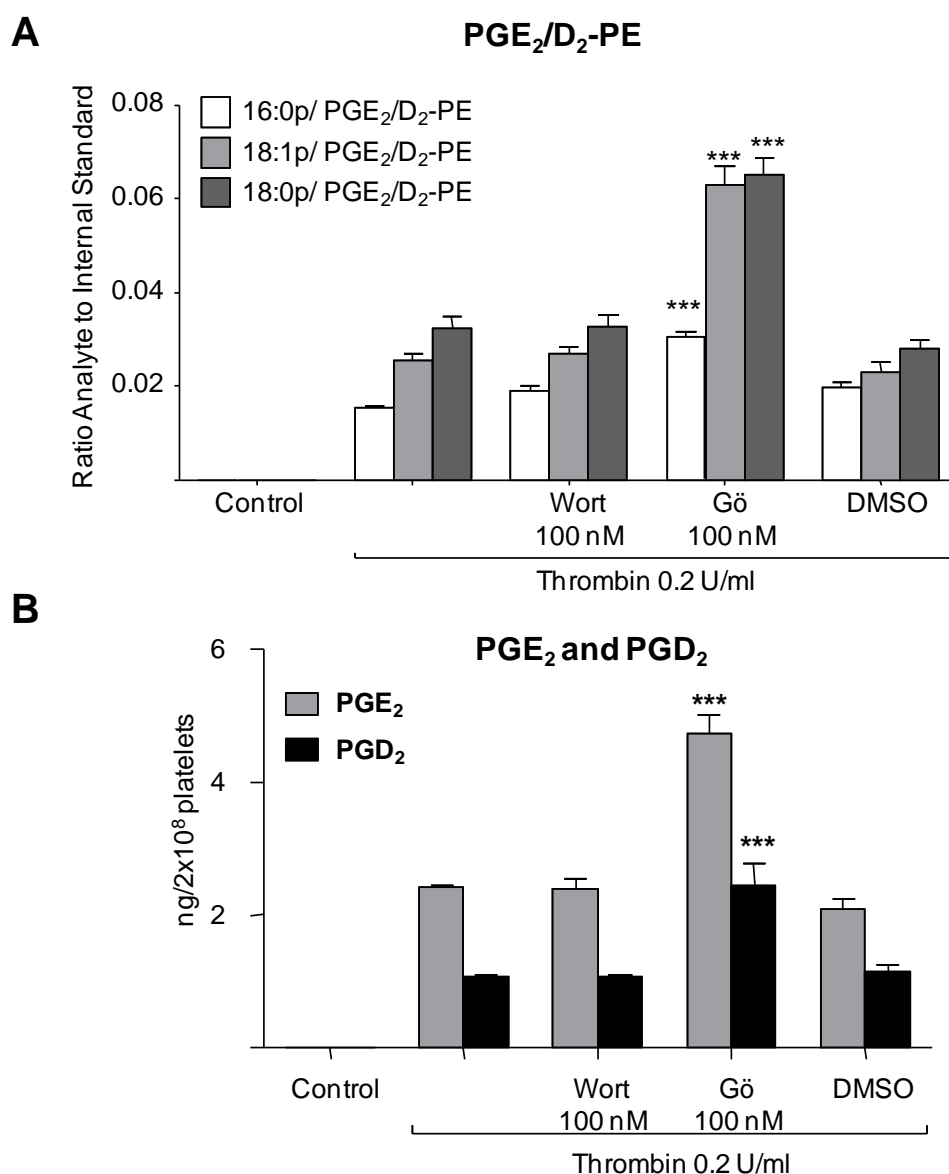
Figure 9.7: Inhibition of PKC enhances generation of PGE$_2$/D$_2$-PEs, PGE$_2$ and PGD$_2$. Washed human platelets were incubated for 10 min at room temperature with each inhibitor prior to thrombin activation (0.2 U/ml, 30 min at 37°C). This was followed by lipid extraction and analysis using reverse-phase LC/MS/MS, as described in Materials and Methods, Section *2.2.3.2* and *2.2.3.3*. Inhibitors used are as follows: wortmannin, 100 nM (PI3ks), Gö 6850, 100 nM (PKC) or vehicle (DMSO, 0.5 %). Levels of PGE$_2$/D$_2$-PEs are expressed as ratio analyte to internal standard while free PGE$_2$ and PGD$_2$ are expressed as ng/2 x 10^8 platelets. Data is presented from one experiment and representative of three (n = 3, mean ± SEM). ***P < 0.001 versus thrombin in the presence of DMSO, using ANOVA and Bonferroni Post Hoc Test. *Panel A*. PGE$_2$/D$_2$-PE formation by platelets incubated with wortmannin or Gö 6850. *Panel B*. PGE$_2$ and PGD$_2$ generation by platelets incubated with wortmannin or Gö 6850.
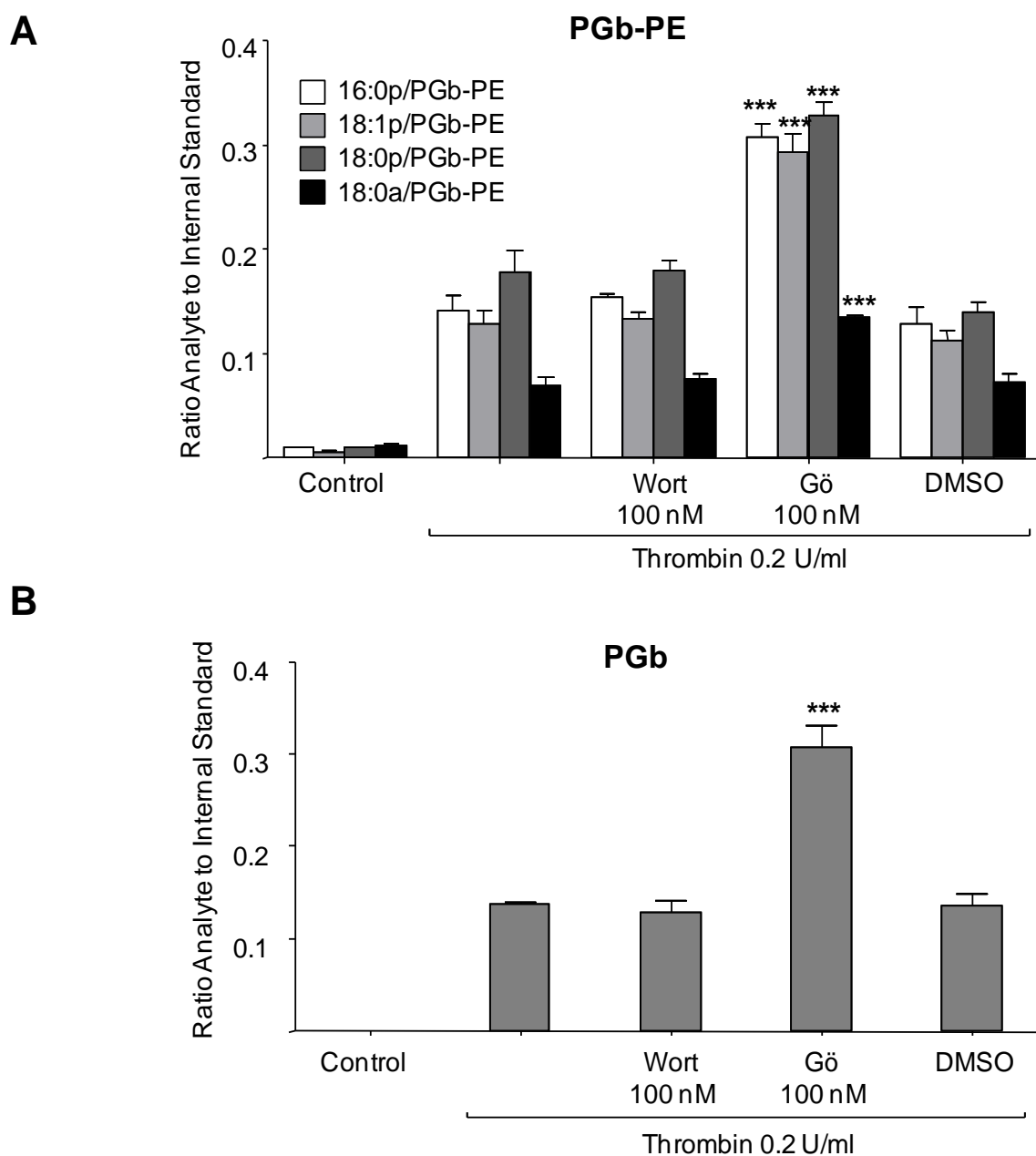
Figure 9.8: Inhibition of PKC enhances generation of PGb-PEs and free PGb. Washed human platelets were incubated for 10 min at room temperature with each inhibitor prior to thrombin activation (0.2 U/ml, 30 min at 37°C). This was followed by lipid extraction and analysis using phospholipid reverse-phase LC/MS/MS, as described in Materials and Methods, section *2.2.3.2* and *2.2.3.3*. Levels of PGb-PEs and free PGb are expressed as ratio analyte to internal standard. Data is presented from one experiment and representative of three (n = 3, mean ± SEM). ***P < 0.001 versus thrombin in the presence of DMSO, using ANOVA and Bonferroni Post Hoc Test. *Panel A*. PGb-PE formation by platelets incubated with wortmannin or Gö 6850. *Panel B*. PGb generation by platelets incubated with wortmannin or Gö 6850.
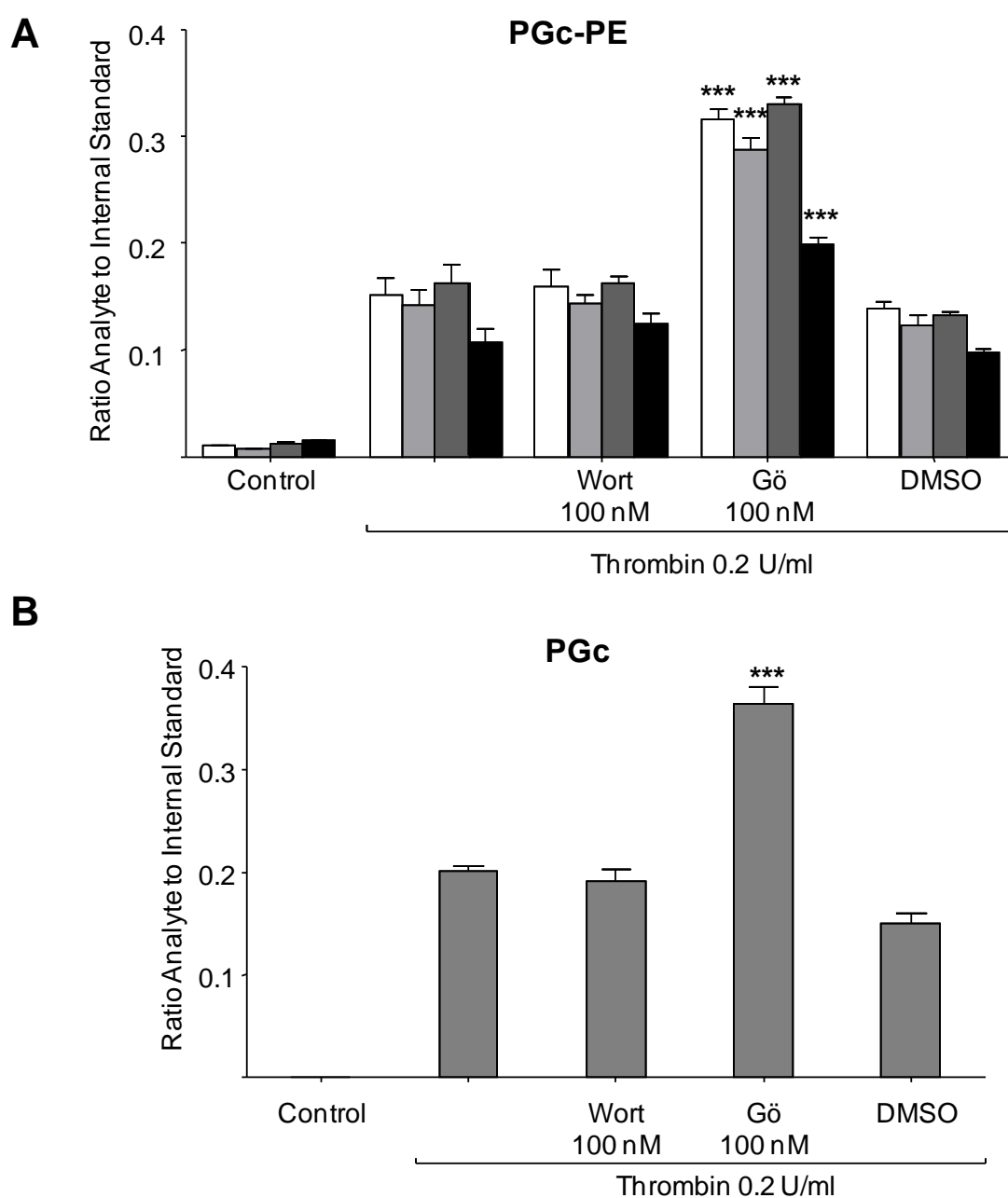
Figure 9.9: Inhibition of PKC enhances generation of PGc-PEs and free PGc. Washed human platelets were incubated for 10 min at room temperature with each inhibitor prior to thrombin activation (0.2 U/ml, 30 min at 37°C). This was followed by lipid extraction and analysis using reverse-phase LC/MS/MS, as describ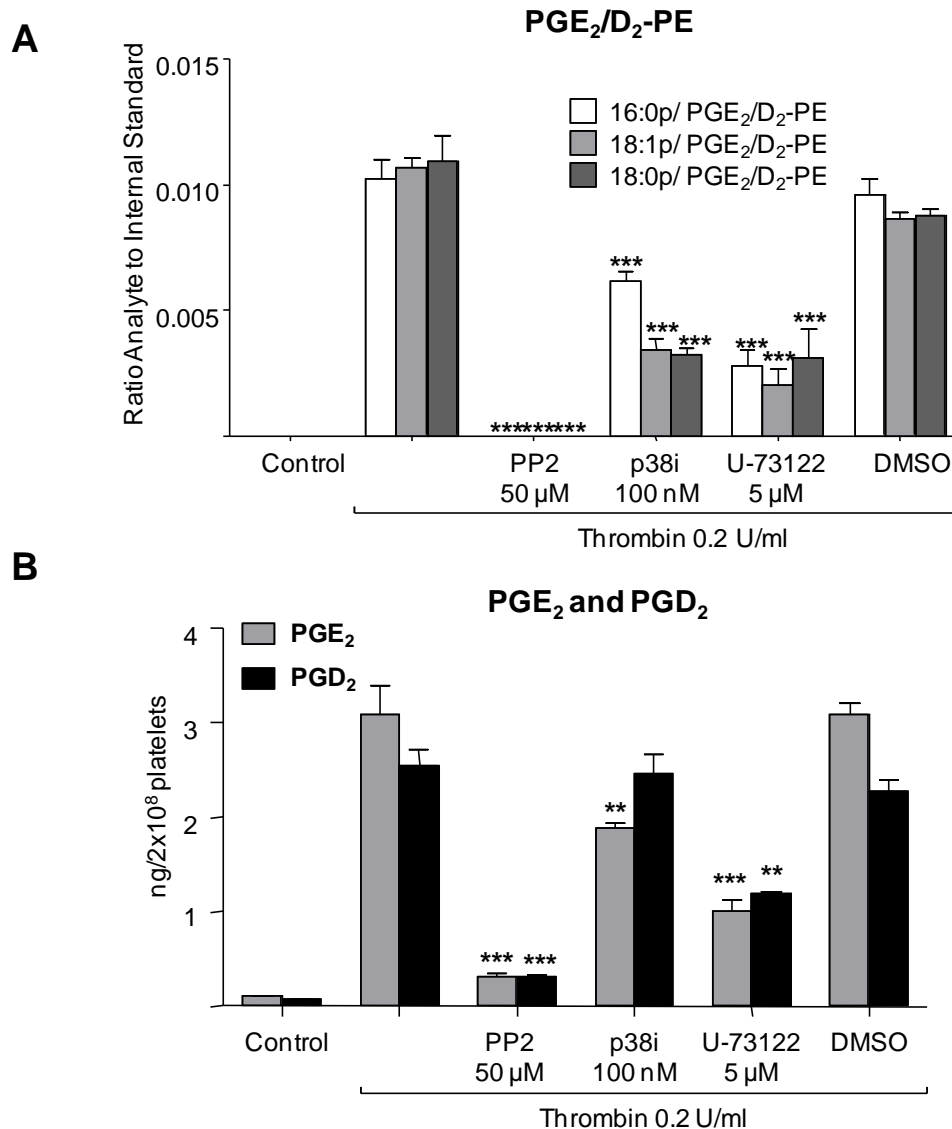ed in Materials and Methods, Section *2.2.3.2* and *2.2.3.3.* Levels of PGc-PEs and PGc are expressed as ratio analyte to internal standard. Data is presented from one experiment and representative of three (n = 3, mean ± SEM). ***P < 0.001 versus thrombin in the presence of DMSO, using ANOVA and Bonferroni Post Hoc Test. *Panel A*. PGc-PE formation by platelets incubated with wortmannin or Gö 6850. *Panel B*. PGc generation by platelets incubated with wortmannin or Gö 6850.
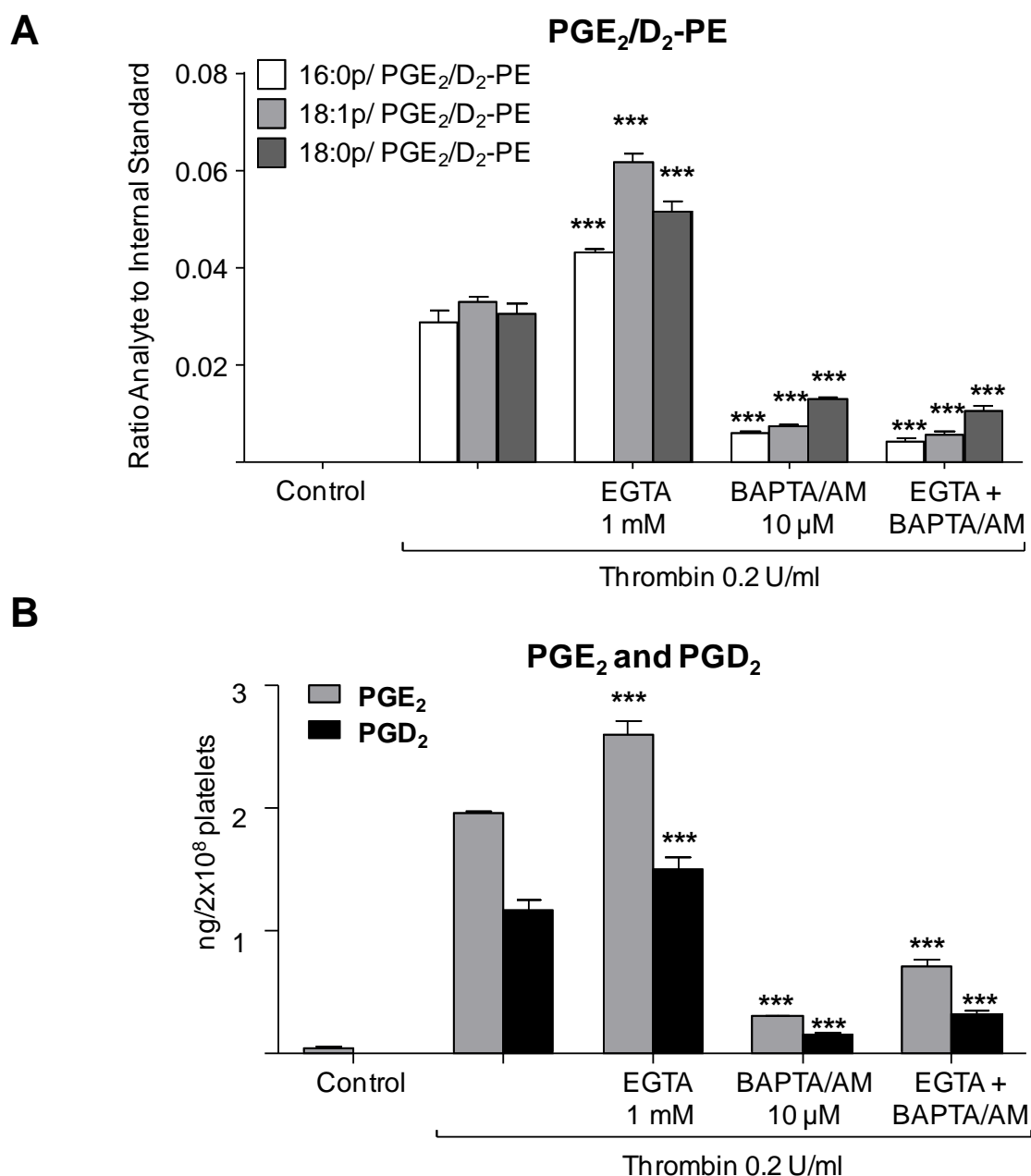
Figure 9.10: Cytosolic Ca^{2+} is required for PGE$_2$/D$_2$-PE, PGE$_2$ and PGD$_2$ formation. Washed human platelets were incubated for 10 min at room temperature with each inhibitor prior to thrombin activation (0.2 U/ml for 30 min for 37°C). Lipids were then extracted and analysed using reverse-phase LC/MS/MS, as described in Materials and Methods, Section *2.2.3.2* and *2.2.3.3*. Levels of PGE$_2$/D$_2$-PEs are expressed as ratio analyte to internal standard while PGE$_2$ and PGD$_2$ are expressed as ng/2 x 10^8 platelets. Data is presented from one experiment and representative of three (n = 3, mean ± SEM). *** P < 0.001 versus thrombin, using ANOVA and Bonferroni Post Hoc Test. *Panel A*. PGE$_2$/D$_2$-PE formation by platelets incubated with 1 mM EGTA and/or 10 µM BAPTA/AM. *Panel B*. PGE$_2$ and PGD$_2$ generation by platelets incubated with 1 mM EGTA and/or 10 µM BAPTA/AM.
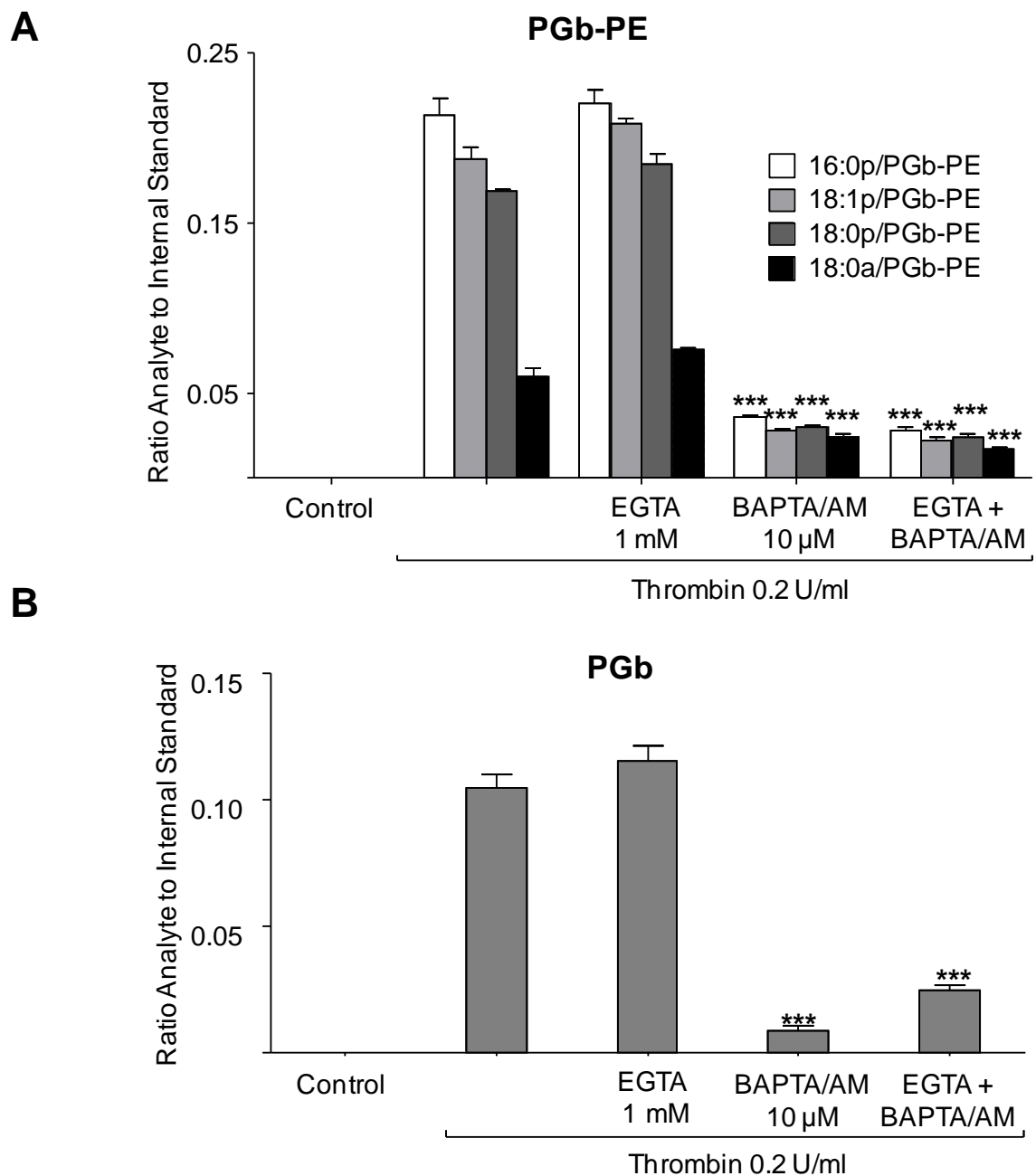
Figure 9.11: Cytosolic Ca²⁺ is required for PGb-PE and free PGb formation. Washed human platelets were incubated for 10 min at room temperature with each inhibitor prior to thrombin activation (0.2 U/ml for 30 min for 37°C). Lipids were then extracted and analysed using reverse-phase LC/MS/MS, as described in Materials and Methods, Section *2.2.3.2* and *2.2.3.3*. Levels of PGb-PEs and PGb are expressed as ratio analyte to internal standard. Data is presented from one experiment and representative of three (n = 3, mean ± SEM). *** P < 0.001 versus thrombin, using ANOVA and Bonferroni Post Hoc Test. *Panel A.* PGb-PE formation by platelets incubated with 1 mM EGTA and/or 10 μM BAPTA/AM. *Panel B.* PGb generation by platelets incubated with 1 mM EGTA and/or 10 μM BAPTA/AM.
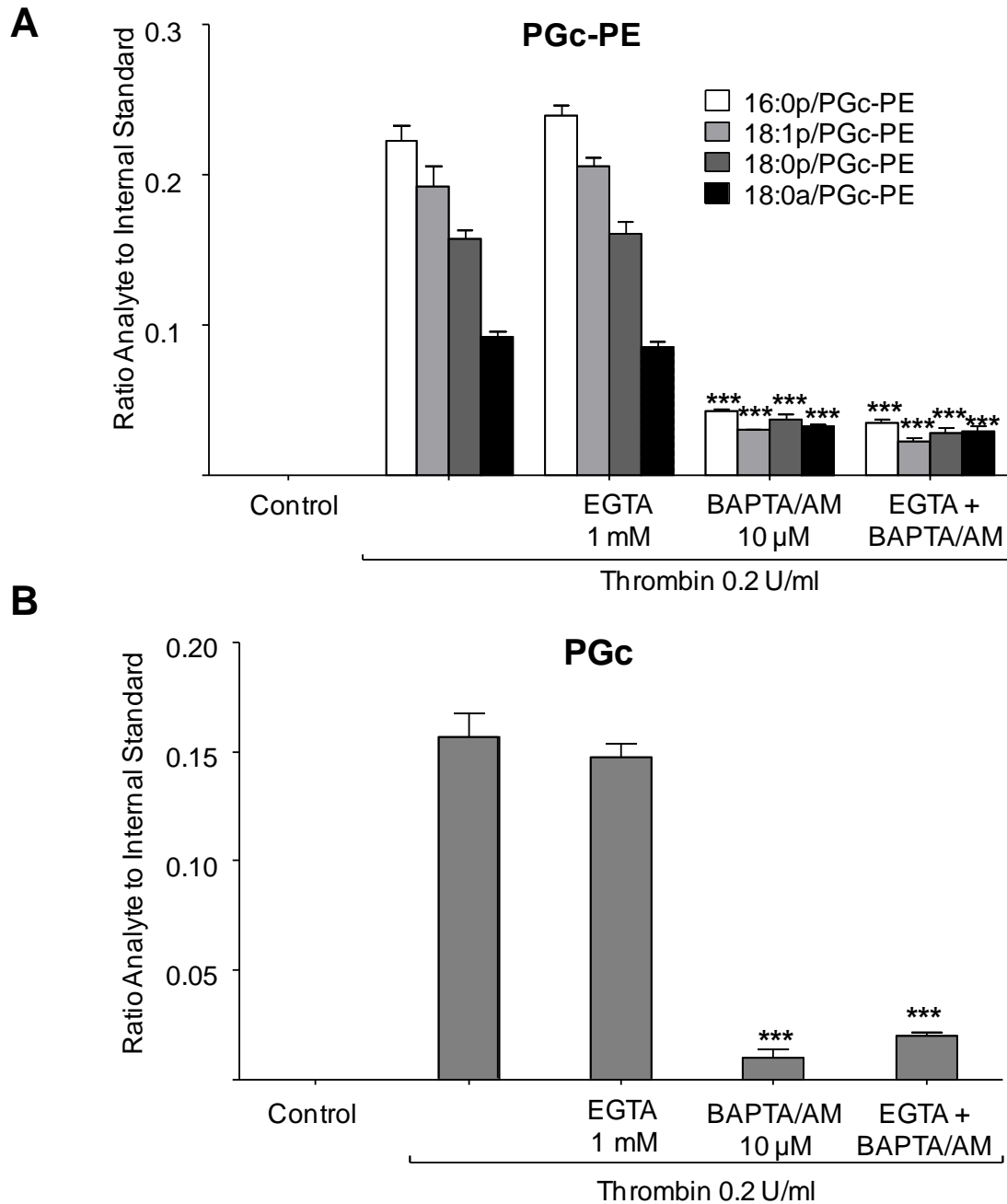
Figure 9.12: Cytosolic Ca^{2+} is required for PGc-PE and free PGc formation. Washed human platelets were incubated for 10 min at room temperature with each inhibitor prior to thrombin activation (0.2 U/ml for 30 min for 37°C). Lipids were then extracted and analysed using reverse-phase LC/MS/MS, as described in Materials and Methods, Section *2.2.3.2* and *2.2.3.3*. Levels of PGc-PEs and PGc are expressed as ratio analyte to internal standard. Data is presented from one experiment and representative of three (n = 3, mean ± SEM). *** P < 0.001 versus thrombin, using ANOVA and Bonferroni Post Hoc Test. *Panel A*. PGc-PE formation by platelets incubated with 1 mM EGTA and/or 10 µM BAPTA/AM. *Panel B*. PGc generation by platelets incubated with 1 mM EGTA and/or 10 µM BAPTA/AM.

9.3 Discussion

In human platelets, thrombin initiates a wide range of responses via stimulation of thrombin receptors PAR-1 and PAR-4, including aggregation, degranulation and TxA$_2$ formation (Sinha *et al*., 1983; Jurk K & Kehrel, 2005). In this chapter, the involvement of PAR-1 and PAR-4 in the generation of free and esterified prostaglandins was confirmed using the thrombin-receptor agonists TFLLRNH$_2$ and AY-NH$_2$ (Figures 9.1 – 9.3). Platelets stimulated with these synthetic peptides generated lower levels of these lipids compared to thrombin. This is most likely due to differences between a built-in tethered ligand generated by thrombin and a ligand free in solution (Chung *et al*., 2002). TFLLRNH$_2$ and AY-NH$_2$ are unable to cleave the receptor; instead, they activate PAR-1 and PAR-4 by mimicking the new amino terminus created by thrombin cleavage (Bahou *et al*., 1993; Gerszten *et al*., 1994). It is also possible that during PAR-1 proteolysis two ligands are formed, a tethered ligand and a PAR-1 amino-terminal peptide cleaved by thrombin, which may potentiate each other inducing a higher thrombin response compared to the synthetic peptides TFLLRNH$_2$ and AY-NH$_2$ (Furman *et al*., 1998; Furman *et al*., 2000). *In vivo*, platelets are activated simultaneously by different agonists, including thrombin and collagen. Although only PAR-1 and PAR-4 were examined, other receptors may be involved, such as collagen receptors glycoprotein VI and integrin $\alpha_2\beta_1$, which on stimulation also leads to platelet activation and TxA$_2$ formation (Li *et al*., 2010).

Separately, I demonstrated that free and esterified prostaglandin formation requires stimulation of several signalling pathways, including *src* tyrosine kinases, p38 MAPK and PLC (Figure 9.4 – 9.6). This is in line with previous reports showing that TxA$_2$ is formed by platelets, following stimulation of PAR-1 and PAR-4, and requires activation of several intracellular signalling intermediates, including cPLA$_2$, p38 MAP kinase, *src* tyrosine kinases, PLC and cytosolic calcium (Bleasdale *et al*., 1990; Jurk & Kehrel, 2005; Banno *et al*., 1998; Agranoff *et al*., 1983; Kramer *et al*., 1996; McNicol & Shibou, 1998). Furthermore, Kawao and colleagues have shown that free PGE$_2$ is formed by human lung-derived A549 epithelial cells via COX-1/-2 in a *src* tyrosine kinase, p38 MAP kinase, PLC, intracellular calcium and cPLA$_2$-dependent manner (Kawao *et al*., 2005). In contrast,

generation of 12-HETE-PE/PCs by activated platelets requires stimulation of *src* tyrosine kinase but not PLC (Thomas *et al.*, 2010). This likely reflects the different signalling pathways involved in 12-LOX versus COX-1 activation.

Furthermore, I observed that inhibition of PKC by Gö 6850 significantly increases levels of free and esterified prostaglandins (Figures 9.7 – 9.9). This suggests that PKC exerts a negative feedback effect on the generation of these lipids. The increase in free and esterified prostaglandin formation may be due to inhibition of PKCθ, which negatively regulates intracellular calcium levels in platelets (Strehl *et al.*, 2007; Cohen *et al.*, 2011; Harper & Poole, 2010). Elevated calcium could enhance the catalytic activity of $cPLA_2$, increasing AA release and formation of free and esterified prostaglandins. To date, there are no commercially available isoform specific PKC inhibitors and Gö 6850 may not be the optimum pharmacological inhibitor to study PKC signalling *in vivo*. Instead, genetically modified mice that lack the expression of a single PKC isoform would be a better approach to study the involvement of PKC in the formation of these lipids.

I showed that generation of free and esterified prostaglandins by activated platelets requires calcium mobilisation from intracellular stores (Figures 9.10 – 9.12) unlike 12-HETE-PE/PC formation, which requires both intra and extracellular calcium (Thomas *et al.*, 2010; Morgan *et al.*, 2010). The difference in calcium requirement likely reflects the different PLA_2 isoforms involved in the formation of these two distinct families of lipids. Esterified 12-HETEs originate from a pool of AA mainly released by $cPLA_2$ but also require $sPLA_2$ that maybe act through generating bioactive lysophospholipids, whereas free and esterified prostaglandins are formed in a $cPLA_2$-dependent manner (Coffey *et al.*, 2004a; Thomas *et al.*, 2010; Morgan *et al.*, 2010; Aldrovandi *et al.*, 2013). While $cPLA_2$ is activated by calcium in a nanomolar level, $sPLA_2$ requires calcium in a milimolar range, suggesting that calcium from intra and extracellular sites are required for $sPLA_2$ stimulation whereas, calcium from intracellular stores may be sufficient to stimulate $cPLA_2$ (Saunders *et al.*, 1999).

In summary, I demonstrated that free and esterified prostaglandins are formed following stimulation of PAR-1/-4 and require *src*-tyrosine kinases, PLC, p38 MAP kinase and

intracellular calcium but not PI3Ks, while PKC exerts a negative feedback inhibition on generation (Scheme 9.2). All these act via stimulating cPLA$_2$ and COX-1, ultimately leading to generation of free PGs. These are subsequently released as free eicosanoids or esterified into lyso PEs via LC-FACS and acyltransferase (Aldrovandi *et al.*, 2013).

In addition, formation of free and esterified prostaglandins is very likely to take place in intracellular membranes where COX-1 and esterification enzymes are localised (Gerrard *et al.*, 1976; Bakken *et al.*, 1994).

Collectively, the data indicate that formation involves a highly coordinated receptor and intracellular signalling pathway that is similar for both free and esterified prostaglandins and further underscores their likely relevance to platelet biology.
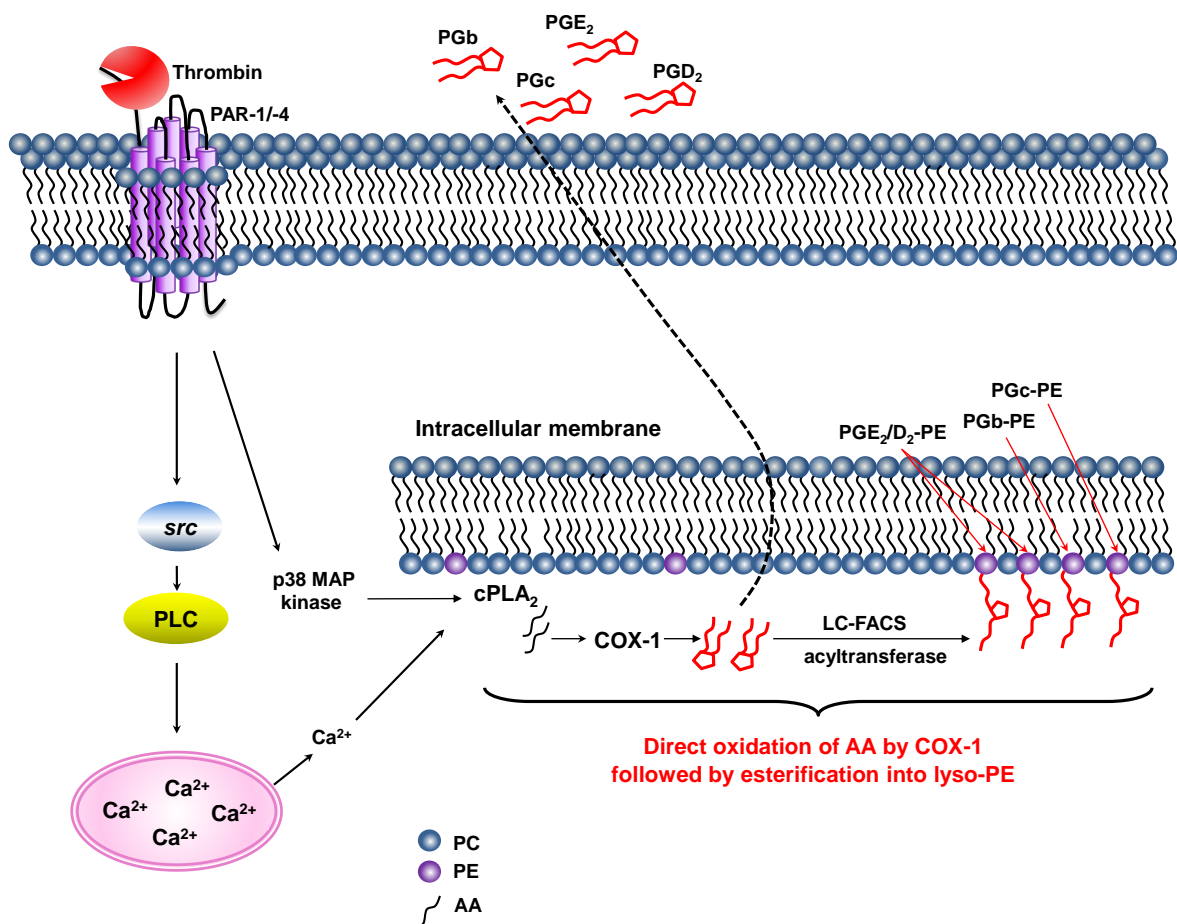
Scheme 9.2: Proposed mechanism for the formation of free and esterified prostaglandins by human platelet COX-1. On platelet activation, AA is released by cPLA$_2$ and oxidised by COX-1, forming PGE$_2$, PGD$_2$, PGb and PGc, which are either esterified into PEs or released as free PGs.

Chapter 10

10 Studying PGE$_2$ Esterification onto Lysophospholipids using Rat Liver Microsomes and Characterising the Ability of Esterified Prostaglandins to Regulate Coagulation

10.1 Introduction

In this chapter, two different studies will be described.

1. Esterification of PGE$_2$ into phospholipids using rat liver microsomes. As previously reported in this thesis, PG-PEs are initially formed as free PGs via COX-1 and subsequently esterified onto lysophospholipid PEs through LC-FACS and acyltransferase. Little is known regarding how oxidised fatty acids are reincorporated into lysophospholipids, and whether LC-FACS and acyltransferase display preferences for different fatty acids or eicosanoids during remodelling of membrane phospholipids in platelets. Rat liver microsomes contain a set of enzymes involved in fatty acid metabolism, including LC-FACS and lysophospholipid acyltransferase (LPLAT), therefore, this is a suitable model to study incorporation of PGE$_2$ into lysophospholipids (Suzuki *et al*., 1990; Yamashita *et al*., 1997; Shindou *et al*., 2013). Here, rat liver microsomes will be isolated and used as a model system to study PGE$_2$ esterification into lysophospholipids.

2. Studying the ability of PG-PEs to regulate coagulation factor activity. Here, I will investigate a potential role for PG-PEs in regulating thrombin formation in human plasma. For this, PG-PE will be purified from total platelet lipid extracts, will then be incorporated into liposomes and added to platelet poor plasma to stimulate thrombin generation. Thrombin is formed following platelet activation and externalisation of the aminophospholipids PS and PE (Heemskerk *et al*., 2002). These phospholipids interact with clotting factors through multiple γ-carboxylated glutamic acids (Gla domains) forming complexes, specifically factor VIIIa/IXa (tenase complex) and factor Va/Xa (prothrombinase complex), that convert prothrombin to thrombin (Morrissey *et al*., 2011; Tavoosi *et al*., 2011; Lentz, 2003; Falls *et al*., 2000). Recently, Thomas and co-workers have shown that liposomes supplemented with 12-HETE-PC dose-dependently enhance tissue factor-dependent thrombin generation in human plasma (Thomas *et al*., 2010).

This oxidised phospholipid is acutely generated by agonist-activated human platelets via 12-LOX, in a highly regulated manner, remaining cell-associated, similar to PG-PEs formed via COX-1. Thus, I propose that PG-PEs may act similarly to 12-HETE-PC, enhancing thrombin generation during platelet activation.

10.1.1 Aims

The studies described in this chapter aim to:

- Isolate rat liver microsomes to be used as a model system to study PGE_2 esterification into phospholipids.
- Purify PG-PEs from total platelet lipid extracts.
- Investigate whether liposomes supplemented with PG-PEs can enhance tissue factor-dependent thrombin generation in human plasma.

10.2 Results

10.2.1 Confirmation of enzymatic activity of microsomal fractions.

In this section, rat liver microsomes were isolated and used as a model system to study PGE_2 esterification into lysophospholipids. Briefly, livers from Wistar male rats were perfused, minced and homogenised. The homogenate underwent three rounds of centrifugation. After final spin, supernatant was aspirated into a clean glass vial, centrifuged at high speed and microsome pellets resuspended in sucrose buffer, as described in Materials and Methods, Section *2.2.12*.

To confirm enzymatic activity, microsomal fractions (0.5 mg/3 ml of Tris – HCL buffer) were incubated with 80 µM of AA-d_8 in the presence of either 80 µM of 18:0 lyso PE or 18:0 lyso PC with the stearic acid (SA) at the sn1, for 60 min at 37°C. Formation of SA-AA-d_8-PE/PC was then determined using reverse-phase LC/MS/MS, in negative and positive mode, as described in Materials and Methods, Section *2.2.12*.

Formation of both SA-AA-d_8-PE and SA-AA-d_8-PC was detected confirming the enzymatic activity of microsomal fractions. Negative LC/MS/MS spectrum of the parent mass *m/z* 774.6 (SA-AA-d_8-PE) yielded fragments with ions characteristic of both lyso PE (*m/z* 480 and 283) and AA-d_8 (*m/z* 311 and 267), confirming the esterification of AA-d_8 to lyso PE (Figure 10.1). Similarly, negative MS/MS spectrum of the parent mass *m/z* 802.7 (SA-AA-d_8-PC) generated daughter ions characteristic of both lyso PC (*m/z* 508 and 283) and AA-d_8 (*m/z* 311 and 267), Figure 10.2. Furthermore, formation of either SA-AA-d_8-PE or SA-AA-d_8-PC was not detected in control samples containing only microsomal fractions (data not shown). The spectrum of AA-d_8 is shown for comparison in Figure 10.3.

10.2.1.1   PGE$_2$-PE generation in vitro was not detected using rat liver microsomes.

The ability of rat liver microsomes to esterify PGE$_2$ to lyso PE/PC was also examined. Briefly, microsomal fractions (0.5 mg/3 ml of Tris – HCL buffer) were incubated with 80 μM of either PGE$_2$ or PGE$_2$-d_4 in the presence of 80 μM 18:0 lyso PE/PC, for 60 min at 37°C. Formation of SA-PGE$_2$-PE/PC and SA-PGE$_2$-d_4-PE/PC was then determined using reverse-phase LC/MS/MS, in negative and positive mode, as described in Materials and Methods, Section *2.2.12*.

However, SA-PGE$_2$-PE, SA-PGE$_2$-d_4-PE, SA-PGE$_2$-PC or SA-PGE$_2$-d_4-PC were not detected. This indicates that platelets display a set of fatty acylation enzymes distinct from rat liver microsomes, which are unable to esterify PGs to lysophospholipids.
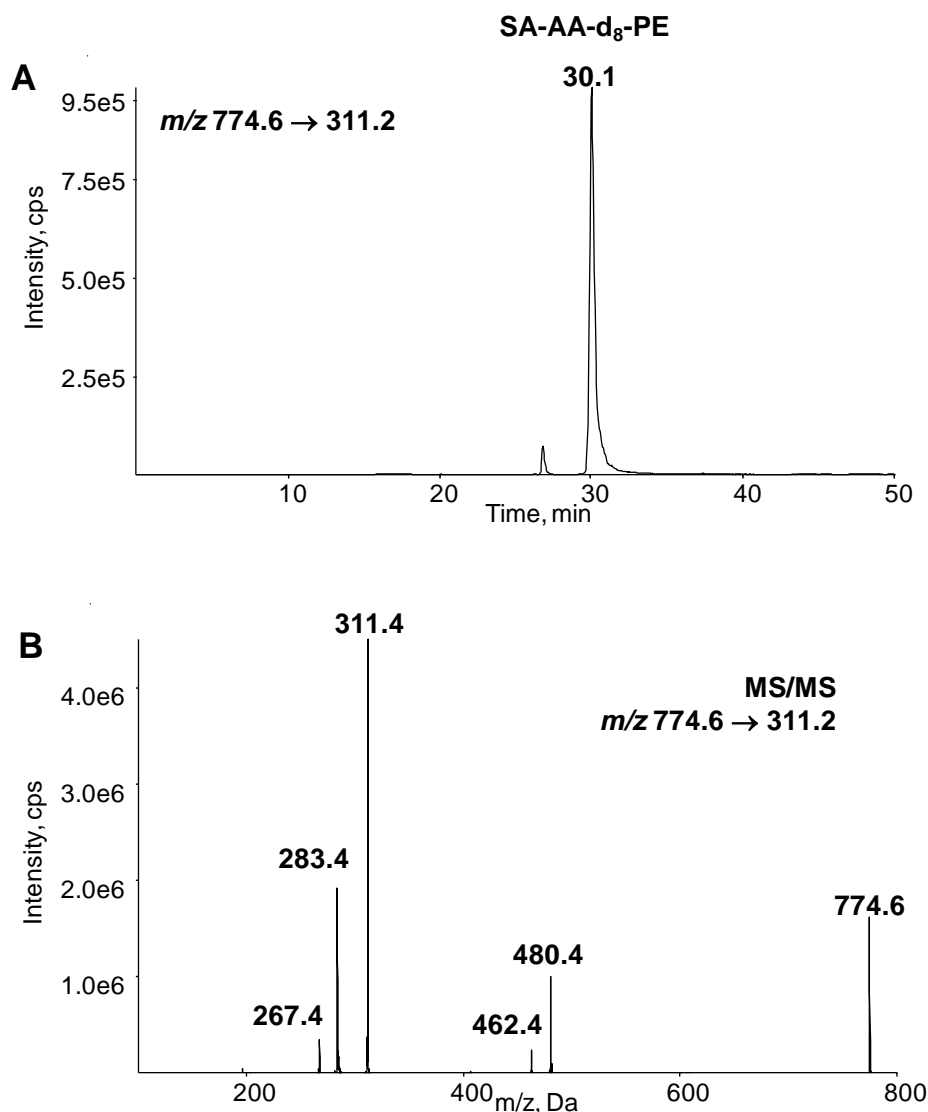
Figure 10.1: Formation of SA-AA-d$_8$-PE by rat liver microsomes. Microsomal fractions (0.5 mg/3 ml of Tris – HCL buffer) were incubated with 18:0 lyso PE (80 µM) and AA-d$_8$ (80 µM), in the presence of ATP (1.6 mM), CoA (80 µM) and MgCl$_2$6H$_2$O (1 mM), for 60 min at 37^{o}C. Lipids were extracted by Bligh and Dyer and analysed using reverse-phase LC/MS/MS, in negative mode, monitoring *m/z* 774.6 → 311.2 as described in Materials and Methods, Section *2.2.13.3*. *Panel A*. Chromatogram showing SA-AA-d$_8$-PE formation *in vitro*. *Panel B.* Negative LC/MS/MS spectrum acquired at the apex of elution of SA-AA-d$_8$-PE at 30.1 min showed fragments at *m/z* 311 and 267 characteristic of AA-d$_8$.
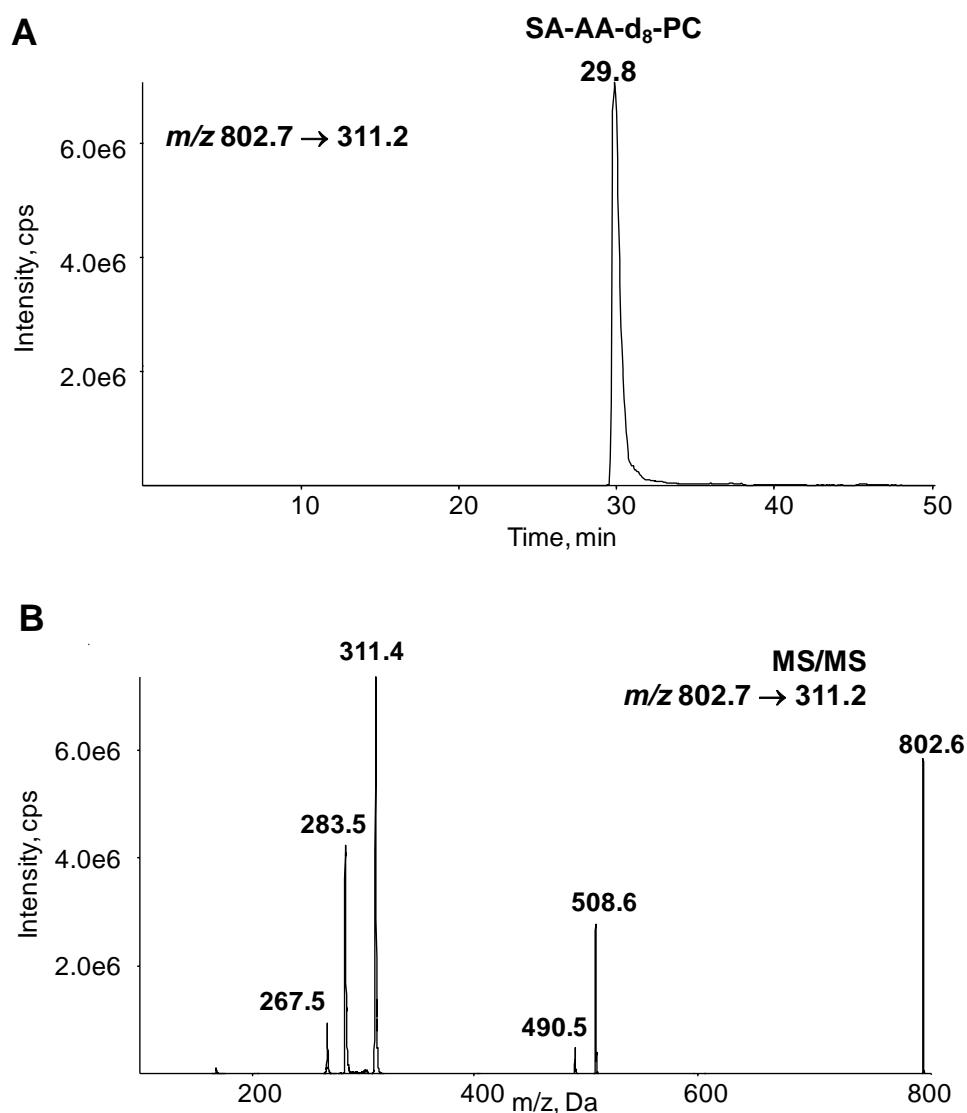
Figure 10.2: Formation of SA-AA-d$_8$-PC by rat liver microsomes. Microsomal fractions (0.5 mg/3 ml of Tris – HCL buffer) were incubated with 18:0 lyso PC (80 µM) or AA-d$_8$ (80 µM), in the presence of ATP (1.6 mM), CoA (80 µM) and MgCl$_2$6H$_2$O (1 mM), for 60 min at 37°C. Lipids were extracted by Bligh and Dyer and analysed using reverse-phase LC/MS/MS, in negative mode, monitoring *m/z* 802.7 → 311.2 as described in Materials and Methods, Section *2.2.13.3*. *Panel A*. Chromatogram showing SA-AA-d$_8$-PC formation *in vitro*. *Panel B.* Negative LC/MS/MS spectrum acquired at the apex of elution of SA-AA-d$_8$-PC at 29.8 min showed fragments at *m/z* 311 and 267 characteristic of AA-d$_8$.
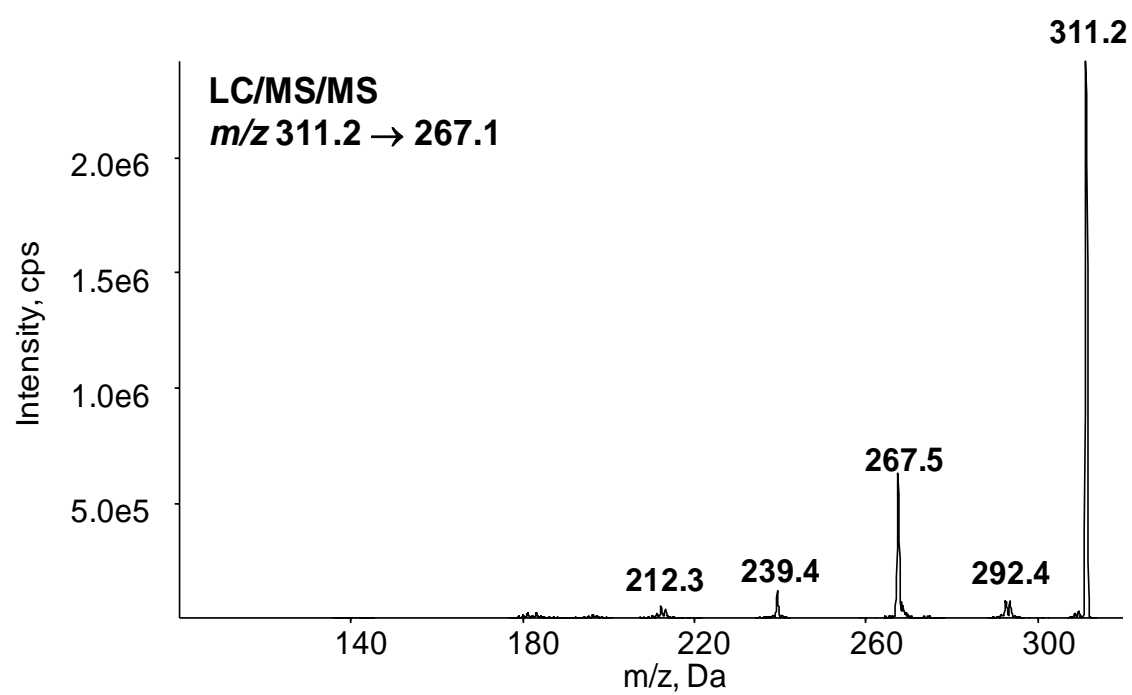
Figure 10.3: Standard AA-d$_8$. An MS/MS spectrum of AA-d$_8$ standard was acquired using the Q-Trap 4000. Fragmentation shows the origin of a major daughter ion at *m/z* 267.5.

10.2.2 Investigating the ability of PG-PEs to regulate thrombin generation in human plasma.

In this section, the ability of PG-PEs to stimulate thrombin generation in human plasma was investigated *in vitro* using liposomes. For this, varying amounts of PG-PE (equivalent to that synthesised by $2 - 12 \times 10^8$ activated platelets) and 4 μM phospholipids (5 % SAPS, 65 % DSPC and 30 % SAPE) were incorporated into liposomes and thrombin generation measured by Calibrated Automated Thrombography (CAT) (Clark *et al*., 2013; Hemker *et al*., 2003). Due to the absence of commercial standards and the inability of enzymes from rat liver microsomes to form PGE$_2$-PE *in vitro*, PG-PE standard was purified from total platelet lipid extracts, as described in Materials and Methods, Section *2.2.4*. Note that other lipids may co-elute with PG-PEs during HPLC separation and, therefore, the PG-PE standard may not be completely pure. PG-PEs were purified from a total of 1×10^{11} activated platelets and resuspended in 1 ml methanol total. The amount (in microliters) of PG-PEs equivalent to that generated by $2 - 12 \times 10^8$ activated platelets was then calculated using the following equation:

$$\mathrm{PG-PEs}_{\,2 \times 10^8 \text{ platelets (μl)}}$$

$$= \frac{2 \times 10^8 \text{ }_{\text{platelets}}}{1 \times 10^{11} \text{ }_{\text{platelets}}} \times 1000 \text{ μl}_{\,(\text{ purified PG−PE total})}$$

PG-PEs equivalent to that generated by $2 - 12 \times 10^8$ activated platelets corresponded to 2 – 12 μl of total purified PG-PE (1 ml).

Initially, liposomes containing varying percentages of SAPS (0 – 10 %), DSPC (60 – 100 %) and SAPE (0 – 30 %) were used to determine the optimum control that would allow changes in tissue factor-dependent thrombin generation *in vitro* to be observed, e.g. submaximal. Liposomes were added to platelet-poor pooled human plasma and coagulation initiated using 10 pM recombinant tissue factor. Thrombin levels were then

measured every 15 seconds, for 60 min by CAT, as described in Materials and Methods, Section *2.2.13*.

10.2.2.1.1 Replacement of DSPC/SAPE with PG-PEs does not enhance thrombin generation *in vitro*.

In this section, varying amounts of both DSPC/SAPE (1 – 30 %) were replaced with PG-PE standard and liposomes generated. Initially, PG-PE standard was quantified by weight and the amounts equivalent to 1 – 30 % of 4 µM phospholipid total calculated. Following extrusion, liposomes were then added to pooled human plasma and tissue factor-dependent thrombin generation measured by CAT.

Liposomes containing 1 – 3 % PG-PEs stimulated thrombin generation to control levels (Figures 10.4). While, 5 – 30 % PG-PEs increased tissue factor-dependent thrombin generation from 64 nM to approximately 72 nM (Figure 10.5), however this was not statistically significant. This suggests that it is unlikely that PG-PEs act regulating thrombin generation *in vivo*.
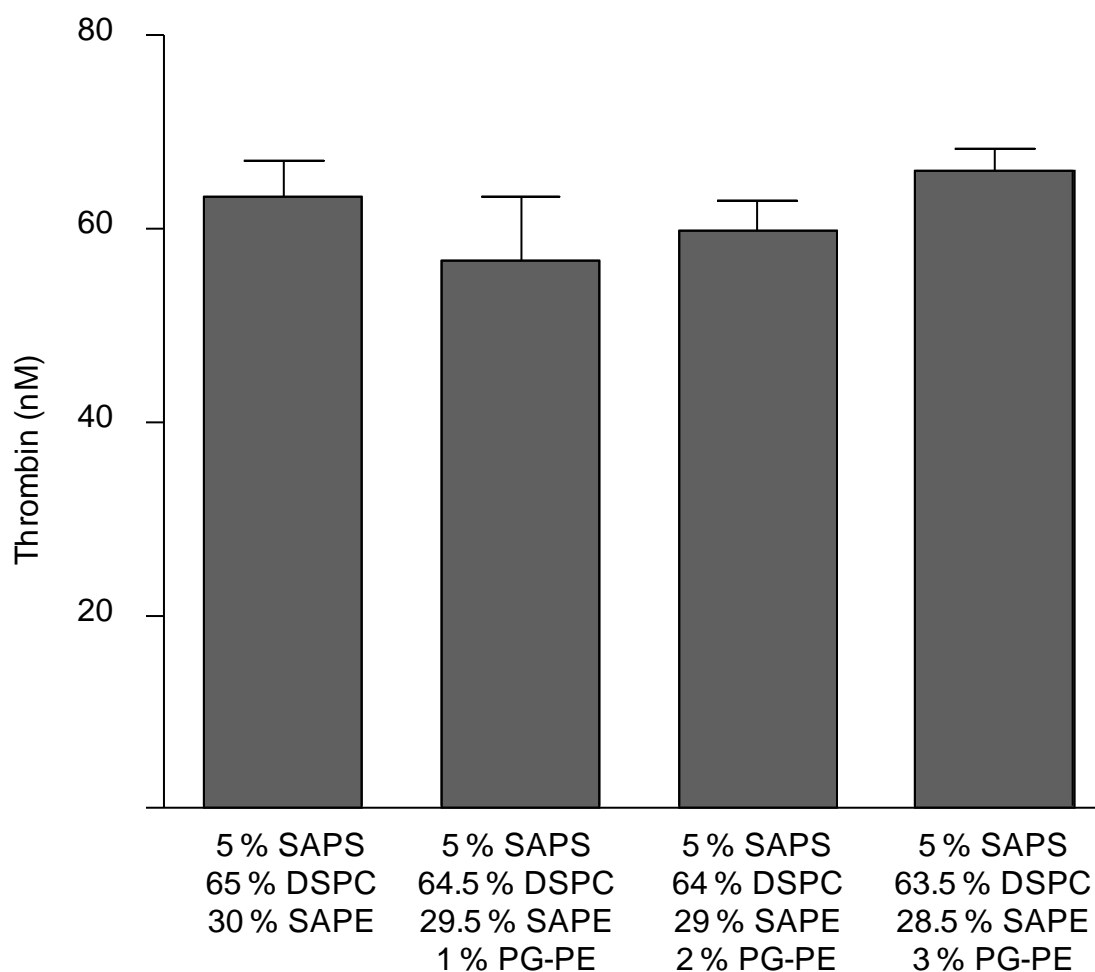
Figure 10.4: Replacement of DSPC/SAPE with 1, 2 or 3 % PG-PEs does not enhance thrombin generation *in vitro*. DSPC and SAPE were replaced with either 1, 2 or 3 % PG-PE and tissue factor-dependent thrombin generation determined, as described in Materials and Methods, Section *2.2.13*. The amount of DSPC, SAPS and PG-PE is varied according to the labels on the figure, but the percentage of PS was maintained throughout. Data from three independent experiments (n = 3, mean ± SEM). Not statisticaly significant, using ANOVA and Bonferroni Post Hoc Test.
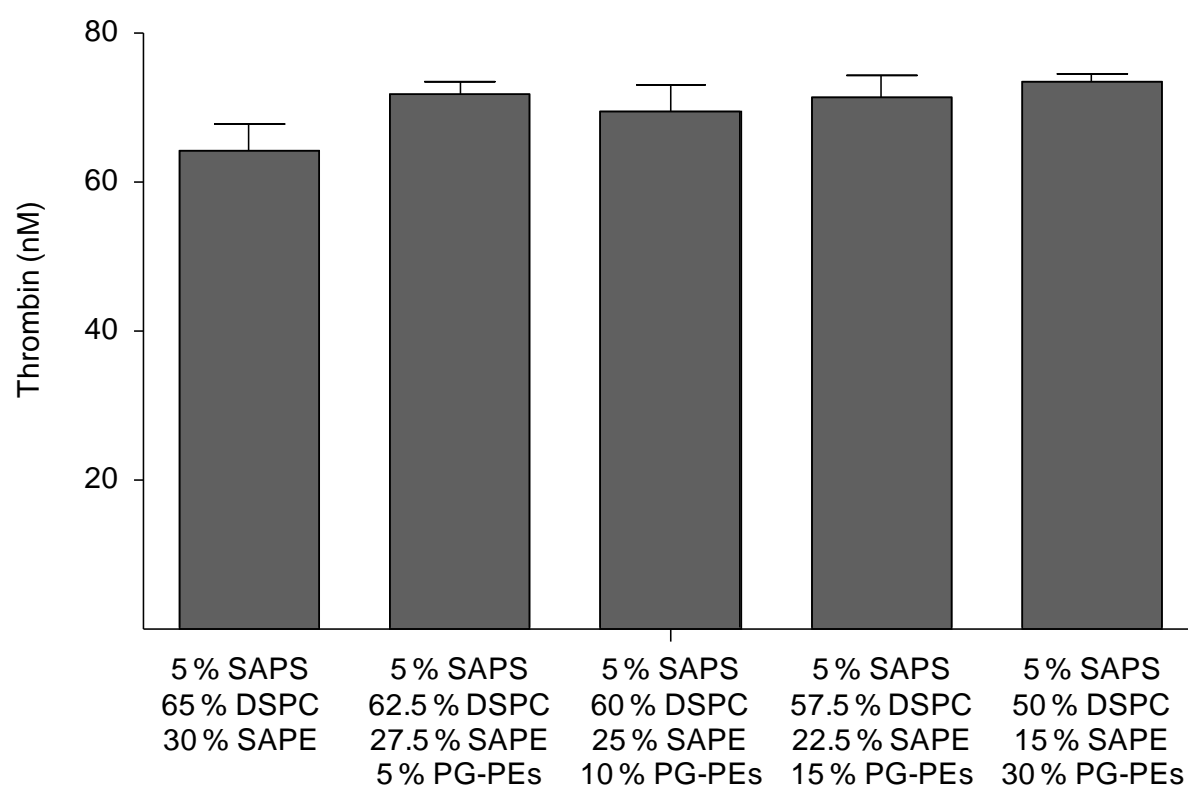
Figure 10.5: Replacement of DSPC/SAPE with 5, 10, 15 or 30 % PG-PEs does not significantly enhance thrombin generation *in vitro*. DSPC and SAPE were replaced with either 5, 10, 15 or 30 % PG-PE and tissue factor-dependent thrombin generation determined, as described in Materials and Methods, Section *2.2.13*. The amount of DSPC, SAPS and PG-PE is varied according to the labels on the figure, but the percentage of PS was maintained throughout. Data from three independent experiments (n = 3, mean ± SEM). Not statisticaly significant, using ANOVA and Bonferroni Post Hoc Test.

10.3   Discussion

In this chapter, two different studies were described. In the first, esterification of PGE_2 to lysophospholipids was assessed using rat liver microsomes. In the second study, the role of PG-PEs in thrombin generation was investigated using liposomes. Whilst the data in these unrelated studies were largely negative, they allowed some key questions to be addressed (e.g. esterification of PGE_2 into phospholipids and PG-PE function).

In the first study, I demonstrated that AA was efficiently esterified into lyso PE/PC (Figures 10.1 and 10.2), however, PGE_2-PE formation was not detected. Previous studies have shown that CoA independent transacylation enzymes that catalyse ether lipid coupling are expressed in platelets but not in rat liver microsomes (Yamashita *et al.*, 1997). This suggests that different tissues and cells are likely to contain very distinct set of enzymes involved in fatty acid acylation (Aldrovandi *et al.*, 2013). Furthermore, specific acyltransferases may have restricted selectivity for lysophospholipid acceptors. This hypothesis is supported by studies demonstrating the absence of activity with alkenyl-glycerophosphocholine by liver microsomal preparations that are active with acyl-glycerophosphocholine (Waku & Lands, 1968). The structural difference between AA and PGE_2 might influence the lysophospholipid acceptance. Future studies using platelet microsomes may generate PGE_2-PE *in vitro*.

In a separate study, I showed that when small amounts of DSPC/SAPE were replaced with PG-PEs, thrombin generation was not significantly elevated (Figures 10.4 – 10.5). Although the data presented in this chapter have not confirmed the role of PG-PEs in coagulation, this does not exclude their function in haemostasis. PG-PEs may act intracellularly as second messenger signalling lipids, similarly to DAG that triggers the activation of PKC and leads to powerful platelet activation responses, such as shape change, aggregation and secretion (Martin, 2001; Rittenhouse, 1996). Thus, PG-PEs could act as mediators of signal transduction during platelet activation. It is hoped that in future, generation of pure PG-PE standards will aid in elucidation of the function of these OxPLs.

Chapter 11

General Discussion

Initially, PGs were considered to only exist as free acid mediators. However, evidence is now emerging that they may also be attached to other functional groups including phospholipids and glycerol (Kozak *et al.*, 2000; Kozak.*et al.*, 2002; Aldrovandi *et al.*, 2013). Although formation of PGE_2-G/PGD_2-G and PGE_2-EA/PGD_2-EA via COX-2 has been reported, COX-1 had not been considered as a source of complex oxidised lipids and had only been shown to generate free acid mediators. In the present study, I demonstrated, with the use of a targeted lipidomic approach, that agonist-activated human platelets generate families of OxPLs via COX-1. These comprise a group of specific lipids, namely PGE_2, PGD_2 and two structurally distinct prostaglandin-like molecules (PGb and PGc), attached to four PE species (16:0p/, 18:1p/, 18:0p/ and 18:0a/). PGb and PGc were also detected as free eicosanoids and their structures remain to be characterised. Nevertheless, comparison of PGb and PGc MS/MS spectra to known eicosanoid standards revealed that these are oxidised fatty acids that have not previously been described in either platelets or other human cells. Hence, a total of sixteen novel OxPLs and two previously undescribed eicosanoids were identified in lipid extracts from thrombin-activated platelets. They are rapidly formed (2 – 5 minutes) through a highly coordinated sequence of receptor and intracellular signalling pathways, in response to physiological agonists. Therefore, the studies presented herein define a new group of OxPLs and COX-1 products. It is also the first demonstration of the involvement of COX-1 in the formation of OxPLs by an agonist-activated cell type.

Esterified prostaglandins belong to a growing family of enzymatically-generated OxPLs that have been described in platelets and other circulating immune cells (Hammond *et al.*, 2012; Bochkov *et al.*, 2010; Clark *et al.*, 2011; Maskrey *et al.*, 2007; Morgan *et al.*, 2009; Morgan *et al.*, 2010; Thomas *et al.*, 2010). To date, all were believed to be generated enzymatically by LOXs, including families of PE and PC that contain 12-HETE or 14-HDOHE formed by agonist-activated human platelets (Thomas *et al.*, 2010; Morgan *et al.*, 2010). In addition, esterified 5-HETEs have been characterised in human neutrophils, while 12/15 LOX-derived PE-esterified HETEs and KETEs have been described in human

monocytes and murine macrophages (Maskrey *et al.*, 2007; Clark *et al.*, 2011; Hammond *et al.*, 2012). Thus, the work presented herein extends this research by showing that other oxidised fatty acids can also be esterified into lysophospholipids.

Quantification of total PGE_2/D_2-PEs revealed that thrombin-activated human platelets generate approximately 28 pg/2 x 10^8 cells. This indicates that less than 1 % of the total PGE_2 and PGD_2 synthesised as free eicosanoids are incorporated into phospholipids. It is postulated that the amount of esterified PGs in platelets may be limited by a number of different mechanisms. Levels of PGE_2/D_2-PEs are considerably lower than 12-HETE-PEs (6 ng/4 x 10^7 platelets) (Thomas *et al.*, 2010). This may be due to the lower amount of free PGE_2/D_2 (6.2 ± 0.3 ng/2 x 10^8 platelets, described in Chapter 4) compared to free 12-HETE (65.5 ± 17.6 ng/4 x 10^7 platelets) being generated by activated platelets, assuming that LC-FACL/LPLAT enzymes have the same affinity for both free PGE_2/D_2 and free 12-HETE (Thomas *et al.*, 2010).

Furthermore, lyso PE acyltransferase (LPEAT)s capable of esterifying PGE_2 might only be expressed at low levels in platelets. For example, LPEAT2 is expressed at high levels in mouse and human brain and poorly expressed in lung and liver (Cao *et al.*, 2008). Therefore, PG-PEs may be formed at significantly higher levels in other cells or tissues, including the brain where both COX and LPEAT are expressed (Cao *et al.*, 2008; Chen & Bazan, 2005).

Alternatively, the amount of PG being esterified in platelets could be limited by carrier-mediated PG transporters, such as the multidrug resistance protein 4 (MRP4). Studies have shown that MRP4 is highly expressed in platelets and functions as a PG efflux carrier, mediating PGE_2 release (Reid *et al.*, 2003; Jedlitschky *et al.*, 2004). In platelets, the rate of PG efflux may potentially be faster than esterification, resulting in lower levels of intracellular PGE_2 available for FACL/LPLATs. Future studies could include investigating whether inhibition of MRP4 in platelets enhances PGE_2/D_2-PE formation.

Unlike free PGs that are secreted, esterified prostaglandins remain membrane-associated, indicating that they are likely to act locally, at the platelet surface or close to the plasma membrane. Due to their shape and polarity, PGE_2 and PGD_2 attached to PEs

are expected to protrude from platelet membranes becoming accessible to cell surface receptors through which they may signal, in a similar fashion to free PGs. Li and colleagues demonstrated that non-enzymatically formed OxPAPC and its component phospholipid 1-palmitoyl-2-epoxyiso-prostane E2-snglycero-3-phosphorylcholine (PEIPC), which accumulates in atherosclerotic lesions, can activate PG receptors, specifically EP2 and DP receptors (Li *et al.*, 2006). They also observed that the level of activation of EP2 by OxPAPC was comparable to that of PGE_2 and both OxPAPC and PEIPC compete for PGE_2 binding to the receptor (Li *et al.*, 2006). Furthermore, in 1976, Kunze and co-workers synthesised PGE_1-PE and PGE_2-PE adducts *in vitro* and compared their effects to the corresponding free PGE_1 and PGE_2 (Kunze *et al.*, 1976). However, these compounds are distinct from PGE_2-PE formed by platelets. They were chemically synthesised by linking the carboxylic group of PGE_1 or PGE_2 with the PE amine group, whilst in platelets, PGE_2 is esterified at the sn2 position of the glycerol backbone. Nevertheless, Kunze demonstrated that chemically synthesised PGE_1-PE and PGE_2-PE mimic the effects of PGE_1 and PGE_2 on isolated smooth muscle preparations, blood pressure and uterine activity, suggesting that the PGE_2-PE adduct was functionally indistinguishable from free PGE_2 (Kunze *et al.*, 1976). Although PGE_2-PEs generated by platelets are structurally distinct from chemically synthesised PGE_2-PEs adducts, this may not affect the binding of platelet-derived PGE_2-PE to EP receptors.

Alternatively, PGE_2-PE and PGD_2-PE may signal through a distinct set of receptors, separate from the PG receptors that mediate the effects of PGE_2 and PGD_2. A study by Nirodi *et al* demonstrated that PGE_2-G, one of the COX-2 metabolites of 2-AG, triggered intracellular calcium mobilisation in a PGE_2-independent manner in RAW264.7 murine macrophage-like cells (Nirodi *et al.*, 2004). Furthermore, PGE_2-G increased the frequency of miniature inhibitory postsynaptic currents in cultured hippocampal neurons, whereas either 2-AG or PGE_2 caused a decrease (Sang *et al.*, 2006). In addition, Sang and co-workers showed that PGE_2-G potentiates excitatory glutamatergic synaptic transmission and produces neurotoxicity independently of endocannabinoid or prostanoid receptors (Sang *et al.*, 2007). Therefore, PGE_2-PEs and PGD_2-PEs can display an array of biological actions that are either distinct or very similar to their free acid analogs. Once sufficient

quantities of PGE$_2$-PE and PGD$_2$-PE can be generated, the affinity of these lipids for PG receptors will be investigated. Future work could also include investigating whether PG-PEs are externalised in human platelets. This would help to elucidate whether the actions of PG-PEs take place at the platelet surface or close to intracellular membranes.

Formation of PG-PEs may be increased in atherosclerotic lesions and other sites of chronic inflammation, where these may facilitate the recruitment of inflammatory cells. Growing evidence now suggests that OxPLs and PGE$_2$ receptor signalling is involved in atherosclerosis. For example, OxPAPC and its component PEIPC activate endothelial cells to bind monocytes via the EP2 receptor (Li *et al.*, 2006). Activation and binding of endothelial cells to monocytes, results in monocyte entry into the vessel wall where they take up lipids, forming foam cells, a common event in atherogenesis. PGE$_2$ has also been reported to contribute to atherosclerosis, mediating inflammatory cytokine production, such as IL-1β and IL-6, via EP2 and EP4, which are expressed in atherosclerotic lesions (Ricciotti & FitzGerald, 2011). It is plausible that PG-PEs may also signal through EP receptors in atherosclerotic lesions mediating similar pro-inflammatory effects.

Studies conducted in collaboration with Dr Robert Murphy, University of Colorado, USA, suggest that free PGc, a novel COX-1 product is 8-hydroxy-9,11-dioxolane eicosatrienoic acid (DXA$_3$), that until now has only ever been described as a product of air oxidation of AA (Yin *et al.*, 2003). Initial studies indicate that DXA$_3$ is formed following conversion of AA into 11-hydroperoxyl radical via COX-1 (Hinz *et al.*, unpublished data 2013). The cyclooxygenase reaction is believed to begin with the tyrosyl radical abstracting a hydrogen from AA at carbon 13 to form an arachidonyl radical. The resulting radical migrates to carbon 11. This is followed by sequential addition of O$_2$ at carbon 11 to generate an 11R-hydroperoxyl radical. This is subsequently released by COX-1 and a dioxolane ring is formed through cyclisation of carbon 11 to carbon 9. The radical is then delocalised over carbon 8 and an O$_2$ is added forming an 8-hydroperoxyl radical, which is reduced forming a hydroperoxide. In the final stage, the hydroperoxide is reduced, possibly by a glutathione peroxidase, leading to DXA$_3$ formation. Additional experiments are currently underway to confirm this hypothesis.

In conclusion, this is the first study demonstrating formation of OxPLs via COX-1 in platelets. They form through a coordinated sequence of receptor and intracellular signalling pathways. The identification of these new metabolites in platelets suggests additional mechanisms regulating platelet function and might be a distinct target for modulation in platelet-dependent pathologies.

Bibliography

Adams RL & Bird RJ. Review article: Coagulation cascade and therapeutics update: relevance to nephrology. Part 1: Overview of coagulation, thrombophilias and history of anticoagulants. Nephrology (Carlton). 2009; 14(5):462-70.

Agranoff BW, Murthy P, Seguin EB. Thrombin-induced phosphodiesteratic cleavage of phosphatidylinositol bisphosphate in human platelets. J Biol Chem. 1983; 258(4):2076-8.

Ahmad SS, London FS, Walsh PN. The assembly of the factor X-activating complex on activated human platelets. J Thromb Haemost. 2003; 1(1):48-59.

Akaogi J, Nozaki T, Satoh M, Yamada H. Role of PGE2 and EP receptors in the pathogenesis of rheumatoid arthritis and as a novel therapeutic strategy. Endocr Metab Immune Disord Drug Targets. 2006; 6(4):383-94.

Albert CJ, Crowley JR, Hsu FF, Thukkani AK, Ford DA. Reactive chlorinating species produced by myeloperoxidase target the vinyl ether bond of plasmalogens: identification of 2-chlorohexadecanal. J Biol Chem. 2001; 276(26):23733-41.

Aldrovandi M & O'Donnell VB. Oxidized PLs and vascular inflammation. Curr Atheroscler Rep. 2013; 15(5):323.

Aldrovandi M, Hammond VJ, Podmore H, Hornshaw M, Clark SR, Marnett LJ, Slatter DA, Murphy RC, Collins PW, O'Donnell VB. Human platelets generate phospholipid-esterified prostaglandins via cyclooxygenase-1 that are inhibited by low dose aspirin supplementation. J Lipid Res. 2013; 54(11):3085-97.

Annesley TM. Ion suppression in mass spectrometry. Clin Chem. 2003; 49(7):1041-4.

Bahou WF, Coller BS, Potter CL, Norton KJ, Kutok JL, Goligorsky MS. The thrombin receptor extracellular domain contains sites crucial for peptide ligand-induced activation. J Clin Invest. 1993; 91(4):1405-13.

Bakken AM, Farstad M, Osmundsen H. The activities of acyl-CoA hydrolase in lysate and subcellular fractions of human blood platelets in relation to activities of acyl-CoA:1-acyl-lysophospholipid acyltransferase. Biochim Biophys Acta. 1994; 1214(2):180-6.

Balgoma D, Astudillo AM, Pérez-Chacón G, Montero O, Balboa MA, Balsinde J. Markers of monocyte activation revealed by lipidomic profiling of arachidonic acid-containing phospholipids. J Immunol. 2010; 184(7):3857-65.

Banno Y, Asano T, Nozawa Y. Stimulation by G protein betagamma subunits of phospholipase C beta isoforms in human platelets. Thromb Haemost. 1998; 79(5):1008-13.

Berg JM, Tymoczo JL & Stryer L. Biochemistry. 5th Edition. 2002. Freeman and Company.

Bergmeier W & Stefanini L. Novel molecules in calcium signaling in platelets. J Thromb Haemost. 2009; 7 Suppl 1:187-90.

Bergström S & Sjövall J. The isolation of prostaglandin E from Sheep prostate glands. Acta.Chem.Scand. 1960a; 14: 1701-1705.

Bergström S & Sjövall J. The isolation of prostaglandin F from sheep prostate glands. Acta.Chem.Scand. 1960b; 14:1693-1700.

Bergstrom S, Danielsson H, Samuelsson B. The enzymatic formation of prostaglandin E2 from arachidonic acid prostaglandins and related factors 32. Biochim Biophys Acta 1964; 90:207–210.

Bevers EM, Comfurius P, Zwaal RF. Changes in membrane phospholipid distribution during platelet activation. Biochim Biophys Acta. 1983; 736(1):57-66.

Bleasdale JE, Thakur NR, Gremban RS, Bundy GL, Fitzpatrick FA, Smith RJ, Bunting S. Selective inhibition of receptor-coupled phospholipase C-dependent processes in human platelets and polymorphonuclear neutrophils. J Pharmacol Exp Ther. 1990; 255(2):756-68.

Bligh EG & Dyer WJ. A rapid method of total lipid extraction and purification. Can J Biochem Physiol. 1959; 37(8):911-7.

Bluteau D, Lordier L, Di Stefano A, Chang Y, Raslova H, Debili N, Vainchenker W. Regulation of megakaryocyte maturation and platelet formation. J Thromb Haemost. 2009; 7 (1):227-234.

Bochkov VN, Oskolkova OV, Birukov KG, Levonen AL, Binder CJ, Stöckl J. Generation and biological activities of oxidized phospholipids. Antioxid Redox Signal. 2010; 12(8):1009-59.

Boutaud O, Brame CJ, Salomon RG, Roberts LJ 2nd, Oates JA. Characterization of the lysyl adducts formed from prostaglandin H2 via the levuglandin pathway. Biochemistry. 1999; 38(29):9389-96.

Braverman NE & Moser AB. Functions of plasmalogen lipids in health and disease. Biochim Biophys Acta. 2012; 1822(9):1442-52.

Brenton AG & Godfrey AR. Accurate mass measurement: terminology and treatment of data. J Am Soc Mass Spectrom. 2010; 21(11):1821-35.

Brose SA, Thuen BT, Golovko MY. LC/MS/MS method for analysis of E(2) series prostaglandins and isoprostanes. J Lipid Res. 2011; 52(4):850-859.

Brown CD, Kilty I, Yeadon M, Jenkinson S. Regulation of 15-lipoxygenase isozymes and mucin secretion by cytokines in cultured normal human bronchial epithelial cells. Inflamm Res. 2001, 50(6):321-6.

Bruno A, Di Francesco L, Coletta I, Mangano G, Alisi MA, Polenzani L, Milanese C, Anzellotti P, Ricciotti E, Dovizio M, Di Francesco A, Tacconelli S, Capone ML, Patrignani P. Effects of AF3442 [N-(9-ethyl-9H-carbazol-3-yl)-2-(trifluoromethyl)benzamide], a novel inhibitor of human microsomal prostaglandin E synthase-1, on prostanoid biosynthesis in human monocytes in vitro. Biochem Pharmacol. 2010; 79(7):974-81.

Cao J, Shan D, Revett T, Li D, Wu L, Liu W, Tobin JF, Gimeno RE. Molecular identification of a novel mammalian brain isoform of acyl-CoA:lysophospholipid acyltransferase with prominent ethanolamine lysophospholipid acylating activity, LPEAT2. J Biol Chem. 2008; 283(27):19049-57.

Carey F, Menashi S, Crawford N. Localization of cyclo-oxygenase and thromboxane synthetase in human platelet intracellular membranes. Biochem J. 1982; 204(3):847-851.

Chandrasekharan NV & Simmons DL. The cyclooxygenases. Genome Biol. 2004; 5(9):241.

Chaurio RA, Janko C, Muñoz LE, Frey B, Herrmann M, Gaipl US. Phospholipids: key players in apoptosis and immune regulation. Molecules. 2009; 14(12):4892-914.

Chell S, Kaidi A, Williams AC, Paraskeva C. Mediators of PGE2 synthesis and signalling downstream of COX-2 represent potential targets for the prevention/treatment of colorectal cancer. Biochim Biophys Acta. 2006; 1766 (1): 104-119.

Chen C & Bazan NG. Lipid signaling: sleep, synaptic plasticity, and neuroprotection. Prostaglandins Other Lipid Mediat. 2005; 77(1-4):65-76.

Chen H, Locke D, Liu Y, Liu C, Kahn ML. The platelet receptor GPVI mediates both adhesion and signaling responses to collagen in a receptor density-dependent fashion. J Biol Chem. 2002; 277(4):3011-9.

Chi Y, Min J, Jasmin JF, Lisanti MP, Chang YT, Schuster VL. Development of a high-affinity inhibitor of the prostaglandin transporter. J Pharmacol Exp Ther. 2011; 339(2):633-41.

Chilton FH, Fonteh AN, Surette ME, Triggiani M, Winkler JD. Control of arachidonate levels within inflammatory cells. Biochim Biophys Acta. 1996; 1299(1):1-15.

Chung AW, Jurasz P, Hollenberg MD, and Radomski MW. Mechanisms of action of proteinase-activated receptor agonists on human platelets. Br J Pharmacol. 2002; 135 (5): 1123–1132.

Clark SR, Guy CJ, Scurr MJ, Taylor PR, Kift-Morgan AP, Hammond VJ, Thomas CP, Coles B, Roberts GW, Eberl M, Jones SA, Topley N, Kotecha S, O'Donnell VB. Esterified eicosanoids are acutely generated by 5-lipoxygenase in primary human neutrophils and in human and murine infection. Blood. 2011; 117(6):2033-43.

Coffey MJ, Coles B, Locke M, Bermudez-Fajardo A, Williams PC, Jarvis GE, O'donnell VB. Interactions of 12-lipoxygenase with phospholipase A2 isoforms following platelet activation through the glycoprotein VI collagen receptor. FEBS Lett. 2004a; 576(1-2):165-8.

Coffey MJ, Jarvis GE, Gibbins JM, Coles B, Barrett NE, Wylie OR, O'Donnell VB. Platelet 12-lipoxygenase activation via glycoprotein VI: involvement of multiple signaling pathways in agonist control of H(P)ETE synthesis. Circ Res. 2004b; 94(12):1598-605.

Cohen S, Braiman A, Shubinsky G, Isakov N. Protein kinase C-theta in platelet activation. FEBS Lett. 2011; 585(20):3208-15.

Corey SJ & Anderson SM. Src-related protein tyrosine kinases in hematopoiesis. Blood. 1999; 93: 1-14.

Coughlin SR. Thrombin signalling and protease-activated receptors. Nature. 2000; 407(6801):258-64.

Dennis EA. Diversity of group types, regulation, and function of phospholipase A2. J Biol Chem. 1994; 269(18):13057-60.

DeWitt DL & Smith WL. Primary structure of prostaglandin G/H synthase from sheep vesicular gland determined from the complementary DNA sequence. Proc Natl Acad Sci USA 1988, 85:1412-1416.

Dietz R, Nastainczyk W, Ruf HH. Higher oxidation states of prostaglandin H synthase. Rapid electronic spectroscopy detected two spectral intermediates during the peroxidase reaction with prostaglandin G2. Eur J Biochem 1988, 171:321-328.

Dioszeghy V, Rosas M, Maskrey BH, Colmont C, Topley N, Chaitidis P, Kühn H, Jones SA, Taylor PR, O'Donnell VB. 12/15-Lipoxygenase regulates the inflammatory response to bacterial products in vivo. J Immunol. 2008; 181(9):6514-24.

Dogné JM, de Leval X, Delarge J, David JL, Masereel B. New trends in thromboxane and prostacyclin modulators. Curr Med Chem. 2000; 7(6):609-28.

Drake TA, Morrissey JH, Edgington TS. Selective cellular expression of tissue factor in human tissues. Implications for disorders of hemostasis and thrombosis. Am J Pathol. 1989; 134(5):1087-97.

Dugan LL, Demediuk P, Pendley CE 2nd, Horrocks LA. Separation of phospholipids by high-performance liquid chromatography: all major classes, including ethanolamine and choline plasmalogens, and most minor classes, including lysophosphatidylethanolamine. J Chromatogr. 1986; 378 (2): 317-327.

Ebbeling L, Robertson C, McNicol A, Gerrard JM. Rapid ultrastructural changes in the dense tubular system following platelet activation. Blood. 1992; 80(3):718-23.

Eigenbrot C, Kirchhofer D, Dennis MS, Santell L, Lazarus RA, Stamos J, Ultsch MH. The factor VII zymogen structure reveals reregistration of beta strands during activation. Structure. 2001; 9 (7): 627-636.

Fahy E, Cotter D, Sud M, Subramaniam S. Lipid classification, structures and tools. Biochim Biophys Acta. 2011; 1811(11):637-47.

Fahy E, Subramaniam S, Brown HA, Glass CK, Merrill AH Jr, Murphy RC, Raetz CR, Russell DW, Seyama Y, Shaw W, Shimizu T, Spener F, van Meer G, VanNieuwenhze MS, White SH, Witztum JL, Dennis EA. A comprehensive classification system for lipids. J Lipid Res. 2005; 46 (5): 839-861.

Falls LA, Furie B, Furie BC. Role of phosphatidylethanolamine in assembly and function of the factor IXa-factor VIIIa complex on membrane surfaces. Biochemistry. 2000; 39(43):13216-22.

Fay PJ. Activation of factor VIII and mechanisms of cofactor action. Blood Rev. 2004; 18(1):1-15.

Fenn JB, Mann M, Meng CK, Wong SF, Whitehouse CM. Electrospray ionization for mass spectrometry of large biomolecules. Science. 1989; 246 (4926): 64-71.

Fiddler GI & Lumley P. Preliminary clinical studies with thromboxane synthase inhibitors and thromboxane receptor blockers. A review. Circulation. 1990; 81(1 Suppl):I69-78; discussion I79-80.

Furman MI, Liu L, Benoit SE, Becker RC, Barnard MR, Michelson AD. The cleaved peptide of the thrombin receptor is a strong platelet agonist. Proc Natl Acad Sci U S A. 1998; 95(6):3082-7.

Furman MI, Nurden P, Berndt MC, Nurden AT, Benoit SE, Barnard MR, Ofosu FA, Michelson AD. The cleaved peptide of PAR1 results in a redistribution of the platelet surface GPIb-IX-V complex to the surface-connected canalicular system. Thromb Haemost. 2000; 84(5):897-903.

Gargalovic PS, Imura M, Zhang B, Gharavi NM, Clark MJ, Pagnon J, Yang WP, He A, Truong A, Patel S, Nelson SF, Horvath S, Berliner JA, Kirchgessner TG, Lusis AJ. Identification of

inflammatory gene modules based on variations of human endothelial cell responses to oxidized lipids. Proc Natl Acad Sci U S A. 2006; 103(34):12741-6.

Gerrard JM, White JG, Rao GH, Townsend D. Localization of platelet prostaglandin production in the platelet dense tubular system. Am J Pathol. 1976; 83(2):283-298.

Gerszten RE, Chen J, Ishii M, Ishii K, Wang L, Nanevicz T, Turck CW, Vu TK, Coughlin SR. Specificity of the thrombin receptor for agonist peptide is defined by its extracellular surface. Nature. 1994; 368(6472):648-51.

Gilroy DW, Tomlinson A, Willoughby DA. Differential effects of inhibitors of cyclooxygenase (cyclooxygenase 1 and cyclooxygenase 2) in acute inflammation. Eur J Pharmacol. 1998; 355(2-3):211-7.

Goldblatt MW. A depressor substance in seminal fluid. J Soc Chem Ind 1933; 52:1056–1057.

Goppelt-Struebe M, Koerner CF, Hausmann G, Gemsa D, Resch K. Control of prostanoid synthesis: role of reincorporation of released precursor fatty acids. Prostaglandins. 1986; 32(3):373-85.

Greenberg ME, Li XM, Gugiu BG, Gu X, Qin J, Salomon RG, Hazen SL. The lipid whisker model of the structure of oxidized cell membranes. J Biol Chem. 2008; 283(4):2385-96.

Greene ER, Huang S, Serhan CN, Panigrahy D. Regulation of inflammation in cancer by eicosanoids. Prostaglandins Other Lipid Mediat. 2011; 96 (1-4): 27-36.

Grob R & Barry E. Modern Practice of Gas Chromatography. Wiley-Interscience, 2004, pp. 817-818.

Gross ML. Accurate Masses for Structure Confirmation. J. Am. Soc. Mass Spectrom 1994; 5 (2): 57.

Gryglewski RJ, Dembínska-Kieć A, Korbut R. A possible role of thromboxane A2 (TXA2) and prostacyclin (PGI2) in circulation. Acta Biol Med Ger. 1978; 37(5-6):715-23.

Habenicht AJ, Goerig M, Grulich J, Rothe D, Gronwald R, Loth U, Schettler G, Kommerell B, and Ross R. Human platelet-derived growth factor stimulates prostaglandin synthesis by activation and by rapid de novo synthesis of cyclooxygenase. J Clin Investig 1985; 75:1381–1387.

Halket JM, Waterman D, Przyborowska AM, Patel RK, Fraser PD, Bramley PM. Chemical derivatization and mass spectral libraries in metabolic profiling by GC/MS and LC/MS/MS. J Exp Bot. 2005; 56(410):219-43.

Hall SL & Lorenc T. Secondary prevention of coronary artery disease. Am Fam Physician. 2010; 81(3):289-96.

Hamberg M & Samuelsson B. Detection and isolation of an endoperoxide intermediate in prostaglandin biosynthesis. Proc Natl Acad Sci USA 1973; 70: 899- 903.

Hamberg M, Svensson J, and Samuelsson B. Prostaglandin endoperoxides. A new concept concerning the mode of action of prostaglandins. Proc Natl Acad Sci USA 1974; 71: 3824–3828.

Hamberg M, Svensson J, Samuelsson B. Thromboxanes: a new group of biologically active compounds derived from prostaglandin endoperoxides. Proc Natl Acad Sci U S A. 1975; 72(8): 2994–2998.

Hammond VJ & O'Donnell VB. Esterified eicosanoids: Generation, characterization and function. Biochim Biophys Acta. 2012; 1818(10):2403-12.

Hammond VJ, Morgan AH, Lauder S, Thomas CP, Brown S, Freeman BA, Lloyd CM, Davies J, Bush A, Levonen AL, Kansanen E, Villacorta L, Chen YE, Porter N, Garcia-Diaz YM, Schopfer FJ, O'Donnell VB. Novel keto-phospholipids are generated by monocytes and macrophages, detected in cystic fibrosis, and activate peroxisome proliferator-activated receptor-γ. J Biol Chem. 2012; 287(50):41651-66.

Harper MT & Poole AW. Diverse functions of protein kinase C isoforms in platelet activation and thrombus formation. J Thromb Haemost. 2010; 8(3):454-62.

Hartman EJ, Omura S, Laposata M. Triacsin C: a differential inhibitor of arachidonoyl-CoA synthetase and nonspecific long chain acyl-CoA synthetase. Prostaglandins. 1989; 37(6):655-71.

Hayaishi O. Sleep-wake regulation by prostaglandins D2 and E2. J Biol Chem. 1988; 263(29):14593-6.

He F, Liu W, Zheng S, Zhou L, Ye B, Qi Z. Ion transport through dimethyl sulfoxide (DMSO) induced transient water pores in cell membranes. Mol Membr Biol. 2012; 29(3-4):107-13.

Heemskerk JW, Bevers EM, Lindhout T. Platelet activation and blood coagulation. Thromb Haemost. 2002; 88(2):186-93.

Heemskerk JW, Farndale RW, Sage SO. Effects of U73122 and U73343 on human platelet calcium signalling and protein tyrosine phosphorylation. Biochim Biophys Acta. 1997; 1355(1):81-8.

Hemker HC, Giesen P, Al Dieri R, Regnault V, de Smedt E, Wagenvoord R, Lecompte T, Béguin S. Calibrated automated thrombin generation measurement in clotting plasma. Pathophysiol Haemost Thromb. 2003; 33(1):4-15.

Hemler M, Lands WEM, Smith WL. Purification of the cyclooxygenase that forms prostaglandins: demonstration of two forms of iron in the holoenzyme. J Biol Chem 1976, 251:5575-5579.

Heptinstall S, Espinosa DI, Manolopoulos P, Glenn JR, White AE, Johnson A, Dovlatova N, Fox SC, May JA, Hermann D, Magnusson O, Stefansson K, Hartman D, Gurney M. DG-041 inhibits the EP3 prostanoid receptor--a new target for inhibition of platelet function in atherothrombotic disease. Platelets. 2008; 19(8):605-13.

Higashi S, Matsumoto N, Iwanaga S. Molecular mechanism of tissue factor-mediated acceleration of factor VIIa activity. J Biol Chem. 1996; 271 (43): 26569-26574.

Hikiji H, Takato T, Shimizu T, Ishii S. The roles of prostanoids, leukotrienes, and platelet-activating factor in bone metabolism and disease. Prog Lipid Res. 2008; 47(2):107-26.

Hirai H, Tanaka K, Yoshie O, Ogawa K, Kenmotsu K, Takamori Y, Ichimasa M, Sugamura K, Nakamura M, Takano S, Nagata K. Prostaglandin D2 selectively induces chemotaxis in T helper type 2 cells, eosinophils, and basophils via seven-transmembrane receptor CRTH2. J Exp Med. 2001; 193(2):255-61.

Hisanaga Y, Ago H, Nakagawa N, Hamada K, Ida K, Yamamoto M, Hori T, Arii Y, Sugahara M, Kuramitsu S, Yokoyama S, Miyano M. Structural basis of the substrate-specific two-step catalysis of long chain fatty acyl-CoA synthetase dimer. J Biol Chem. 2004; 279(30):31717-26.

Hisatsune C, Nakamura K, Kuroda Y, Nakamura T, Mikoshiba K. Amplification of Ca2+ signaling by diacylglycerol-mediated inositol 1,4,5-trisphosphate production. J Biol Chem. 2005; 280(12):11723-30.

Hornberger W & Patscheke H. Primary stimuli of icosanoid release inhibit arachidonoyl-CoA synthetase and lysophospholipid acyltransferase. Mechanism of action of hydrogen peroxide and methyl mercury in platelets. Eur J Biochem. 1990; 187(1):175-81.

Huang JT, Welch JS, Ricote M, Binder CJ, Willson TM, Kelly C, Witztum JL, Funk CD, Conrad D, Glass CK. Interleukin-4-dependent production of PPAR-gamma ligands in macrophages by 12/15-lipoxygenase. Nature. 1999; 400(6742):378-82.

Hunter SA, Burstein S, Sedor C. Stimulation of prostaglandin synthesis in WI-38 human lung fibroblasts following inhibition of phospholipid acylation by p-hydroxymercuribenzoate. Biochim Biophys Acta. 1984; 793(2):202-12.

Igal RA, Wang P, Coleman RA. Triacsin C blocks de novo synthesis of glycerolipids and cholesterol esters but not recycling of fatty acid into phospholipid: evidence for functionally separate pools of acyl-CoA. Biochem J. 1997; 324(Pt 2): 529-534.

Italiano JE, Patel-Hett S, Hartwig JH. Mechanics of proplatelet elaboration. J Thromb Haemost. 2007; 5 (1):18-23.

Jakobsson A, Westerberg R, Jacobsson A. Fatty acid elongases in mammals: their regulation and roles in metabolism. Prog Lipid Res. 2006; 45(3):237-49.

Jedlitschky G, Tirschmann K, Lubenow LE, Nieuwenhuis HK, Akkerman JW, Greinacher A, Kroemer HK. The nucleotide transporter MRP4 (ABCC4) is highly expressed in human platelets and present in dense granules, indicating a role in mediator storage. Blood. 2004; 104(12):3603-10.

Jurk K & Kehrel BE. Platelets: physiology and biochemistry. Semin Thromb Hemost. 2005; 31(4):381-92.

Kahn ML, Zheng YW, Huang W, Bigornia V, Zeng D, Moff S, Farese RV Jr, Tam C, Coughlin SR. A dual thrombin receptor system for platelet activation. Nature. 1998; 394(6694):690-4.

Kalinski P. Regulation of immune responses by prostaglandin E2. J Immunol. 2012; 188(1):21-8.

Kang YJ, Mbonye UR, DeLong CJ, Wada M, Smith WL. Regulation of intracellular cyclooxygenase levels by gene transcription and protein degradation. Prog Lipid Res. 2007; 46(2):108-25.

Kaplan ZS & Jackson SP. The role of platelets in atherothrombosis. Hematology Am Soc Hematol Educ Program. 2011; 2011:51-61.

Karni R, Mizrachi S, Reiss-Sklan E, Gazit A, Livnah O, Levitzki A. The pp60c-Src inhibitor PP1 is non-competitive against ATP. FEBS Lett. 2003; 537(1-3):47-52.

Kasirer-Friede A, Legrand C, Frojmovic MM. Thrombin receptor occupancy modulates aggregation efficiency and platelet surface expression of vWF and thrombospondin at low thrombin concentrations. Thromb Haemost. 1999; 81(6):967-75.

Kawao N, Nagataki M, Nagasawa K, Kubo S, Cushing K, Wada T, Sekiguchi F, Ichida S, Hollenberg MD, MacNaughton WK, Nishikawa H, Kawabata A. Signal transduction for proteinase-activated receptor-2-triggered prostaglandin E2 formation in human lung epithelial cells. J Pharmacol Exp Ther. 2005; 315(2):576-89.

Kim Y, George D, Prior AM, Prasain K, Hao S, Le DD, Hua DH, Changa K. Novel Triacsin C Analogs as Potential Antivirals against Rotavirus Infections. Eur J Med Chem. 2012; 50: 311–318.

Knapp HR, Oelz O, Roberts LJ, Sweetman BJ, Oates JA, Reed PW. Ionophores stimulate prostaglandin and thromboxane biosynthesis. Proc Natl Acad Sci U S A. 1977; 74(10): 4251-4255.

Kondo M, Tamaoki J, Takeyama K, Isono K, Kawatani K, Izumo T, Nagai A. Elimination of IL-13 reverses established goblet cell metaplasia into ciliated epithelia in airway epithelial cell culture. Allergol Int. 2006; 55(3):329-36.

Kondo M, Tamaoki J, Takeyama K, Nakata J, Nagai A. Interleukin-13 induces goblet cell differentiation in primary cell culture from Guinea pig tracheal epithelium. Am J Respir Cell Mol Biol. 2002; 27(5):536-41.

Kozak KR & Marnett LJ. Oxidative metabolism of endocannabinoids. Prostaglandins Leukot Essent Fatty Acids. 2002; 66(2-3):211-20.

Kozak KR, Crews BC, Morrow JD, Wang LH, Ma YH, Weinander R, Jakobsson PJ, Marnett LJ. Metabolism of the endocannabinoids, 2-arachidonylglycerol and anandamide, into prostaglandin, thromboxane, and prostacyclin glycerol esters and ethanolamides. J Biol Chem. 2002; 277(47):44877-85.

Kozak KR, Rowlinson SW, Marnett LJ. Oxygenation of the endocannabinoid, 2-arachidonylglycerol, to glyceryl prostaglandins by cyclooxygenase-2. J Biol Chem. 2000; 275(43):33744-9.

Kraemer SA, Meade EA, DeWitt DL. Prostaglandin endoperoxide synthase gene structure: identification of the transcriptional start site and 5'-flanking regulatory sequences. Arch Biochem Biophys. 1992; 293(2):391-400.

Kramer RM, Roberts EF, Manetta JV, Hyslop PA, Jakubowski JA. Thrombin-induced phosphorylation and activation of Ca(2+)-sensitive cytosolic phospholipase A2 in human platelets. J Biol Chem. 1993; 268(35):26796-804.

Kramer RM, Roberts EF, Strifler BA, Johnstone EM. Thrombin induces activation of p38 MAP kinase in human platelets. J Biol Chem. 1995; 270(46):27395-8.

Kramer RM, Roberts EF, Um SL, Börsch-Haubold AG, Watson SP, Fisher MJ, Jakubowski JA. p38 mitogen-activated protein kinase phosphorylates cytosolic phospholipase A2 (cPLA2) in thrombin-stimulated platelets. Evidence that proline-directed phosphorylation is not required for mobilization of arachidonic acid by cPLA2. J Biol Chem. 1996; 271(44):27723-9.

Kuhn H & Thiele BJ. The diversity of the lipoxygenase family. Many sequence data but little information on biological significance. FEBS Lett. 1999; 449(1):7-11.

Kunze H, Ghooi RB, Bohn E, Le-Kim D. Phosphatidylethanolamide derivatives of prostaglandins E1 and E2. Prostaglandins. 1976; 12(6):1005-17.

Kurumbail RG, Stevens AM, Gierse JK, McDonald JJ, Stegeman RA, Pak JY, Gildehaus D, Miyashiro JM, Penning TD, Seibert K, Isakson PC, Stallings WC. Structural basis for selective inhibition of cyclooxygenase-2 by anti-inflammatory agents. Nature. 1996; 384(6610):644-8.

Kyrle PA, Eichler HG, Jäger U, Lechner K. Inhibition of prostacyclin and thromboxane A2 generation by low-dose aspirin at the site of plug formation in man in vivo. Circulation. 1987; 75(5):1025-9.

Langenbach R, Morham SG, Tiano HF, Loftin CD, Ghanayem BI, Chulada PC, Mahler JF, Lee CA, Goulding EH, Kluckman KD, Kim HS, Smithies O. Prostaglandin synthase 1 gene disruption in mice reduces arachidonic acid-induced inflammation and indomethacin-induced gastric ulceration. Cell. 1995; 83(3):483-92.

Legler DF, Bruckner M, Uetz-von Allmen E, Krause P. Prostaglandin E2 at new glance: novel insights in functional diversity offer therapeutic chances. nt J Biochem Cell Biol. 2010; 42(2):198-201.

Lentz BR. Exposure of platelet membrane phosphatidylserine regulates blood coagulation. Prog Lipid Res. 2003; 42(5):423-38.

Levy R. The role of cytosolic phospholipase A2-alfa in regulation of phagocytic functions. Biochim Biophys Acta. 2006; 1761(11):1323-34.

Lewin TM, Kim JH, Granger DA, Vance JE, Coleman RA. Acyl-CoA synthetase isoforms 1, 4, and 5 are present in different subcellular membranes in rat liver and can be inhibited independently. J Biol Chem. 2001; 276(27):24674-9.

Li R, Mouillesseaux KP, Montoya D, Cruz D, Gharavi N, Dun M, Koroniak L, Berliner JA. Identification of prostaglandin E2 receptor subtype 2 as a receptor activated by OxPAPC. Circ Res. 2006; 98(5):642-50.

Li Z, Delaney MK, O'Brien KA, Du X. Signaling during platelet adhesion and activation. Arterioscler Thromb Vasc Biol. 2010; 30(12):2341-9.

Liberty IF, Raichel L, Hazan-Eitan Z, Pessach I, Hadad N, Schlaeffer F, Levy R. Cytosolic phospholipase A2 is responsible for prostaglandin E2 and leukotriene B4 formation in phagocyte-like PLB-985 cells: studies of differentiated cPLA2-deficient PLB-985 cells. J Leukoc Biol. 2004; 76(1):176-84.

Loll PJ, Picot D, Garavito RM. The structural basis of aspirin activity inferred from the crystal structure of inactivated prostaglandin H2 synthase. Nat Struct Biol. 1995; 2(8):637-643.

Lordkipanidzé M, Pharand C, Schampaert E, Turgeon J, Palisaitis DA, Diodati JG. A comparison of six major platelet function tests to determine the prevalence of aspirin resistance in patients with stable coronary artery disease. Eur Heart J. 2007; 28(14):1702-8.

Luong C, Miller A, Barnett J, Chow J, Ramesha C, Browner MF. Flexibility of the NSAID binding site in the structure of human cyclooxygenase-2. Nat Struct Biol. 1996; 3(11):927-33.

Lysz TW & Needleman P. Evidence for two distinct forms of fatty acid cyclooxygenase in brain. J Neurochem 1982; 38:1111–1117.

Lysz TW, Zweig A, Keeting PE. Examination of mouse and rat tissues for evidence of dual forms of the fatty acid cyclooxygenase. Biochem Pharmacol 1988; 37:921–927.

Macfarlane SR, Seatter MJ, Kanke T, Hunter GD, Plevin R. Proteinase-activated receptors. Pharmacol Rev. 2001; 53(2):245-82.

Mackman N. The role of tissue factor and factor VIIa in hemostasis. Anesth Analg. 2009; 108(5):1447-52.

Mahmud I, Ueda N, Yamaguchi H, Yamashita R, Yamamoto S, Kanaoka Y, Urade Y, Hayaishi O. Prostaglandin D synthase in human megakaryoblastic cells. J Biol Chem. 1997; 272(45):28263-6.

Makarov A & Scigelova M. Coupling liquid chromatography to Orbitrap mass spectrometry. J Chromatogr A. 2010; 1217 (25): 3938-3945.

Makarov A. Electrostatic axially harmonic orbital trapping: a high-performance technique of mass analysis. Anal Chem. 2000; 72 (6): 1156-1162.

Mann M, Hendrickson RC, Pandey A. Analysis of proteins and proteomes by mass spectrometry. Annu Rev Biochem. 2001; 70: 437-473.

Marcus AJ, Ullman HL, Safier LB. Lipid composition of subcellular particles of human blood platelets. J Lipid Res. 1969; 10 (1): 108-114.

Marnett LJ, Rowlinson SW, Goodwin DC, Kalgutkar AS, Lanzo CA. Arachidonic acid oxygenation by COX-1 and COX-2. Mechanisms of catalysis and inhibition. J Biol Chem. 1999; 274 (33): 22903-22906.

Marshall PJ & Kulmacz RJ. Prostaglandin H synthase: distinct binding sites for cyclooxygenase and peroxidase substrates. Arch Biochem Biophys 1988; 266:162–170.

Marshall PJ, Kulmacz RJ, Lands WE. Constraints on prostaglandin biosynthesis in tissues. J Biol Chem. 1987; 262(8):3510-7.

Martin TF. PI(4,5)P(2) regulation of surface membrane traffic. Curr Opin Cell Biol. 2001; 13(4):493-9.

Maskrey BH & O'Donnell VB. Analysis of eicosanoids and related lipid mediators using mass spectrometry. Biochem Soc Trans. 2008; 36 (Pt 5): 1055-1059.

Maskrey BH, Bermudez-Fajardo A, Morgan AH, Stewart-Jones E, Dioszeghy V, Taylor GW, Baker PR, Coles B, Coffey MJ, Kuhn H, O'Donnell VB. Activated platelets and monocytes generate four hydroxyphosphatidylethanolamines via lipoxygenase. J Biol Chem. 2007; 282(28):20151-20163.

Masoodi M, Eiden M, Koulman A, Spaner D, Volmer DA. Comprehensive lipidomics analysis of bioactive lipids in complex regulatory networks. Anal Chem. 2010; 82 (19): 8176-8185.

McClelland S, Gawaz M, Kennerknecht E, Konrad CS, Sauer S, Schuerzinger K, Massberg S, Fitzgerald DJ, Belton O. Contribution of cyclooxygenase-1 to thromboxane formation, platelet-vessel wall interactions and atherosclerosis in the ApoE null mouse. Atherosclerosis. 2009; 202(1):84-91.

McNicol A & Shibou TS. Translocation and phosphorylation of cytosolic phospholipase A2 in activated platelets. Thromb Res. 1998; 92(1):19-26.

Merlie JP, Fagan D, Mudd J, Needleman P. Isolation and characterization of the complementary DNA for sheep seminal vesicle prostaglandin endoperoxide synthase (cyclooxygenase). J Biol Chem 1988, 263:3550-3553.

Michalski A, Damoc E, Lange O, Denisov E, Nolting D, Müller M, Viner R, Schwartz J, Remes P, Belford M, Dunyach JJ, Cox J, Horning S, Mann M, Makarov A. Ultra high resolution linear ion trap Orbitrap mass spectrometer (Orbitrap Elite) facilitates top down LC MS/MS and versatile peptide fragmentation modes. Mol Cell Proteomics. 2012; 11 (3): O111.013698.

Miller YI, Chang MK, Funk CD, Feramisco JR, Witztum JL. 12/15-lipoxygenase translocation enhances site-specific actin polymerization in macrophages phagocytosing apoptotic cells. J Biol Chem. 2001; 276(22):19431-9.

Miyamoto T, Ogino N, Yamamoto S, Hayaishi O. Purification of prostaglandin endoperoxide synthetase from bovine vesicular gland microsomes. J Biol Chem 1976, 251:2629-2636.

Miyamoto T, Yamamoto S, Hayaishi O. Prostaglandin synthetase system-resolution into oxygenase and isomerase components. Proc Natl Acad Sci U S A. 1974; 71 (9): 3645-3648.

Morcillo EJ & Cortijo J. Mucus and MUC in asthma. Curr Opin Pulm Med. 2006, 12(1):1-6.

Morgan AH, Dioszeghy V, Maskrey BH, Thomas CP, Clark SR, Mathie SA, Lloyd CM, Kühn H, Topley N, Coles BC, Taylor PR, Jones SA, O'Donnell VB. Phosphatidylethanolamine-esterified eicosanoids in the mouse: tissue localization and inflammation-dependent formation in Th-2 disease. J Biol Chem. 2009; 284(32):21185-91.

Morgan LT, Thomas CP, Kuhn H, O'Donnell VB. Thrombin-activated human platelets acutely generate oxidized docosahexaenoic-acid-containing phospholipids via 12-lipoxygenase. Biochem J. 2010; 431(1):141-148.

Morita I, Schindler M, Regier MK, Otto JC, Hori T, DeWitt DL, Smith WL. Different intracellular locations for prostaglandin endoperoxide H synthase-1 and -2. J Biol Chem. 1995; 270(18):10902-8.

Morrissey JH, Tajkhorshid E, Rienstra CM. Nanoscale studies of protein-membrane interactions in blood clotting. J Thromb Haemost. 2011; 9 Suppl 1:162-7.

Murakami M. Lipid mediators in life science. Exp Anim. 2011; 60(1):7-20.

Murphy R. Mass Spectrometry of Phospholipids: Tables of Molecular and Product Ions. Illuminati Press, Denver. 2002

Murphy RC, Barkley RM, Zemski Berry K, Hankin J, Harrison K, Johnson C, Krank J, McAnoy A, Uhlson C, Zarini S. Electrospray ionization and tandem mass spectrometry of eicosanoids. Anal Biochem. 2005; 346(1):1-42.

Murugappan S, Shankar H, Bhamidipati S, Dorsam RT, Jin J, Kunapuli SP. Molecular mechanism and functional implications of thrombin-mediated tyrosine phosphorylation of PKCdelta in platelets. Blood. 2005; 106(2):550-7.

Mustard JF, Kinlough-Rathbone RL, Packham MA. Prostaglandins and platelets. Annu Rev Med. 1980; 31:89-96.

Nagan N & Zoeller RA. Plasmalogens: biosynthesis and functions. Prog Lipid Res. 2001; 40(3):199-229.

Nakahata N. Thromboxane A2: physiology/pathophysiology, cellular signal transduction and pharmacology. Pharmacol Ther. 2008; 118(1):18-35.

Nayak MK, Kulkarni PP, Dash D. Regulatory role of proteasome in determination of platelet life span. J Biol Chem. 2013; 288(10):6826-34.

Necela BM, Su W, Thompson EA. Toll-like receptor 4 mediates cross-talk between peroxisome proliferator-activated receptor gamma and nuclear factor-kappaB in macrophages. Immunology. 2008; 125(3):344-58.

Niki E. Lipid peroxidation: physiological levels and dual biological effects. Free Radic Biol Med. 2009; 47(5):469-84.

Nirodi CS, Crews BC, Kozak KR, Morrow JD, Marnett LJ. The glyceryl ester of prostaglandin E2 mobilizes calcium and activates signal transduction in RAW264.7 cells. Proc Natl Acad Sci U S A. 2004; (7):1840-1845.

Noguchi K, Shitashige M, Yanai M, Morita I, Nishihara T, Murota S, Ishikawa I. Prostaglandin production via induction of cyclooxygenase-2 by human gingival fibroblasts stimulated with lipopolysaccharides. Inflammation. 1996; 20(5):555-68.

O'Brien PJ & Rahimtula A. The possible involvement of a peroxidase in prostaglandin biosynthesis. Biochem Biophys Res Commun. 1976; 70 (3): 832-838.

Ogino N, Ohki S, Yamamoto S, and Hayaishi O. Prostaglandin endoperoxide synthetase from bovine vesicular gland microsomes: inactivation and activation by heme and other metalloporphyrins. J Biol Chem 1978; 253:5061–5068.

Otto JC & Smith WL. Prostaglandin endoperoxide synthases-1 and -2. J Lipid Mediat Cell Signal. 1995; 12(2-3):139-56.

Otto JC & Smith WL. The orientation of prostaglandin endoperoxide synthases-1 and -2 in the endoplasmic reticulum. J Biol Chem. 1994; 269 (31): 19868-19875.

Parazzoli S, Harmon JS, Vallerie SN, Zhang T, Zhou H, Robertson RP. Cyclooxygenase-2, not microsomal prostaglandin E synthase-1, is the mechanism for interleukin-1β-induced prostaglandin E2 production and inhibition of insulin secretion in pancreatic islets. J Biol Chem. 2012; 287(38):32246-53.

Perry RH, Cooks RG, Noll RJ. Orbitrap mass spectrometry: instrumentation, ion motion and applications. Mass Spectrom Rev. 2008; 27 (6): 661-699.

Petrucci G, De Cristofaro R, Rutella S, Ranelletti FO, Pocaterra D, Lancellotti S, Habib A, Patrono C, Rocca B. Prostaglandin E2 differentially modulates human platelet function through the prostanoid EP2 and EP3 receptors. J Pharmacol Exp Ther. 2011; 336(2):391-402.

Pickering W, Gray E, Goodall AH, Barrowcliffe TW. Effects of apoptosis and lipid peroxidation on T-lymphoblastoid phospholipid-dependent procoagulant activity. J Thromb Haemost. 2008, 6(7):1122-30.

Pickett WC, Jesse RL, Cohen P. Initiation of phospholipase A2 activity in human platelets by the calcium ion ionophore A23187. Biochim Biophys Acta. 1976; 486(1):209-13.

Picot D, Loll PJ, Garavito RM. The X-ray crystal structure of the membrane protein prostaglandin H2 synthase-1. Nature. 1994; 367(6460):243-9.

Podrez EA, Poliakov E, Shen Z, Zhang R, Deng Y, Sun M, Finton PJ, Shan L, Febbraio M, Hajjar DP, Silverstein RL, Hoff HF, Salomon RG, Hazen SL. A novel family of atherogenic oxidized phospholipids promotes macrophage foam cell formation via the scavenger receptor CD36 and is enriched in atherosclerotic lesions. J Biol Chem. 2002; 277(41):38517-23.

Powis G, Bonjouklian R, Berggren MM, Gallegos A, Abraham R, Ashendel C, Zalkow L, Matter WF, Dodge J, Grindey G, Vlahos CJ. Wortmannin, a potent and selective inhibitor of phosphatidylinositol-3-kinase. Cancer Res. 1994; 54(9):2419-23.

Putney JW Jr. The role of phosphoinositide metabolism in signal transduction in secretory cells. J Exp Biol. 1988; 139:135-50.

Rajtar G, Cerletti C, Castagnoli MN, Bertelé V, de Gaetano G. Prostaglandins and human platelet aggregation. Implications for the anti-aggregating activity of thromboxane-synthase inhibitors. Biochem Pharmacol. 1985; 34(3):307-10.

Regier MK, Otto JC, DeWitt DL, Smith WL. Localization of prostaglandin endoperoxide synthase-1 to the endoplasmic reticulum and nuclear envelope is independent of its C-terminal tetrapeptide-PTEL. Arch Biochem Biophys. 1995; 317(2):457-463.

Reid G, Wielinga P, Zelcer N, van der Heijden I, Kuil A, de Haas M, Wijnholds J, Borst P. The human multidrug resistance protein MRP4 functions as a prostaglandin efflux transporter and is inhibited by nonsteroidal antiinflammatory drugs. Proc Natl Acad Sci U S A. 2003; 100(16):9244-9.

Ricciotti E & FitzGerald GA. Prostaglandins and inflammation. Arterioscler Thromb Vasc Biol. 2011; 31(5):986-1000.

Rittenhouse SE. Phosphoinositide 3-kinase activation and platelet function. Blood. 1996; 88(12):4401-14.

Rocca B & Petrucci G. Variability in the responsiveness to low-dose aspirin: pharmacological and disease-related mechanisms. Thrombosis. 2012; 2012:376721.

Rodrigues M, Fitscha P, Sinzinger H. Synergistic antiplatelet action of nitric oxide (NO) with PGD2 and its metabolite PGJ2--relevance for cerebral circulation? J Physiol Pharmacol. 1994; 45(4):533-9.

Rosenthal MD & Hill JR. Elongation of arachidonic and eicosapentaenoic acids limits their availability for thrombin-stimulated release from the glycerolipids of vascular endothelial cells. Biochim Biophys Acta. 1986; 875(2):382-91.

Roth GJ, Stanford N, Majerus PW. Acetylation of prostaglandin synthase by aspirin. Proc Natl Acad Sci U S A. 1975; 72(8):3073-6.

Rouzer CA & Marnett LJ. Cyclooxygenases: structural and functional insights. J Lipid Res. 2009; 50 Suppl:S29-34.

Rouzer CA & Marnett LJ. Endocannabinoid oxygenation by cyclooxygenases, lipoxygenases, and cytochromes P450: cross-talk between the eicosanoid and endocannabinoid signaling pathways. Chem Rev. 2011; 111(10): 5899-5921.

Rouzer CA & Marnett LJ. Mechanism of free radical oxygenation of polyunsaturated fatty acids by cyclooxygenases. Chem Rev. 2003; 103(6):2239-304.

Roy B & Cathcart MK. Induction of 15-lipoxygenase expression by IL-13 requires tyrosine phosphorylation of Jak2 and Tyk2 in human monocytes. J Biol Chem. 1998; 273(48):32023-9.

Salomon R, Miller, DB, Raychaudhuri, SR, Avasthi, K, Lal, K, Levison, BS. Asymmetric Total Synthesis of Levuglandin E2. J Am Chem Soc. 1984; 106:8296-8298.

Sandig H, Pease JE, Sabroe I. Contrary prostaglandins: the opposing roles of PGD2 and its metabolites in leukocyte function. J Leukoc Biol. 2007; 81(2):372-82.

Sang N, Zhang J, Chen C. COX-2 oxidative metabolite of endocannabinoid 2-AG enhances excitatory glutamatergic synaptic transmission and induces neurotoxicity. J Neurochem. 2007; 102(6):1966-77.

Sang N, Zhang J, Chen C. PGE2 glycerol ester, a COX-2 oxidative metabolite of 2-arachidonoyl glycerol, modulates inhibitory synaptic transmission in mouse hippocampal neurons. J Physiol. 2006; 572(Pt 3):735-45.

Saunders MA, Belvisi MG, Cirino G, Barnes PJ, Warner TD, Mitchell JA. Mechanisms of prostaglandin E2 release by intact cells expressing cyclooxygenase-2: evidence for a 'two-component' model. J Pharmacol Exp Ther. 1999; 288(3):1101-6.

Schick PK & Panetti TS, Platelet and megakaryocyte lipids, in Hemostasis and thrombosis: basic principles and clinical practice, R.W. Colman, Editor. Lippincott Williams & Wilkins: Philadelphia, PA. 2006: 591-604.

Schmidt EE, MacDonald IC, Groom AC. Changes in splenic microcirculatory pathways in chronic idiopathic thrombocytopenic purpura. Blood. 1991; 78 (6): 1485-1489.

Schober LJ, Khandoga AL, Dwivedi S, Penz SM, Maruyama T, Brandl R, Siess W. The role of PGE(2) in human atherosclerotic plaque on platelet EP(3) and EP(4) receptor activation and platelet function in whole blood. J Thromb Thrombolysis. 2011; 32(2):158-66.

Scigelova M, Hornshaw M, Giannakopulos A, Makarov A. Fourier transform mass spectrometry. Mol Cell Proteomics. 2011; 10 (7): M111.009431.

Semple JW, Italiano JE Jr, Freedman J. Platelets and the immune continuum. Nat Rev Immunol. 2011; 11(4):264-74.

Seno T, Inoue N, Gao D, Okuda M, Sumi Y, Matsui K, Yamada S, Hirata KI, Kawashima S, Tawa R, Imajoh-Ohmi S, Sakurai H, Yokoyama M. Involvement of NADH/NADPH oxidase in human platelet ROS production. Thromb Res. 2001; 103(5):399-409.

Shindou H, Hishikawa D, Harayama T, Eto M, Shimizu T. Generation of membrane diversity by lysophospholipid acyltransferases. J Biochem. 2013; 154(1):21-8.

Simmons DL, Botting RM, Hla T. Cyclooxygenase isozymes: the biology of prostaglandin synthesis and inhibition. Pharmacol Rev. 2004; 56(3):387-437.

Simmons DL, Xie W, Chipman JG, Evett GE. Multiple cyclooxygenases: Cloning of an inducible form, in Prostaglandins, Leukotrienes, Lipoxins and PAF. Bailey JM ed. 1991; 67–78, Plenum Press, New York.

Sims PJ, Wiedmer T, Esmon CT, Weiss HJ, Shattil SJ. Assembly of the platelet prothrombinase complex is linked to vesiculation of the platelet plasma membrane. Studies in Scott syndrome: an isolated defect in platelet procoagulant activity. J Biol Chem. 1989; 264(29):17049-57.

Sinha AK, Rao AK, Willis J, Colman RW. Inhibition of thromboxane A2 synthesis in human platelets by coagulation factor Xa. Proc Natl Acad Sci U S A. 1983; 80(19):6086-90.

Smith CJ, Zhang Y, Koboldt CM, Muhammad J, Zweifel BS, Shaffer A, Talley JJ, Masferrer JL, Seibert K, Isakson PC. Pharmacological analysis of cyclooxygenase-1 in inflammation. Proc Natl Acad Sci U S A. 1998; 95(22):13313-8.

Smith JB, Dangelmaier C, Mauco G. Measurement of arachidonic acid liberation in thrombin-stimulated human platelets. Use of agents that inhibit both the cyclooxygenase and lipoxygenase enzymes. Biochim Biophys Acta. 1985; 835(2):344-51.

Smith JB, Silver MJ, Ingerman CM, Kocsis JJ. Prostaglandin D2 inhibits the aggregation of human platelets. Thromb Res. 1974; 5(3):291-9.

Smith JP, Haddad EV, Downey JD, Breyer RM, Boutaud O. PGE2 decreases reactivity of human platelets by activating EP2 and EP4. Thromb Res. 2010; 126(1):e23-9.

Smith WL & Lands WE. Oxygenation of polyunsaturated fatty acids during prostaglandin biosynthesis by sheep vesicular gland. Biochemistry 1972; 11: 3276–3285.

Smith WL, DeWitt DL, Garavito RM. Cyclooxygenases: structural, cellular, and molecular biology. Annu Rev Biochem. 2000; 69:145-182.

Smith WL, Garavito RM, DeWitt DL. Prostaglandin endoperoxide H synthases (cyclooxygenases)-1 and -2. J Biol Chem. 1996; 271(52):33157-60.

Smith WL, Urade Y, Jakobsson PJ. Enzymes of the cyclooxygenase pathways of prostanoid biosynthesis. Chem Rev. 2011; 111(10):5821-65.

Smith WL. Prostanoid biosynthesis and mechanisms of action. Am J Physiol. 1992; 263(2 Pt 2):F181-91.

Song WL, Stubbe J, Ricciotti E, Alamuddin N, Ibrahim S, Crichton I, Prempeh M, Lawson JA, Wilensky RL, Rasmussen LM, Puré E, FitzGerald GA. Niacin and biosynthesis of PGD_2 by platelet COX-1 in mice and humans. J Clin Invest. 2012; 122(4):1459-68.

Spencer AG, Woods JW, Arakawa T, Singer II, Smith WL. Subcellular localization of prostaglandin endoperoxide H synthases-1 and -2 by immunoelectron microscopy. J Biol Chem. 1998; 273(16):9886-93.

Stefanini L, Roden RC, Bergmeier W. CalDAG-GEFI is at the nexus of calcium-dependent platelet activation. Blood. 2009; 114(12):2506-14.

Stoke SH. General, Organic, and Biological Chemistry: Structure of Carboxylic acids and their Derivatives. 6th edition. 2013. Belmont, CA, USA.

Strehl A, Munnix IC, Kuijpers MJ, van der Meijden PE, Cosemans JM, Feijge MA, Nieswandt B, Heemskerk JW. Dual role of platelet protein kinase C in thrombus formation: stimulation of pro-aggregatory and suppression of procoagulant activity in platelets. J Biol Chem. 2007; 282(10):7046-55.

Suzuki H, Kawarabayasi Y, Kondo J, Abe T, Nishikawa K, Kimura S, Hashimoto T, Yamamoto T. Structure and regulation of rat long-chain acyl-CoA synthetase. J Biol Chem. 1990; 265(15):8681-5.

Sweeny JM, Gorog DA, Fuster V. Antiplatelet drug 'resistance'. Part 1: mechanisms and clinical measurements. Nat Rev Cardiol. 2009; 6(4):273-82.

Tanabe T & Tohnai N. Cyclooxygenase isozymes and their gene structures and expression. Prostaglandins Other Lipid Mediat. 2002; 68-69:95-114.

Tavoosi N, Davis-Harrison RL, Pogorelov TV, Ohkubo YZ, Arcario MJ, Clay MC, Rienstra CM, Tajkhorshid E, Morrissey JH. Molecular determinants of phospholipid synergy in blood clotting. J Biol Chem. 2011; 286(26):23247-53.

Thomas CP, Morgan LT, Maskrey BH, Murphy RC, Kuhn H, Hazen SL, Goodall AH, Hamali HA, Collins PW, O'Donnell VB. Phospholipid-esterified eicosanoids are generated in agonist-activated human platelets and enhance tissue factor-dependent thrombin generation. J Biol Chem. 2010; 285(10):6891-6903.

Thon JN & Italiano JE. Platelet formation. Semin Hematol. 2010; 47 (3):220-226.

Thon JN & Italiano JE. Platelets: production, morphology and ultrastructure. Handb Exp Pharmacol. 2012; (210):3-22.

Thun MJ, Jacobs EJ, Patrono C. The role of aspirin in cancer prevention. Nat Rev Clin Oncol. 2012; 9(5):259-67.

Tilley SL, Coffman TM, Koller BH. Mixed messages: modulation of inflammation and immune responses by prostaglandins and thromboxanes. J Clin Invest. 2001; 108(1):15-23.

Tohgi H, Konno S, Tamura K, Kimura B, Kawano K. Effects of low-to-high doses of aspirin on platelet aggregability and metabolites of thromboxane A2 and prostacyclin. Stroke. 1992; 23(10):1400-3.

Tomoda H, Igarashi K, Cyong JC, Omura S. Evidence for an essential role of long chain acyl-CoA synthetase in animal cell proliferation. Inhibition of long chain acyl-CoA synthetase by triacsins caused inhibition of Raji cell proliferation. J Biol Chem. 1991; 266(7):4214-9.

Tong L, Pav S, White DM, Rogers S, Crane KM, Cywin CL, Brown ML, Pargellis CA. A highly specific inhibitor of human p38 MAP kinase binds in the ATP pocket. Nat Struct Biol. 1997; 4(4):311-6.

Toullec D, Pianetti P, Coste H, Bellevergue P, Grand-Perret T, Ajakane M, Baudet V, Boissin P, Boursier E, Loriolle F, Duhamel L, Charon D, Kirilovsky J. The bisindolylmaleimide GF 109203X is a potent and selective inhibitor of protein kinase C. J Biol Chem. 1991; 266(24):15771-81.

Triggiani M, Granata F, Giannattasio G, Marone G. Secretory phospholipases A2 in inflammatory and allergic diseases: not just enzymes. J Allergy Clin Immunol. 2005; 116(5):1000-6.

Tsai AL & Kulmacz RJ. Prostaglandin H synthase: resolved and unresolved mechanistic issues. Arch Biochem Biophys. 2010; 493(1):103-24.

Tsien RY. A non-disruptive technique for loading calcium buffers and indicators into cells. Nature. 1981; 290(5806):527-8.

Uderhardt S, Herrmann M, Oskolkova OV, Aschermann S, Bicker W, Ipseiz N, Sarter K, Frey B, Rothe T, Voll R, Nimmerjahn F, Bochkov VN, Schett G, Krönke G. 12/15-lipoxygenase orchestrates the clearance of apoptotic cells and maintains immunologic tolerance. Immunity. 2012; 36(5):834-46.

Ueno R, Narumiya S, Ogorochi T, Nakayama T, Ishikawa Y, Hayaishi O. Role of prostaglandin D2 in the hypothermia of rats caused by bacterial lipopolysaccharide. Proc Natl Acad Sci U S A. 1982; 79(19):6093-7.

van der Ouderaa FJ, Buytenhek M, Nugteren DH, and Van Dorp DA. Purification and characterisation of prostaglandin endoperoxide synthetase from sheep vesicular glands. Biochim Biophys Acta 1977; 487:315–333.

van Dorp DA, Beerthuis RK, Nugteren DH, and Vonkeman H Enzymatic conversion of all-cis-polyunsaturated fatty acids into prostaglandins. Nature (Lond) 1964; 203:839–841.

Vance DE & Vance JE. Biochemistry of Lipids, Lipoproteins and Membranes. 4th edition. 2002; Amsterdam, The Netherlands: Elsevier Science.

Vane JR. Inhibition of prostaglandin synthesis as a mechanism of action for aspirin-like drugs. Nat New Biol. 1971; 231 (25): 232-235.

Vane JR, Bakhle YS, Botting RM. Cyclooxygenases 1 and 2. Annu Rev Pharmacol Toxicol. 1998; 38:97-120.

Varga-Szabo D, Braun A, Nieswandt B. Calcium signaling in platelets. J Thromb Haemost. 2009; 7(7):1057-66.

Vessey DA, Kelley M, Warren RS. Characterization of triacsin C inhibition of short-, medium-, and long-chain fatty acid: CoA ligases of human liver. J Biochem Mol Toxicol. 2004; 18(2):100-6.

Vesterqvist O & Gréen K. Urinary excretion of 2,3-dinor-thromboxane B2 in man under normal conditions, following drugs and during some pathological conditions. Prostaglandins. 1984; 27(4):627-44.

Vezza R, Roberti R, Nenci GG, Gresele P. Prostaglandin E2 potentiates platelet aggregation by priming protein kinase C. Blood. 1993; 82(9):2704-13.

von Euler US. The specific blood pressure lowering substance in human prostate and seminal vesicle secretions. Klin Wochenschr 1935; 14:1182–1183.

Vu TK, Hung DT, Wheaton VI, Coughlin SR. Molecular cloning of a functional thrombin receptor reveals a novel proteolytic mechanism of receptor activation. Cell. 1991; 64(6):1057-68.

Waddington E, Sienuarine K, Puddey I, Croft K. Identification and quantitation of unique fatty acid oxidation products in human atherosclerotic plaque using high-performance liquid chromatography. Anal Biochem. 2001; 292(2):234-44.

Waku K & Lands WE. Acyl coenzyme A:1-alkenyl-glycero-3-phosphorylcholine acyltransferase action in plasmalogen biosynthesis. J Biol Chem. 1968; 243(10):2654-9.

Wang LH, Hajibeigi A, Xu XM, Loose-Mitchell D, Wu KK.Characterization of the promoter of human prostaglandin H synthase-1 gene. Biochem Biophys Res Commun. 1993; 190(2):406-11.

Watanabe T, Narumiya S, Shimizu T, Hayaishi O. Characterization of the biosynthetic pathway of prostaglandin D2 in human platelet-rich plasma. J Biol Chem. 1982; 257(24):14847-53.

Watson AD, Leitinger N, Navab M, Faull KF, Hörkkö S, Witztum JL, Palinski W, Schwenke D, Salomon RG, Sha W, Subbanagounder G, Fogelman AM, Berliner JA. Structural identification by mass spectrometry of oxidized phospholipids in minimally oxidized low density lipoprotein that induce monocyte/endothelial interactions and evidence for their presence in vivo. J Biol Chem. 1997; 272(21):13597-607.

Watts IS, Wharton KA, White BP, Lumley P. Thromboxane (Tx) A2 receptor blockade and TxA2 synthase inhibition alone and in combination: comparison of anti-aggregatory efficacy in human platelets. Br J Pharmacol. 1991; 102(2):497-505.

Weber A, Ni J, Ling KH, Acheampong A, Tang-Liu DD, Burk R, Cravatt BF, Woodward D. Formation of prostamides from anandamide in FAAH knockout mice analyzed by HPLC with tandem mass spectrometry. J Lipid Res. 2004; 45(4):757-63.

Weinstein EA, Li H, Lawson JA, Rokach J, FitzGerald GA, Axelsen PH. Prothrombinase acceleration by oxidatively damaged phospholipids. J Biol Chem. 2000; 275(30):22925-30.

Williams PC, Coffey MJ, Coles B, Sanchez S, Morrow JD, Cockcroft JR, Lewis MJ, O'Donnell VB. In vivo aspirin supplementation inhibits nitric oxide consumption by human platelets. Blood. 2005; 106(8):2737-43.

Wolfs JL, Comfurius P, Rasmussen JT, Keuren JF, Lindhout T, Zwaal RF, and Bevers EM. Activated scramblase and inhibited aminophospholipid translocase cause phosphatidylserine exposure in a distinct platelet fraction. Cell Mol Life Sci, 2005; 62(13): 1514-25.

Wong-Ekkabut J, Xu Z, Triampo W, Tang IM, Tieleman DP, Monticelli L. Effect of lipid peroxidation on the properties of lipid bilayers: a molecular dynamics study. Biophys J. 2007; 93(12):4225-36.

Wu G, Kulmacz RJ, Tsai AL. Cyclooxygenase inactivation kinetics during reaction of prostaglandin H synthase-1 with peroxide. Biochemistry. 2003; 42(46):13772-7.

Wu G, Rogge CE, Wang JS, Kulmacz RJ, Palmer G, Tsai AL. Oxyferryl heme and not tyrosyl radical is the likely culprit in prostaglandin H synthase-1 peroxidase inactivation. Biochemistry. 2007; 46(2):534-42.

Wu G, Vuletich JL, Kulmacz RJ, Osawa Y, Tsai AL. Peroxidase self-inactivation in prostaglandin H synthase-1 pretreated with cyclooxygenase inhibitors or substituted with mangano protoporphyrin IX. J Biol Chem. 2001; 276(23):19879-88.

Wu G, Wei C, Kulmacz RJ, Osawa Y, Tsai AL. A mechanistic study of self-inactivation of the peroxidase activity in prostaglandin H synthase-1. J Biol Chem. 1999; 274(14):9231-7.

Xu WF, Andersen H, Whitmore TE, Presnell SR, Yee DP, Ching A, Gilbert T, Davie EW, Foster DC. Cloning and characterization of human protease-activated receptor 4. Proc Natl Acad Sci U S A. 1998; 95(12):6642-6.

Xu XM, Tang JL, Chen X, Wang LH, Wu KK. Involvement of two Sp1 elements in basal endothelial prostaglandin H synthase-1 promoter activity. J Biol Chem 1997; 272:6943–50

Yamashita A, Sugiura T, Waku K. Acyltransferases and transacylases involved in fatty acid remodeling of phospholipids and metabolism of bioactive lipids in mammalian cells. J Biochem. 1997; 122(1):1-16.

Yeung J & Holinstat M. 12-lipoxygenase: a potential target for novel anti-platelet therapeutics. Cardiovasc Hematol Agents Med Chem. 2011, 9(3):154-64.

Yin H, Havrilla CM, Gao L, Morrow JD, Porter NA. Mechanisms for the formation of isoprostane endoperoxides from arachidonic acid. "Dioxetane" intermediate versus beta-fragmentation of peroxyl radicals. J Biol Chem. 2003; 278(19):16720-5.

Yin H, Havrilla CM, Gao L, Morrow JD, Porter NA. Mechanisms for the formation of isoprostane endoperoxides from arachidonic acid. "Dioxetane" intermediate versus beta-fragmentation of peroxyl radicals. J Biol Chem. 2003; 278(19):16720-5.

Yin H, Morrow JD, Porter NA. Identification of a novel class of endoperoxides from arachidonate autoxidation. J Biol Chem. 2004; 279(5):3766-76.

Yokoyama C & Tanabe T. Cloning of human gene encoding prostaglandin endoperoxide synthase and primary structure of the enzyme. Biochem Biophys Res Commun 1989, 165:888-894.

Zamocky M, Jakopitsch C, Furtmüller PG, Dunand C, Obinger C. The peroxidise cyclooxygenase superfamily: Reconstructed evolution of critical enzymes of theinnate immune system. Proteins. 2008; 72 (2): 589-605.

Zhang R, Brennan ML, Shen Z, MacPherson JC, Schmitt D, Molenda CE and Hazen SL. Myeloperoxidase functions as a major enzymatic catalyst for initiation of lipid peroxidation at sites of inflammation. J Biol Chem 2002; 277: 46116–46122.

Zhao J, Maskrey B, Balzar S, Chibana K, Mustovich A, Hu H, Trudeau JB, O'Donnell V, Wenzel SE. Interleukin-13-induced MUC5AC is regulated by 15-lipoxygenase 1 pathway in human bronchial epithelial cells. Am J Respir Crit Care Med. 2009; 179(9):782-90.

Zhao J, O'Donnell VB, Balzar S, St Croix CM, Trudeau JB, Wenzel SE. 15-Lipoxygenase 1 interacts with phosphatidylethanolamine-binding protein to regulate MAPK signaling in human airway epithelial cells. Proc Natl Acad Sci U S A. 2011; 108(34):14246-51.

Zhu X, Kim JL, Newcomb JR, Rose PE, Stover DR, Toledo LM, Zhao H, Morgenstern KA. Structural analysis of the lymphocyte-specific kinase Lck in complex with non-selective and Src family selective kinase inhibitors. Structure. 1999; 7(6):651-61.

Zwaal RF & Schroit AJ. Pathophysiologic implications of membrane phospholipid asymmetry in blood cells. Blood. 1997; 89(4):1121-32.

Zwaal RF, Comfurius P, and Bevers EM. Lipid-protein interactions in blood coagulation. Biochim Biophys Acta, 1998; 1376(3): 433-53.